Aus dem Institut für Klinische Zytobiologie und Zytopathologie
Direktor: Prof. Dr. Roland Lill
des Fachbereichs Medizin der Philipps-Universität Marburg

Function of the Myc-binding protein Miz1 in the mouse mammary gland

Inaugural-Dissertation
zur Erlangung des Doktorgrades der Naturwissenschaften
(Dr. rer. nat.)

dem Fachbereich Medizin der Philipps-Universität Marburg
vorgelegt von

Adrián Sanz Moreno
aus Gijón (Asturias, Spanien)
Marburg, 2014

Aus dem Institut für Klinische Zytobiologie und Zytopathologie
Direktor: Prof. Dr. Roland Lill
des Fachbereichs Medizin der Philipps-Universität Marburg

Function of the Myc-binding protein Miz1 in the mouse mammary gland

Inaugural-Dissertation
zur Erlangung des Doktorgrades der Naturwissenschaften
(Dr. rer. nat.)

dem Fachbereich Medizin der Philipps-Universität Marburg
vorgelegt von

Adrián Sanz Moreno
aus Gijón (Asturias, Spanien)
Marburg, 2014

Angenommen vom Fachbereich Medizin der Philipps-Universität Marburg am:
10 März 2014

Gedruckt mit Genehmigung des Fachbereichs

Dekan: Prof. Dr. Helmut Schäfer
Referent: Prof. Dr. Hans-Peter Elsässer
1. Korreferent: Prof. Dr. Thorsten Stiewe
2. Korreferent: Prof. Dr. Alexander Brehm

TABLE OF CONTENTS

2.2. Methods

1. INTRODUCTION

1.1. The murine mammary gland

1.1.1. Mouse mammary gland: cellular architecture and comparison to the human breast

The mammary gland is believed to have evolved from apocrine sweat glands associated with hair follicles more than 310 millions of years ago (Oftedal, 2002). It represents an evolutionary achievement of mammals due to the ability of the gland to secrete milk, allowing the availability of its nutrients and antimicrobial agents for the growth and proper development of the suckling newborns (Peaker, 2002). The mouse mammary gland is a suitable organ for developmental studies due to the cyclical rounds of proliferation, differentiation and apoptosis that occur in each pregnancy and the presence of mammary stem cells in the pubertal gland and in the adult. In addition, relevant mouse models for the study of the origin and progression of human breast cancer have been successfully developed and are extensively used in laboratories worldwide (Allred and Medina, 2008). Although the murine gland is a valuable research model and resembles the human organ, there are noticeable differences between the mouse and human mammary gland. The ductal network ends in clustered structures called terminal ductal lobular units (TDLUs) in the human breast while alveolar buds formed in each estrous cycle are characteristic of the mouse mammary gland. In addition, the elongation of the ductal tree in the mouse is possible due to the existence of club-shaped structures called terminal end buds (TEBs) which migrate through the gland during puberty and these are not as prominent in human glands (Sarkar, 2009). Finally, the murine gland has less fibrous connective tissue and more adipocytes in the fat pad than the human breast (Visvader, 2009).

Two main compartments constitute the mouse mammary gland: the epithelium and the surrounding stroma or fat pad which is mainly formed by adipocytes but also consists of fibroblasts, vasculature, macrophages and eosinophils (Gouon-Evans et al., 2000; Hennighausen and Robinson, 2005). The epithelium is comprised of two main cell types: basal and luminal (Macias and Hinck, 2012). The main basal cell type are myoepithelial cells which are contractile and responsible for the ejection of milk during lactation as a response to pup suckling and oxytocine release from the pituitary gland (Moumen et al., 2011). A population of mammary

stem cells is also regarded to reside in the basal compartment of the mouse mammary gland (Joshi et al., 2010) probably corresponding with small light cells (SLC) visualized in a frequency of around 3% within the epithelium using electron microscopy (Chepko and Smith, 1997). The luminal compartment is composed of ductal and alveolar epithelium. In virgin mice, the ductal tree has lateral buds that partially differentiate in each estrous cycle and these undergo complete differentiation during pregnancy and lactation when the cleavage of small alveolar buds results in the formation of mature alveoli, capable of milk synthesis and secretion (Robinson et al., 1995).

1.1.2. The development of the mouse mammary gland

The development of the murine mammary gland starts at embryonic day 10 (E10) with the formation of stripes of ectoderm called milk lines on the ventral side of the embryo (Robinson et al., 1999). 5 pairs of symmetrically localized placodes become visible asynchronously at determined areas of the mammary line by E11.5 (Hens and Wysolmerski, 2005). Then, a ball-shaped cell aggregate from the placode invaginates into the mesenchyme to form mammary buds at around E12.5 (Watson and Khaled, 2008). The differentiation of this mesenchyme correlates with androgen receptor expression and fetal androgens provoke the destruction of the mammary anlage in male embryos (Neville and Daniel, 1987). The buds remain quiescent in female embryos until the final stages of embryonic development by E16. Then epithelial cells proliferate and sprout into the fat pad precursor mesenchyme where they start branching by cellular division at the terminal end bud. Epidermal cells from the bud differentiate into the nipple and at birth, a primary rudimentary ductal tree, which consists of 15-20 branches, is already formed (Hens and Wysolmerski, 2005; Macias and Hinck, 2012). In humans, this basic ductal system is able to synthesize milk, popularly known as witch´s milk, upon exposure of the baby to hormones from maternal origin (Yap et al., 1980). With the onset of puberty at around 20-30 days of age (Otto et al., 2007), the murine ductal tree migrates through the fat pad guided by terminal end bud (TEB) bifurcation at the tips of the ducts (Hinck and Silberstein, 2005). These bulbous shaped structures are formed by two types of cells: cap and body cells (Fig. 1.1). The cap cells are organized as an outer layer and are considered to be the progenitors of the basal myoepithelial cells in the adult duct. The body cells form 6-10 inner layers in the TEB and finally constitute the luminal epithelial compartment in the mature gland. High proliferation at the TEBs drives the pubertal morphogenesis of the ductal tree through the stroma. The development of the adolescent

mammary gland is disrupted in animals lacking growth hormone (*Gh*), insulin-like growth factor 1 (*Igf1*) or estrogen receptor alpha (*Esr1*) (Macias and Hinck, 2012). In addition, a number of proteins which are also important for ductal morphogenesis have been described and the phenotypes observed after overexpression or knockout in mice were also reviewed (Howlin et al., 2006). Contrary to this, development of the gland during puberty is normal in animals in which prolactin (*Prl)* or progesterone receptor (*Pgr*) were depleted, pointing to the importance of these proteins for alveologenesis and mammary differentiation (Macias and Hinck, 2012).

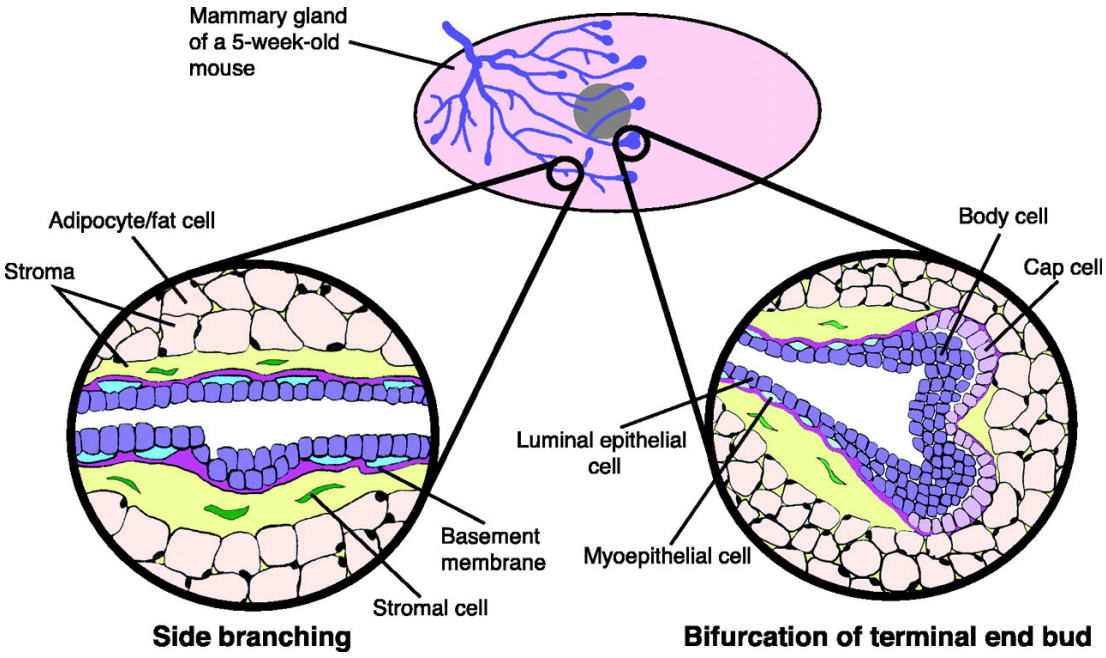

Fig. 1.1: Development of the pubertal mammary gland. The ductal tree (blue) migrates through the fat pad (pink) in a virgin 5-week-old gland (up) while side branches are formed (left) and club-shaped terminal end buds (TEBs; right) actively divide subsequently forming the two compartments of the adult mammary epithelium: luminal and basal (figure reprinted from Wiseman and Werb, 2002).

The central cells of the TEB will suffer apoptosis for the establishment of the hollow ductal system of the adult gland only after branching morphogenesis has occurred (Affolter et al., 2003). An *in vitro* three-dimensional (3D) model has been developed trying to recapitulate some features of mammary morphogenesis *in vivo* using a gel-like mixture of different basement membrane proteins (Hebner et al., 2008). The central cells of these 3D acini suffer apoptosis (Debnath et al., 2002) and autophagy (Debnath, 2008), forming a lumen after culture in the appropriate conditions (Debnath et al., 2003). This method is useful for the elucidation of the pathways which regulate lumen formation (Mailleux et al., 2008) and mammary ductal morphogenesis.

As can be seen in Fig. 1.2, which illustrates mouse mammary gland development by whole-mount preparations at different time points, only a rudimentary tree is visible close to the nipple at day 10 postpartum (Fig. 1.2A). The TEBs reach the lymph node after around one month of growth (Fig. 1.2B), keep proliferating and migrating through the stroma (Fig. 1.2C) and finally disappear once the ductal tree fills the whole fat pad after around 9-12 weeks postpartum (Fig. 1.2D). Under hormonal stimulation, mainly by progesterone during the estrous cycle, ductal side branches form and disappear in the virgin gland (Atwood et al., 2000). Further differentiation of these mammary buds will only occur at pregnancy (Robinson et al., 1995). Three key processes coordinate the transformation of the virgin ductal tree into a milk-producing secretory organ during pregnancy and lactation: proliferation, differentiation and survival of the alveolar epithelium (Hennighausen and Robinson, 2005). An extensive increase in secondary and tertiary branching (Fig. 1.2E) precedes the formation of alveolar buds which cleave and differentiate into alveoli (Fig. 1.2F-G) in the second half of pregnancy (Macias and Hinck, 2012). The pituitary gland secretes the peptide hormone prolactin during pregnancy and lactation which acts directly by binding to the prolactin receptor, triggering the Jak2/Stat5 pathway, and indirectly by sustaining ovarian progesterone secretion (Oakes et al., 2008).

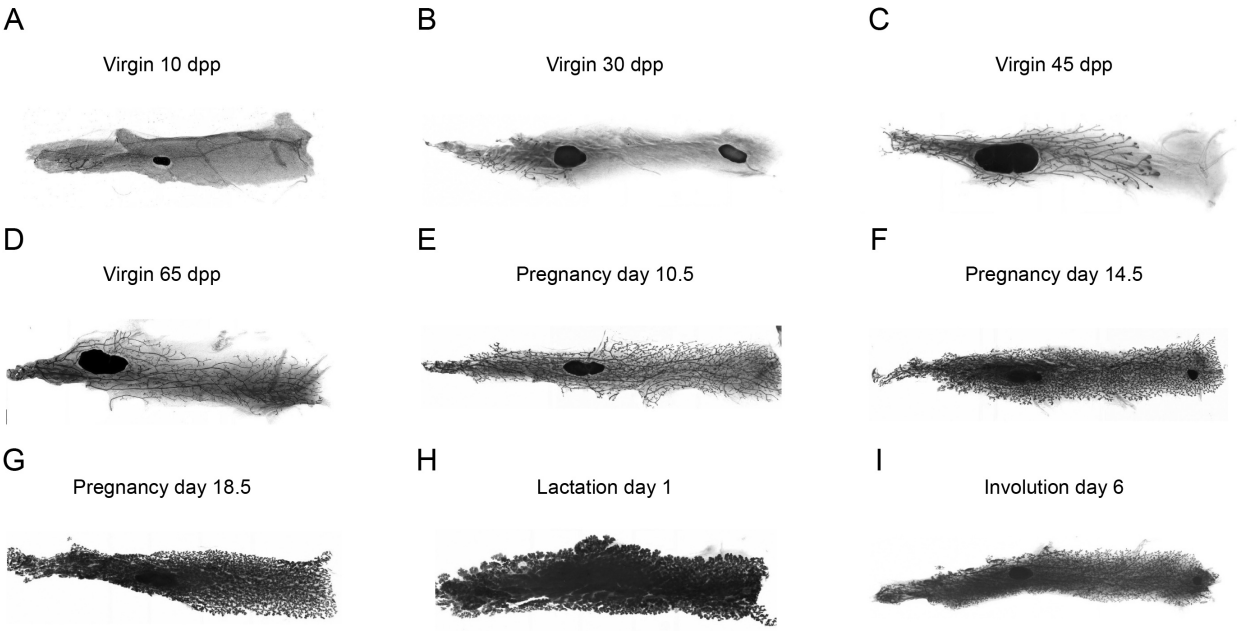

Fig. 1.2: Mouse mammary gland development. Whole-mount preparations of virgin (**A**-**D**), pregnant (**E**-**G**), lactating (**H**) and involuting (**I**) inguinal mouse mammary glands photographed under a stereomicroscope after carmine alum staining (See Materials and Methods for experimental details). Individual pictures were submitted to the Grayscale mode in Adobe Photoshop CS5.

Prolactin is synthesized mainly by lactotrophs in the anterior pituitary gland under the control of the hypothalamus, but it is also produced in other organs including the mammary gland itself (Naylor et al., 2003). As alveolar cells expand and differentiate for milk protein production, adipocytes are depleted from the stroma and this process is more efficient in the presence of epithelium than in a cleared fat pad (Hovey and Aimo, 2010). Lipid cell depletion also depends on the number of pups and the duration of lactation (Elias et al., 1973). The exact milk composition produced by the lactating mammary gland (Fig. 1.2H) varies between species. Mouse milk contains around 12% proteins (including caseins, whey acidic protein, lactoferrin or lactalbumin), a very high concentration of lipids (around 30%) and 5% lactose (Anderson et al., 2007). Once pups are fully weaned, milk accumulates in the gland and the process of involution is initiated. The regressing mammary gland (Fig. 1.2I) suffers massive apoptosis and alveolar cells are cleared leading to a virgin-like architecture of the gland. Of note, parity induces a distinct gene expression program than in the virgin gland (D'Cruz et al., 2002) and a new population of parity-induced mammary epithelial cells (PI-MECs) with stem cell properties originate after the first pregnancy (Wagner et al., 2002). Autophagy has also been linked to mammary involution although evidence is preliminary (Zarzynska and Motyl, 2008; Sobolewska et al., 2011). Two distinct phases of involution have been described. The first phase lasts around 48 hours, is reversible and involves apoptosis of alveolar cells and their accumulation in the lumina of the alveoli. In a second irreversible phase, matrix metalloproteinases (MMPs) remodel the stroma, macrophages are recruited for clearing dead cells and adipocytes refill the gland (Watson and Kreuzaler, 2011a).

1.1.3. The undifferentiated state: the quest for mammary stem cells

Stem cells are able to self-renew and to differentiate into specific cellular lineages maintaining the homeostasis of the tissues in which they reside. Stem cell-related therapies hold great promise for regenerative medicine or cancer treatment (Blanpain et al., 2012). This is especially true after the development of the induced pluripotent stem cell (iPSC) technology which allows the reprogramming of adult somatic cells into pluripotent progenitors (Takahashi and Yamanaka, 2006) and the formulation of the cancer stem cell hypothesis (a recent update on current views on the topic can be found in Nguyen et al., 2012).

Great efforts have been made to elucidate the pathways which regulate mammary stem cell function (Fridriksdottir et al., 2011) and their relationship with breast cancer heterogeneity (Pece et al., 2010). The experiments which first hinted to the existence of mammary stem cells were performed by DeOme and coworkers and consisted on the serial transplantation of mammary gland tissue or hyperplastic alveolar nodules into the cleared mammary fat pad of syngeneic mice (Deome et al., 1959). Unlike transformed cells, transplanted normal mammary gland cells become senescent after 5-8 serial transplant generations (Daniel, 1975), while the host age and reproductive history of the animal does not impact the mammary stem cell frequency (Young et al., 1971). More recently, a whole mammary gland could be generated after transplantation of a single mammary stem cell with the $Lin^{-}CD29^{hi}CD24^{+}$ signature (Shackleton et al., 2006). The quest for the identification and isolation of mammary stem cells has been intense during the last years. A type of small light cells (SLCs) with stem cell properties was identified by electron microscopy (Chepko and Smith, 1997) and several groups reported findings describing potential markers characteristic of mammary stem cells (Shackleton et al., 2006; Stingl et al., 2006; Santos et al., 2013). Moreover, new mouse models confirmed the presence of these rare dividing cells at the tips of the TEBs of the pubertal gland and at the alveolar buds during pregnancy (Bai and Rohrschneider, 2010).

The hierarchical organization of the different stem/progenitor cells that give rise to the functionally differentiated luminal (ductal and alveolar) and myoepithelial cells of the adult gland is still not clear. At least two distinct models exist: one considers the existence of multipotent stem cells which could potentially differentiate into myoepithelial and luminal cell types and the second model suggests the presence of lineage-restricted stem cells which can form either myoepithelial cells or luminal cells but not both (Visvader and Smith, 2011). Recent evidence speaks in favor of both the former (van Amerongen et al., 2012) and the latter hypotheses (Van Keymeulen et al., 2011a), but more experimental data would be required for the completion of a functional model. Also, a population of parity-induced mammary epithelial cells (PI-MECs) has been described (Wagner et al., 2002; Matulka et al., 2007). These cells are pluripotent, self-renewing and able to maintain their alveolar-restricted function upon transplantation (Visvader and Smith, 2011). Their origin is still controversial as PI-MECs have been described to arise from luminal cells which do not undergo apoptosis during involution (Wagner et al., 2002). Alternatively, others argue that these cells are already present in the virgin gland (Booth et al., 2007). The Notch and Hedgehog pathways have been reported to control mammary stem cell

function (Liu, 2006; Bouras et al., 2008). As will be addressed in more depth later, Miz1 has recently been shown to positively regulate the Hedgehog pathway by binding to Smo and Gli2 (Lu et al., 2013b, 1). Also, the increase on progesterone concentration during the estrous cycle has been reported to expand the mammary stem cell pool (Joshi et al., 2010). In addition, new methods for the study of stem cells *in vitro* were developed (Dontu et al., 2003; Dontu and Wicha, 2005a). The mammosphere assay, a mammary stem/progenitor cell culture technique, allows the maintenance in suspension of undifferentiated mammary stem/progenitor cells which can be subjected to passage for several generations until cells differentiate or undergo senescence (Dey et al., 2009a).

1.1.4. Hormonal control of alveologenesis and lactogenesis

The beginning of pregnancy is characterized by high proliferation, side branching and formation of alveolar buds. Alveoli extend throughout the whole ductal tree at around pregnancy day 16.5. These hollow alveolar cavities are dilated or enlarged by the secretions produced by luminal mammary cells at the end of pregnancy. Alveologenesis, final phase of mammary morphogenesis and essential for the formation of alveoli, is tightly linked to the functional differentiation of mammary cells within the alveoli for milk production and secretion, a process called lactogenesis (Brisken and Rajaram, 2006). Two separate phases have been described during lactogenesis (Neville et al., 2002). The first one starts at mid-pregnancy when milk protein gene expression is initiated and lipid droplets are visible in the cytoplasms of mammary cells. The second stage begins at around parturition and is characterized by a boost in milk protein gene expression, tight junction closure and the occurrence of lipid droplets and milk proteins in the alveolar lumina. This first post-partum secretion product from the mammary gland is called colostrum and contains immunoglobulins and protective proteins like the iron-binding protein lactoferrin (Neville et al., 2002). Several hormones control the precise sequence of events which take place during alveologenesis and lactogenesis (Brisken and Rajaram, 2006). Prolactin has been reported to be the main regulator of these processes. Heterozygous knockout females for the prolactin receptor allele have a lactation defect in their first pregnancy and homozygous knockout animals are sterile (Ormandy et al., 1997). When mammary epithelium from prolactin receptor knockout glands is transplanted into wildtype mammary fat pads, normal side branching and formation of alveolar buds occurs but no lobuloalveolar development is observed (Brisken et al., 1999). The

genetic depletion of downstream components of prolactin signalling (e.g. Jak2 and Stat5a/b) or negative regulators of the pathway (e.g. SOCS proteins) clearly affects alveolar formation and mammary differentiation (Brisken and Rajaram, 2006). Another hormone which is required for alveolar expansion is progesterone. There are two distinct isoforms of the progesterone receptor (A and B) encoded by the same gene (Hennighausen and Robinson, 2005). Deletion of both isoforms results in impaired lobuloalveolar development (Lydon et al., 1995), but only isoform B (PR-B) is essential (Mulac-Jericevic et al., 2003). Progesterone receptor deficient epithelium transplanted into wildtype fat pads showed that this hormone acts by a paracrine mechanism (Brisken et al., 1998) with receptor activator of nuclear factor kB ligand (RANKL) as a paracrine mediator of progesterone-dependent alveolar formation (Mulac-Jericevic et al., 2003).

1.2. Prolactin signalling and the Jak2/Stat5 pathway

1.2.1. Stat5 as the master mammary regulator

Signal Transducer and Activator of Transcription 5 (Stat5), originally termed Mammary Gland Factor (Wakao et al., 1994), is the central transcriptional switch for proper mammary gland cell proliferation, differentiation and survival (Hennighausen and Robinson, 2005). Stat5 comprises two closely related isoforms, Stat5a and Stat5b, which are 96% identical at the protein level. Both are encoded by a gene which localizes on chromosome 11 in mouse and in chromosome 17 in humans and this region contains also the *Stat3* gene (Hennighausen and Robinson, 2008). Stat5a is the main actor in normal mammary gland development representing 70% of total Stat5 levels (Yamaji et al., 2012), while both isoforms are important for mammary tumorigenesis (Furth et al., 2011). Stat proteins are normally activated by phosphorylation at tyrosine residues after binding of ligands to cytokine receptors. Once phosphorylated, Stat proteins dimerize and translocate into the cell nucleus where they bind to γ-interferon-activated (GAS) DNA sequences (Hennighausen and Robinson, 2008) and stimulate mammary cell proliferation and differentiation (see Fig. 1.3). *Stat5a/b* constitutive knockout embryos are perinatal lethal due to severe anemia and conditional *Stat5a/b* ablation in late pregnancy results in an increase in mammary cell apoptosis (Cui et al., 2004). *Stat5a* deletion causes a lactation defect by the occurrence of a severely reduced alveologenesis in mutant glands during pregnancy and lactation, although ductal development is normal (Liu et al., 1997). *Stat5b* knockout males are smaller, but

no severe lactation defect is observed in female mutant glands (Udy et al., 1997; Teglund et al., 1998). In the absence of Stat5a, the Stat5b isoform can compensate after several pregnancies, partially rescuing the lactation defect observed in *Stat5a* knockout mice (Liu et al., 1998). Stat5a/b loss does not affect stem cell population frequencies, but luminal progenitor mammary cells are greatly reduced, suggesting that Stat5a is necessary and sufficient for the formation and maintenance of luminal progenitor cells (Yamaji et al., 2009). Around 70% of the mRNAs found in the lactating mammary gland encode for milk proteins and most of the genes with the highest expression during lactation are bound by Stat5a/b within promoter proximal regions (Yamaji et al., 2012). The protein abundance of Stat5a and Stat5b determines the correct functioning of genetic programs which grant a proper mammary proliferation and milk synthesis during pregnancy and lactation (Yamaji et al., 2012).

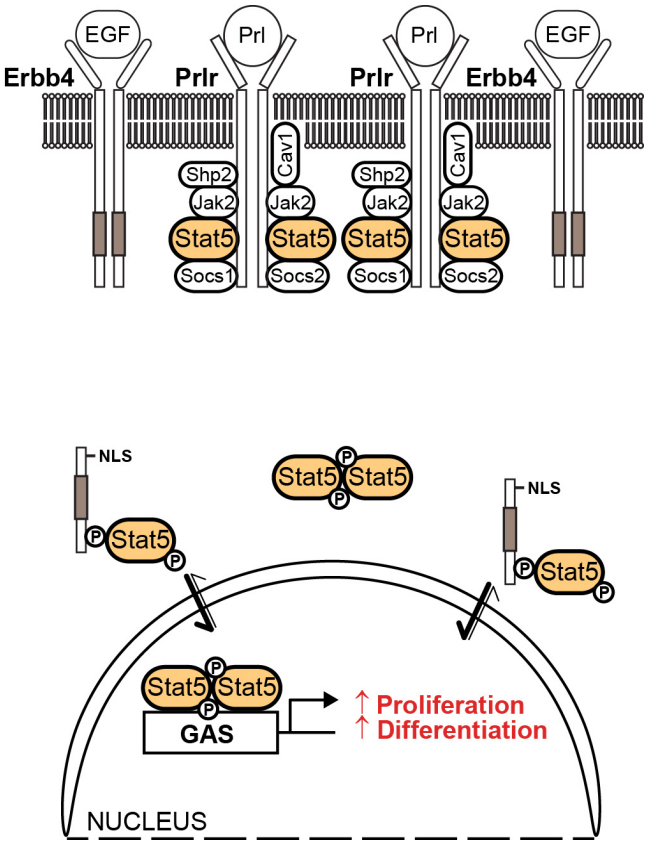

Fig. 1.3: Stat5 signalling regulates mammary cell proliferation and differentiation. Schematic representation of the activation of Stat5 by phosphorylation through either Jak2 via Prolactin Receptor (Prlr) or by direct interaction with a short version of ErbB4 which translocates pStat5 into the nucleus. Once there, Stat5 dimers bind to GAS sequences and activate the expression of genes which are pivotal for proper mammary proliferation and differentation (modified according to Hennighausen and Robinson, 2008; Williams et al., 2004).

1.2.2. The prolactin and ErbB4 receptors

Stat5 is regulated by a number of pathways during mammary pubertal development, lactation and tumorigenesis. Prolactin, ErbB4 or other factors like EGF, estrogen, GH and IGF can affect the phosphorylation of Stat5 (reviewed in Furth et al., 2011). During pregnancy and lactation, two of the main upstream regulators of Stat5 activation via phosphorylation are the prolactin and ErbB4 receptors (Hennighausen and Robinson, 2008).

Prolactin, a 23 kD peptide, is synthesized by lactotrophic cells of the anterior pituitary, but it can additionally be produced in several extrapituitary sites, like the mammary gland itself (Lkhider et al., 1997). Prolactin is the main ligand binding to the prolactin receptor and placental lactogens can also associate with it. The prolactin receptor is a transmembrane protein from the cytokine receptor superfamily and is expressed in long and short forms which are originated from a single *Prlr* gene by alternative splicing (Ormandy et al., 1997). Only the long form is able to participate in the activation of Stat5 (Gouilleux et al., 1994), although the receptor lacks intrinsic kinase function (Shillingford et al., 2002). Binding of prolactin to the long form of its receptor results in the tyrosine phosphorylation of Jak2 (Janus kinase 2), which is permanently associated with the receptor, independently of prolactin ligand levels (Campbell et al., 1994). Subsequently, activated Jak2 proteins phosphorylate each other and specific residues of the cytoplasmic domain of the receptor, which are docking sites for the binding of Stat5 (Sutherland et al., 2007). Upon association with these sites of the prolactin receptor, Stat5 is phosphorylated at tyrosine residues and this event leads to the dissociation of Stat5 from the receptor, the formation of Stat5 dimers and their translocation into the nucleus for transcriptional regulation (reviewed in Wagner and Rui, 2008). Homozygous prolactin receptor knockout females are sterile and heterozygous dams display a lactation defect in their first pregnancy (Ormandy et al., 1997). Accordingly, Jak2 null epithelium transplanted into wildtype hosts fills the fat pad but alveologenesis is impaired and mutant dams also suffer a lactation defect (Shillingford et al., 2002). Taken together, prolactin binding to its receptor is the signal for the activation of Stat5 via Jak2 and this network is essential for proper mammary gland cell proliferation and differentiation during pregnancy and lactation. Another important regulator of Stat5 phosphorylation is ErbB4 which belongs to the ErbB family of receptor tyrosine kinases comprising EGF receptor, ErbB2/HER2/Neu, ErbB3 and ErbB4. From these, ErbB4 is unique with respect to two aspects: it is required for the differentiation of mammary gland cells, while the others stimulate proliferation (Muraoka-Cook

et al., 2008) and its short intracellular form harbors three nuclear localization and three putative nuclear export sequences (Carpenter, 2003). ErbB4 expression is low during proliferative phases of development like puberty or early pregnancy and high when the mammary differentiation program is activated during late pregnancy and lactation (Schroeder and Lee, 1998). ErbB4 knockout dams feature a lactation defect by defective differentiation due to impaired lobuloalveolar development (Jones et al., 1999; Long et al., 2003). In addition, ErbB4 depleted mammary cells fail to activate Stat5a, even in the presence of an intact prolactin/prolactin receptor/Jak2/Stat5a signalling pathway (Muraoka-Cook et al., 2008). This observation led to the notion that ErbB4 could be a direct mediator of Stat5 phosphorylation. Further, it was shown that subsequent to binding of EGF-like ligands (e.g. neuregulins, betacellulin or HG-EGF), ErbB4 is cleaved by TACE and presenilin-dependent γ-secretase resulting in an 80 kDa intracellular form named 4ICD or $s80^{HER4}$. This short version of ErbB4 displays kinase activity essential for Stat5a activation and is able to act as a molecular chaperone, which translocates Stat5a into the cell nucleus due to its nuclear localization and export sequences (Williams et al., 2004; Muraoka-Cook et al., 2006). In conclusion, the sustained activation of Stat5 via phosphorylation and its correct nuclear transport depend on the appropriate expression of the prolactin receptor and ErbB4 at the cell membrane of mammary cells during pregnancy and lactation (see Fig. 1.3).

1.2.3. Negative regulators of the Jak2/Stat5 pathway

A balanced functioning of the Jak2/Stat5 pathway is essential for a tightly regulated cell proliferation and differentiation at the distinct stages of mammary gland development. Suppressor of Cytokine Signalling (SOCS) proteins and Caveolin-1 have been described as part of a negative feedback loop, which attenuates the phosphorylation of Stat5 upon activation, keeping the Jak2/Stat5 pathway under strict regulatory control (Jasmin et al., 2006).

The SOCS protein family comprises eight members, which are induced by cytokines: SOCS 1-7 and Cytokine-Inducible Sh2-containing protein (CIS). The most well-known members of the family are SOCS1, SOCS2, SOCS3 and CIS (Jasmin et al., 2006). All contain a SOCS-box domain, functionally related to protein degradation by targeting through ubiquitination (Hennighausen and Robinson, 2008). CIS does not play a big role in mammary gland development as knockout animals and their progeny are phenotypically normal, although its expression increases during lactation (Marine et al., 1999; Sutherland et al., 2007). Overexpression of SOCS1-3 and CIS diminishes ß-casein synthesis (Lindeman et al., 2001) in

SCp2 mammary epithelial cells (Desprez et al., 1998). In addition, *Socs1* deletion (accompanied of IFNγ knockout to rescue from neonatal lethality) leads to an accelerated alveolar formation during pregnancy due to a premature upregulation of the levels of pStat5, which leads to a precocious lactogenesis. Further, the lactation defect observed in prolactin receptor-heterozygous females (Ormandy et al., 1997) can be rescued by the deletion of just one allele of *Socs1* (Lindeman et al., 2001). SOCS1 has been shown to bind Jak2 and inhibit its kinase activity, while the N-terminus and SH2 domains of SOCS1 are essential in this process (Nicholson et al., 1999). In contrast to SOCS1, SOCS2 does not directly interact with Jak2 and its mechanism of action remains poorly understood (Sutherland et al., 2007; Hennighausen and Robinson, 2008). SOCS2 was found not to be essential for lactogenesis, although the deletion of both alleles of *Socs2* can rescue the lactation defect of prolactin receptor-heterozygous females (Harris, 2006). Finally, SOCS3 is a critical repressor of Stat3-mediated apoptosis during involution. Wap-Cre mediated deletion of *Socs3* in the mammary gland results in accelerated remodeling and apoptosis due to high levels of pStat3 and Myc during an established lactation (Sutherland et al., 2006). When *Socs3* is knocked out with MMTV-Cre (line D) (Wagner et al., 2001) and BLG-Cre (Selbert et al., 1998) no lactation defect is observed (Harris et al., 2006), but MMTV-Cre (line A) deletion results in impaired proliferation of mammary epithelium and reduced alveologenesis (Robinson et al., 2007). Collectively, SOCS1 and SOCS2 function as critical repressors of prolactin signalling during mammary differentiation and SOCS3 is a negative regulator of apoptosis during the remodelling of the gland characteristic of the involution phase while its concrete role in lactation has not been elucidated.

The Jak2/Stat5 pathway can also be attenuated by membrane-bound proteins called caveolins. These proteins are the main constituents of the caveolae, which are membrane invaginations playing a role in endocytosis and mammary tumorigenesis (Patani et al., 2012). The family comprises three members encoded by the genes *Cav1*, *Cav2* and *Cav3*, respectively. *Cav1* expression is significantly downregulated during late pregnancy and lactation coinciding with prolactin secretion (Park et al., 2001). Further, Caveolin-1 depletion in the mammary gland leads to a premature alveolar development during pregnancy due to hyperactivation of Stat5, while Caveolin-2 is not required for alveologenesis (Park et al., 2002). In addition, Caveolin-1 could be co-immunoprecipitated with Jak2 (Park et al., 2002) and the current model suggests that Caveolin-1 prevents the access of Jak2 to the prolactin receptor, negatively affecting Stat5 phosphorylation and proper mammary differentiation (Hennighausen and Robinson, 2008).

1.3. Function of the transcription factors Miz1 and Myc

1.3.1. Miz1

1.3.1.1. Discovery and structure

Myc-interacting zinc finger protein 1 (Miz1) was identified in a yeast two-hybrid screen aimed at searching for Myc partners capable of joint transcriptional repression (Peukert et al., 1997). Miz1 belongs to the POK family of transcription factors characterized by harboring an N-terminal POxvirus and Zink finger/ Broad complex, Tramtrack, Bric à brac (POZ/BTB) domain and a number of Krüppel-type zinc fingers at the C-terminus (Fig. 1.4A; Costoya, 2007). The human Miz1 protein is formed by 803 amino acids being 92% identical to the murine ortholog which contains 794 amino acids (Schulz et al., 1995; Peukert et al., 1997). The evolutionary-conserved POZ domain is constituted by approximately 100 amino acids and is involved in transcriptional repression, cytoskeleton function, dimerization, gating of ion channels and ubiquitination (Stogios et al., 2005; Kelly and Daniel, 2006). More than 40 POK proteins have been identified in humans and these play a pivotal role in development, stem cell biology or cancer (Stogios et al., 2005; Costoya, 2007). In particular, the Miz1 POZ domain serves for homo- or hetero-oligomerization and recruitment of non-POZ partners, so that Miz1 is in dynamic tetramer/dimer equilibrium in solution. The Miz1 tetramer results from the interaction of dimers through two five-stranded β-sheet interfaces (Fig. 1.4B; Stead et al., 2007). The POZ domain is essential for Miz1 function as a transcription factor and mutants lacking this domain are unable to stably associate with chromatin (Fig. 1.5A; Wanzel et al., 2008; Kosan et al., 2010; Möröy et al., 2011). Miz1 binding to DNA occurs in a long non-palindromic sequence located mainly in regions close to the transcriptional start site of its target genes (Wolf et al., 2013). In addition to the N-terminal POZ domain, the C-terminus of Miz1 contains 13 consensus Cys_2His_2 zinc finger domains. Twelve of these are consecutive and the thirteenth is separated from the others by a region involved in the interaction with Myc (Peukert et al., 1997). Cys_2His_2 zinc fingers are one of the main ways in which transcription factors bind DNA (Wolfe et al., 2000). These zinc fingers are formed by around 30 amino acids adopting a ββα conformation secured by two cysteines and two histidines, which are responsible of the coordination of a Zn^{++} ion. The structures of the zinc fingers 5-10 of Miz1 have been recently resolved by solution-state NMR (Fig. 1.4C; Bédard et al., 2012; Bernard et al., 2013).

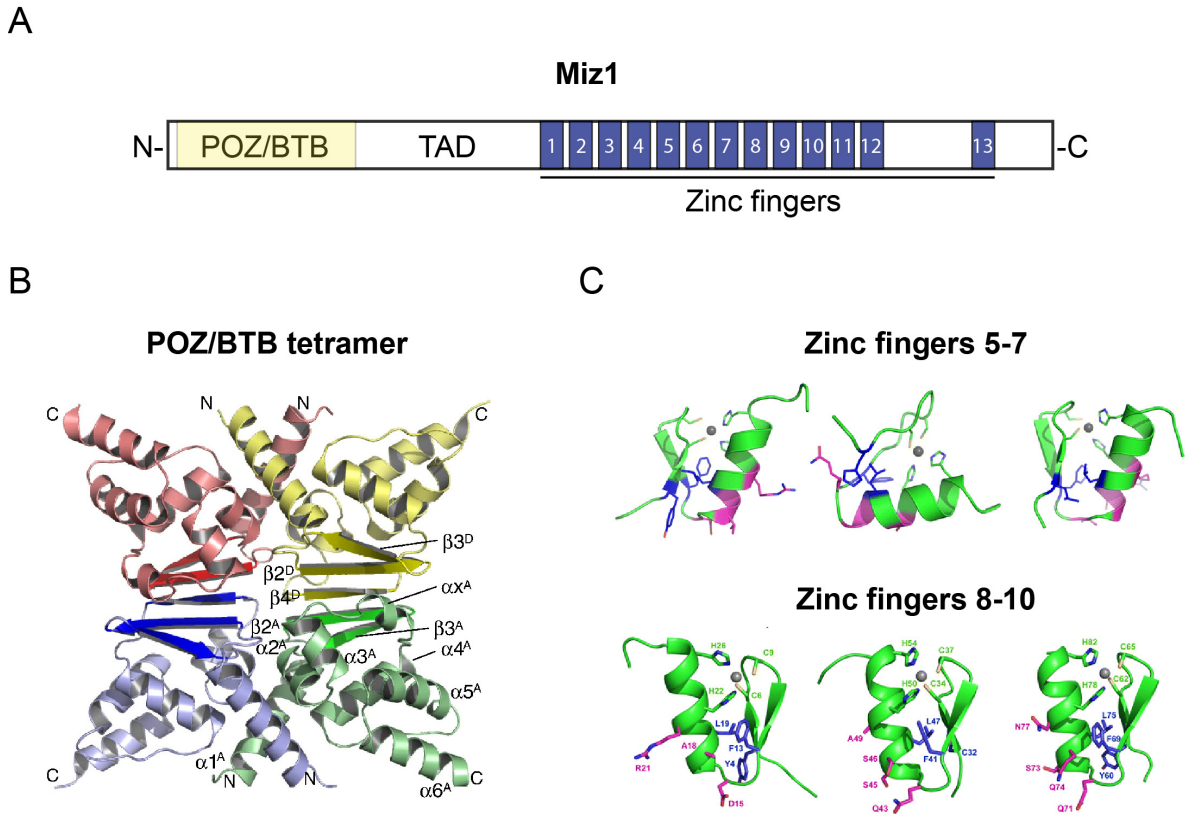

Fig. 1.4: Miz1 protein structure. (**A**) Schematic representation of the Miz1 protein. Miz1 contains a POZ/BTB domain at the N-terminus, a transactivation domain (TAD) and 13 Krüppel-type zinc fingers for binding to DNA. Miz1 interacts with Myc in a region between zinc fingers 12 and 13. (**B**) X-ray crystal structure of a tetramer of POZ/BTB domains which results from the formation of two five-stranded beta-sheet interaction interfaces (reprinted from Stead et al., 2007). (**C**) The crystal structures of the zinc fingers 5-10 of Miz1 have been recently determined (reprinted from Bédard et al., 2012; Bernard et al., 2013).

1.3.1.2. Miz1 as a critical regulator of cell cycle arrest

Miz1 can either activate or repress transcription depending on the identity of its binding partners (Fig. 1.5B; Herkert and Eilers, 2010; Möröy et al., 2011). Miz1 has been shown to transactivate in association with the histone acetyltransferase p300 (Staller et al., 2001) and nucleophosmin (Wanzel et al., 2008). Miz1 can repress transcription by forming a number of distinct complexes with other proteins like Bcl-6, Gfi1 or Zbtb4. In addition, Myc restrains Miz1-dependent activation of gene expression by interfering in the association of Miz1 with its coactivators (e.g. p300 and Myc have overlapping binding sites in the Miz1 protein as reported in Staller et al., 2001). Myc binds Miz1 through its helix-loop-helix (HLH) domain, forming a ternary complex which comprises Miz1, Myc and Max (Herkert and Eilers, 2010). This dual role of Miz1 in

activation and repression of transcription has been extensively studied in regard to the cyclin-dependent kinase inhibitors *Cdkn2b* (encoding $p15^{Ink4b}$) and *Cdkn1a* (encoding $p21^{Cip1}$), which negatively affect cellular proliferation by inducing cell cycle arrest and are of crucial relevance in cancer (Krimpenfort et al., 2007; Abbas and Dutta, 2009).

Miz1 was shown to activate the expression of $p15^{Ink4b}$ by interacting with the cysteine/histidine rich region 3 of p300 and to repress it via ternary complex formation with the Myc/Max heterodimer (Staller et al., 2001). As Miz1 seems to lack a functional nuclear localization signal, it was suggested that the protein might access the cell nucleus by association with other interacting partners like p300 or Myc (Peukert et al., 1997; Staller et al., 2001). In addition to the transcriptional regulation exerted in the nucleus, Miz1 is located also in the cytoplasm where it stably associates to microtubules (Ziegelbauer et al., 2001; Ziegelbauer et al., 2004). In conjunction to the cell cycle, a two-input model was proposed in which in the absence of TGFβ, Myc represses $p15^{Ink4b}$ expression by association with Miz1 at the initiator region of *Cdkn2b*. Upon TGFβ activation, Myc is downregulated allowing the formation of a Smad activator complex upstream of the *Cdkn2b* promoter, including Smad3 and Smad4, which may contact both Miz1 and Sp1 for $p15^{Ink4b}$ transcriptional activation (Seoane et al., 2001). The Miz1/Myc complex has shown to be important in the repression of *Cdkn2b* and cell adhesion genes also *in vivo* (Gebhardt, 2006; Riggelen et al., 2010a). In a similar way and short after these reports, Miz1 was demonstrated to positively regulate $p21^{Cip1}$ by binding to the proximal promoter of *Cdkn1a*, while Myc recruitment represses the expression of $p21^{Cip1}$ in HaCaT, Cos7 and HL-60 cells (Seoane et al., 2002; Wu et al., 2003b). In addition, Miz1 forms other repressive complexes independently of Myc. For instance, Bcl6 suppresses $p21^{Cip1}$ by interaction with Miz1, allowing the proliferation of B-cells in germinal centers during the normal immune response and in B cell lymphomas (Fig. 1.5B; Phan et al., 2005). Also, SB transposase interacts with Miz1, participating in the repression of cyclin D1 in a Miz1-dependent manner (Walisko et al., 2006). Analogously to Myc, the SNAG domain repressor Gfi1 has been shown to suppress the expression of $p15^{Ink4b}$ and $p21^{Cip1}$ in association with Miz1 (Fig. 1.5B; Basu et al., 2009; Liu et al., 2010). Finally, the POZ domain zinc finger protein Zbtb4 recruits the Sin3/histone deacetylase and forms a complex with Miz1 for repression of $p21^{Cip1}$ (Weber et al., 2008). Taken together, Miz1 activates transcription by binding close to the transcriptional start sites of different cell cycle arrest genes and a number of proteins can negatively influence this activation by binding to Miz1 and forming repressor complexes.

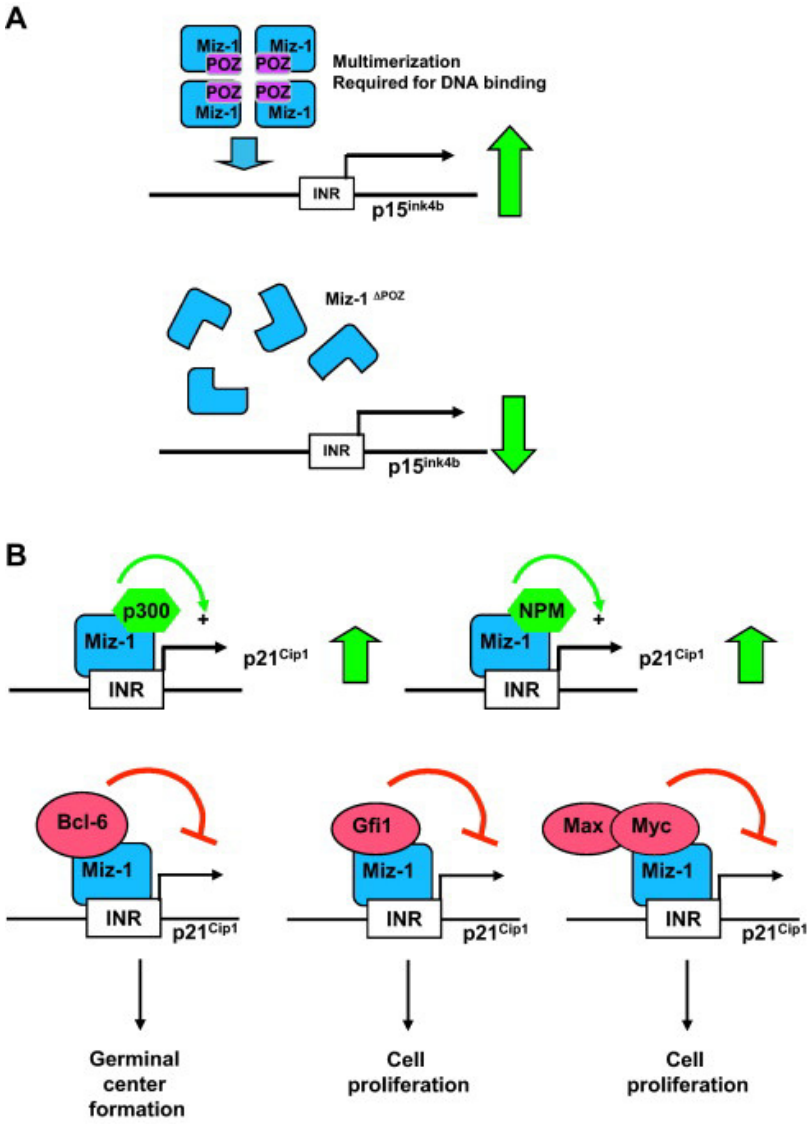

Fig. 1.5: Regulation of gene expression by the transcription factor Miz1. (**A**) Miz1 binds to DNA as a multimer, most probably as a tetramer, and the POZ-BTB domain is required for multimerization and association of Miz1 with chromatin. The $p15^{Ink4b}$ locus is shown as an example of Miz1-transcriptional activation. (**B**) Miz1 can act as an activator (in association with p300 and nucleophosmin) or as a repressor (e.g. after binding of Bcl6, Gfi1 or Myc/Max complexes to Miz1). The regulation of $p21^{Cip1}$ is shown as an example of this dual regulation (figure reprinted from Möröy et al., 2011).

1.3.1.3. Miz1 and apoptosis

As seen in many biological contexts, Myc sensitizes cells to apoptosis when overexpressed (Hoffman and Liebermann, 2008) and the binding to Miz1 was reported as essential for this function of Myc (Patel and McMahon, 2006). Later, Miz1 was shown to activate the anti-apoptotic gene B cell leukemia/lymphoma 2 (*Bcl2*). By interacting with Miz1, Myc represses

Bcl2 and apoptosis follows (Patel and McMahon, 2007). The authors conclude that Miz1 is critical for cellular survival by preventing Myc-mediated apoptosis. In addition to Myc, Bcl6 restrains the expression of Bcl2 by binding to Miz1 and this process is relevant in lymphomagenesis (Saito et al., 2009). Another report describes how Miz1 associates with the tumor suppressors p53 and $p19^{ARF}$, which compete for Miz1 binding (Miao et al., 2009). Miz1 interacts with the DNA-binding domain (DBD) of p53, abrogating the active transcription of apoptotic genes by p53. When levels of murine $p19^{ARF}$ increase, this protein binds Miz1 and p53 is relieved from the complex with Miz1 leading to p53-mediated transcriptional activation of apoptotic genes like *Bax*. Finally, the binding of Myc to Miz1 has been shown to switch the cellular response to human $p14^{ARF}$ from cell cycle arrest to apoptosis (Herkert et al., 2010).

1.3.1.4. Miz1 and stress induced by DNA damage

UV irradiation stimulates the release of an inhibitory complex formed by the topoisomerase II binding protein (TopBP1) and Miz1, allowing the latter to bind and activate the $p21^{Cip1}$ promoter (Herold et al., 2002). TopBP1 expression in human keratinocytes declines 2 hours after UV irradiation and levels keep low till at least 10 hours after exposure. Thus, Miz1 is important for DNA damage-induced cell cycle arrest. In addition, Myc represses the expression of $p21^{Cip1}$ by direct binding to Miz1 as a point mutant of Myc (MycV394D; hereafter referred to as MycVD), which is unable to bind to Miz1 but is still proficient for Max interaction, lacks the ability to repress $p21^{Cip1}$ in response to UV irradiation (Herold et al., 2002). Furthermore, knockdown of Miz1 increases apoptosis and impairs the ability of cells to arrest in G1 by a diminished $p21^{Cip1}$ induction after exposure to UV-induced DNA damage (Wanzel et al., 2004). In the same publication, a new Myc-independent repressive function of Miz1 is described. Akt phosphorylates Miz1 at Ser428 and this post-translational modification is required for the association of Miz1 with the 14-3-3η protein, which in turn inhibits Miz1 function by direct interaction with its 1^{st} and 5^{th} zinc fingers (Wanzel et al., 2004).

Finally, Myc was shown to be ubiquitinated by the E3-ligase HectH9 (also known as Mule, ARF-BP1 and HUWE1) and Miz1 inhibits this ubiquitination (Adhikary et al., 2005). Also, Miz1 is required for the binding of TopBP1 to chromatin and to prevent HectH9-mediated proteasomal degradation of TopBP1 (Herold et al., 2008).

1.3.1.5. Miz1 POZ domain deletion phenotypes *in vivo*

The constitutive deletion of the three first coding exons of Miz1 in the mouse by homologous recombination, comprising the POZ domain and a transactivation region with a neomycin resistance cassette, results in embryonic lethality at around E7.5. At this time point, massive apoptosis and reduced proliferation are observed in knockout embryos which seem to express mesodermal markers but fail to undergo a complete gastrulation (Adhikary et al., 2003). In order to study Miz1 function *in vivo* and due to the lethality associated with its constitutive deletion, a conditional knockout mouse model was developed in which the exons coding for the POZ domain (E3 and E4) are flanked by LoxP sites and depleted by the expression of a tissue-specific Cre recombinase (Gebhardt et al., 2007; Kosan et al., 2010). As described before, the POZ domain is essential for oligomerization and association of Miz1 with chromatin (Möröy et al., 2011). The first report of Miz1 POZ domain deletion *in vivo* describes a complex phenotype after K14-Cre mediated POZ recombination in the keratinocytes of the interfollicular epidermis, the hair follicle and sebaceous glands. Mutant animals display an irregular arrangement of hair follicles, a catagen delay in the hair cycle, development of hair cysts, loss of zig-zag hairs and pigment incontinence (Gebhardt et al., 2007). In addition, K14-Cre *Miz1ΔPOZ* animals exhibit a decreased formation of chemically-induced skin papillomas (DMBA/TPA treatment), due to high levels of $p21^{Cip1}$ in their skin accompanied by a reduced proliferation and increased differentiation (Hönnemann et al., 2012). In this context, Miz1 binds to the *Cdkn1a* promoter and the phenotype can be rescued in a $p21^{Cip1}$ null background stressing that Miz1 is a critical repressor of $p21^{Cip1}$ during skin tumorigenesis (Hönnemann et al., 2012). These observations were recently confirmed by the analysis of papilloma formation in Mule (also known as HectH9, ARF-BP1 and HUWE1) null mice, which exhibit an increase of Miz1/Myc complexes. This leads to a sustained repression of cell cycle arrest genes (*Cdkn1a* and *Cdkn2b*), subsequently resulting in a boosted tumorigenesis in mutant animals. Mule ubiquitinates Myc, and to a lesser extent Miz1, providing a rational explanation for the accumulation of Miz1/Myc complexes in Mule knockout mice (Inoue et al., 2013). Mule had previously been shown to ubiquitinate Miz1, targeting it for proteosomal degradation, especially in the context of TNFα-induced JNK activation (Yang et al., 2010; Liu et al., 2012). In this scenario of active TNF signalling, POZ domain deletion in the lung, by intratracheal administration of adenoviruses encoding Cre

recombinase, results in hyperinflammation and increased mortality of mutant animals after lipopolysaccharide (LPS) treatment (Do-Umehara et al., 2013).

Finally, deletion of the Miz1 POZ domain in the hematopoietic system under the Vav-Cre promoter leads to a largely reduced population of mature B cells in knockout mice, due to a block at the Pre-Pro-B to Pro-B cellular differentiation transition (Kosan et al., 2010). Mutant animals display a decreased Stat5 phosphorylation and very high levels of SOCS1 mRNA. The data show that Miz1 binds to the *Socs1* promoter and the authors suggest that Miz1 is a SOCS1 repressor in this system. In addition, SOCS1 downregulation only partially rescues the phenotype and the re-expression of Bcl2 and Ebf1 is required to completely restore the differentiation of B cells from Vav-Cre *Miz1ΔPOZ* animals (Kosan et al., 2010). Using the same mouse model (Vav-Cre), T cell cellularity was also found greatly reduced in the thymus of *Miz1ΔPOZ* mice. Mutant T cells suffer a block at the transition from $CD4^-CD8^-$ to $CD4^+CD8^+$ cells and inhibition of SOCS1 or Bcl2 overexpression rescue the number of T cells and their differentiation capabilities (Saba et al., 2011). Both of these phenotypes during early lymphocyte development seem to be largely Myc-independent, as $Myc^{VD/VD}$ knock-in animals, in which the interaction between Miz1 and Myc is not possible, have normal numbers of B and T cells (Möröy et al., 2011; Saba et al., 2011). Deletion of the POZ domain of Miz1 in the central nervous system (CNS) under the Nestin-Cre promoter leads to progressive cerebellar neurodegeneration associated with loss of Purkinje cells (Wolf et al., 2013). In this recent publication, 261 Miz1-binding sites in the whole genome are revealed by ChIP-Sequencing performed with chromatin from neural progenitor cells cultivated as neurospheres. The majority of these regions are located close to the transcriptional start site and a long non-palindromic Miz1-binding sequence is present in approximately 70% of them. There is a fair overlap of Miz1-bound genes in the nervous system and in MDA-MB231 human breast cancer cells although the absolute number of binding sites differs, most probably due to the use of distinct antibodies for ChIP-Seq. Despite the fact that Miz1 seems to have a pleiotropic function, not showing Miz1-bound sites a clear functional gene enrichment by bioinformatic analysis, many of its target genes are related to vesicular transport, endocytosis and lysosomal biogenesis. In line with these data, *Miz1ΔPOZ* cerebella accumulate ubiquitinated proteins and p62, which facilitates the elimination of ubiquitinated protein aggregates by autophagy (Pankiv et al., 2007). This leads to the observation of an impaired autophagic flux (Komatsu et al., 2006), as proteasomal activity is unchanged, which progressively causes the late-onset neurodegeneration observed in Nestin-Cre *Miz1ΔPOZ* animals (Wolf et al., 2013).

1.3.2. Myc

The Myc proto-oncogene family comprises the evolutionary conserved c-Myc (Sheiness et al., 1978), N-Myc (Schwab et al., 1983) and L-Myc (Nau et al., 1985) proteins. c-Myc, usually referred to as Myc, has been extensively studied since its discovery and is associated with a plethora of cellular functions like proliferation, differentiation, apoptosis, cellular growth (ribosome biogenesis, protein synthesis and metabolism) and inhibition of cell cycle arrest (Eilers and Eisenman, 2008; Hoffman and Liebermann, 2008; van Riggelen et al., 2010). Myc is commonly deregulated in a wide variety of cancers by either insertional mutagenesis, chromosomal translocation or amplification (Meyer and Penn, 2008).

The 439 amino acid human Myc protein harbors a transactivation domain (TAD) and the Myc homology boxes I and II at the N-terminus (Fig. 1.6A). The homology box I (aa 44-63) is important for the phosphorylation of Myc at Thr58 and Ser62 and the homology box II (aa 128-143) serves for the interaction with the transactivation/transformation-associated protein (TRRAP; McMahon et al., 1998). These two Myc homology boxes are required for transformation, the first in conjunction with Ras and the second with TRRAP (Meyer and Penn, 2008). The Myc homology boxes IIIa, IIIb and IV are located in the middle part of the protein, together with a nuclear localization signal (NLS; aa 320-328; Dang and Lee, 1988). At the C-terminus, Myc has a Basic Region (BR; aa 355-369) for the binding to canonical and non-canonical E-boxes and a basic helix-loop-helix-leucine zipper domain (HLH-LZ; aa 370-439) for dimerization and interaction with the small protein Max, also called “myc-associated factor X” (Fig. 1.6; Blackwell et al., 1990; Blackwood and Eisenman, 1991). Myc/Max heterodimers bind mainly to the E-box sequence CACGTG, while the formation of the complex typically results in transactivation. Further, Myc requires association with Max through its HLH-LZ for exerting its oncogenic activity (Dang et al., 1989; Amati et al., 1993).

The Mxd family of proteins also interact with Max competing with Myc/Max complexes for binding to DNA and resulting in the repression of bound genes (Grinberg et al., 2004). In addition to its role in positively regulating transcription, Myc can also repress gene expression through interaction of its HLH domain with Miz1 which, in turn, directly binds to the repressed genes (Peukert et al., 1997; Herkert and Eilers, 2010). Max has been shown to be essential in Myc-dependent repression (Mao et al., 2003), although functions of Myc which are Max-independent have been described as well (Gallant and Steiger).

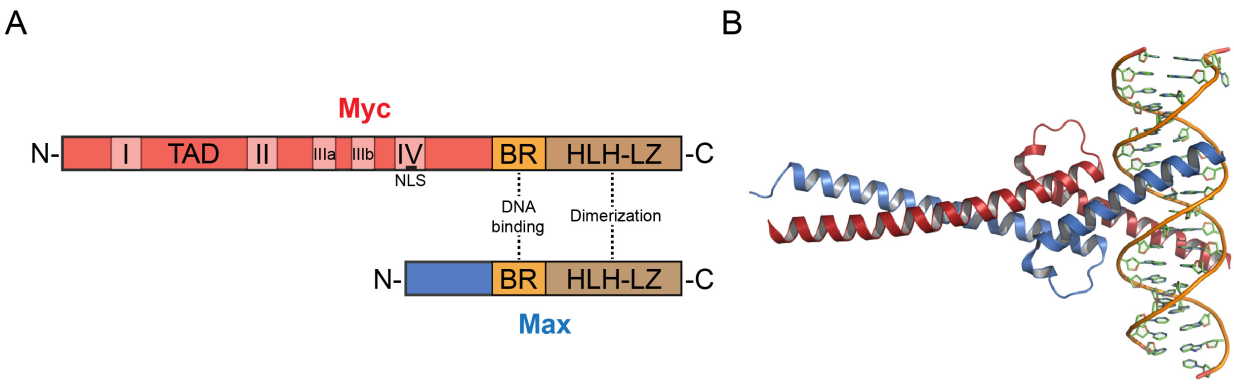

Fig. 1.6: The Myc/Max heterodimer. (**A**) Schematic representation of the structure of human Myc and Max proteins. Myc harbors 4 homology boxes (I-IV) and a transactivation domain (TAD). Myc and Max-share a Basic Region (BR) for DNA binding and the helix-loop-helix-leucine zipper (HLH-LZ) domain required for their interaction (modified according to Meyer and Penn, 2008). (**B**) X-ray crystal structure of the Myc/Max heterodimer recognizing DNA. Myc is represented in red and Max in blue (reprinted from Wikipedia; originally published by Nair and Burley, 2003).

The Myc protein has a relatively short half-life of around 25 minutes (Hann and Eisenman, 1984), is regulated by various post-translational mechanisms (Vervoorts et al., 2006; Wang et al., 2011) and it also represses its own transcription (Penn et al., 1990). The constitutive knockout of *Myc* is lethal before 10.5 days of gestation (Davis et al., 1993) and decreasing its expression *in vivo* reveals that Myc controls cell number and not cell size in mice (Trumpp et al., 2001). Although Myc is generally considered to block differentiation in many biological contexts, it can also promote differentiation in the epidermis by driving stem cells into the transit amplifying compartment (Gandarillas and Watt, 1997; Watt et al., 2008; Eilers and Eisenman, 2008). Myc transcriptional targets seem to be context-dependent, as little overlap can be found after comparing microarray expression data in different systems. Also, genome-wide binding experiments have shown that tens of thousands of Myc-binding sites exist and that the levels of Myc determine the relative occupancy of these DNA regions (Lüscher and Vervoorts, 2012). Myc has been recently proposed to be a "universal amplifier" of the expression of active genes in a particular cellular context by promoting transcriptional elongation, however, this model cannot explain Myc´s role as a transcriptional repressor (Lin et al., 2012; Nie et al., 2012; Rahl et al., 2010). Myc has been reported to regulate Hox genes in collaboration with Miz1 after analyzing genome-wide binding of Miz1 and Myc in human embryonic stem cells by ChIP-on-chip analysis (Varlakhanova et al., 2011). In addition, Myc is critical in the establishment and maintenance of pluripotency (Chappell and Dalton, 2013) and to enhance the efficiency of the reprogramming of somatic cells into induced pluripotent stem (iPS) cells, although Myc can be substituted by other

factors (Takahashi and Yamanaka, 2006; Nakagawa et al., 2008; Nakagawa et al., 2010). Myc seems to regulate a different set of genes (the so-called "Myc module") than other pluripotency factors such as Nanog, Oct4 or Sox2, which share a great amount of transcriptional targets (Chen and Daley, 2008; Kim et al., 2008; Kim et al., 2010). In line with these reports, deletion of Myc in the basal compartment of the mammary gland using K5-Cre leads to a decreased population of mammary stem cells as assessed by limiting dilution and serial transplantation experiments (Moumen et al., 2012). Finally, Myc has been shown to increase self-renewal in neural progenitor cells and its association with Miz1 is important in this process (Kerosuo et al., 2008).

Myc is often deregulated in human breast cancer (Hynes and Stoelzle, 2009) and its overexpression in the mouse mammary gland leads to tumorigenesis (Stewart et al., 1984; Schoenenberger et al., 1988a). Myc is highly expressed in the beginning of pregnancy (Blakely, 2005), most probably contributing to alveolar expansion by boosting mammary proliferation, while its synthesis is sensitive to estrogen and progesterone levels (Hynes and Stoelzle, 2009). Furthermore, overexpression of Myc between days 12.5 and 15.5 of gestation in the mouse mammary epithelium leads to a precocious lactation due to downregulation of Caveolin-1 which leads to hyperactivation of Stat5 and premature involution (Blakely, 2005). A link between a positive regulation of mammary gland differentiation and Myc expression had already been described (Schoenenberger et al., 1988a). Also, Myc overexpression in mammary cells has been shown to induce epithelial to mesenchymal transition (EMT) *in vitro* (Cho et al., 2010). Wap-Cre-mediated Myc conditional deletion in mouse mammary alveolar cells during mid-pregnancy causes a delayed proliferative response, reduced milk production, decreased translational efficiency and impaired repopulation ability upon transplantation in NOD-SCID mice (Stoelzle et al., 2009).

1.4. Aim of the work

Miz1 (Myc-interacting zinc finger protein 1) is a transcription factor which can both activate and repress gene expression depending on the identity of its binding partners. It can activate transcription in association with p300 or nucleophosmin and repress gene expression by recruitment of proteins like the Myc/Max heterodimer, Gfi1 or Bcl-6. Miz1 harbors 13 zinc fingers and an evolutionary-conserved BTB/POZ domain at the amino terminus. The latter domain is essential for multimerization and for the association of Miz1 with chromatin. Miz1 function as a transcription factor is abrogated after deletion of the BTB/POZ domain. As constitutive ablation of *Miz1* is embryonic lethal at E7.5, a conditional knockout mouse model was developed. In this model, the exons which code for the BTB/POZ domain are flanked by LoxP sites for Cre-mediated recombination. Using this *in vivo* tool, the function of the transcription factor Miz1 in the skin, hematopoetic system or cerebellum was described. Miz1 was shown to be important for hair follicle structure and hair morphogenesis, proper differentiation of B and T cells of the hematopoetic system and for the regulation by direct binding of several vesicular transport and autophagy genes in the cerebellum. The repression exerted by the Myc/Max heterodimer on cell cycle arrest genes is also crucial for tumor formation after induction of skin papilloma or in lymphomagenesis.

Miz1 expression is elevated in epithelial tissues and the mammary gland, as a skin appendage, represented a promising target organ for further research. Also, Myc is often deregulated in breast cancer and the function of the Miz1/Myc complex in the mammary gland is still poorly understood. The murine mammary gland constitutes an invaluable tool for developmental studies, due to the consecutive rounds of proliferation, differentiation and apoptosis which occur after each pregnancy. Miz1 expression could be analysed in virgin, pregnant, lactating and involuting mammary glands *in vivo*. Also, deletion of the POZ domain of Miz1 was accomplished by using two different mouse strains: MMTV- and Wap-Cre. MMTV-Cre is already active in the embryo and is suitable for the study of virgin gland development and stem cell research. Interestingly, stem cell function and frequency can be analysed by cultivation of mammospheres, cell aggregates enriched in stem and progenitor mammary cells. The role of the interaction between Miz1 and Myc on mammary stem cells was investigated using a mutant Myc unable to bind Miz1 *in vivo* ($Myc^{VD/VD}$).

Wap-Cre allows a highly-specific gene recombination in luminal mammary alveolar cells starting during mid-pregnancy and allowed the study of the role of Miz1 on mammary differentiation and alveologenesis. Miz1 was investigated *in vitro* using HC11 mammary cells, able to synthesize milk proteins upon addition of a lactogenic hormone cocktail. In conclusion, we aimed to focus on the function of the Miz1/Myc complex in the regulation of the distinct mammary gland developmental stages concentrating on its possible influence on mammary cellular proliferation, differentiation and adult mammary stem cell regulation.

2. MATERIALS AND METHODS

2.1. Materials

2.1.1. Equipment

Autoclaves	Tuttnauer 5075 EL	Tuttnauer (Netherlands)
	Tuttnauer 5075 ELV	Tuttnauer (Netherlands)
	Heraeus ST5042	Heraeus (Hanau, Germany)
Balances	Sartorius Type 1474	Sartorius (Göttingen, Germany)
	Sartorius Analytic AC2105	Sartorius (Göttingen, Germany)
Blotters	Perfect Blue Semi-dry	Peqlab (Erlangen, Germany)
Cameras	MicroPublisher 3.3 RTV	Q-Imaging (Canada)
	F-view	Olympus (Japan)
	Canon EOS 450D	Canon (Japan)
	Lumenera Infinity 1	Lumenera (Canada)
Cell Counter	Cellometer Auto T4	Nexcelom (USA)
Centrifuges	Refrigerated centrifuge 3K30	Sigma (Osterode am Harz, Germany)
	Refrigerated centrifuge 5810R	Eppendorf (Hamburg, Germany)
	Refrigerated centrifuge J2-21	Beckman (USA)
	Bench centrifuge Biofuge pico	Hereaus (Düsseldorf, Germany)
Freezers (-80°C)	Sanyo MDF-594	Sanyo (Japan)
	Colora UF85-360T	Colora (Lorch, Germany)
Heating block	Techne Dri-Block DB2A	Techne (UK)
Heating oven	Binder ED240	Binder (Tuttlingen, Germany)
Homogenizer	Ultra-Turrax T25	Janke & Kunkel (Staufen, Germany)
Incubators	Nuaire DH Autoflow	Integra (Fernwald, Germany)
	Heidolph Unimax 1010	Heidolph (Schwabach, Germany)
Laminar Flow Hood	Faster BHA 48	Faster (Italy)
Magnetic Stirrer	Heidolph MR2000	Heidolph (Schwabach, Germany)

Microplate Reader	Infinite 200	Tecan (Crailsheim, Germany)
Microplate Sealer	Alps 50V Heat Sealer	Thermo Scientific (USA)
Microscopes	Leitz Diaplan MPS 46/52 Olympus BX61 Zeiss IM35 Leica TCS SP2 AOBS Olympus SZ61	Leitz (Wetzlar, Germany) Olympus (Japan) Zeiss (Jena, Germany) Leica (Wetzlar, Germany) Olympus (Japan)
Mixer	Eppendorf Mixer 5432	Eppendorf (Hamburg, Germany)
pH meter	Wtw pH 521	Wtw (Weilheim, Germany)
Power supplies	Biometra Power Pack P25 Lkb 2301 Macrodrive 1	Biometra (Göttingen, Germany) Lkb Bromma (Sweden)
qPCR System	Stratagene Mx3005P	Agilent (USA)
Sonicator	Bioruptor Standard	Diagenode (Belgium)
Spectrophotometer	Hitachi U-2000	Hitachi (Japan)
Thermocyclers	Personal Cycler UNO Peqstar 96 Universal	Biometra (Göttingen, Germany) Peqlab (Erlangen, Germany)
UV Transilluminator	IBI UVT 400-M	Ibi Scientific (USA)
Vortexer	Vortex Genie 2	Bender & Hobein (Switzerland)
Waterbath	GFL Typ 1004	GFL (Burgwedel, Germany)
Water purification	Elix 5 UV	Millipore (USA)

2.1.2. Plastic and glassware

Cell counting	Fuchs Rosenthal Chamber	Schreck (Hofheim, Germany)
Cell culture plates	100 x 20 mm, plastic 24-well plates, plastic 24-well ultra low attachment	Sarstedt (Nümbrecht, Germany) Greiner (Frickenhausen, Germany) Corning (USA)
Cell scrapers	25 cm	Sarstedt (Nümbrecht, Germany)
Cell strainers	70 µm	BD Biosciences (USA)

Containers	Sterile, 50 ml	Labcor (USA)
Cover slips	Glass	Menzel-Gläser (Braunschweig, Germany)
Cryo container	Nalgene “Mr. Frosty”	Thermo Scientific (USA)
Cryotubes	1.8 ml	Nunc, Thermo (USA)
Dispenser	Multipette	Eppendorf (Hamburg, Germany)
Glass pipettes	1, 2, 5 and 10 ml	Hirschmann Laborgeräte (Eberstadt, Germany)
Labteks	8-well Labtek II Chamber Slide	Nunc, Thermo (USA)
Microtiter plates	96-well Microplates, PS, F-bottom	Greiner bio-one (Frickenhausen, Germany)
	96-well PCR plate	Thermo Scientific (USA)
Needles	BD Microlance 3 (20G) TSK (18G) Fine-ject (26 G)	BD Biosciences (USA) Tsk (Japan) Henke Sass Wolf (Tuttlingen, Germany)
Pasteur pipettes	230 mm	Roth (Karlsruhe, Germany)
PCR tubes	0.2 ml	Greiner bio-one (Frickenhausen, Germany)
Plastic pipettes	10 ml	Greiner bio-one (Frickenhausen, Germany)
	50 ml	Sarstedt (Nümbrecht, Germany)
RNase free tips	Biosphere fil. tip	Sarstedt (Nümbrecht, Germany)
Slides	Glass, 76 x 26 mm	Thermo Scientific (USA)
Sterile filter	Filtropur 0.2	Sarstedt (Nümbrecht, Germany)
Syringes	1 ml plastic 50 ml perfusor, plastic	Terumo (USA) Braun (Melsungen, Germany)
Tubes	1.5 and 2 ml, safe-lock 15 and 50 ml	Eppendorf (Hamburg, Germany) Sarstedt (Nümbrecht, Germany)

2.1.3. Solutions and buffers

$CaCl_2$ Solution (2M)
14.7 g $CaCl_2$; Merck (Darmstadt, Germany)
Fill volume to 50 ml with H_20dd and mix
Sterile filter

Carmine Alum stain
1 g Carmine; Merck (Darmstadt, Germany)
2.5 g $KAl(SO_4)_2$; Merck (Darmstadt, Germany)
Add 450 ml of H_20dd and boil mix for 20 minutes
Fill volume to 500 ml with H_20dd
Cool solution and filter

Carnoy´s solution
60% Ethanol; Roth (Karlsruhe, Germany)
30% Chloroform; Roth (Karlsruhe, Germany)
10% Acetic acid; Roth (Karlsruhe, Germany)

EDTA (0.5 M)
18.61 g EDTA; Roth (Karlsruhe, Germany)
Add 80 ml H_20dd
Adjust pH to 8 with 5 M NaOH; Applichem (Darmstadt, Germany)
Fill volume to 100 ml with H_20dd

2x HBS buffer
5.96 g HEPES; Roth (Karlsruhe, Germany)
0.106 g Na_2HPO_4; Roth (Karlsruhe, Germany)
8.18 g NaCl; Roth (Karlsruhe, Germany)
Add 450 ml of H_20dd
Adjust pH to 7.05 with 5 M NaOH
Fill volume to 500 ml with H_20dd
Sterile filter volume desired

10x Laemmli buffer
30 g Tris; Roth (Karlsruhe, Germany)
144 g Glycine; Roth (Karlsruhe, Germany)
10 g SDS; Roth (Karlsruhe, Germany)
Fill volume to 1 liter with H_20dd

LB (**L**ysogeny **b**roth) **media**
10 g Tryptone; Fluka (Switzerland)
5 g Yeast extract; Sigma (USA)
10 g NaCl; Roth (Karlsruhe, Germany)
Adjust pH to 7 with NaOH
Fill volume to 1 liter with H_20dd

PBS (**P**hosphate **b**uffered **s**aline)
0.138 M NaCl
0.0027 M KCl
pH=7.4
Sigma (USA); P-3813

Red blood cell lysis solution	4.5 g NH_4Cl; Merck (Darmstadt, Germany) 0.5 g $KHCO_3$; Sigma (USA) 20 µl 0.5 M EDTA Fill volume to 500 ml with H_20dd
RIPA buffer	50 mM Tris (pH=8) 150 mM NaCl; Roth (Karlsruhe, Germany) 1% Triton X-100; Sigma (USA) 0.5% Sodium deoxycholate; Merck (Darmstadt, Germany) 0.1% SDS; Roth (Karlsruhe, Germany)
4x SDS-PAGE loading buffer	8% SDS; Roth (Karlsruhe, Germany) 20% ß-mercaptoethanol; Merck (Darmstadt, Germany) 40% Glycerol; Fisher Scientific (USA) 0.1% Bromophenol Blue; Sigma (USA) 0.250 M Tris-HCl
Sudan III solution	0.3 g Sudan III; Merck (Darmstadt, Germany) 100 ml hot 70% ethanol Mix well and 60°C o/n incubation Let cool down and filter
Sudan Black B solution	0.1 g Sudan Black B; Merck (Darmstadt, Germany) Add 100 ml 70% ethanol and boil Let cool down and filter
5x TBE (**T**ris/**B**orate/**E**DTA)	54 g Tris; Roth (Karlsruhe, Germany) 27.5 g Boric acid; Roth (Karlsruhe, Germany) 20 ml 0.5M EDTA (pH=8) Fill volume to 1 liter with H_20dd
10x TBS (**T**ris **b**uffered **s**aline)	80 g NaCl; Roth (Karlsruhe, Germany) 2 g KCl; Roth (Karlsruhe, Germany) 30 g Tris; Roth (Karlsruhe, Germany) Add H_20dd and adjust pH to 7.4 with HCl; Merck (Darmstadt, Germany) Fill volume to 1 liter with H_20dd
TE (**T**ris/**E**DTA) pH=8	10 mM Tris; Roth (Karlsruhe, Germany) 1 mM EDTA; Roth (Karlsruhe, Germany)
Tissue fixation (Histology)	3.7% PFA (Roth) in PBS; Sigma (USA)
10x Transfer buffer	48 mM Tris; Roth (Karlsruhe, Germany) 39 mM Glycine; Roth (Karlsruhe, Germany) 0.04% SDS; Roth (Karlsruhe, Germany) 20% Methanol; Roth (Karlsruhe, Germany)

2.1.4. Kits, reagents and special materials

Kits

Absolute qPCR SYBR Green Mix (AB1167; Thermo Scientific, USA)

AEC (red) Substrate Kit (00-2007; Invitrogen, USA)

DeadEnd Fluorometric TUNEL System (G3250; Promega, USA)

Mouse on Mouse (MOM) Basic Kit (BMK-2202; Vector Laboratories, USA)

NucleoBond Xtra plasmid purification system (#740416.50; Macherey-Nagel, Düren, Germany)

NucleoSpin RNA clean-up Kit (740948; Macherey-Nagel, Düren, Germany)

rDNase Set (740963; Macherey-Nagel, Düren, Germany)

REDExtract-N-Amp Tissue PCR Kit (XNATR; Sigma, USA)

RevertAid First Strand cDNA Synthesis Kit (#K1622; Thermo Scientific, USA)

Reagents and special materials

BCA Protein Assay (B9643; Sigma, USA)

Benzonase Nuclease (70664-3; Novagen; Darmstadt, Germany)

Collagenase/Hyaluronidase 10x (#07912; Stem Cell Technologies, Canada)

Cultrex BME Growth Factor Reduced Pathclear (#3433-005-02; Trevigen, USA)

Hoechst 33342 (14533; Sigma, USA)

Lumi-Light and Lumi-Light^{PLUS} Western Blotting Substrates (Roche, Switzerland)

Methyl Cellulose (M0512; Sigma, USA)

Nitrocellulose transfer membranes 0.45 µm (10401196; Whatman, UK)

PageRuler Plus Prestained Protein Ladder (26619; Thermo Scientific, USA)

Phalloidin-TRITC (P1951; Sigma, USA)

Phosphatase Inhibitor Cocktail (P5726; Sigma, USA)

Protease Inhibitor Cocktail (P8340; Sigma, USA)

PVDF transfer membranes 0.20 µm (741260; Macherey-Nagel, Düren, Germany)

Restore Western Blot Stripping Buffer (#21059; Thermo Scientific, USA)

RNA later (R0901; Sigma, USA)

Supersignal West Dura Substrate (#34075; Thermo Scientific, USA)

TriDye 2-Log DNA Ladder (N3270S; New England BioLabs, UK)

TRI Reagent (T9424; Sigma, USA)

2.1.5. Primer sequences (qPCR, semiq-PCR and genotyping)

QUANTITATIVE PCR PRIMERS		
Gene	***Sequence***	***Amplicon (bp)***
Ambra1	**fw:** GAGCACCCAATTTACCCAGA **rv:** GATCATCCTCTGGGCGTAGTA	66
Ano4	**fw:** CGCTTATGACTGGGATCTGATT **rv:** GCTTCAAACTGGGGTCGTAT	66
Camk2b	**fw:** AATGCAAGGAGGAAGCTCAA **rv:** TCCATCTGCTTTCTTGTTGAGTAA	96
αcasein (s1)	**fw:** GACATCTCTCAGGAACTCCACA **rv:** TCCATAGAATGAATAGAGAGACATGAG	92
βcasein	**fw:** GGTGAATCTCATGGGACAGC **rv:** TGACTGGATGCTGGAGTGAA	70
Cav1	**fw:** CCAGGGAAACCTCCTCAGA **rv:** CCGGATGGGAACAGTGTAGA	100
Cdkn1a	**fw:** TCCACAGCGATATCCAGACA **rv:** GGCACACTTTGCTCCTGTG	90
Clca1	**fw:** CATCTACAAGTGGCAGCGTCT **rv:** TGCCCCTGCTCTGACATC	72
Clca2	**fw:** CCAACAGGCTACTGGTGGA **rv:** TGCTCTGGTCACTGGAGGTA	80
Erbb4	**fw:** AATGCTGATGGTGGCAAGA **rv:** CATCACTTTGATGTGTGAATTTCC	82
Exoc2	**fw:** GGGAGAACCTGGGTACTGGT **rv:** CCGTGAGGAGGCAATTATGT	72
Lrp12	**fw:** CAGGCTGGCGTATTTTTCA **rv:** ATTTCCACAGCGGAACTGAT	70
Miz1	**fw:** AGGCACACTGTCTGAGAAGAGA **rv:** TGGTTCAGCTGCTCCAAGA	96
Mki67	**fw:** GCTGTCCTCAAGACAATCATCA **rv:** GGCGTTATCCCAGGAGACT	71
Myc	**fw:** CCTAGTGCTGCATGAGGAGA **rv:** TCCACAGACACCACATCAATTT	93
Pikfyve	**fw:** GGCCGACTGATCTGGATTC **rv:** CCAGCAAATGACCATCAAATAC	60
Prlr	**fw:** GCAGTGGCTTTGAAGGGTTA **rv:** CAGACTTGCCCTTCTCTAGCA	106
Socs1	**fw:** GTGGTTGTGGAGGGTGAGAT **rv:** CCTGAGAGGTGGGATGAGG	61
Socs2	**fw:** CGCGAGCTCAGTCAAACAG **rv:** AGTTCCTTCTGGAGCCTCTTTT	87

Gene	*Sequence (5´ to 3´ direction)*	*Amplicon (bp)*
Socs3	**fw:** ATTTCGCTTCGGGACTAGC **rv:** AACTTGCTGTGGGTGACCAT	126
Spast	**fw:** CAGCCCTGGGTCCTATCC **rv:** TTCTCATCTCACTGGCAGACAT	69
Stat5a	**fw:** AAGATCAAGCTGGGGCACTA **rv:** CATGGGACAGCGGTCATAC	60
Stat5b	**fw:** CGAGCTGGTCTTTCAAGTCA **rv:** CTGGCTGCCGTGAACAAT	64
Vamp4	**fw:** TGCAAGAGAATATTACAAAGGTAATTG **rv:** GAAAGCGGTGGCATTATCC	95
Vps13d	**fw:** CTGACTAACCTAGAGCACCAGATCTAT **rv:** TGTGGTTCCGAAGAGCAAA	94
Vps28	**fw:** AGCTTCTGTCGCCATCTCC **rv:** CCCAGGCAGCTATACAGCAC	65
WAP	**fw:** TGACATGTACACCCCCAGTG **rv:** CTGGTCACTCCCGACAGG	81
SEMI-QUANTITATIVE PCR PRIMERS		
β actin	**fw:** CTAAGGCCAACCGTGAAAAG **rv:** ACCAGAGGCATACAGGGACA	104
β casein	**fw:** ACTGTATCCTCTGAGACTG **rv:** TCTAGGTACTGCAGAAGGTC	578
GENOTYPING PRIMERS		
Cre	**fw:** GAACGCACTGATTTCGACCA **rv:** AACCAGCGTTTTCGTTCTGC	200
Miz1	**Primer 1:** GTATTCTGCTGTGGGGCTATC **Primer 2:** GGCTGTGCTGGGGGAAATC **Primer 3:** GGCAGTTACAGGCTCAGGTG	floxed: 311 wildtype: 276 recombinant: 180
MycVD	**fw:** TGTCCATTCAAGCAGACGAG **rv:** AATTCCAGCGCATCAGTTCT	Myc wildtype: 200 VD knock-in: 300

Table 2.1: **List of primers**. Sequences in 5´ to 3´ direction. Amplicon length is indicated in base pairs.

2.1.6. Informatic Resources

Figure design	Adobe Illustrator/Photoshop CS5	Adobe Systems (USA)
Image acquisition	Cell^F	Olympus (Japan)
	QCapture Pro 5	QImaging (Canada)
	Leica LAS AF Lite	Leica (Wetzlar, Germany)
	Infinity Capture 5.0.0	Lumenera (Canada)
Image quantifications	ImageJ 1.43u	NIH (USA)

Microarray analysis	David Bioinformatics 6.7	NIH (USA)
Primer design	Universal Probe Library Assay	Roche (Switzerland)
Quantitative PCR	Stratagene Mx Pro 4.10d GenEx 5	Agilent (USA) MultiD Analyses (Sweden)
References	Zotero 4.0.11	GMU (USA)
Sequence alignment	Clustal Omega BLAST	EMBL-EBI (UK) NCBI (USA)
Statistics	GraphPad Prism 5.03	GraphPad Software (USA)
Translate tool	ExPASy	SIB (Switzerland)
Whole-mount edition	Autostitch v2.2 Demo	UBC (Canada)

2.2. Methods

2.2.1. Mice

2.2.1.1. Mouse lines

MMTV-Cre Line A and Wap-Cre animals (Wagner et al., 1997; Wagner et al., 2001) were crossed with $Miz1^{lox/lox}$ mice (Gebhardt et al., 2007) in order to conditionally knockout the POZ domain of Miz1 in the mammary gland. MMTV-Cre and Wap-Cre lines were kindly provided by Prof. Lothar Hennighausen (NIDDK, Bethesda, USA). $Miz1^{lox/lox}$ mice were generated in the laboratory of Prof. Tarik Möröy (IRCM, Montreal, Canada). Wap-Cre and $Miz1^{lox/lox}$ lines were backcrossed for six generations, and MMTV-Cre for four generations, to a 129S2/SvHsd background. In the present Thesis, Cre + $Miz1^{+/+}$ animals are referred to as control (*Ctr)* and Cre + $Miz^{lox/lox}$ as *Miz1ΔPOZ*. $Myc^{VD/VD}$ knock-in animals were generated in the laboratory of Prof. Tarik Möröy (IRCM, Montreal, Canada) and generously provided by Prof. Martin Eilers (Biocenter, Würzburg, Germany). Experiments with mice followed the German Animal Protection Law (Tierschutzgesetz) and were approved by the experimental animal local authorities (Regierungspraesidium Giessen; Geschäftszeichen V54-19c20/15cMR 20/10 Nr. A 1/2010).

2.2.1.2. Pup weights and pregnancy/lactation analysis

Pup weights (Fig. 3.16) were measured every 3 days using a Kern EMB balance (Kern & Sohn; Balingen, Germany). The number of the progeny was standardized to 6 pups after birth and for each genotype pups from 6 mothers were monitored. Wap-Cre females were mated at 65 dpp for 1st pregnancy and lactation analysis and 2 weeks after completion of the 1st lactation for the study of the 2nd pregnancy and lactation. For pregnancy samples, mating plugs were checked every day and mammary dissection was performed at the indicated time points.

2.2.1.3. Mammary gland dissection

Thoracic mammary glands (3rd and 8th gland pair) were dissected for obtaining RNA and protein samples. Inguinal mammary glands (4th and 9th gland pair) were collected for whole-mount staining and histology. A schematic representation of the systematization of mammary gland sample collection is shown in Fig. 2.1.

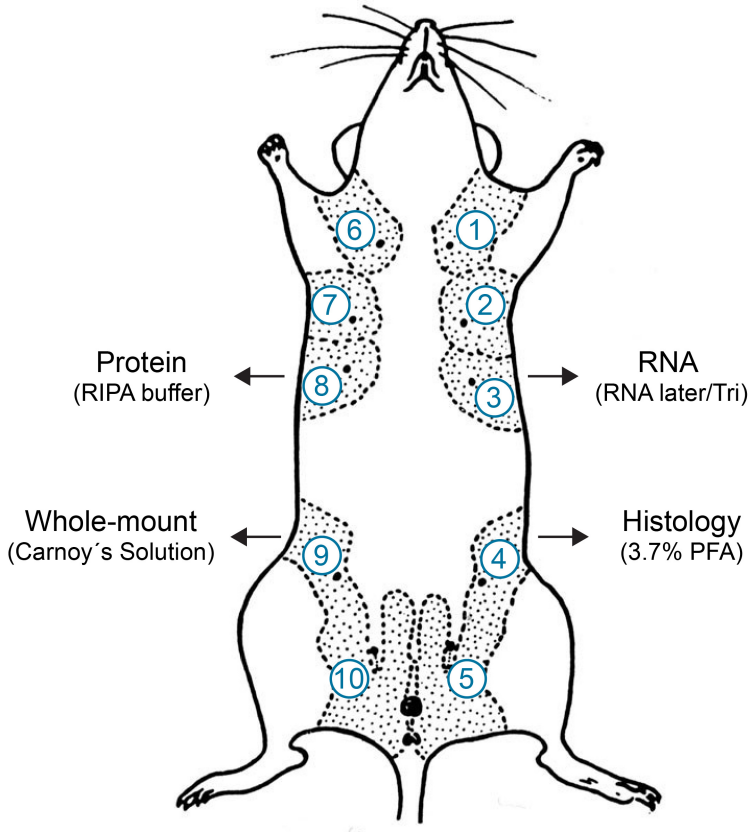

Fig. 2.1. Schematic representation of mammary gland sample collection. The solutions used for the different samples after mammary gland dissection are shown in brackets (modified according to Ip and Asch, 2000).

2.2.2. Cell culture

2.2.2.1. HC11 cell culture and differentiation

HC11 mammary epithelial cells (Ball et al., 1988) were routinely cultured in complete growth medium consisting of RPMI 1640, 10% FBS, 60 µg/ml gentamicin, 2 mM glutamine (all from PAA, Austria), 20 µg/ml insulin from bovine pancreas (I6634; Sigma, USA) and 10 ng/ml of EGF (E4127; Sigma, USA). To induce competence to differentiate, 2-day confluent HC11 cells were incubated for 48 hours in medium without EGF and with low serum (2%). To induce differentiation, competent cells were incubated with DIP medium based on RPMI 1640 and supplemented with 2% FBS, 60 µg/ml gentamicin, 2 mM glutamine (all from PAA, Austria), 10 µg/ml insulin (I6634; Sigma, USA), 1 µM dexamethasone (D4902; Sigma, USA) and 5 µg/ml of prolactin from sheep pituitary gland (L6520; Sigma, USA). A scheme of the protocol followed for HC11 differentiation is shown in Fig 2.2.

2.2.2.2. Miz1 knockdown in HC11 cells

Phoenix packaging cells (Orbigen, USA) were transfected by the calcium phosphate method with *shscr* or *shMiz1* expression vectors (Herkert et al., 2010) using standard protocols. Briefly, 30 µg of each plasmid were mixed with 63 µl of 2M $CaCl_2$ filling the volume to 500 µl with sterile H_20dd. This mix was applied drop by drop into 15 ml Falcon tubes (Sarstedt; Nümbrecht, Germany) containing 500 µl of 2x HBS buffer in agitation. Recipes for preparation of the solutions required for transfection can be found in Section 2.1.3. After incubation for 5 minutes at room temperature, the solution obtained in the last step was added to Phoenix cells and carefully mixed. Cells were then incubated at 37°C and medium was replaced after 15 hours post-transfection with 7 ml of fresh medium. Retroviral supernatants were obtained in two harvests (48 and 66 hours after transfection) and stored at -80°C.

Half a million HC11 cells per 10 cm dish were plated 24 hours before infection. Then, cells were incubated with 3 ml of retroviral supernatant (*shscr* or *shMiz1*), 4 µg/ml of polybrene and 2 ml of growth medium. Next, 5 ml of medium were added to the cells 15 hours post-infection. When cells reached confluency, they were split 1:3 and selected with 2 µg/ml of puromycin (P8833; Sigma, USA). Histone H2B-GFP infected HC11 cells were used to estimate the efficiency of infection and to determine the end of the antibiotic selection.

2.2.2.3. HC11 acinar morphogenesis 3D culture

Three-dimensional acini forming culture of HC11 cells was performed as described elsewhere (Debnath et al., 2003; Xian, 2005; Hebner et al., 2008). Briefly, 24-well plates (662160; Greiner bio-one, Frickenhausen, Germany) coated with 40 µl sterile Cultrex basement membrane extract (BME) Growth Factor Reduced (#3433-005-02; Trevigen, USA) per well on sterilized 13 mm coverslips (Menzel-Gläser, Braunschweig, Germany) were used. Coated coverslips were allowed to solidify for at least 30 minutes at 37° C. HC11 cells were seeded at a concentration of 25.000 cells per ml in 3D medium: RPMI 1640 supplemented with 2% FBS, 60 µg/ml gentamicin, 2 mM glutamine (all from PAA, Austria), 10 µg/ml insulin (I6634; Sigma, USA), 5 ng/ml of EGF (E4127; Sigma, USA), 2 µg/ml of puromycin (P8833; Sigma, USA) for selection and 2% Cultrex. 3D medium was replaced every 4 days using a total volume of 1 ml per well. Acini were fixed in 4% PFA for 20 minutes, washed twice in PBS and stored at 4° C until staining. Next, three 15-minute incubations with 1 ml/well of 100 mM Glycin/PBS (Roth, Karlsruhe, Germany) followed. Acini were permeabilized for 60 minutes in 1 ml of 0.5% TritonX100/PBS (Sigma, USA), blocked for 2 hours in IF-buffer (0.1% BSA, 7.7 mM NaN_3, 0.2% TritonX100, 0.05% Tween20 in PBS) with 1% milk powder. This buffer was used for dilution of primary and secondary antibodies. 300 µl/well of primary antibody were incubated overnight at 4° C and the next morning at RT. After three 15-minute washes with 1 ml IF buffer, 500 µl of secondary antibody were incubated overnight at 4° C and for 2 hours of the next morning at RT. Actin filaments in acini were stained with 10 µg/ml Phalloidin-TRITC (P1951; Sigma) incubated for 40 minutes. Images were captured using a TCS SP2 AOBS confocal microscope (Leica, Wetzlar, Germany) and analysed with LAS AF lite freeware (Leica Microsystems, Wetzlar, Germany).

2.2.2.4. Mammosphere culture of primary mammary cells from MMTV-Cre and $Myc^{VD/VD}$ mouse lines

Primary cell mammosphere culture was largely performed according to the protocol provided with the collagenase/hyaluronidase mix (#07912) from Stem Cell Technologies (Canada) using MMTV-Cre and $Myc^{VD/VD}$ mouse lines (Figures 3.10 and 3.11) and 4 technical replicates per mouse. Thoracic (3^{rd} and 8^{th} gland pair) and inguinal (4^{th} and 9^{th} gland pair) mammary glands (Fig. 2.1) were rendered into a paste in a Petri dish using sterilized scissors after adding 4.5 ml of digestion media containing DMEM (Lonza, Switzerland), 1 mM glutamine, 5% FBS and 60 µg/ml gentamicin (all from PAA, Austria). Next, minced mammary fragments were transferred in

digestion media into a 15 ml Falcon (Sarstedt; Nümbrecht, Germany). This procedure was performed for the number of animals used in each experiment and then digestion was started in all gland fragments synchronously with 500 µl of 10x collagenase/hyaluronidase mix (#07912; Stem Cell Technologies, Canada) per animal. After mixing well, samples were incubated for 7 hours at 37° C. Then, cells were centrifuged (350 g, 5 minutes, break on) and the supernatant discarded. Next, the pellet was resuspended in 5 ml of a mix containing 25% of Cold Hanks Balanced Salt Solution Modifed (Sigma, USA) with 2% FBS (hereinafter referred to as HF) and 75% of Red blood cell lysis solution. See Section 2.1.3. for details on the preparation of this solution. After a 5 minute incubation for red blood cell lysis, cells were centrifuged (350 g, 5 min, break on) and the supernatant discarded. The pellet was resuspended in 3 ml of pre-warmed trypsin-EDTA (0.05% trypsin and 0.02% EDTA in PBS; PAA, Austria) and incubated for around 2 minutes while mixing well with a Pasteur pipette operated on an automatic pipettor (Automatic Sarpette; Sarstedt, Nümbrecht, Germany). Then, the reaction was stopped adding 10 ml of cold HF (see above) and samples were centrifuged (350 g, 5 minutes, break on).

The supernatants were carefully removed and the pellet was resuspended in 2 ml of pre-warmed 5 mg/ml dispase (17105-041; Gibco, Life Technologies, USA) previously diluted in Cold Hanks Balanced Salt Solution Modifed (Sigma, USA) and 200 µl of 1 mg/ml DNase I (buffer included in the kit; 740963; Macherey-Nagel, Düren, Germany) were added. After mixing well, samples were incubated for 10 minutes at 37° C. Next, the cell suspension was diluted with additional 10 ml of cold HF and filtered through a 70 µm cell strainer (BD Falcon; BD Biosciences, USA) on a 50 ml Falcon (Sarstedt; Nümbrecht, Germany). Then, cells were centrifuged (350 g, 5 minutes, break on) and the supernatant was carefully removed. The pellet was resuspended in 2 ml of complete liquid mammosphere medium consisting of MEBM (CC-3151; Lonza, Switzerland), 60 µg/ml gentamicin (P11-004; PAA, Austria), 20 ng/ml EGF (E4127; Sigma, USA), 5 µg/ml insulin (I6634; Sigma, USA), 4 µg/ml heparin (H4784; Sigma, USA), 0.5 µg/ml hydrocortisone (H0888; Sigma, USA), 2% of 50x B27 without vitamin A (12587-010; Gibco, Life Technologies, USA) and 20 ng/ml bFGF (354060; BD Biosciences, USA). Next, cells were counted using a Fuchs Rosenthal Chamber (Schreck; Hofheim, Germany) and 100.000 cells per well were plated on 24-well ultra low attachment plates (3473; Corning, USA) already containing 2 ml of semisolid mammosphere medium (see above) with 1% methyl cellulose (M0512; Sigma, USA). Fresh liquid mammosphere medium was added every 5-6 days of culture. After 2 weeks of

culture, spheres were disaggregated, counted and 2000 cells per well were replated for the formation of secondary or tertiary mammospheres.

2.2.2.5. Mammosphere quantification and size determination

Mammospheres were harvested into a 15 ml Falcon tube (Sarstedt; Nümbrecht, Germany) using a total volume of 7 ml of liquid mammosphere medium. Next, they were centrifuged (350 g, 5 minutes, break off) and the pellet was carefully resuspended in 200 µl mammosphere medium. Then, 50 µl of each of the 4 technical replicates per animal were transferred into different wells of a sterile 96-well plate previously marked with a cross in the bottom using a syringe needle under the stereomicroscope Olympus SZ61 (Olympus, Japan). Spheres in each of the 4 areas of the well were counted for each of the 4 technical replicates using a 5x magnification on a Zeiss IM35 microscope (Zeiss, Jena, Germany). For size determination, diameters of secondary or tertiary mammospheres were scored using ImageJ 1.43u software (NIH, USA). The number of spheres measured per animal is indicated in Figures 3.10 and 3.11.

2.2.2.6. Cultrex 3D culture of primary cells from $Myc^{+/+}$ and $Myc^{VD/VD}$ mice

Primary cells from mammary glands of $Myc^{+/+}$ and $Myc^{VD/VD}$ animals, which had undergone the treatments described in Section 2.2.2.4, were plated on 8-well Labtek II Chamber Slides (Nunc, Thermo, USA) coated with 50 µl of sterile and solidified Cultrex basement membrane extract (#3433-005-02; Trevigen, USA). Similarly, as already described for MCF-10A cells (Debnath et al., 2003), primary cells were counted and 25.000 cells per animal were resuspended in 500 µl of MEBM (CC-3151; Lonza, Switzerland) and mixed with another 500 µl of 2x 3D medium. Then, 400 µl/well of this mix were plated on top of the solidified Cultrex-coated Labteks.
3D medium consisted of MEBM (CC-3151; Lonza, Switzerland), 20 ng/ml EGF (E4127; Sigma, USA), 0.5 µg/ml hydrocortisone (H0888; Sigma, USA), 100 ng/ml cholera toxin (C-8052; Sigma, USA), 10 µg/ml insulin (I6634; Sigma, USA), 80 µg/ml gentamicin and 2% Cultrex basement membrane extract (#3433-005-02; Trevigen, USA).

2.2.2.7. Sudan Black staining of primary cells from $Myc^{+/+}$ and $Myc^{VD/VD}$ mice

Primary cells, from mammary glands of $Myc^{+/+}$ and $Myc^{VD/VD}$ animals, growing on Cultrex-coated (#3433-005-02; Trevigen, USA) Labteks (Nunc, Thermo, USA) were stained for lipids 25 days after plating. After two PBS washes, cells were fixed with 4% PFA (Merck, Darmstadt, Germany) in PBS for 30 minutes at room temperature. Then, mammary cells were washed first in PBS, secondly in H_2Odd and finally in 50% ethanol. Subsequently, cells were stained with Sudan Black B (Merck, Darmstadt, Germany; see Section 2.1.3 for preparation) for 20 minutes. After two H_2Odd washes, cells were counterstained with Nuclear Fast Red (Kernechtrot with Aluminiumsulfat; Fluka, Switzerland) for 10 minutes at room temperature. Next, two H_2Odd washes were performed and slides were mounted with Mowiol (Roth, Karlsruhe, Germany).

2.2.3. Molecular Biology

2.2.3.1. Transformation of competent bacteria

In order to obtain plasmids to stably knockdown Miz1, three different vectors were inserted in competent *Escherichia coli*: a *shscr* (short hairpin scrambled control) and two different specific short hairpins to downregulate Miz1 (*shMiz1#1* and *shMiz1#2*), all kindly provided by Prof. Martin Eilers´ lab (Biocenter, Würzburg, Germany). Briefly, 20 µl of *E. coli* (RapidTrans; Active Motif, USA) and 100 ng of each plasmid were incubated for 45 minutes on ice and then for 45 seconds at 42° C in a waterbath. Next, 180 µl of LB medium (see Section 2.1.3 for preparation) were added to each tube and incubated for 45 minutes at 37° C. After this, 20 µl of bacteria (undiluted, 1:10 and 1:100) were plated into agar plates containing antibiotic (50 µg/ml of ampicillin) and incubated at 37° C overnight. Then, one isolated bacterial colony for each vector was allowed to multiply for 8 hours in the presence of 2 ml of LB medium in a shaker at 37° C. Finally, 500 µl of transformed bacteria were further cultivated in 200 ml LB media flasks containing 50 µg/ml of ampicillin at 37° C overnight.

2.2.3.2. Plasmid DNA purification (Maxiprep)

Transformed bacteria, carrying the *shscr*, *shMiz1#1* and *shMiz1#2* vectors, were centrifuged at 5000 rpm for 10 minutes. Then, the NucleoBond Xtra system (#740416.50; Macherey-Nagel, Düren, Germany) was used to purify DNA plasmids. In brief, bacterial pellets were mixed with

resuspension buffer including RNaseA and then lysis buffer was added to the suspensions and incubated at room temperature for 5 minutes. Next, columns and filters were exposed to equilibration buffer. Neutralization buffer was added to the suspensions and the lysates were mixed by repeated inversion (10-15 times). The suspensions were carefully poured into the columns, washed and the filters discarded. After a new wash, the different plasmid DNAs were eluted and precipitated with room temperature isopropanol (Roth, Karlsruhe, Germany). Next, plasmids were centrifuged (9400 g, 30 minutes, 4° C) and 70% ethanol (Roth, Karlsruhe, Germany) was added to the pellets. After a new centrifugation (9400 g, 5 minutes, room temperature), ethanol was carefully removed and the pellets allowed to dry. DNA pellets were then dissolved in 400 µl of TE buffer (see Section 2.1.3 for preparation) and plasmid yield was determined by UV Spectrophotometry (U-2000; Hitachi, Japan) at 260 nm.

2.2.3.3. Mouse genotyping

Genotyping was performed according to existing protocols (Gebhardt et al., 2007; Hönnemann et al., 2012) using the REDExtract-N-Amp Tissue PCR Kit (XNATR; Sigma, USA). In short, DNA from ear punches was extracted using 50 µl of Extract Solution and 12.5 µl of Tissue Preparation Solution and incubated for 10 minutes at room temperature. Then, samples were digested at 95° C for 3 minutes in a heating block (Dri-Block DB2A; Techne, UK). Immediately after that, 50 µl of Neutralization Solution were added per sample. After agitation, neutralized tissue was stored at 4° C till PCR amplification: 2 µl of DNA were mixed with 10 µl of a solution containing 4 µl of specific primers (See Section 2.1.5.) already in H_2Odd (at a concentration of 100 µM per primer) and 6 µl of REDExtract-N-Amp PCR Reaction Mix included in the kit. The program of the PCR consisted of 30 cycles, after a 3 minute initial denaturation at 95° C, with the following steps:

a) Denaturation: 95° C for 45 seconds.
b) Annealing: 60° C for 45 seconds.
c) Elongation: 72° C for 2 minutes.

Before storage at 4° C, samples were submitted to 1 cycle at 72° C for 10 minutes. Finally, the different animal genotypes were unveiled by 2% agarose gel electrophoresis using TriDye 2-Log (N3270S; New England BioLabs, UK) as DNA marker.

2.2.3.4. RNA harvesting and isolation from cells and tissue

For obtaining RNA from cells, 1 ml of TRI Reagent (T9424; Sigma, USA) was homogeneously distributed on 10 cm Petri dishes, cells were harvested using cell scrapers (Sarstedt; Nümbrecht, Germany) and samples were immediately stored at -80° C till RNA isolation. For obtaining RNA from murine tissue, thoracic mammary gland fragments (maximum 0.5 cm in all dimensions) were stored in RNA later (R0901; Sigma, USA) at 4° C till homogenization in 2 ml of TRI Reagent on ice using the Ultra-Turrax T25 homogenizer (Janke & Kunkel; Staufen, Germany) and submitting each sample to 5 cycles of 5 seconds at a speed set to 13500 rpm. As for cell culture, samples were immediately stored at -80° C after homogenization. RNase-free tips with filters (Biosphere, Sarstedt; Nümbrecht, Germany) were used when pipetting samples containing RNA while surfaces and dissection instruments were rinsed in RNase AWAY (7003; Molecular BioProducts, Thermo, USA).

For RNA isolation from both cell culture and tissue, the protocol from the Tri Reagent bulletin was followed (T9424; Sigma, USA) (Chomczynski and Sacchi, 1987). In short, 200 µl of chloroform (Roth; Karlsruhe, Germany) were added per 1 ml Tri Reagent sample and, after vigorous shaking, probes were incubated for 5 minutes at room temperature. A centrifugation step followed (12000 rpm, 15 minutes, 4° C) and subsequently the upper transparent phase containing RNA was carefully transferred to a tube. Then, 500 µl of isopropanol (Roth, Karlsruhe, Germany) were added to the samples, mixed and incubated for 10 minutes at room temperature. Next, samples were again centrifuged (12000 rpm, 15 minutes, 4° C) and the RNA pellet dissolved in 90 µl of RNase-free water. A DNA digestion followed using 10 µl of the rDNase Set (740963; Macherey-Nagel, Düren, Germany) and incubation for 10 minutes at 37° C. Next, the NucleoSpin RNA clean-up Kit (740948; Macherey-Nagel, Düren, Germany) was used. Briefly, RNA binding conditions were adjusted, mixing samples with 600 µl of Buffer RA1-ethanol premix. Then, each probe was loaded onto a NucleoSpin RNA Binding Column and RNA was bound to the silica membrane by centrifugation for 30 seconds at 10000 g. After replacing collection tubes, the membranes were washed with 700 µl of buffer RA3 and centrifuged again for 30 seconds at 10000 g. The flow-through was discarded, 350 µl of buffer RA3 were added and columns were centrifuged for 2 minutes at 10000 g. The columns were then transferred to fresh 1.5 ml tubes (provided with the kit) and RNA was eluted in 50 µl RNase-free water by centrifugation for 1 minute at 10000 g. Finally, RNA was stored at -80° C.

2.2.3.5. Determination of DNA and RNA concentrations

DNA and RNA concentrations were determined by UV Spectrophotometry (U-2000; Hitachi, Japan) at 260 nm (OD_{260}). The samples were diluted using TE buffer (See Section 2.1.3) which served as blank. The following formula was used to calculate DNA and RNA concentrations: OD_{260} * F * dilution. The F factor value depends on the type of nucleic acid and whether it is single or double-stranded. An OD of 1 corresponds approximately to 50 µg/ml of DNA for double-stranded DNA, 40 µg/ml for single-stranded DNA and RNA and 20 µg/ml for oligonuclotides (Sambrook et al., 1989). The dilution of 1:100 with TE buffer gave normally absorbance values between 0.1 and 1 and was used for most concentration determinations.

2.2.3.6. First strand cDNA synthesis

Methods for synthesis of first strand cDNA depend on the enzyme RNA-dependent DNA polymerase (reverse transcriptase) to catalyze the reaction (Sambrook et al., 1989). The RevertAid First Strand cDNA Synthesis Kit (#K1622; Thermo Scientific, USA) was used. This kit relies on a genetically engineered version of the Moloney Murine Leukemia Virus reverse transcriptase (RevertAid M-MuLV RT) with a low RNase activity. According to the kit, synthesis of full-length cDNAs can be achieved using long templates (up to 13 kb). Random hexamers primers were used in all cDNA synthesis reactions performed in this Thesis. These primers bind non-specifically along an RNA template and all RNAs (not only mRNAs) serve as templates for cDNA synthesis. In short, for one cDNA synthesis reaction, 1 µg of RNA, 1 µl of random hexamer primer (0.2 µg/µl) and DEPC-treated water to a final volume of 12 µl were pipetted into a 0.2 ml tube (Greiner bio-one; Frickenhausen, Germany). After gentle mixing, samples were incubated at 70° C for 5 minutes. In order to prepare a master mix for the amount of samples desired, the following components were added per reaction: 4 µl of 5x reaction buffer, 1 µl of Ribolock Ribonuclease inhibitor (20 u/µl), 2 µl of 10 mM dNTP mix and 1 µl of RevertAid M-MuLV Reverse Transcriptase (200 u/µl). 8 µl from this master mix were added to the preheated sample as described above. Next, the samples were incubated first at 25° C for 10 minutes, then at 42° C for 60 minutes and finally the reaction was stopped heating at 70° C for 10 minutes. All these incubations at different temperatures were performed on a Personal Cycler (Biometra; Göttingen, Germany). Synthesized first strand cDNA was then stored at 4° C for short-term use.

2.2.3.7. Semiquantitative RT-PCR

The polymerase chain reaction (PCR) allows the amplification of any fragment of DNA resulting in the formation of millions of copies which can be used in downstream applications like gene expression analysis, sequencing or genetic fingerprinting. It was developed by Kary Mullis and colleagues (Saiki et al., 1985; Mullis and Faloona, 1987) by improving pre-existing methods (Agarwal et al., 1970; Kleppe et al., 1971) and shortly after that successfully used in combination with a thermostable polymerase (Saiki et al., 1988). The different steps of the polymerase chain reaction (PCR) are the following:

a) Initialization: The temperature rises to 94-98° C for those DNA polymerases which require heat for activation.
b) Denaturation: DNA melts at 94-98° C resulting in single-stranded DNA.
c) Annealing: Temperature is lowered to 50-60° C to allow the binding of specific oligonucleotides (primers) and the polymerase to template DNA.
d) Elongation: The heat-stable DNA polymerase synthesizes a new strand complementary to the template in 5´ to 3´ direction at a temperature which varies with the enzyme used. Taq polymerase (from the thermophilic bacterium *Thermus aquaticus*) has an optimum temperature of 70-80° C and is normally used at 72° C.
e) Final elongation: This step is performed to ensure that any remaining single-stranded template is extended (normally 10 minutes at 72° C).
The mix for the semiquantitative RT-PCR reaction showed in Fig. 3.25 (expression of ß casein and actin in HC11 cells) consisted of:

- 1 µl dNTPs 10 mM (R0191; Fermentas, Thermo, USA)
- 0,5 µl cDNA from mammary tissue and 6 µl for HC11 cells samples
- 5 µl 10x PCR master mix (P2192; Sigma, USA)
- 10 µl primer mix (stock:10 picomol/ µl). Ordered from Metabion (Martinsried, Germany)
- 2 µl REDTaq polymerase (D0688; Sigma, USA)
- 5 µl $MgCl_2$ (R0971; Fermentas, Thermo, USA)
- till 50 µl with H_20dd

Samples were then amplified using a thermocycler (Personal Cycler UNO; Biometra, Göttingen, Germany) and the following PCR program:

- Initialization: 94° C for 3´
- Denaturation: 94° C for 30´´ / Annealing: 58° C for 30´´ / Elongation: 72° C for 2´ (x35)
- Final elongation: 72° C for 10´

Once the PCR was over, 2 µl of 6x DNA-loading buffer (0.4% xylene cyanol, 50% glycerin, 1 mM EDTA pH 8 and 0.4% bromophenol blue) were added to 10 µl of the samples and 10 µl of this mix were run in an agarose gel (see next Section) using TriDye 2-Log (N3270S; New England BioLabs, UK) as DNA marker.

2.2.3.8. Agarose gel electrophoresis

When applying an electric field across an agarose gel, the negatively charged DNA and RNA, due to their phosphate backbone, move in the direction of the positively-charged anode (Sambrook et al., 1989). Nucleic acids can be separated by size due to their distinct migration through the gel and the fragment size can be determined by running the samples side by side with an appropriate marker. The higher the percentage of the agarose gel, the smaller the nucleic acids that can be resolved. A DNA or RNA intercalating agent like ethidium bromide is tipically used to visualize the bands under a UV lamp. For the casting of a 2% gel, 2.4 g of agarose (2267.3; Roth, Karlsruhe, Germany) were introduced into a 500 ml Erlenmeyer flask (Schott; Mainz, Germany). Then, 120 ml of TBE buffer (See Section 2.1.3 for preparation) were poured into the flask and microwaved until the mix was clear due to the complete melting of agarose. The evaporated volume was substituted with H_2Odd. Subsequently, 2 µl of ethidium bromide were added (10 mg/ml stock; Sigma, USA) for visualization of the nucleic acids and the liquid agarose was poured into a cast accompanied by a comb to form the wells for sample loading. After 35-45 minutes, the solidified agarose gel was placed in a TBE-filled running chamber and 10 µl of the samples were loaded using 6x DNA-loading buffer, reserving one lane for 7 µl of TriDye 2-Log (N3270S; New England BioLabs, UK) DNA ladder. The samples were run at a constant voltage of 100 V for approximately 45 minutes. Finally, bands on the gel were visualized using an IBI UV transilluminator (Ibi Scientific, USA) and photographed with a FinePix JZ300 camera (Fujifilm, Japan).

2.2.3.9. Quantitative Reverse Transcription PCR (qPCR)

Quantitative Reverse Transcription PCR (qRT-PCR) or simply Quantitative PCR (qPCR) allows the simultaneous amplification of DNA by the polymerase chain reaction (PCR) and real time detection of newly synthesized nucleic acid by the use of a fluorescent reporter molecule. It provides the capability of precisely quantifying the amplified product, which is useful in e.g. gene expression analysis, diagnosis of diseases or microRNA quantification. The earliest reports of the use of qPCR were done by Higuchi and colleagues (Higuchi et al., 1992; Higuchi et al., 1993). After each amplification cycle, the increase in fluorescence is proportional to the amount of newly synthesized DNA and the qPCR instrument collects data in real time. A threshold level of fluorescence is set above the background and the cycle at which an amplification plot reaches this fluorescence threshold is called Ct value or threshold cycle. If the initial amount of DNA template is high, then the Ct value will be low (it will reach the threshold in an earlier cycle) and vice versa. After an exponential phase of amplification a plateau is reached as the reaction components are consumed. In short, specific intron-spanning primers were designed using the Universal Probe Library Assay (Roche, Switzerland). SYBR Green-based real-time polymerase chain reactions (AB1167; Thermo Scientific) were run in triplicate using a Mx3005P qPCR System (Stratagene, Heidelberg, Germany) and 96-well non-skirted plates (AB-0600/W; Thermo Scientific, USA). A typical qPCR reaction would include:

- 2.5 µl of cDNA diluted 1:10 with nuclease-free H_2O
- 10 µl of primer mix containing nuclease-free H_2O (200 nM primer final concentration)
- 12.5 µl of Absolute qPCR SYBR Green Mix (AB1167; Thermo Scientific, USA)

After all components of the qPCR reaction were included, the plates were sealed using Clear Seal Diamond film (AB-0812; Thermo Scientific, USA) and an Alps 50V Heat Sealer (Thermo Scientific, USA). A quick centrifugation followed (400 g, 30 seconds, room temperature) and then the samples were submitted to the following PCR program:

- Initialization: 95° C for 15´
- Denaturation: 95° C for 30´´ / Annealing: 60° C for 30´´ / Elongation: 72° C for 30´´ (x45)
- Denaturation: 95° C for 1´
- Dissociation curve analysis: 60° C → 95° C

The ΔΔCt method was used for relative quantification of gene expression (Livak and Schmittgen, 2001). In short, for calculation of the ΔCt between the gene of interest (GOI) and the housekeeping or reference gene (e.g. GAPDH) the following formula was used for each sample:

$$\Delta Ct = Ct_{GOI} - Ct_{GAPDH}$$

Then, the difference between the ΔCt of the different samples and the ΔCt of the group selected as control was calculated (ΔΔCt) with the formula:

$$\Delta\Delta Ct = (Ct_{GOI} - Ct_{GAPDH})_{sample} - (Ct_{GOI} - Ct_{GAPDH})_{control}$$

Finally, the normalized target amount in the sample is $2^{-\Delta\Delta Ct}$ and gene expression levels can be compared between samples. The ΔΔCt method was applied using Office Excel 2003 (Microsoft, USA) and statistical analysis was performed with GraphPad Prism 5.03 (GraphPad Software, USA). For *in vivo* experiments, gene expression in one of the control (*Ctr*) animals was arbitrarily set to 1 and the relative fold change expression was calculated for the rest of the mice. 'No template' controls (NTC) were included in each run and product specificity was verified by dissociation curve analysis (Bustin et al., 2009). All primer sequences and amplicon sizes are available in Section 2.1.5.

2.2.3.10. Analysis of qPCR reference gene stability in mammary cells

An optimal reference or housekeeping gene should have a stable expression in the different experimental conditions used. In order to find the most reliable gene in proliferative, arrested and differentiating mammary cells with distinct levels of Miz1 and Myc, several cDNAs from HC11 cells were used for qPCR (see time points surrounded by a square in Fig. 2.2):

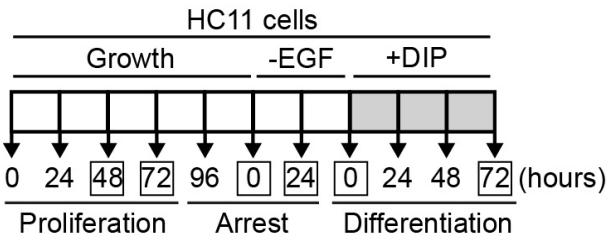

Fig. 2.2. HC11 cDNAs used for reference gene analysis with geNorm and Normfinder.

In samples from 0 and 72 hours of differentiation (see grey squares in Fig. 2.2), cDNAs from control or from HC11 cells overexpressing Miz1 or Myc were also used. The following reference genes were tested: GAPDH, 18s, Hprt, ß Actin, Hmbs, Sdha and Ubqln1. The expression of 18s, Hmbs and ß Actin in these experimental conditions was highly variable and the other four genes behaved more robustly when analyzed in GenEx 5 software (MultiD Analyses, Sweden). GAPDH has been described to be a suitable reference gene in pregnant and lactating mouse mammary glands *in vivo* (Han et al., 2010). Our own analysis on proliferative and differentiating HC11 cells confirms this notion. The M-value of this gene using geNorm (Vandesompele et al., 2002) was 0.4669 and the SD with Normfinder (Andersen et al., 2004) was 0.3072. In consequence, GAPDH was selected as reference gene for qPCR analysis.

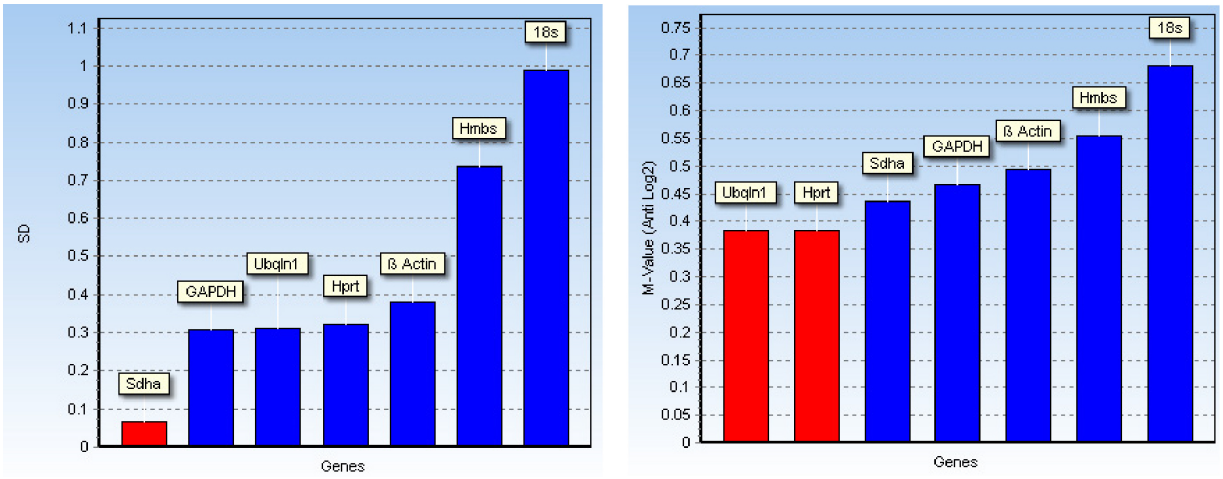

Fig. 2.3. Housekeeping gene analysis. Normfinder (left) and Genorm (right) software were used for the analysis.

2.2.3.11. Microarray analysis and bioinformatics

Microarray analysis of gene expression using first pregnancy lactation day 6 mammary gland samples from Wap-Cre + Miz1$^{+/+}$ (*Ctr*) and Wap-Cre + Miz1$^{lox/lox}$ (*Miz1ΔPOZ*) animals (n=4 per genotype) was performed. RNA integrity (RQI>9 in all samples with 10 as the highest score available) and concentration were assessed with the Experion automated electrophoresis station (Bio-Rad Laboratories, USA). 100 ng of total RNA were employed for cDNA synthesis. Next, the Quick-Amp Labeling Kit (Agilent, USA) was used and Cy3 and Cy5 marked probes were hybridized for 16 hours at 65° C with a mouse genome Agilent-028005 array. The resulting intensity values for the red and green channels were normalized using the lowest method within

the limma package in R/BioConductor (Gentleman et al., 2004; Smyth, 2004). Regulated probes were selected on the basis that the logarithmic (base 2) average intensity value (A-Value) was ≥ 5. Microarrays were performed by Dr. Michael Krause in the Genomics Unit of the Institute of Molecular Biology and Tumor research (IMT, Marburg). Data were generated by Florian Finkernagel and Lukas Rycak (IMT, Marburg) and are available on ArrayExpress under the accession code E-MTAB-1718. Gene numbers from Venn diagrams of Fig. 3.31A were obtained by introducing the lists of regulated genes in *Miz1ΔPOZ* versus control animals (for fold changes equal or higher than 1.5 or 2) under the Official Gene Symbol identifier in the Functional Annotation tool of David Bioinformatics 6.7 (NIH, USA). In Fig. 3.31B, the 4 most significant Gene Ontology (GO) terms were obtained using also the Functional Annotation tool of David Bioinformatics v6.7 (Huang et al., 2008; Huang et al., 2009). Cell functions are represented by relative gene abundance between groups.

2.2.4. Protein Biochemistry

2.2.4.1. Protein extraction from HC11 cells and mammary tissue

For protein extraction, HC11 cells were washed with 10 ml of sterile PBS (P-3813; Sigma, USA) and then harvested using cell scrapers (Sarstedt; Nümbrecht, Germany) and 1 ml of ice cold RIPA buffer (See Section 2.1.3 for preparation). In addition, the buffer contained protease (P8340; Sigma, USA) and phosphatase (P5726; Sigma, USA) inhibitor cocktails and benzonase nuclease (70664-3; Novagen Darmstadt, Germany). Snap frozen thoracic mammary gland fragments were stored at -20° C, homogenized with the Ultra Turrax T25 Homogenizer (Ika, Staufen, Germany) and each sample was submitted to 5 cycles of 5 seconds at an idle (no load) speed of 13500 rpm using 2 ml of ice cold RIPA buffer for virgin, pregnant and involuting glands and 5 ml for lactation samples (due to the high protein concentration of these). After overnight incubation of the cell and tissue samples at 4°C for efficient benzonase nuclease action, lysates were centrifuged (12000 rpm, 15 minutes, 4°C) to remove cellular debris and supernatants were subsequently stored at -20°C.

2.2.4.2. Determination of protein concentration: BCA assay

The bicinchoninic acid (BCA) protein assay allows the quantitative determination of protein concentration and is compatible with the use of detergents and buffer salts (Smith et al., 1985). Under alkaline conditions, a Cu^{++}-protein complex is formed and then the Cu^{++} is reduced to Cu^{+}. Different aminoacids are able to reduce Cu^{++} to Cu^{+}: cysteine, cystine, tryptophan and tyrosin (Wiechelman et al., 1988). Thus, the extent of the reduction is directly proportional to the protein concentration in the samples. BCA forms a purple complex with Cu^{+}, allowing a quantification of the protein content of the samples by comparison with a bovine serum albumin (BSA) calibration curve. In brief, 30 µl of the BSA standards (11 standards from 0 till 5 µg of BSA) and 10 µl of our protein samples with 20 µl of $H20_{dd}$ were added to 96 well plates (655101; Greiner bio-one, Frickenhausen, Germany). Different dilutions with $H20_{dd}$ of our protein samples (for example 1:10, 1:30 and 1:50) were normally used to correctly extrapolate the absorbance data from the standard curve to our sample results. Then, 200 µl of bicinchoninic acid (BCA) solution (B9643; Sigma, USA) with 2% $CuSO_4$ were included in each well using a Transferpette-8 multipipette (Brand, Wertheim, Germany). The absorbance of the reactions was measured at 37°C and 562 nm on three time points (0, 15 and 30 minutes after starting the measurement) using an Infinite

M200 microplate reader (Tecan, Männedorf, Germany). Finally, the protein concentration of our samples (µg/µl) was calculated using Office Excel 2003 (Microsoft, USA), averaging the absorbances obtained in the three different time points.

2.2.4.3. SDS-PAGE (**S**odium **D**odecyl **S**ulfate **P**oly**A**crylamide **G**el **E**lectrophoresis)

SDS-PAGE allows the separation of a complex mixture of proteins by their molecular weight based on the differential migration of these through a matrix under an electric field (Shapiro et al., 1967). The first reports on its use (Pederson, 2008) were related to resolving viral proteins in a gel with SDS (Summers et al., 1965) and for studying immunoglobulin chain synthesis (Shapiro et al., 1966). SDS is an anionic detergent that, after boiling, denatures proteins and provides a negatively-charged coat around the protein and the negative charge is proportional to the mass of the protein. At saturation, 1.4 g of SDS binds to each 1.0 g of protein. A reducing agent (ß mercapto-ethanol or dithiothreitol) is used to break down disulphide bonds disrupting the tertiary and quaternary structure of the proteins so that they are linearized. SDS-coated proteins have the same charge to mass ratio so that differential migration depends entirely on mass but not on charge of the proteins. Negatively charged proteins will then migrate towards the cathode through a polyacrilamide gel matrix. The polyacrylamide chains are crosslinked by N,N-methylene bisacrylamide. The polymerization is initiated by ammonium persulfate (Hunkeler, 1991) and TEMED accelerates the formation of free radicals from persulfate and these catalyze the polymerization reaction. As the percentage of acrylamide increases, the pore size decreases, allowing the separation of differently sized proteins. Proteins with a higher molecular mass should be resolved with low acrylamide percentage and smaller proteins in higher percentage gels. Discontinuous buffer systems are characterized by distinct buffer ions in the gel compared to those in the electrode reservoirs (Ornstein, 1964; Davis, 1964), being the Laemmli SDS-discontinuous system the most widely used (Laemmli, 1970). The stacking gel (1 M Tris-HCl, pH=6.8) allows proteins to migrate in a tight band moving behind chloride ions while the resolving gel (1.5 M Tris-HCl, pH=8.8), once glycine has been deprotonated, permits the migration of proteins according to their size using differential pore sizes (6-15% acrylamide gels are normally used) for accurate protein band discrimination (modified from Mullins lab SDS-PAGE protocol, UCSF, USA). 8% and 15% acrylamide gels were used in the present thesis. In

short, for the preparation of 20 ml of an 8% resolving gel (Sambrook et al., 1989), the following components were mixed adding APS and TEMED at the end to ensure proper polymerization:

- 9.3 ml H_2Odd
- 5.3 ml of a 30% acrylamide/bisacrylamide 37.5:1 mix (3029.1; Roth, Karlsruhe, Germany)
- 5.0 ml 1.5 M Tris-HCl (pH=8.8)
- 200 µl 10% SDS (4360.2; Roth, Karlsruhe, Germany)
- 200 µl 10% APS (17874; Thermo Scientific, USA)
- 12 µl TEMED (161-0800; Bio-Rad Laboratories, USA)

After pouring the acrylamide solution for the resolving gel into the space between glass plates, 500 µl of isopropanol were added to ensure the formation of a flat gel. Next, the isopropanol was removed and H_2Odd was used to wash the upper part of the resolving gel. Once the matrix had polymerized (about 30 minutes), the stacking gel was added on top of the resolving gel including a comb for well formation. For the preparation of 5 ml of stacking gel (Sambrook et al., 1989) the following components were combined:

- 3.4 ml H_2Odd
- 830 µl of a 30% acrylamide/bisacrylamide 37.5:1 mix (3029.1; Roth, Karlsruhe, Germany)
- 630 µl 1 M Tris-HCl (pH=6.8)
- 50 µl 10% SDS (4360.2; Roth, Karlsruhe, Germany)
- 50 µl 10% APS (17874; Thermo Scientific, USA)
- 5 µl TEMED (161-0800; Bio-Rad Laboratories, USA)

During the polymerization of the stacking gel, protein samples (20-60 µg) were prepared by mixing them with 4x SDS-PAGE loading buffer (see Section 2.1.3), and were incubated for 5 minutes at 95° C on a heating block (Techne Dri-Block DB2A; Techne, UK) for protein denaturation. Once the polymerization of the stacking gel was complete (about 30 minutes), the gel was mounted in the electrophoresis apparatus and combs were removed. Samples were then loaded including 5 µl of PageRuler Plus Prestained Protein Ladder (26619; Thermo Scientific, USA) for proper estimation of the molecular weights of our proteins of interest. With the help of a power supply (see Section 2.1.1 for equipment details), 15 mA of constant current per gel were applied till the dye front migrated into the resolving gel. Then, current was increased to 30 mA until bromophenol blue reached the bottom of the resolving gel.

2.2.4.4. Western blotting

Western blotting involves the transfer of proteins from the SDS-PAGE gel on nitrocellulose or polyvinylidene difluoride (PVDF) membranes and the detection of antigenic epitopes using specific antibodies (Towbin et al., 1979). This technique is very useful not only for the identification but also for the quantification of proteins and does not require radiolabelling (Sambrook et al., 1989).

For semi-dry western blotting, 1 mm filter paper rectangles of 9 cm x 6 cm were cut. In addition, PVDF (741260; 0.20 µm; Macherey-Nagel, Düren, Germany) and nitrocellulose transfer membranes (10401196; 0.45 µm; Whatman, UK) were also cut slightly smaller than the filter paper (approximately 8.3 cm x 5.8 cm). PVDF membranes were then submerged into methanol for 1 minute for activation due to their high hydrophobicity. After this, filter papers, membranes and gels were incubated for 15 minutes in transfer buffer with methanol (see Section 2.1.3) at room temperature with gentle rotation. Then, the following components were arranged in order: anode/filter paper/SDS-PAGE gel/nitrocellulose or PVDF membrane/filter paper/cathode inside of a Perfect Blue Semi-dry blotting chamber (Peqlab, Erlangen, Germany). The transfer of the proteins of the gel into the membrane was performed using 2.5 mA per cm^2 of membrane during 45 minutes. After the transfer, membranes were blocked for 45 minutes using 5% milk (T145.2; Roth, Karlsruhe, Germany) or 2% albumin (T844.2; Roth, Karlsruhe, Germany) diluted in TBST (TBS with 0.1% of Tween; Merck, Darmstadt, Germany) at room temperature with gentle rotation. Next, membranes were incubated inside of sealed plastic bags overnight at 4° C with one of the diluted primary antibodies indicated in Table 2.2. Blocking substance (milk or albumin) was used for dilution of antibodies. All primary antibody incubations were performed at 4°C overnight except for the rabbit anti-milk serum, which was done at room temperature for 1 hour (Marte et al., 1995).

After primary antibody incubation, membranes were washed 3 times (10 minutes each) with TBST inside of plastic containers or cassettes under agitation. Next, membranes were incubated with the appropriate HRP-conjugated secondary antibody (See Table 2.2) for one hour at room temperature with rotation. Membranes were then washed again 3 times (10 minutes each) with TBST and transferred to TBS for detection of the protein bands using either the Supersignal West Dura Extended Duration (#34075; Thermo Scientific, USA) or the Lumi-Light (Roche, Switzerland) chemiluminescent Western blotting substrates which were applied to the

membranes for 5 minutes at room temperature. After this, autoradiography films (SC-201696; Santa Cruz Biotechnology, USA) were exposed to the membranes. Finally, for visualization of the protein bands, films were submerged in paper developer solution Neutol Liquid (Agfa, Belgium), washed in H_20dd to remove the excess of developer and protected using Sistan Image Silver Stabilizer (Agfa, Belgium). Dried films were scanned using a ScanJet 3400C scanner (Hewlett-Packard, USA) and images of blots were displayed in Grayscale mode using Photoshop CS5 (Adobe Systems, USA) for blot representation in figures.

Primary antibodies			
Antigen	*Info*	*Company/Provider*	*Dilution*
Actin (A2103)	rabbit polyclonal	Sigma (USA)	1:1000
Milk proteins	rabbit polyclonal	Prof. Nancy Hynes (Basel, Switzerland)	1:5000
β-Casein (S-15)	goat polyclonal	Santa Cruz (USA)	1:200
Cytokeratin 18 (C-04)	mouse monoclonal	Abcam (UK)	1:1000
Miz1 (10E2)	mouse monoclonal	Prof. Martin Eilers (Würzburg, Germany)	1:400
Miz1 (B10)	mouse monoclonal	Santa Cruz (USA)	1:250
Myc (N262)	rabbit polyclonal	Santa Cruz (USA)	1:400
pStat5a/b (#05-495)	mouse monoclonal	Millipore (USA)	1:500
Stat5a/b (C-17)	rabbit polyclonal	Santa Cruz (USA)	1:250
α-Tubulin	mouse monoclonal	Thermo Scientific (USA)	1:5000
Secondary antibodies			
Antibody	*Host*	*Company*	*Dilution*
Anti-Goat IgG	Rabbit	Bio-Rad (#172-1034)	1:7500
Anti-Mouse IgG	Goat	Bio-Rad (#172-1011)	1:7500
Anti-Rabbit IgG	Goat	Bio-Rad (#172-1019)	1:7500

Table 2.2: **List of primary and secondary antibodies used for Western Blotting**. Dilution of antibodies was performed using blocking solution: either 5% milk (T145.2; Roth, Karlsruhe, Germany) or 2% albumin (T844.2; Roth, Karlsruhe, Germany) diluted in TBST (TBS with 0.1% of Tween; Merck, Darmstadt, Germany). Blocking of any of the milk protein or phosphoprotein blots was performed with 2% albumin to avoid cross-reactions between the primary antibodies and the blocking solution.

2.2.5. Histology

2.2.5.1. Whole-mount carmine alum staining

For proper visualization of the ductal development of whole mouse mammary glands, a carmine alum staining was performed. The protocol followed for staining with this bright-red pigment was done according to the one described by Ip and Asch (Ip and Asch, 2000). In short, inguinal mammary glands (4^{th} and 9^{th} gland pair in Fig. 2.1) were spread on a glass slide, fixed in Carnoy's solution (see Section 2.1.3) for 4 hours at room temperature, washed in 70%, 50% and 25% ethanol for 15 minutes each, rinsed in tap water for 5 minutes and stained in carmine alum (see Section 2.1.3) overnight. Then, mammary glands were washed in 70%, 95% and 100% ethanol for 15 minutes each. Next, mammary glands were cleared in xylene (Roth, Karlsruhe, Germany) for 30 minutes and subsequently for 2 hours replacing with fresh xylene. Mammary glands inside of a glass Petri dish containing xylene were photographed using a stereomicroscope Olympus SZ61 (Olympus, Japan) equipped with a Lumenera Infinity 1 camera (Lumenera, Canada). Finally, 2-3 individual pictures spanning the whole gland were stitched together using Autostitch v2.2 Demo software (UBC, Canada).

2.2.5.2. Fixation and paraffin embedding of mammary tissues

Inguinal mammary glands (see Fig. 2.1) were dissected, cut in 0.5-1 cm long fragments and fixed overnight at 4°C using 50 ml per animal of freshly prepared 3.7% paraformaldehyde (Roth, Karlsruhe, Germany) in PBS. The edges of the glands were discarded and only "central" mammary gland fragments surrounding the lymph node were used for histological analysis. Then, samples were washed in tap water for 3 hours applying a constant flux and stored in 70% ethanol at 4°C. For paraffin embedding, samples were placed in embedding cassettes (Leica, Wetzlar, Germany) and dehydrated by two-hour baths in first 80% ethanol, then 96 % ethanol and finally 2 separate incubations in 100% isopropanol. Samples were then bathed in Paraffin I (melting temperature: 42-44° C) at 60° C overnight. Next morning, cassettes were transferred to Paraffin II (melting temperature: 51-53° C) and incubated for 8 hours at 60° C. Finally, an overnight incubation on Paraplast (melting temperature: 56-58° C) at 60°C followed. For embedding, molds were filled with paraffin wax and tissue was placed in the mold. After paraffin covered cassettes and molds completely, they were chilled in a cold plate and blocks were removed from the molds.

2.2.5.3. Paraffin block sectioning

Paraffin blocks were cooled down on an ice tray and cut in 3-4 µm sections using a Microm HM 400 sliding microtome (Microm, Thermo Scientific, USA). Paraffin ribbons were carefully stretched on a 40° C waterbath and sections were mounted onto Poly-L-Lysine (Biochrom, Merck-Millipore, Darmstadt, Germany) coated slides. Slides were then dried either at 40° C overnight or at 60° C for 30 minutes and stored at room temperature until use.

2.2.5.4. Hematoxylin and eosin (H&E) staining

H&E double staining was first employed in 1876 by Wissowzky (Gill, 2012) and remains the most commonly used staining technique in pathology laboratories until today. Hematoxylin stains nucleic acids in dark-blue or purple color (basophilic) and eosin binds to most proteins in the cytoplasm (eosinophilic or acidophilic) giving them a pink coloration (Fischer et al., 2008). In brief, slides were deparaffinized with two 5-minute baths in Roti-Histol (Roth, Karlsruhe, Germany). Then, samples were rehydrated incubating successively in 100% isopropanol and decreasing ethanol concentrations: 96%, 80% and 70% for 5 minutes each. After 5 minutes in H_20dd, slides were bathed in Mayer´s hemalum solution (Merck, Darmstadt, Germany) for 3 minutes at room temperature and immersed in running tap water for 5-10 minutes. Next, slides were incubated for 10-15 minutes with 0.1% eosin (Merck, Darmstadt, Germany) and dehydrated in baths of increasing ethanol concentrations: firstly 80% ethanol for 10 seconds, then 96% ethanol for further 10 seconds and lastly 100% isopropanol for 5 minutes. Finally, slides were cleared with two 5-minute incubations in xylene (Roth, Karlsruhe, Germany) and cover slipped with a drop of Enthelan mounting media (Merck, Darmstadt, Germany). Paraffin embedding, block sectioning and H&E stainings were routinarily performed by Waltraud Ackermann (Institute of Cellular Biology, Marburg, Germany).

2.2.5.5. Immunohistochemistry

Immunohistochemistry (IHC) allows the detection of antigens in tissue samples by the use of specific antibodies. This antibody-antigen interaction can be detected utilizing antibodies conjugated to enzymes which catalyse a colored reaction (e.g. immunoperoxidase staining) or by antibodies tagged to a fluorophore (immunofluorescence). The technique was developed and first

used in 1941 by Dr. Albert Coons and colleagues (Coons and Kaplan, 1950). The following general protocol was used for formalin-fixed and paraffin-embedded tissue sections. First, tissue slides were deparaffinized with two 5-minute baths in Roti-Histol (Roth, Karlsruhe, Germany) and rehydrated incubating in 100% isopropanol and decreasing ethanol concentrations: 96%, 80% and 70% for 5 minutes each. Next, slides were transferred to a 5-minute bath in H_20dd. In some cases, antigen retrieval was necessary and improved the quality of the stainings substantially (see Table 2.3A for details). Aldehyde-containing fixatives crosslink proteins in the sample and exposure of the slides to heat allows the unmasking of epitopes, which favors binding of the antibodies. Antigen retrieval was achieved with either 10mM Tris/1mM EDTA (pH 9) or 10mM citrate buffer (pH 6) for 15-30 minutes in a steamer.

For reduction of the background in immunofluorescence, samples were incubated with 10 mg/ml Glycine (Roth, Karlsruhe, Germany) in PBS for 10 minutes. Glycine binds free aldehyde groups that can potentially also bind primary or secondary antibodies resulting in high background. In immunoperoxidase stainings, slides were incubated for 10-15 minutes with 3% H_2O_2 diluted in PBS which suppresses endogenous peroxidase activity, leading also to a reduced background. After washing the slides twice in PBS for 5 minutes each, a PAP pen was used to draw hydrophobic circles around the tissue sections. Blocking was accomplished by incubating the samples with 10% goat serum (X0907; Dako, Denmark) in PBS for 45 minutes at room temperature. Serum was carefully removed from the slides which were not negative controls and mammary sections were incubated overnight at 4° C in a humidified chamber with distinct primary antibodies diluted in blocking solution (see Table 2.3A). Slides were then washed 3 times in PBS (5 minutes each) and incubated with the secondary antibody. Next steps differ depending on the immunodetection method employed and are explained separately in the following sections.

2.2.5.5.1. Immunoperoxidase staining

Secondary antibody incubation was performed using biotinylated antibodies, diluted 1:500 in blocking solution, against the species in which the primary antibody was raised (see Table 2.3B for details). Sections were incubated with specific secondary antibodies for 45 minutes at room temperature inside of a humidified chamber and then 3 PBS washes (5 minutes each) followed. Horseradish peroxidase-labeled Streptavidin (KPL, USA), having a very high affinity for biotin, was added to the tissue sections at a concentration of 2 µg/ml and incubated for 30 minutes at

room temperature inside of the chamber. After 3 PBS washes of 5 minutes each, the 3-amino-9-ethylcarbazole (AEC) Substrate Kit (00-2007; Invitrogen, USA) was utilized in all immunoperoxidase stainings. The AEC substrate was prepared, trying to avoid exposure to light, adding 1 drop of reactive A to 1 ml of H_2Odd. Then, 1 drop of reactive B and 1 drop of reactive C were also included and mixed. Around 200 µl of the AEC substrate were used per slide and the progress of the reaction was observed in real-time under a light microscope. Once the staining strength was adequate, sections were transferred to H_2Odd and counterstained in Mayer´s hemalum solution (Merck, Darmstadt, Germany) for 3 minutes at room temperature and subsequently immersed in running tap water for 5-10 minutes. Finally, slides were mounted with Mowiol and kept at room temperature till documentation utilizing a Leitz Diaplan MPS 46/52 (Leitz, Wetzlar, Germany) microscope equipped with a MicroPublisher 3.3 RTV camera (Q-Imaging, Canada).

Primary antibodies					
Antigen	*Info*	*Company/Provider*	*Dilution*	*Technique*	*Antigen Retrieval*
Cleaved Caspase-3 (5A1E)	Rabbit Monoclonal	Cell Signalling (USA)	1:200	Peroxidase	15 min. Tris/EDTA
Cleaved Caspase-3 (5A1E)	Rabbit Monoclonal	Cell Signalling (USA)	1:100	Fluorescence	NO
Cre	Rabbit Polyclonal	Dr. Christoph Kellendonk (NY, USA)	1:1500	Peroxidase	15 min. Tris/EDTA
ErbB4 (C-18)	Rabbit Polyclonal	Santa Cruz (USA)	1:200	Fluorescence	30 min. Citrate
Ki67 (#VP-K452)	Mouse Monoclonal	Vector Laboratories (USA)	1:100	Peroxidase	15 min. Citrate
Ki67 (#VP-K452)	Mouse Monoclonal	Vector Laboratories (USA)	1:50	Fluorescence	NO
Milk proteins	Rabbit Polyclonal	Prof. Nancy Hynes (Basel, Switzerland)	1:5000	Fluorescence	NO
Miz1 (10E2)	Mouse Monoclonal	Prof. Martin Eilers (Würzburg, Germany)	1:10	Peroxidase	30 min. Tris/EDTA
Myc (Y69)	Rabbit Monoclonal	Abcam (UK)	1:100	Peroxidase	30 min. Citrate
PrlR (M170)	Rabbit Polyclonal	Santa Cruz (USA)	1:150	Fluorescence	NO
pStat5 (#71-6900)	Rabbit Polyclonal	Invitrogen (USA)	1:25	Peroxidase	20 min. Citrate

Table 2.3A: **List of primary antibodies used for immunohistochemistry.**

Secondary antibodies					
Antibody	*Info*	*Company/Provider*	*Dilution*	*Technique*	*Reference*
Anti-Rabbit Ig/Biotinylated	Goat Polyclonal	Dako (Denmark)	1:500	Peroxidase	E0432
Anti-Mouse Ig/Biotinylated	Rabbit Polyclonal	Dako (Denmark)	1:500	Peroxidase	E0464
Anti-Rabbit Alexa Fluor 488	Goat Polyclonal	Molecular Probes (USA)	1:500	Fluorescence	A-11008
Anti-Mouse Alexa Fluor 647	Goat Polyclonal	Molecular Probes (USA)	1:500	Fluorescence	A-21235
Anti-Rabbit Alexa Fluor 546	Goat Polyclonal	Molecular Probes (USA)	1:500	Fluorescence	A-11010

Table 2.3B: **List of secondary antibodies used for immunohistochemistry.**

2.2.5.5.2. Immunofluorescence

Secondary antibodies tagged to a fluorophore (see Table 2.3B for details) were diluted using blocking substance (10% goat serum in PBS) and exposed to the tissue sections inside of a humidified chamber for 1 hour at room temperature. Then, samples were incubated with 0.7 µg/ml Hoechst 33342 (14533; Sigma) for 5 minutes at room temperature for nuclei visualization. After 3 PBS washes (5 minutes each), covering slides to protect them from light, sections were transferred to H_2Odd and washed for 5 minutes. Subsequently, slides were mounted with Mowiol and kept covered at 4° C till documentation with an Olympus BX61 fluorescence microscope (Olympus, Japan) assembled with an F-view digital camera (Olympus, Japan).

2.2.5.6. TUNEL assay

This method was first described by Gavrieli and colleagues (Gavrieli et al., 1992). Nuclear DNA fragmentation, a hallmark of the last phases of apoptosis, can be detected and quantified using the Terminal desoxynucleotidyl transferase-mediated dUTP Nick End Labeling (TUNEL) assay (DeadEnd Fluorometric TUNEL System, G3250; Promega, USA). Fluorescein-12-dUTP is incorporated at 3´ -OH ends and labeled DNA can be visualized and documented by fluorescence microscopy. Briefly and according to manufacturer´s instructions, slides were deparaffinized washing twice in xylene (Roth, Karlsruhe, Germany) and immersed in 100% ethanol (each step

for 5 minutes). Then, sections were rehydrated in decreasing concentrations of ethanol: 96%, 80% and 70% for 3 minutes each. Samples were then washed in PBS for 5 minutes and fixed in 4% formaldehyde in PBS for 15 minutes. Next, sections were incubated at room temperature for 10 minutes with a 20 µg/ml Proteinase K solution, washed for 5 minutes in PBS and fixed again with 4% formaldehyde in PBS for 5 minutes. After this, slides were incubated with 100 µl of equilibration buffer for 5-10 minutes at room temperature. Tissue sections were labeled for 60 minutes at 37° C, covering slides with plastic coverslips in a humidified chamber, using 50µl of TdT reaction mix per slide containing: 45µl of equilibration buffer, 5 µl of nucleotide mix and 1 µl of rTdT enzyme (the 1 µl of rTdT enzyme was substituted with 1 µl of H_2Od in negative controls). After removing plastic coverslips, reactions were stopped by immersing the slides in 2x SSC for 15 minutes. Finally, sections were washed twice in PBS (5 minutes each) and exposed to 0.7 µg/ml Hoechst 33342 (14533; Sigma) for 5 minutes at room temperature. After 2 PBS washes (5 minutes each) and a H_2Odd bath, slides were mounted with Mowiol.

2.2.5.7. Sudan III lipid staining

Sudan III lipid staining was performed on first pregnancy lactation day 6 cryosections following standard protocols. Briefly, sections were fixed in 4% PFA for 30 minutes at 4°C and subsequently washed with 50% Ethanol for 3 minutes. A 25-minute incubation with 0.3% Sudan III-solution (see Section 2.1.3.) in 70% ethanol followed. Then, sections were washed again with 50% Ethanol and transferred to H_2Od. Next, slides were counterstained with Mayer´s hemalum solution (Merck, Darmstadt, Germany) and washed in running tap water for 10 minutes. Finally, sections were transferred to H_2Od and mounted with Mowiol.

2.2.6. Ultrastructural analysis

For transmission electron microscopy, tissue was fixed in a mixture of 2.5% glutaraldehyde, 2.5% paraformaldehyde and 0.05% picric acid in 67 mM cacodylate buffer (pH 7.4) according to Ito und Karnovsky (Ito and Karnovsky, 1968). Postfixation was performed in 1% osmium tetroxide followed by an overnight incubation with 0.3% uranyl acetate dissolved in 50 mM maleate buffer (pH 5.0). Samples were embedded in Epon according to standard procedures. Thin sections were contrasted with lead citrate and examined with a Zeiss EM 109S electron microscope (Zeiss, Jena, Germany).

2.2.7. Morphometric analysis in lactating mammary glands

2.2.7.1. Adipocyte percentage determination

The percentage of fat (Fig. 3.18) was calculated by estimating the area occupied by adipocytes divided by the total mammary area in H&E stained sections using the wand tool from ImageJ 1.43u software (NIH, USA). 10 pictures per animal were used for the analysis of first pregnancy (n=4 per genotype) and second pregnancy (n=3 per genotype) lactation day 6 sections of *Ctr* and *Miz1ΔPOZ* mammary glands.

2.2.7.2. TUNEL assay quantification

TUNEL positive cells, rare in both *Ctr* and *Miz1ΔPOZ* animals, were counted in 10 pictures per animal (20x magnification) on lactation day 1 and 6 samples of a first pregnancy (Fig. 3.20). ImageJ 1.43u software (NIH, USA) was used for both quantifications and at least 3 animals per genotype and time point were analysed.

2.2.7.3. Percentage of Ki67 positive cells

The percentage of Ki67 positive cells (Fig. 3.22A) on lactation day 6 of a first pregnancy was calculated by quantifying the number of Ki67 positive cells among all epithelial cells in representative 25x magnification immunohistochemical sections utilizing ImageJ 1.43u software (NIH, USA). More than 1000 cells per animal were scored in 3 animals per genotype.

2.2.8. Statistics

All comparisons between *Ctr* vs *Miz1ΔPOZ* animals or *shscr* vs *shMiz1* HC11 cells were analysed by two-tailed Student´s t-tests. A two-way ANOVA with a Bonferroni's post-hoc test was used for the analysis of the percentage of cells containing lipid droplets over time in Fig. 3.13. Also, a two-way ANOVA followed by Bonferroni's post-hoc test but for multiple pairwise comparisons was employed for pup weight analysis in Fig. 3.16. All statistical tests were performed using GraphPad Prism 5.03 (GraphPad Software, USA). *P-values*: NS (p>0.05); * (p= 0.01-0.05); ** (p= 0.001-0.01); *** (p<0.001). Data are shown as mean ± s.d.

3. RESULTS

3.1. Miz1/Myc expression in mammary gland development and HC11 mammary cells.

3.1.1. Miz1 expression during mammary gland development

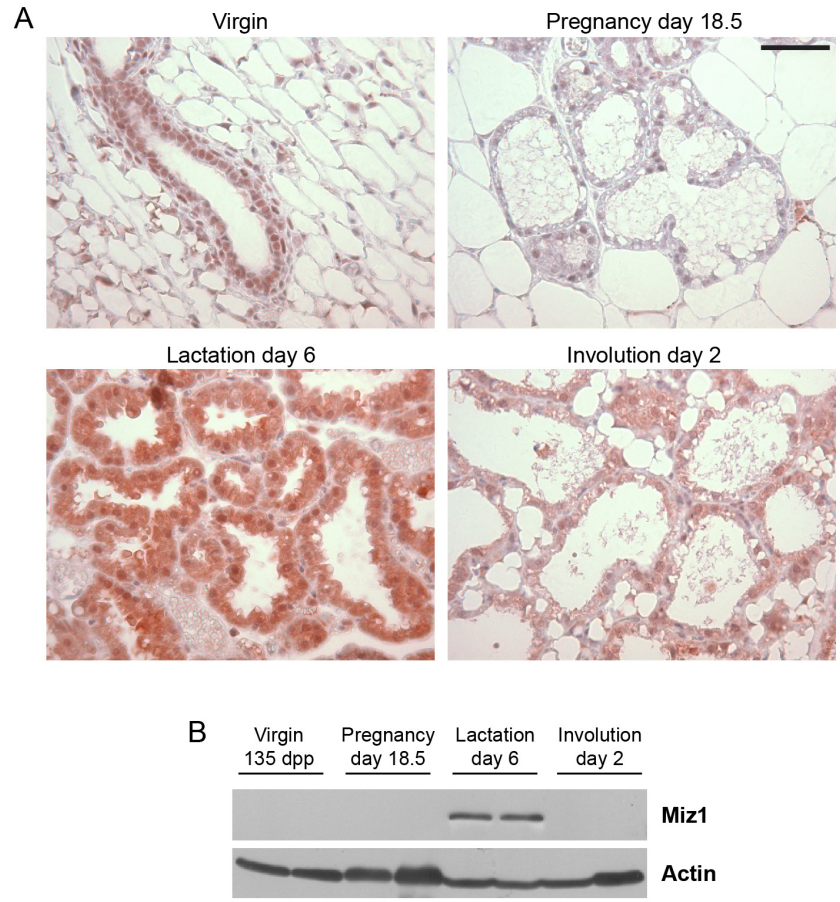

Figure 3.1: Miz1 expression during mammary gland development. Immunohistochemistry (**A**) and western blotting (**B**) showing Miz1 localization and expression levels in mammary glands from control animals (Wap-Cre+ $Miz1^{+/+}$) at the indicated time points. Actin was used as a loading control in B. Scale bar in A: 50 µm.

Miz1 expression during mammary gland development was assessed by immunohistochemistry and western blotting (Fig. 3.1) using Miz1 wildtype mice (Wap-Cre+ $Miz1^{+/+}$). The first method revealed a nuclear staining in the virgin gland (45 dpp), during pregnancy (day 18.5) and involution (day 2). In lactation (day 6), also a cytoplasmic staining was visible in addition to the nuclear stain. Miz1 expression increased substantially during lactation as also seen by Western

blotting. The 10E2 antibody was used in Fig. 1B, but other commercially available Miz1 antibodies were also utilized leading to comparable results (N17, H190 and B10; data not shown). Miz1 was only occasionally detected in virgin gland protein lysates, possibly due to the small fraction of ductal tissue compared to the more abundant fat pad. At pregnancy day 18.5, Miz1 was always undetectable albeit the glandular tissue had expanded until this time point. Miz1 expression increased in the transition from pregnancy to lactation as the protein could be detected at lactation day 1 and remained strongly expressed throughout lactation (lactation days 1, 6 and 10 were analysed by western blotting; data not shown). After 48 hours of removal of the pups from the mother, commonly regarded as forced involution of the mammary gland, Miz1 levels decreased considerably to the baseline levels observed in the virgin gland or during late pregnancy.

3.1.2. Myc expression during mammary gland development

Analogously to the study of the expression of Miz1 described above, immunohistochemistry against c-Myc was performed on sections from control mice spanning different stages of mammary gland development (Fig. 3.2). Nuclear Myc expression was visible in virgin mammary ducts and in the forming alveoli during early pregnancy as described elsewhere by gene expression analysis (Blakely, 2005; Master et al., 2002) and by immunohistochemistry of pregnancy day 6.5 animals (Stoelzle et al., 2009). During late pregnancy, a clear nuclear Myc staining was visible in the lymph node but not in the surrounding mammary alveoli (see arrows in Fig. 3.2D). Myc expression was not detectable during lactation as described before (Klinakis et al., 2006) and was hardly discernible at involution day 2.

Taken together, Miz1 and Myc are expressed in the ductal epithelium of the virgin mammary gland (Fig. 3.1A and 3.2A). Myc levels increase at the beginning of pregnancy when mammary epithelial cells proliferate heavily and the gland expands to fill the fat pad. Blakely et al. show data from an oligonucleotide array analysis in the mammary gland and describe high expression of Myc during early pregnancy (days 6.5 and 12.5). Our own immunohistochemical analysis supports this view (Fig. 3.2B and C). At the end of pregnancy (day 18.5), Myc levels decrease (Blakely, 2005) and were detectable only in the lymph node but not in the mammary epithelium (Fig. 3.2D). At the onset of lactation, Miz1 expression increases (Fig. 3.1 and data not shown) while Myc keeps at low levels throughout lactation (Blakely, 2005; Klinakis et al., 2006) as seen

in Fig. 3.2E. Once lactation is terminated, Miz1 levels decrease and both Miz1 and Myc are expressed at low levels during early mammary involution (Fig. 3.1 and 3.2F).

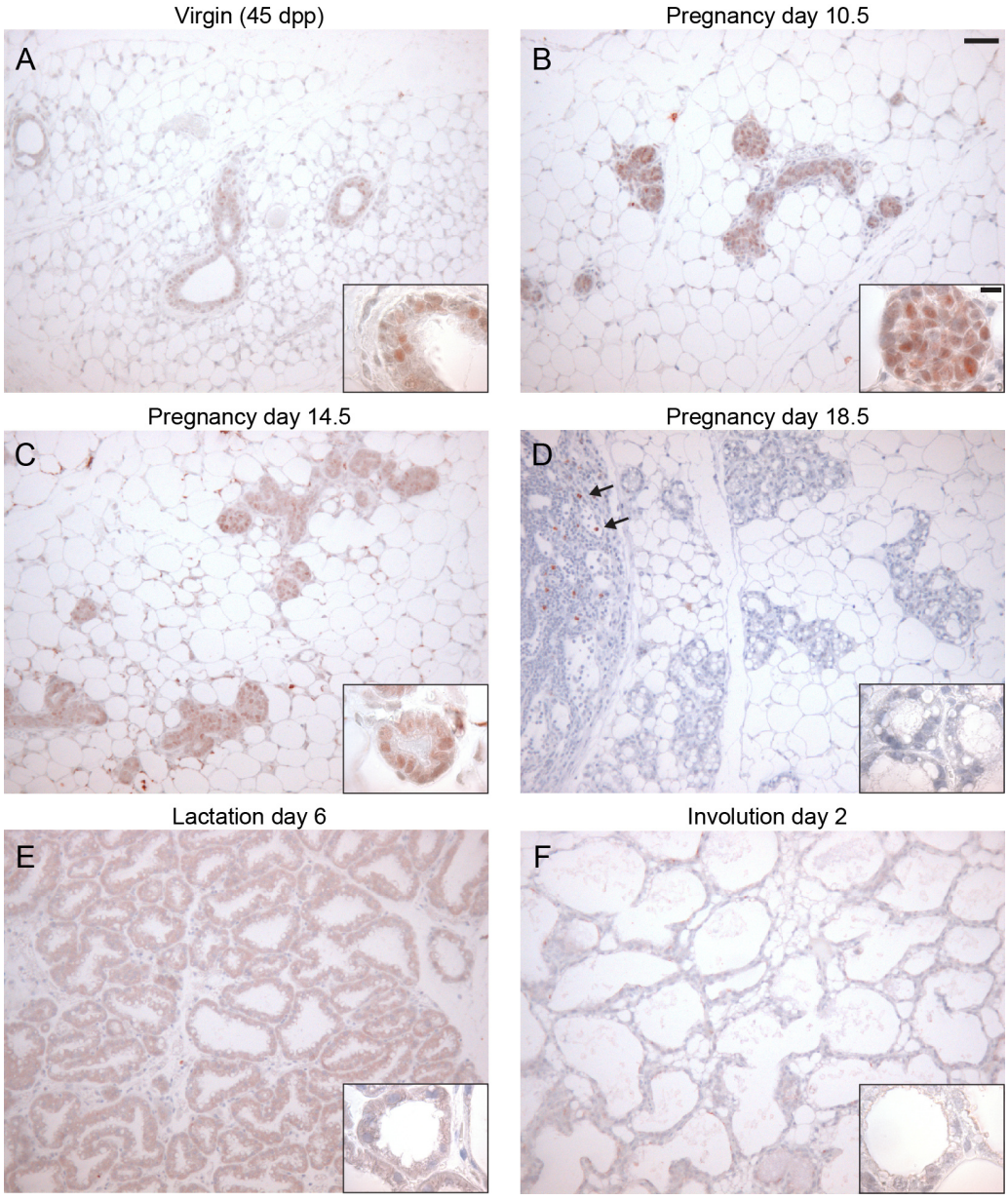

Figure 3.2: Myc immunohistochemistry during mammary gland development. Paraffin-embedded inguinal mammary glands were stained with a Myc-specific antibody (see Material & Methods for details). Time points analysed were the following: virgin gland at 45 dpp (**A**; n=3), pregnancy day 10.5 (**B**; n=2), 14.5 (**C**; n=2) and 18.5 (**D**; n=3), lactation day 6 (**E**; n=3) and involution day 2 (**F**; n=3). Scale bars: 50 µm and 10 µm in the inset.

3.1.3. Miz1 expression during HC11 cell mammary differentiation

HC11 cells were used as an *in vitro* mammary cell culture model in the present thesis. HC11 cells are immortalized, non-transformed mammary epithelial cells obtained from the COMMA-1D cell line which in turn derives from mid-pregnant mammary tissue of BALB/c mice (Ball et al., 1988; Danielson et al., 1984). This cell line can functionally differentiate and produce milk proteins upon addition of a lactogenic hormone cocktail referred to as DIP (includes dexamethasone, insulin and prolactin). A schematic representation of the protocol followed for HC11 mammary cell differentiation is represented in Fig. 3.3A. Briefly, HC11 cells are seeded in a RPMI-based complete growth medium and allowed to remain confluent for 48 hours. Then, EGF-free and low-serum medium is added to the cells in order to induce competence for differentiation (Chammas et al., 1994; Hynes et al., 1990). After further 48 hours, the hormonal cocktail (DIP) is included in fresh EGF-free medium in order to differentiate the cells, which subsequently start producing milk proteins. ß-casein expression can be detected as soon as 3 hours after hormone stimulation (Ball et al., 1988). HC11 cells represent a valuable tool for the study of mammary cell proliferation and differentiation *in vitro*.

In relation with the study of the expression of Miz1 and Myc in different developmental stages *in vivo*, a similar approach was used in HC11 cells across the above-mentioned differentiation protocol. Miz1 mRNA and protein levels increased when HC11 cells became confluent (Fig. 3.3B and C), as expected for a transcription factor that activates cell cycle arrest genes like *Cdkn2b*, encoding $p15^{Ink4}$, or *Cdkn1a* which translates into $p21^{Cip1}$ (Seoane et al., 2001; Staller et al., 2001; Wu et al., 2003a). Miz1 levels increased even before EGF was withdrawn from the medium. Two different housekeeping genes were used for normalization of qPCR data (GAPDH and Hprt) as shown in Fig. 3.3B. Importantly, Miz1 levels did not increase after addition of the lactogenic hormone cocktail (Fig. 3.3B and C) but remained steady or slightly decreased and this was true for a period of 7 days after induction of differentiation (data not shown). This observation contrasts with the clear upregulation of Miz1 *in vivo* at the onset of lactation. The trigger of Miz1 expression in early lactation might therefore not be prolactin. Other possible candidate molecule which could be responsible for Miz1 upregulation in early lactation *in vivo* is the cyclic peptide oxytocin, which is released after pups are born and contracts mammary myoepithelial cells allowing milk ejection or let-down (Reversi et al., 2005). The actual mechanism engaged in Miz1 upregulation during lactation *in vivo* remains to be elucidated.

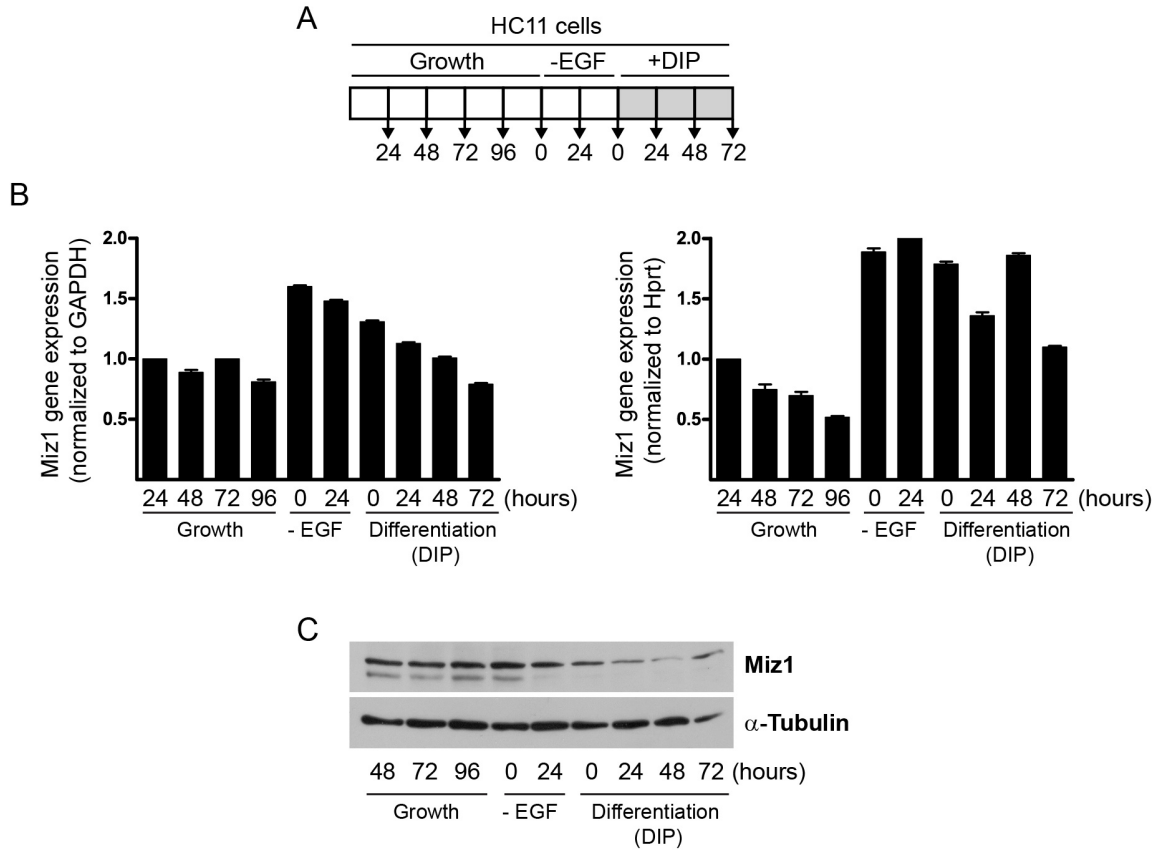

Figure 3.3: Miz1 expression during HC11 mammary cell growth and differentiation. (**A**) Schematic representation of the protocol for differentiation of HC11 cells. EGF: Epidermal growth factor. DIP: Differentiation media containing dexamethasone, insulin and prolactin (See Material & Methods for experimental details). (**B**) qPCR analysis of Miz1 gene expression normalized to GAPDH and Hprt in HC11 cells during proliferation and differentiation. (**C**) Western blot of Miz1 expression in HC11 cells using tubulin as a loading control.

3.1.4. Myc expression during HC11 cell mammary differentiation

In contrast to Miz1, Myc is downregulated when HC11 mammary cells become confluent as has been already reported (Grolli et al., 1997). Myc promotes proliferation, but when cells become contact-inhibited it is reasonable that Myc levels decrease and cells arrest. Our own data support this assumption as can be seen by qPCR and Western blotting analysis on Fig. 3.4. Myc levels are high after 24 hours of HC11 seeding when cell proliferation is active and rapid. Myc mRNA and protein levels gradually decrease after this time point till Myc is hardly detectable by Western blotting. Myc expression decreases even before EGF is removed from the HC11

medium. Finally, only after 72 hours of differentiation, mRNA levels seem to elevate while protein is still negligible.

A similar analysis of Miz1 and Myc expression in HC11 cells shows that Myc levels are high in actively cycling cells and decrease when the cells arrest in their proliferation after removal of serum and growth factors from the medium (Si et al., 2010). In this publication, Miz1 levels are not altered in the two physiological states analysed.

To sum up, Miz1 and Myc have an opposing regulation when HC11 cells become confluent (Miz1 increases its expression while Myc is downregulated), but their expression levels do not seem to be directly regulated by prolactin hormonal treatment or prolactin receptor downstream signalling.

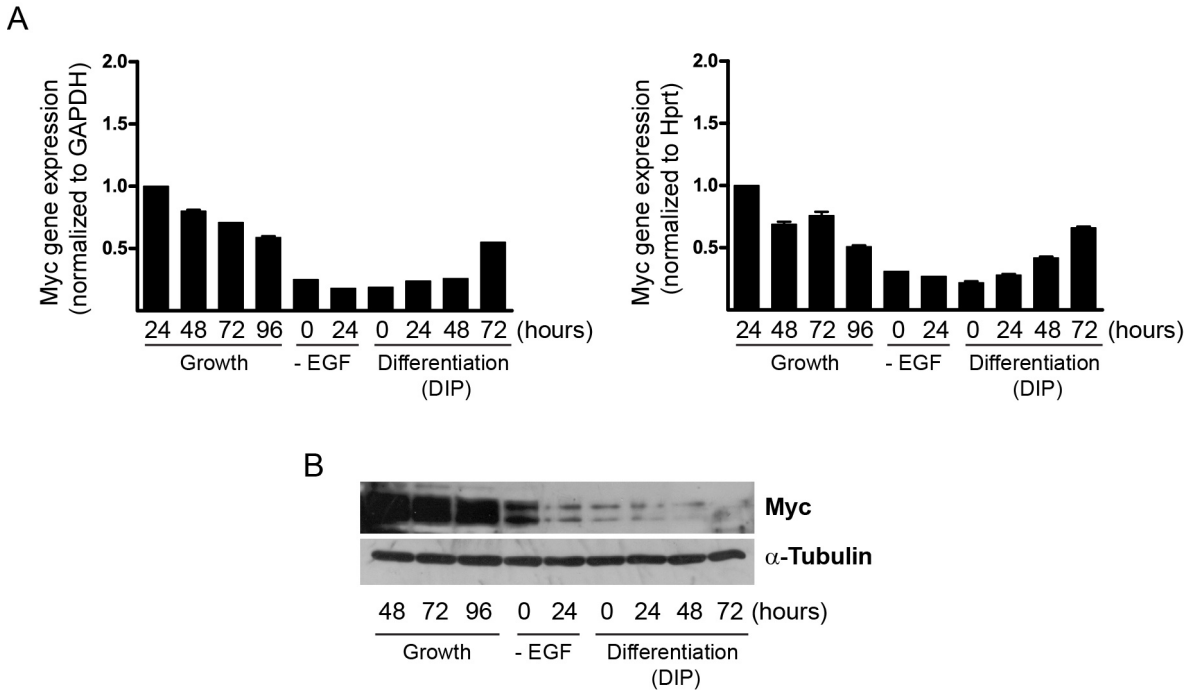

Figure 3.4: Myc expression during HC11 mammary cell growth and differentiation. (**A**) qPCR analysis of Myc gene expression normalized to GAPDH and Hprt in HC11 cells during proliferation and differentiation. (**B**) Western blot of Myc expression in HC11 cells using tubulin as a loading control.

3.2. MMTV-Cre mediated deletion of the Miz1 POZ domain in the virgin mammary gland and its effect on ductal morphogenesis and mammary stem/progenitor cells.

3.2.1. Conditional knockout of the Miz1 POZ domain in the virgin mammary gland.

Miz1 constitutive knockout mice are embryonic lethal at E7.5 due to massive apoptosis of ectodermal cells during gastrulation (Adhikary et al., 2003). In order to conditionally knockout Miz1 in the mammary gland, the Cre/loxP system was employed. Cre recombinase can excise a DNA segment by homologous recombination at a pair of 34 bp LoxP sequences which flank the desired genomic region to be deleted. The use of a cell specific promoter for Cre recombination allows the study of the function of a certain gene in a desired tissue during a particular developmental stage (Orban et al., 1992; Rossant and McMahon, 1999).

In the case of the conditional deletion of Miz1, Dr. Werner Lutz engineered a plasmid in which the exons 3 and 4 of the Miz1 gene, which code for the POZ/BTB transactivation and tetramerization domain of the Miz1 protein, are flanked by LoxP sites (Fig. 3.5A). Afterwards, a transgenic mouse line was generated by Dr. Christian Kosan and Prof. Tarik Möröy (IRCM, Montreal, Canada). The knockout mice in which the POZ/BTB domain of Miz1 is excised will be referred to as *Miz1ΔPOZ* in this thesis.

Miz1 gene deletion in the mammary gland was accomplished by using two distinct Cre strains which have different tissue specificity and temporal expression (Wagner et al., 1997) and were kindly provided by Prof. Lothar Hennighausen (NIDDK, Bethesda, USA). Wap (Whey acidic protein)-Cre is expressed specifically in mammary alveolar luminal cells during pregnancy and was useful for the study of the role of Miz1 in mammary differentiation and lactation. More details about this strain will be addressed in the Section 3.4 of the present thesis. The MMTV (Mouse mammary tumor virus) long terminal repeat (LTR)-Cre strain (Line A) was employed for the study of Miz1 function in the virgin mammary gland. Specifically, ductal morphogenesis and mammary stem/progenitor cell biology were investigated in *Miz1ΔPOZ* animals.

MMTV-Cre, in the Line A mouse strain, is expressed already in the embryo and in the luminal and basal compartments of the adult mammary gland. It is also reported to be active in other tissues like oocytes, salivary gland or skin (Wagner et al., 2001). This line is not desirable for the study of mammary differentiation due to a lactation defect of the dams (Robinson and

Hennighausen, 2011; Yuan et al., 2011) but it is useful for mammary morphogenesis and stem cell research in the virgin gland due to the early Cre expression and its activity in mammary stem/progenitor cells of the newborn (Buono et al., 2006; Jiang et al., 2010).

MMTV-Cre mediated deletion of the POZ/BTB domain of Miz1 is represented in Fig. 3.5B. Due to the mosaic expression of MMTV-Cre, the Miz1 recombinant band can be observed also in skin earclips. Cre and Miz1 genotyping of 4 knockout or *Miz1ΔPOZ* (MMTV-Cre + and $Miz1^{lox/lox}$) and 4 wildtype/control (hereafter referred to as *Ctr*) animals (MMTV-Cre + and $Miz1^{+/+}$) is shown in Fig. 3.5B.

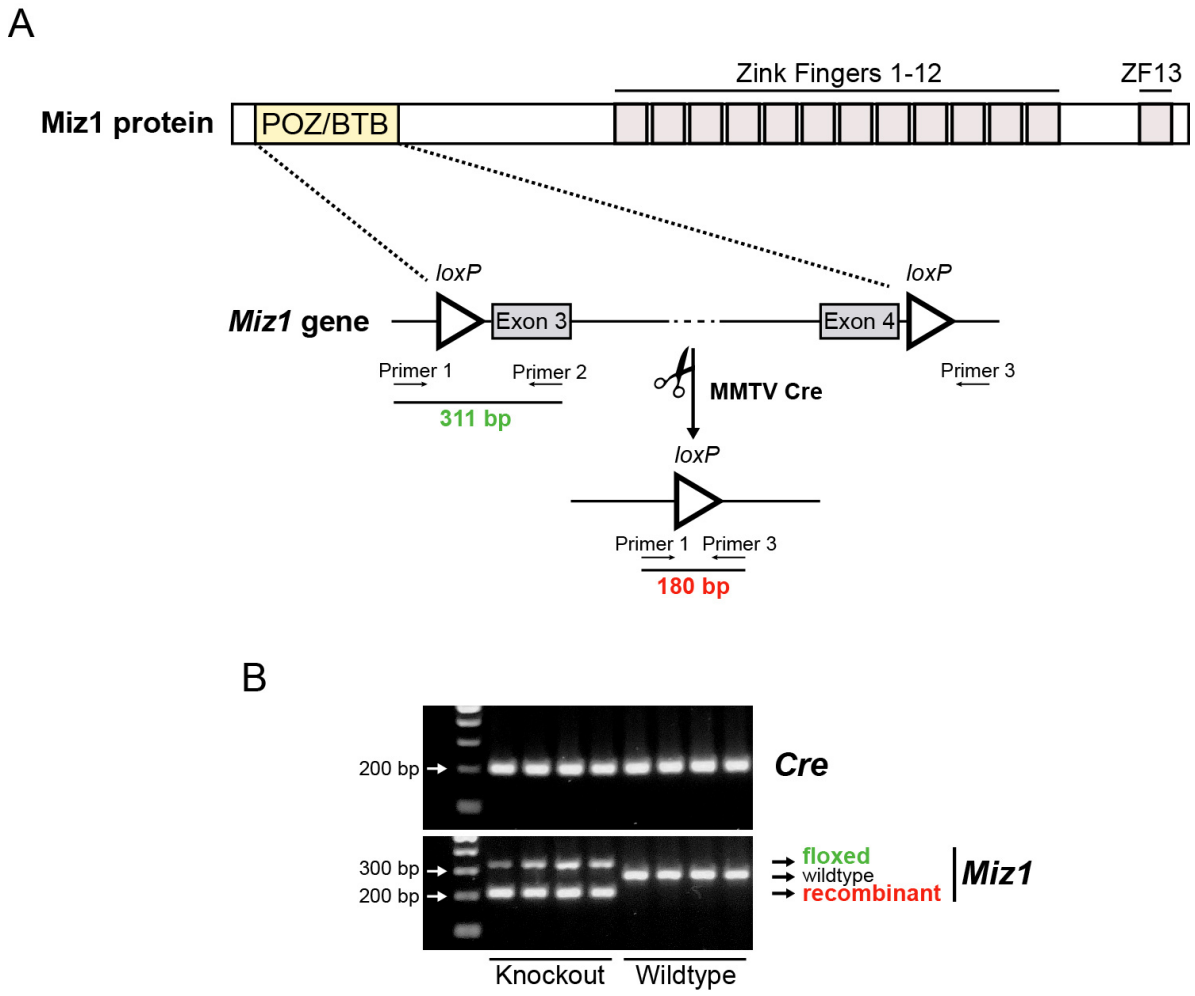

Figure 3.5: MMTV-Cre mediated Miz1 POZ domain recombination in the virgin mammary gland. (**A**) Schematic representation of the MMTV Cre-loxP system strategy used to conditionally knockout the exons 3 and 4 of the Miz1 gene, which code for the POZ/BTB transactivation and tetramerization domain of the Miz1 protein, in the virgin mammary gland. (**B**) Genotyping of *Cre* and *Miz1* from earclips of knockout (n=4) or wildtype (n=4) mice. Fig. 3.5A was greatly inspired by Fig. 3.24 in Dr. Anneli Gebhardt´s thesis.

3.2.2. Mammary ductal morphogenesis in *Ctr* and *Miz1ΔPOZ* animals after MMTV-Cre mediated deletion.

The mouse mammary gland develops from a rudimentary tree mainly postnatally. Pubertal mammary gland development is driven by club-shaped structures termed terminal end buds (TEBs). Cells of TEBs exhibit a high-rate proliferation and migration resulting in the formation of a ductal tree which fills the fat pad in the virgin adult mouse. This process is tightly controlled by estrogen and progesterone which support ductal outgrowth and branching morphogenesis, respectively (Hennighausen and Robinson, 2005; Macias and Hinck, 2012).

In order to address the function of Miz1 in virgin mammary gland development, MMTV-Cre *Ctr* and *Miz1ΔPOZ* inguinal mammary glands were harvested, fixed and carmine alum-stained at different time points of pubertal growth. Miz1 deficient glands showed a slight developmental delay as observed in 30 days old mammary whole-mounts shown in Fig. 3.6. While TEBs already reached the lymph node in *Ctr* animals, the migration of the ductal tree and the formation of TEBs in *Miz1ΔPOZ* animals seemed to be impaired after one month of postnatal mammary development.

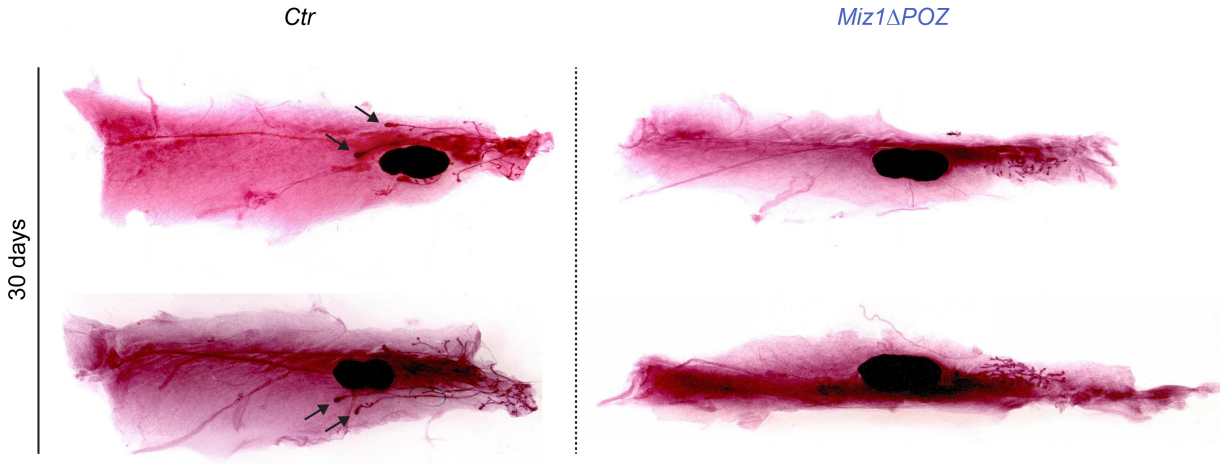

Figure 3.6: Mammary whole-mounts of 30 days old *Ctr* and *Miz1ΔPOZ* animals. Representative stereomicroscopic pictures of carmine alum-stained 30 days old inguinal mammary glands from MMTV-Cre *Ctr* (n=7) and *Miz1ΔPOZ* (n=3) dams. TEBs are indicated by arrows.

After 45 days postpartum, the ductal tree of *Miz1ΔPOZ* animals reached a similar extent and size as in *Ctr* mice, except for one of the three knockout dams analysed which seemed to have a more severe developmental delay phenotype than its age-matched genetically identical counterparts (Fig. 3.7).

The reason for this obvious developmental deviation in *Miz1ΔPOZ* mice is currently unknown but could be related to the extent of Miz1 recombination due to a distinct Cre expression in the different animals.

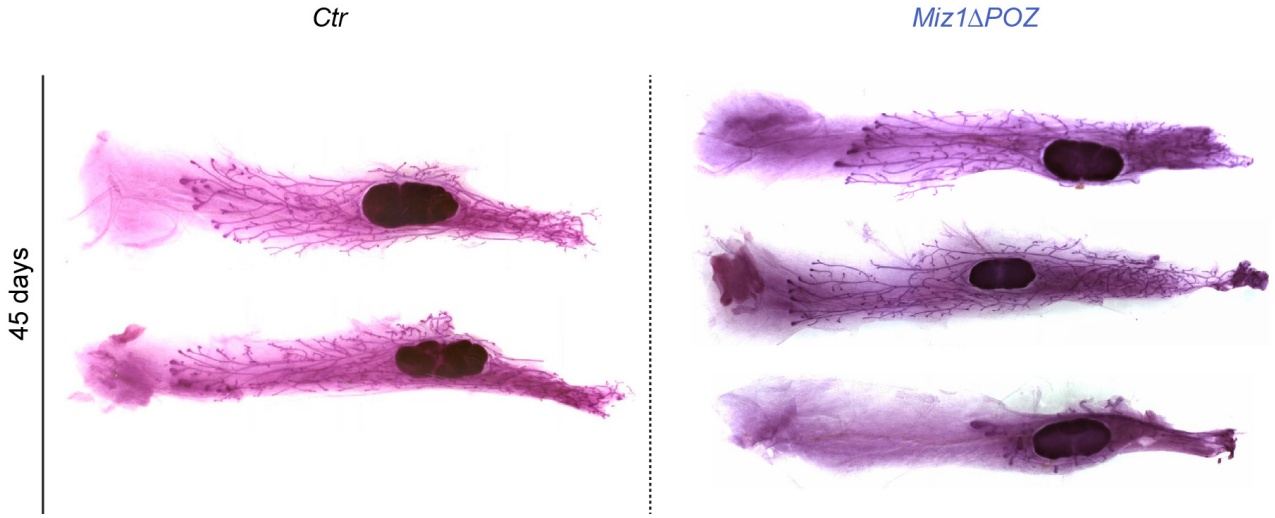

Figure 3.7: Mammary whole-mounts of 45 days old *Ctr* and *Miz1ΔPOZ* animals. Representative stereomicroscopic pictures of carmine alum-stained 45 days old inguinal mammary glands from MMTV-Cre *Ctr* (n=6) and *Miz1ΔPOZ* (n=3) dams.

After 65 days of virgin mammary gland development, no overt differences were observed between Ctr and *Miz1ΔPOZ* mice and the developmental delay phenotype is rescued (Fig. 3.8). The ductal tree fills the complete fat pad in both *Ctr* and *Miz1ΔPOZ* mice at this time point.

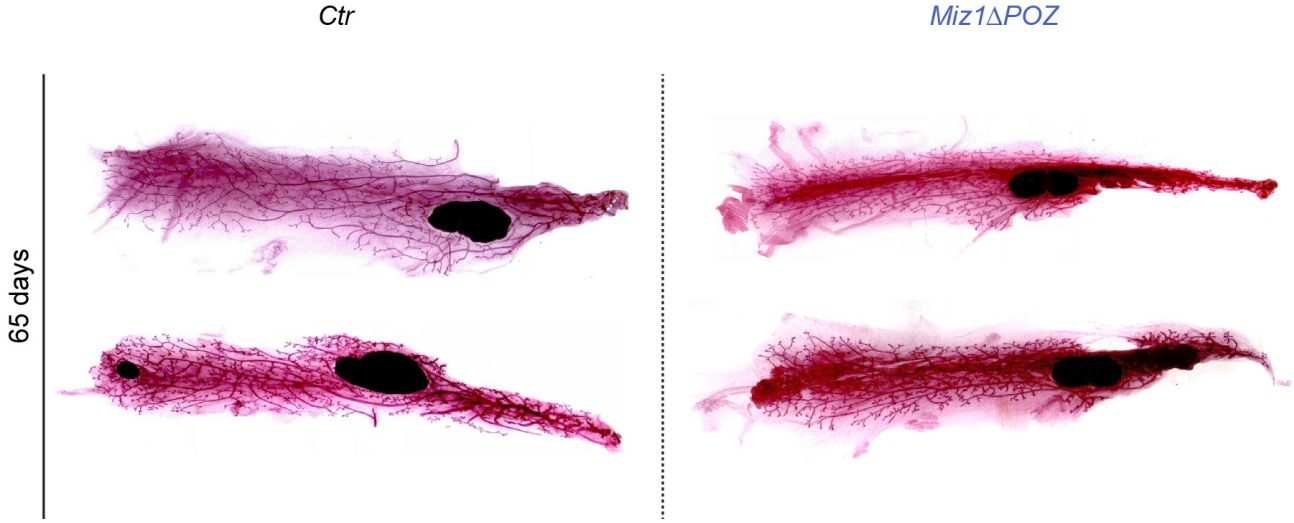

Figure 3.8: Mammary whole-mounts of 65 days old *Ctr* and *Miz1ΔPOZ* animals. Representative stereomicroscopic pictures of carmine alum-stained 65 days old inguinal mammary glands from MMTV-Cre *Ctr* (n=7) and *Miz1ΔPOZ* (n=3) dams.

Histological sections of 45 days old *Ctr* and *Miz1ΔPOZ* mammary glands were stained with hematoxylin and eosin (H&E) in order to examine carefully the ductal compartment. As seen in Fig. 3.9, the cellularity or amount of cells per duct is greatly decreased in *Miz1ΔPOZ* mice. This phenotype could be explained by the decreased proliferation observed in ducts from *Miz1ΔPOZ* mice, probably due to reduced levels of the EGF-like ligand amphiregulin (data not shown; collaboration with Hedyeh Kiaveh). However, the expression of luminal (E-cadherin and ß-catenin) and basal (SMA and cytokeratin 14) markers was not seemingly different in *Ctr* and *Miz1ΔPOZ* 45 days old virgin mammary glands (data not shown; collaboration with Hedyeh Kiaveh).

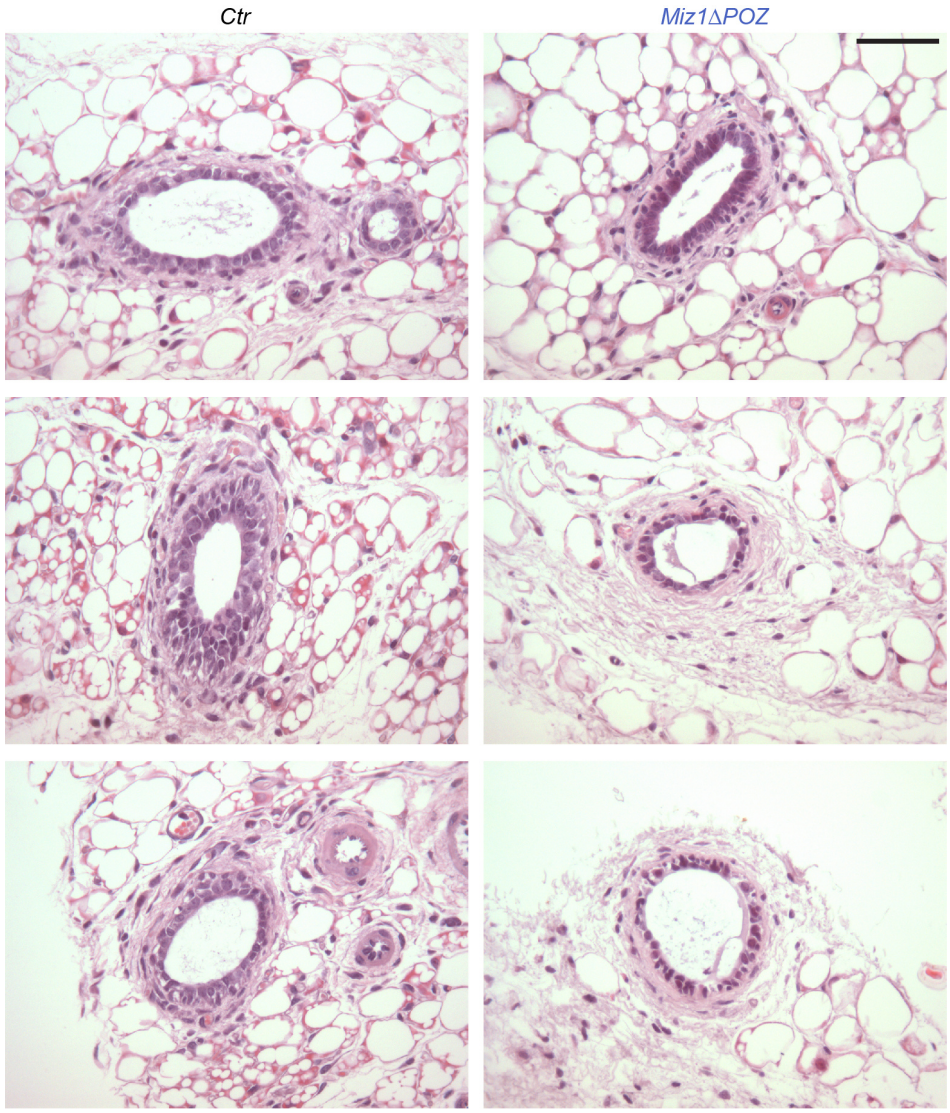

Figure 3.9: H&E staining of 45 days old mammary ducts. Representative pictures of hematoxylin and eosin-stained (H&E) and transversally cut mammary ducts of MMTV-Cre *Ctr* and *Miz1ΔPOZ* animals after 45 days of postpartum development are shown. Scale bar: 50 µm.

3.2.3. MMTV-Cre *Miz1ΔPOZ* animals accumulate mammary stem/progenitor cells

The function of Miz1 in mammary stem/progenitor cells was investigated using *Ctr* and *Miz1ΔPOZ* MMTV-Cre virgin animals as a source of primary cells. The mammary gland serves as a convenient system for stem/progenitor cell research due to the possibility of transplantation of mammary tissue into a cleared fat pad (Deome et al., 1959) and to the ability of mammary stem cells to form undifferentiated cellular spheres, termed mammospheres, when cultured in serum-free methylcellulose-based medium (Dontu et al., 2003). The latter method derives from the use of neurospheres for the study of neural stem cells (Reynolds et al., 1992). Mammospheres are able to self-renew and differentiate in the absence of attachment to any substratum and the mammary stem/progenitor cells contained in a sphere are able to form colonies which express markers of all three lineages of the adult mammary gland (Dontu and Wicha, 2005a). It is possible to estimate the frequency of stem/progenitor cells in a particular cellular population by using this method, but mammospheres can only be cultivated for several passages *in vitro* and not indefinitely due to occurrence of cellular senescence (Dey et al., 2009a).

Culture of primary mammary cells as mammospheres was employed in order to investigate if Miz1 has any impact on the frequency of mammary stem/progenitor cells *in vivo*. Two pairs of mammary glands (thoracic and inguinal) from virgin MMTV-Cre *Ctr* (n=5) and *Miz1ΔPOZ* (n=4) animals were subjected to chemical digestion by a mix of collagenase and hyaluronidase, and after several treatments, described in detail in Material & Methods, cells were counted and seeded into 24-well low-attachment plates which contained medium with 1% methylcellulose. 4 technical replicates per animal were used in all passages.

After two weeks encompassing the formation of primary spheres, these were disaggregated, cells were counted and 2000 cells per well were seeded. Another two weeks of culture yielded secondary mammospheres which were quantified. Results from these experiments are shown in Fig. 3.10A. The number of secondary mammospheres formed was significantly higher (about 3-fold) when cells were isolated from *Miz1ΔPOZ* mammary glands. To test the hypothesis of accumulation of stem/progenitor cells in *Miz1ΔPOZ* animals, these secondary spheres were disaggregated, counted and 2000 cells per well were seeded. As shown in Fig. 3.10B, the number of tertiary spheres was again significantly higher when mammary cells derived from *Miz1ΔPOZ* mice. Although the tertiary sphere number was greatly reduced in comparison to the number of secondary spheres in both *Ctr* and *Miz1ΔPOZ* animals, possibly due to cellular senescence (Dey

et al., 2009a), the relative amounts were similar to the ones measured for secondary spheres: about 3-fold more mammospheres in *Miz1ΔPOZ* mice. Representative pictures of secondary mammospheres obtained are shown in Fig. 3.10C. Although the number of secondary and tertiary spheres formed is higher in cells derived from *Miz1ΔPOZ* mammary glands, the sizes of growing secondary spheres measured were not significantly different between *Ctr* and *Miz1ΔPOZ* animals as shown in Fig. 3.10D (mammosphere diameters were measured using ImageJ software). Taken together, a higher frequency of stem/progenitor cells was observed when primary cells from *Miz1ΔPOZ* animals were seeded for the formation of secondary and tertiary mammospheres, but no differences in sphere size were found between *Ctr* and *Miz1ΔPOZ* mice.

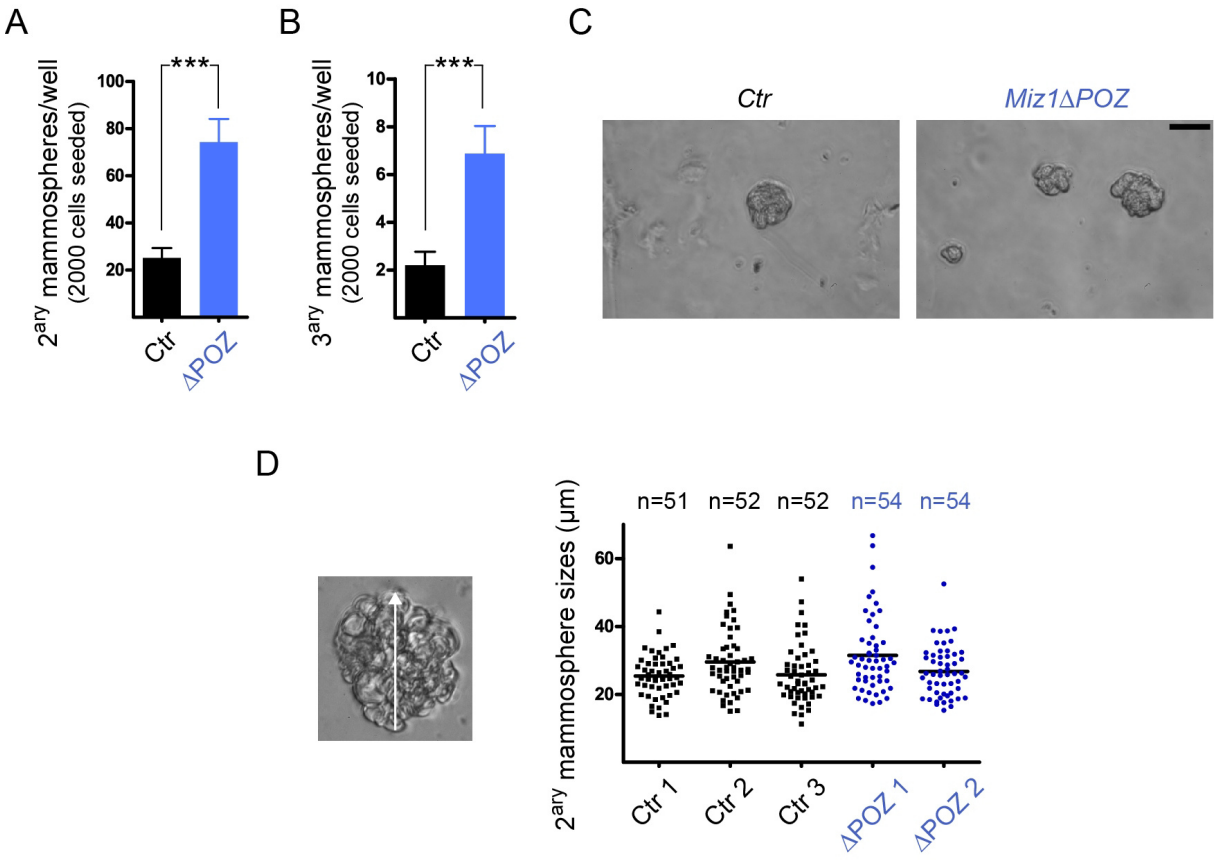

Figure 3.10: Stem/progenitor cells accumulate in *Miz1ΔPOZ* mammary glands. (**A** and **B**) Representation of the number of secondary and tertiary mammospheres quantified two weeks after seeding 2000 cells per well in methylcellulose-based medium. Primary cells from 5 *Ctr* and 4 *Miz1ΔPOZ* MMTV-Cre virgin mice, using 4 technical replicates per animal, were scored. (**C**) Representative pictures of *Ctr* and *Miz1ΔPOZ* secondary mammospheres. (**D**) Diameters of growing secondary spheres from 3 *Ctr* and 2 *Miz1ΔPOZ* animals were measured using ImageJ software. Scale bar in C: 50 µm.

The expression of different stem cells markers was analysed by quantitative PCR (qPCR) in mammary glands of 45 days old *Ctr* and *Miz1ΔPOZ* animals. This approach resulted in the discovery of a highly active Hedgehog pathway in *Miz1ΔPOZ* mice (data not shown; collaboration with Hedyeh Kiaveh). Miz1 has been recently described as a positive regulator of the Hedgehog pathway *in vitro* (Lu et al., 2013a) but its impact on the regulation of this signalling cascade *in vivo* has not been addressed in this recent report. Further experiments are required to elucidate the reason for the accumulation of stem/progenitor cells in *Miz1ΔPOZ* mammary glands and to determine the role of Miz1 in the Hedgehog pathway *in vivo*.

3.3. Role of the interaction of Miz1 and Myc in mammary stem/progenitor cell biology and adipocyte differentiation.

The transcription factor c-Myc plays a major role in stem cell biology (Laurenti et al., 2009) and its properties in cellular reprogramming have been widely investigated using the induced pluripotent stem cell (iPS) technology (Folmes et al., 2013; Nakagawa et al., 2010; Takahashi and Yamanaka, 2006). Deletion of Myc from the mammary epithelium leads to impaired stem cell self-renewal and to a decreased population of luminal progenitors (Moumen et al., 2012; Stoelzle et al., 2009). Myc overexpression, using MMTV-c-Myc animals, is accompanied by an increased proportion of ductal cells in relation to lobular cells and an alteration of the stem cell niche (Chepko et al., 2005).

After assessing the increased mammary stem/progenitor cell frequency in *Miz1ΔPOZ* animals described above, the next step was to test whether the phenotype observed was dependent on the interaction of Miz1 with Myc. Myc interacts with Miz1 through a region outside the helix-loop-helix domain of Myc and a specific Myc mutant (MycV394D) can still transactivate gene expression via binding with Max, but cannot repress gene expression by association with Miz1 (Herold et al., 2002). Subsequently, $Myc^{VD/VD}$ knock-in animals were generated by Dr. Christian Kosan and Prof. Tarik Möröy (IRCM, Montreal, Canada). Thoracic and inguinal mammary glands from these mice ($Myc^{+/+}$ as control and $Myc^{VD/VD}$) were digested and seeded for mammosphere formation using methylcellulose-based medium in analogy to the experiments performed with *Miz1ΔPOZ* animals. As represented in Fig. 3.11, the number and sizes of secondary (Fig. 3.11A and B) and tertiary (Fig. 3.11C and D) mammospheres originated from $Myc^{+/+}$ and $Myc^{VD/VD}$ mammary tissue were not significantly different after seeding 2000 cells per well in both passages.

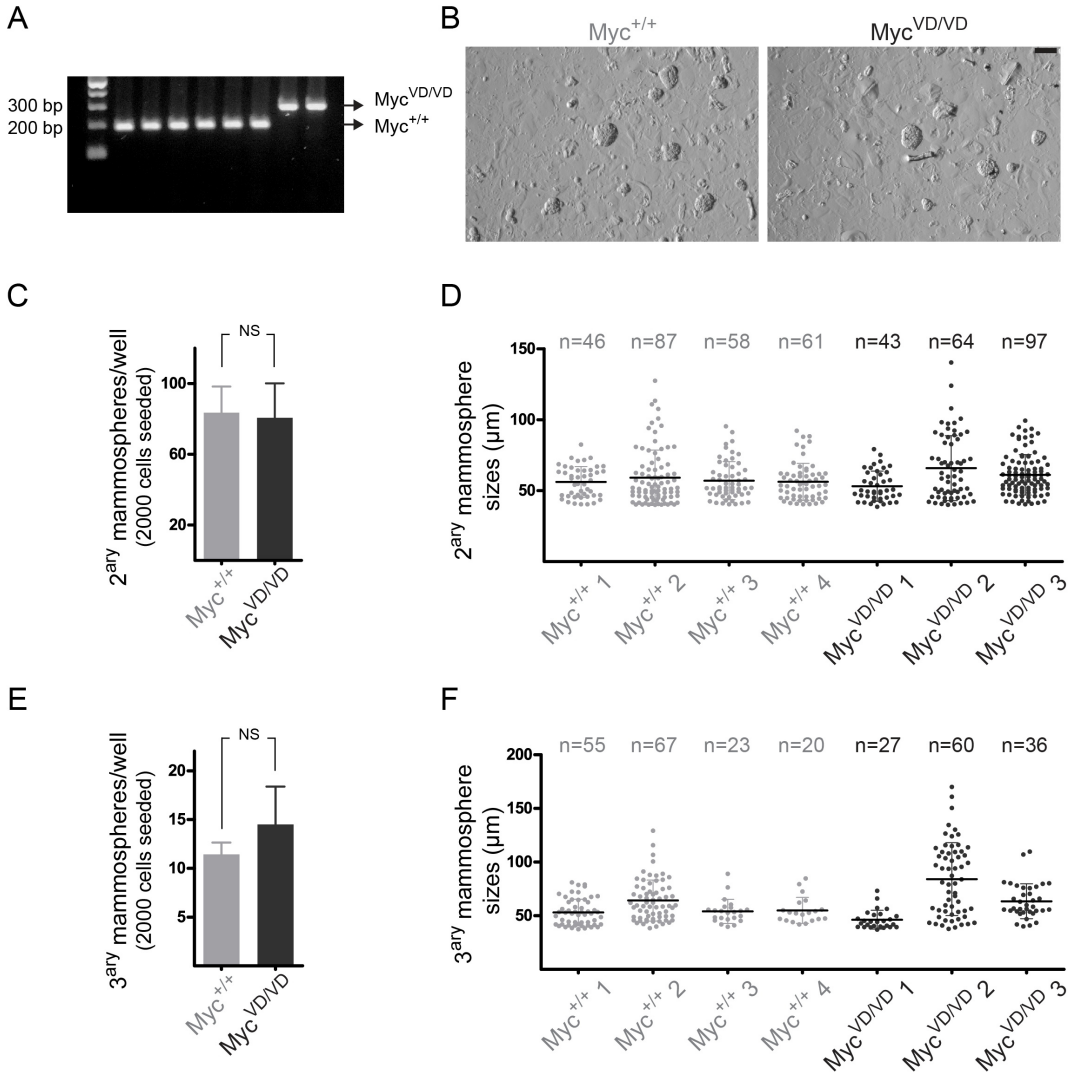

Figure 3.11: Mammosphere number and size in Myc$^{+/+}$ and Myc$^{VD/VD}$ animals. (**A**) Example of genotyping of 6 Myc$^{+/+}$ and 2 Myc$^{VD/VD}$ animals. (**B**) Representative pictures of secondary mammospheres formed. Number (**C** and **E**) and size (**D** and **F**) of secondary and tertiary mammospheres, respectively, originated after seeding 2000 mammary cells per well from 4 Myc$^{+/+}$ and 3 Myc$^{VD/VD}$ mice. 4 technical replicates per animal were used. Scale bar in B: 100 µm.

As can be seen in Fig. 3.11E, secondary mammospheres were not overtly different morphologically in Myc$^{+/+}$ and Myc$^{VD/VD}$ animals. Taken together, the abolishment of the interaction between Miz1 and Myc did not affect the frequency of stem/progenitor cells and the size of the spheres, using Myc$^{VD/VD}$ knock-in animals as a model system. Thus, the increased numbers of stem/progenitor cells observed in *Miz1ΔPOZ* glands may occur by a Myc-independent mechanism.

In order to investigate if the interaction between Miz1 and Myc has any effect on 3D culture morphogenesis, cells isolated from $Myc^{+/+}$ and $Myc^{VD/VD}$ mammary glands were seeded on Lab-Tek chambers (Nunc, Thermo Scientific) coated with basement membrane extract (Cultrex, Trevigen) at a density of 12500 cells/ml. This extract is purified from Engelbreth-Holm-Swarm (EHS) sarcomas and includes laminin, collagen IV, entactin and heparin sulfate proteoglycan. Representative pictures of the culture, which spanned 21 days, are shown in Fig. 3.12.

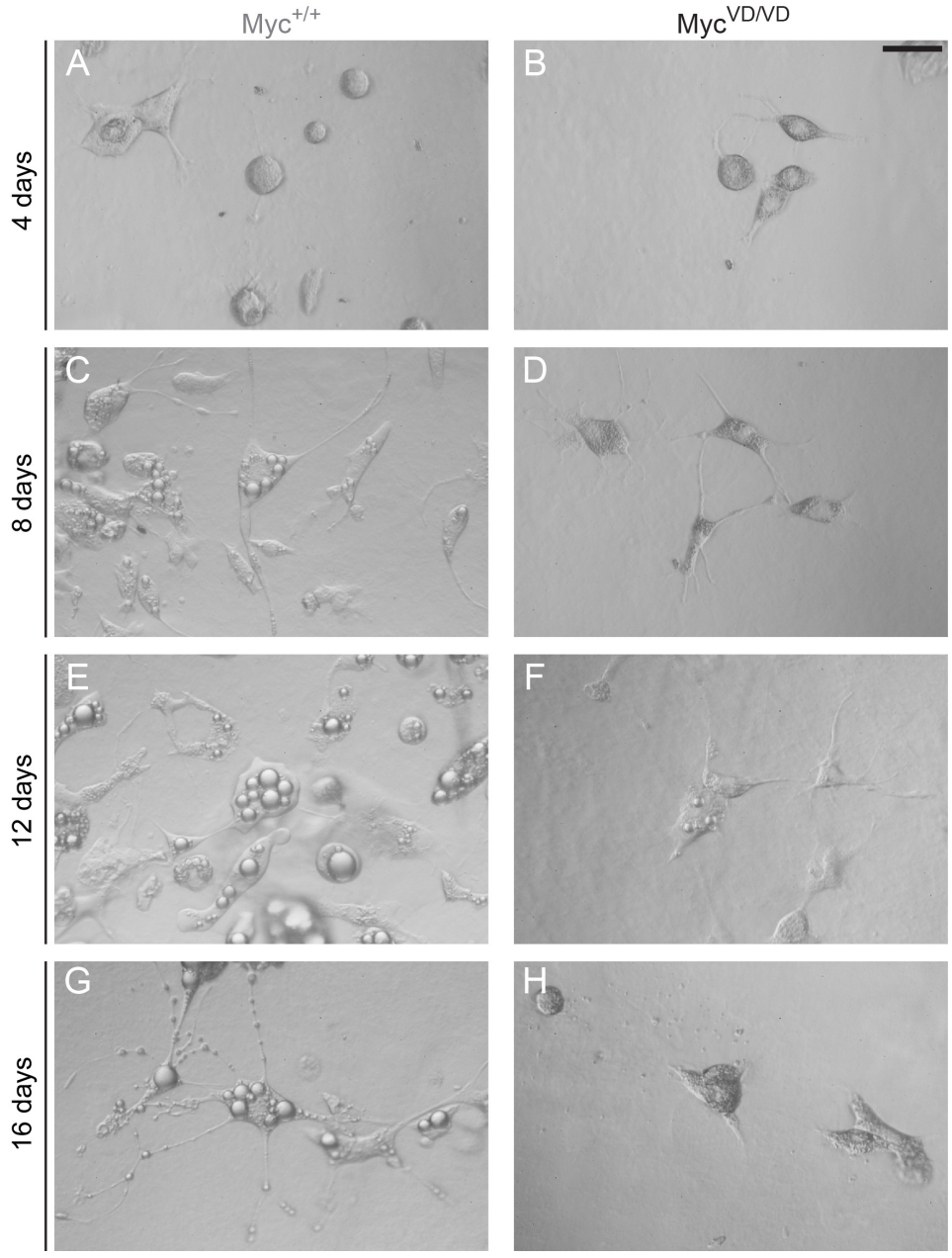

Figure 3.12: 3D culture of primary cells from $Myc^{+/+}$ and $Myc^{VD/VD}$ mammary glands. Representative pictures of the growth and differentiation of primary cells from $Myc^{+/+}$ (n=4) and $Myc^{VD/VD}$ (n=3) mammary glands cultured on a basement membrane matrix. Scale bar in B: 50 µm.

The protocol used has been described in the literature (Debnath et al., 2003) and details can be found in the Materials & Methods section. The primary cells seeded could have arisen from epithelium or from the stromal compartment of the virgin mammary gland as whole thoracic and inguinal glands were enzymatically digested in order to obtain single-cell suspensions. In the presence of the basement membrane matrix (Cultrex, Trevigen) a fraction of the mammary gland cells isolated, most possibly preadipocytes of stromal origin, differentiated and started producing large droplets after one week of culture. Adipocytes successfully grow on matrigel-based culture (Hazen et al., 1995) and, most interestingly, around 60% of stromal cells harvested from human adipose mammary tissue have been shown to differentiate into adipocytes in the presence of matrigel (O'Connor et al., 2003). As described in the latter article, other extracellular matrix substrata have less efficiency inducing *de novo* lipogenesis: 5% of the cells differentiated into adipocytes on fibronectin and 13-28% on tissue culture plastic and collagen I.

To characterize the droplets formed by primary mammary cells in 3D culture, a Sudan Black staining was carried out confirming their lipidic nature (Fig. 3.13A). Lipid droplets were not visible in any cell from both genotypes in the first 4 days of culture. After one week, 47.06 ± 24.77% of all $Myc^{+/+}$ seeded cells had differentiated into lipid-droplet-producing adipocytes but only 9.47 ± 4.76% of $Myc^{VD/VD}$ cells had done so at this time point (Fig. 3.13C). After 10 days of culture, the $Myc^{+/+}$ cells producing lipid droplets expanded to 73.23 ± 13.20% of the total cells while the percentage of $Myc^{VD/VD}$ which had undergone functional differentiation to produce lipids was of only 24.30 ± 4.78%. The culture continued till 21 days after seeding but the proportion of differentiated cells between $Myc^{+/+}$ and $Myc^{VD/VD}$ mammary primary cells was not markedly altered during the period ranging from 10-21 days of culture (Fig. 3.13C).

The number of primary mammary gland cells seeded per well was the same from both genotypes and no lipid droplets were observed at the beginning (first four days) of the culture. Then, either the amount of preadipocytes originally present in $Myc^{VD/VD}$ mammary tissue was low or $Myc^{VD/VD}$ preadipocytes were not efficiently differentiating and producing lipid droplets in the absence of a functional Miz1/Myc complex. More experimental data would be required to ascertain which of these two possible explanations is more accurate.

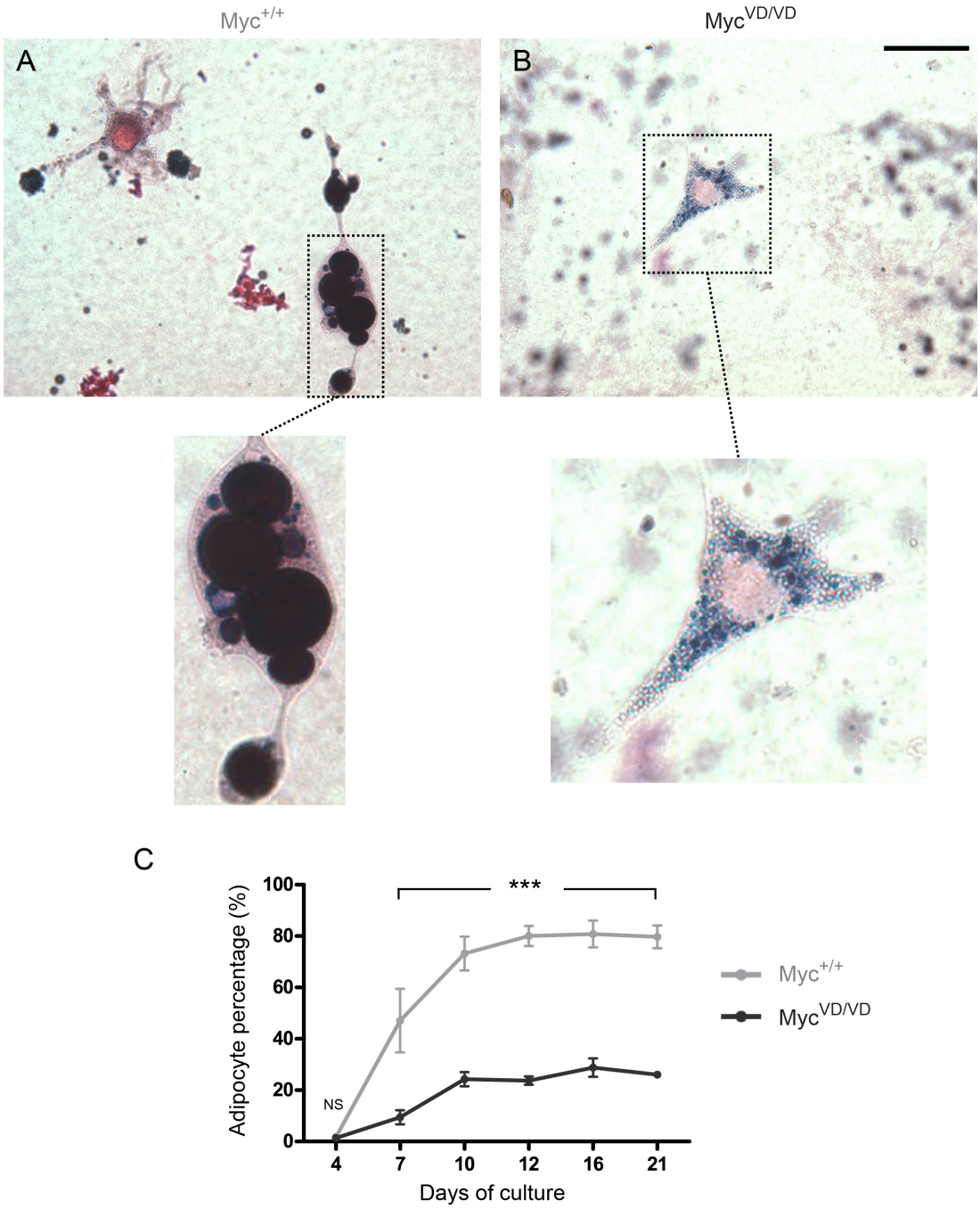

Figure 3.13: Lipid staining and quantification of the percentage of Myc$^{+/+}$ and Myc$^{VD/VD}$ adipocytes. (**A**) Sudan Black staining demonstrated the lipidic nature of the droplets analysed. (**B**) Myc$^{VD/VD}$ cell showing negativity after Sudan Black staining. (**C**) Quantification of the percentage of primary cells derived from Myc$^{+/+}$ and Myc$^{VD/VD}$ mammary glands which produced lipid droplets in the 21 days of culture. A two-way ANOVA with a Bonferroni's post-hoc test was used for statistical analysis. Scale bar in B: 50 µm.

3.4. Wap-Cre mediated deletion of the Miz1 POZ domain in the pregnant mammary gland causes a lactation defect by attenuated Stat5 expression and phosphorylation.

3.4.1. Conditional knockout of the Miz1 POZ domain in the pregnant and lactating mammary gland.

In analogy to the mouse model used for the deletion of the POZ domain of Miz1 in the virgin mammary gland, Miz1$^{lox/lox}$ mice (Gebhardt et al., 2007) were crossed to Whey acidic protein (Wap)-Cre animals (Wagner et al., 1997) in order to conditionally knockout the Miz1 POZ domain in luminal mammary epithelial cells during late pregnancy and lactation (Fig. 3.14). Prior to mating, both lines were backcrossed six generations to a 129S2/SvHsd background.

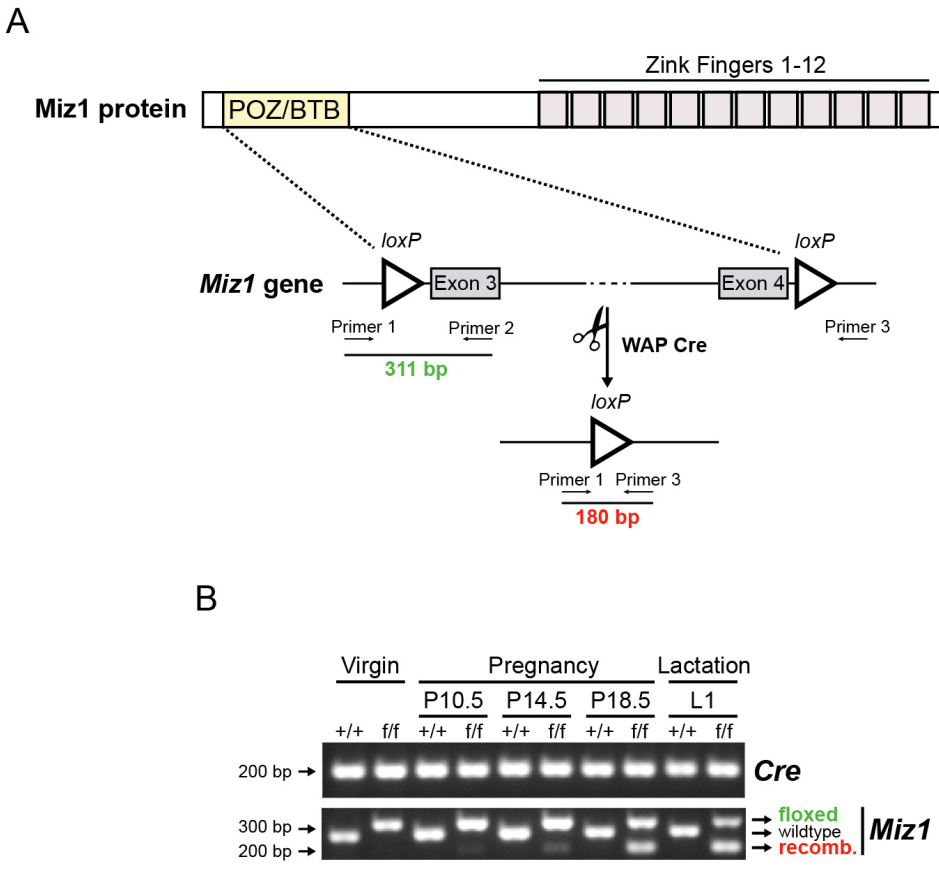

Figure 3.14: Conditional deletion of the Miz1 POZ domain in luminal mammary epithelial cells during pregnancy and lactation. (**A**) Schematic representation of the Wap-Cre mediated recombination strategy used to delete the exons which code for the Miz1 POZ domain and the relative position of the primers to detect it (Gebhardt et al., 2007). (**B**) Time course of the appearance of the Miz1 recombinant band performed on genomic DNA isolated from mammary glands at the indicated time points.

Wap promoter expression is more restricted to mammary epithelium than MMTV. As described before, MMTV-Cre recombination is detectable also in the salivary gland, the Harderian gland, seminal vesicles and lymphoid cells, while Wap deletion is specific for luminal epithelial mammary cells with expression in other tissues being several orders of magnitude lower than in the mammary gland (Pittius et al., 1988; Wagner et al., 1997). Wap-Cre represents a suitable model for the study of mammary differentiation during pregnancy and lactation *in vivo* due to the specificity of the deletion and precise timing. As can be seen in Fig. 3.14B, the appearance of the Miz1 recombinant band after PCR amplification occurs during mid-pregnancy and is sustained throughout lactation as already reported for the Wap-Cre mouse line (Wagner et al., 1997).

Immunohistochemistry against Cre (Stoelzle et al., 2009) was performed on mammary gland sections during pregnancy and lactation and its nuclear expression could be detected at the end of pregnancy (pregnancy day 18.5) and during lactation (lactation days 1 and 6; day 6 not shown) in the luminal mammary epithelium of the forming alveoli but not in the stroma (Fig. 3.15). Cre expression at day 14.5 of pregnancy was almost negligible by immunohistochemical analysis (Fig. 3.15A) although the Miz1 recombinant band was already visible at this time point after PCR amplification (Fig. 3.14B). Taken together, the Miz1 POZ domain was efficiently recombined *in vivo* using the Wap-Cre promoter in the luminal mammary epithelial compartment starting at mid-pregnancy and during lactation.

Due to the fact that Cre expression could affect mammary differentiation as reported for the MMTV-Cre model (Robinson and Hennighausen, 2011; Yuan et al., 2011) only Wap-Cre positive animals (Wap+ $Miz1^{+/+}$ or *Ctr* and Wap+ $Miz1^{lox/lox}$ or *Miz1ΔPOZ*) were employed to study the role of Miz1 during mammary differentiation *in vivo*.

Wap-Cre females of both genotypes were mated at 65 dpp for 1st pregnancy/lactation analysis and 2 weeks after completion of the 1st lactation for the study of the 2nd pregnancy/lactation. For pregnancy samples, mating plugs were checked every day and mammary dissection was performed at the indicated time points.

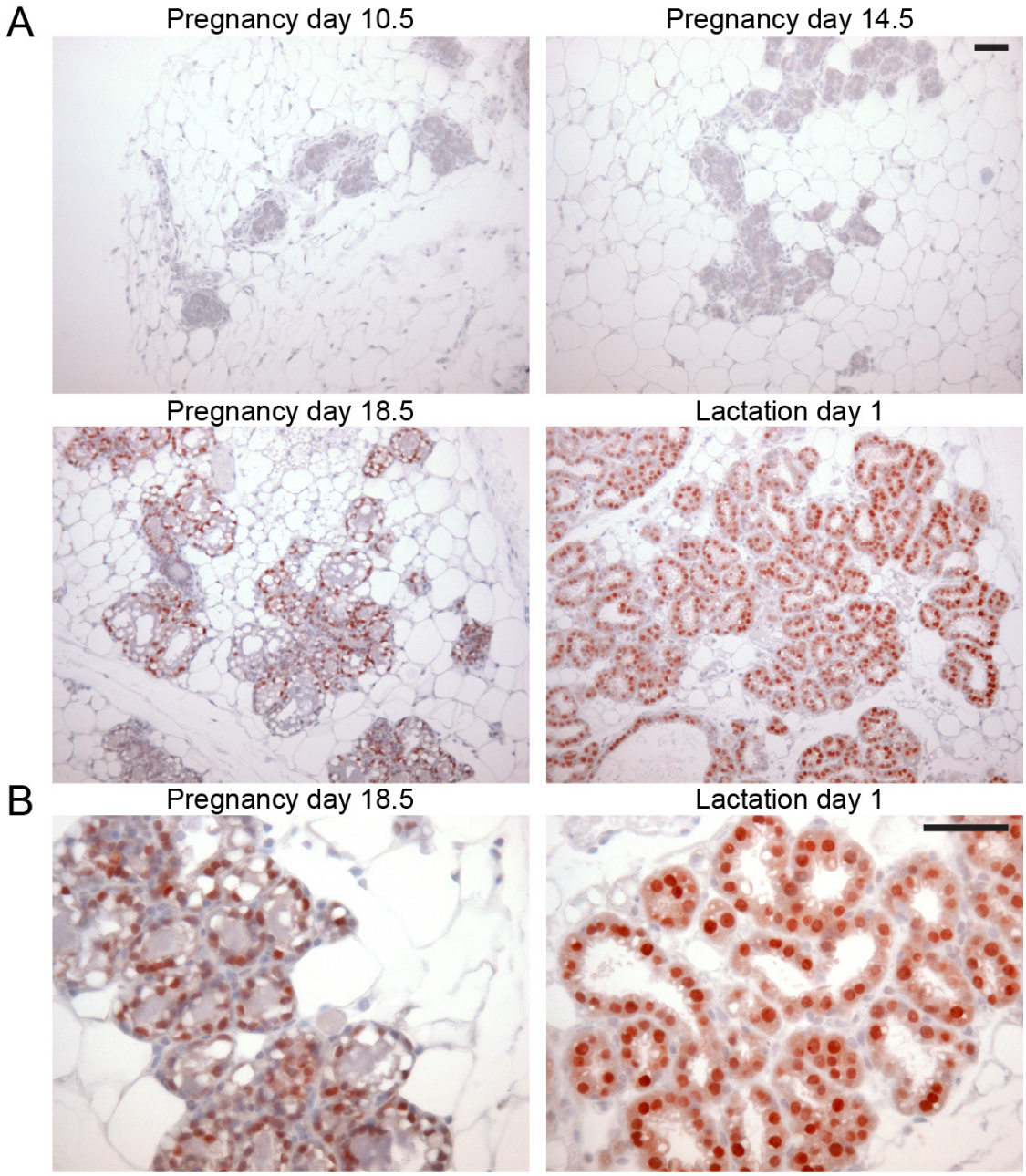

Figure 3.15: Cre immunohistochemistry in pregnant and lactating *Ctr* mammary glands. (**A**) Cre expression was analysed via peroxidase immunostaining in paraffin-embedded sections of *Ctr* mammary glands at pregnancy days 10.5 (n=2), 14.5 (n=2) and 18.5 (n=3) and lactation days 1 (n=3) and 6 (n=4; data not shown). (**B**) Higher magnification pictures of the Cre staining at pregnancy day 18.5 and lactation day 1. Scale bars: 50 µm.

3.4.2. *Miz1ΔPOZ* females feature a lactation defect.

Newborn pup weights (Palmer et al., 2006) were monitored for 24 days after being fostered by *Ctr* and *Miz1ΔPOZ* mothers. The number of pups per mother was set to six at birth and the offspring from six mothers per genotype were analysed (n=6). No significant difference was observed on day 3 postpartum (3 dpp), but at 6 dpp the weight of the pups nursed by *Miz1ΔPOZ* mothers was significantly reduced ($p<0.01$) and this difference increased until 24 dpp ($p<0.001$; Fig. 3.16A). The described variation in weight from the age-matched pups was sex-independent (Fig. 3.16B). In conclusion, *Miz1ΔPOZ* mothers featured a lactation defect and their pups were found significantly smaller than the ones fostered by *Ctr* dams between 6 and 24 days of age in the period of time analysed.

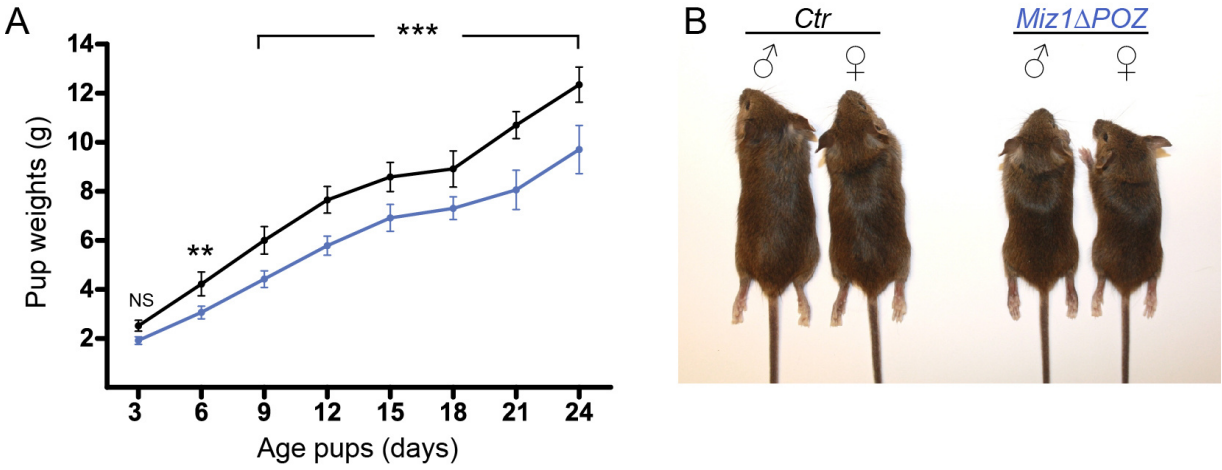

Figure 3.16: *Miz1ΔPOZ* mothers feature a lactation defect. (**A**) Pup weights of the offspring nursed by *Ctr* (black, n=6) and *Miz1ΔPOZ* (blue, n=6) mothers during 24 days postpartum. A two-way ANOVA followed by a Bonferroni's post-hoc test for multiple pairwise comparisons was employed for pup weight analysis. (**B**) Size differences were gender-independent. A representative picture of 24 days old male and female mice fostered by either *Ctr* or *Miz1ΔPOZ* mothers is shown.

Hematoxylin and eosin (H&E) stainings revealed a higher proportion of adipose tissue in sections from *Miz1ΔPOZ* mammary glands compared to *Ctr* animals at lactation day 6 (Fig. 3.17A). This phenotype was also observed after a second pregnancy (Fig. 3.17A) and was further proved by carmine alum-stained whole-mount mammary preparations. In these, *Miz1ΔPOZ* mammary glands exhibited less alveolar density in lactation day 1 as shown in Fig. 3.17B.

In order to quantify the proportion of adipose tissue in lactation day 6 samples from *Ctr* and *Miz1ΔPOZ* mammary glands, a morphometric approach was used. The percentage of fat was calculated measuring the area occupied by adipocytes and the total area of mammary gland in

H&E stained mammary sections corresponding to first and second pregnancies. The wand tool of ImageJ 1.43u software was employed for this quantification (Fig. 3.18). As shown in Fig. 3.17C, the percentages of fat measured in lactation day 6 first pregnancy sections were in average 2.65% in *Ctr* and 14.39% in *Miz1ΔPOZ* mammary glands (n=4; p=0.021). After a second pregnancy, the adipocyte proportion at lactation day 6 was 3.71% in *Ctr* and 16.55% in *Miz1ΔPOZ* glands (n=3; p=0.041).

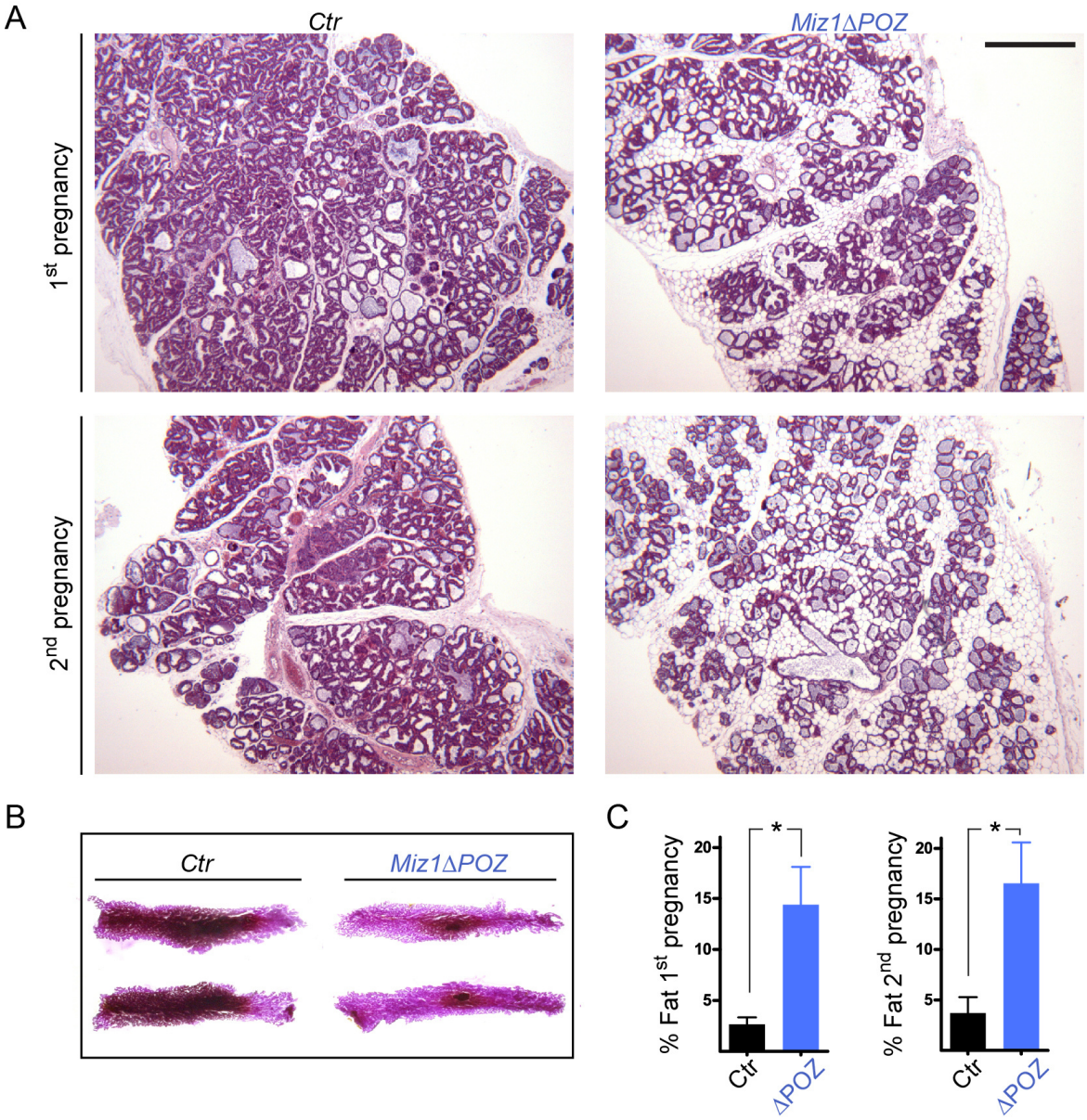

Figure 3.17: Increased proportion of adipose tissue in early lactation *Miz1ΔPOZ* mammary glands. (**A**) Representative H&E stainings of lactation day 6 mammary glands from *Ctr* and *Miz1ΔPOZ* animals. The first two pregnancies are shown. (**B**) Carmine-alum stained mammary whole-mount preparations at lactation day 1. (**C**) Adipocyte percentage quantification in lactation day 6 sections from *Ctr* and *Miz1ΔPOZ* mammary glands. Scale bar in A: 500 µm.

Thus, the difference in the ratio of glandular to adipose tissue measured during early lactation was similar after the first and second pregnancies.

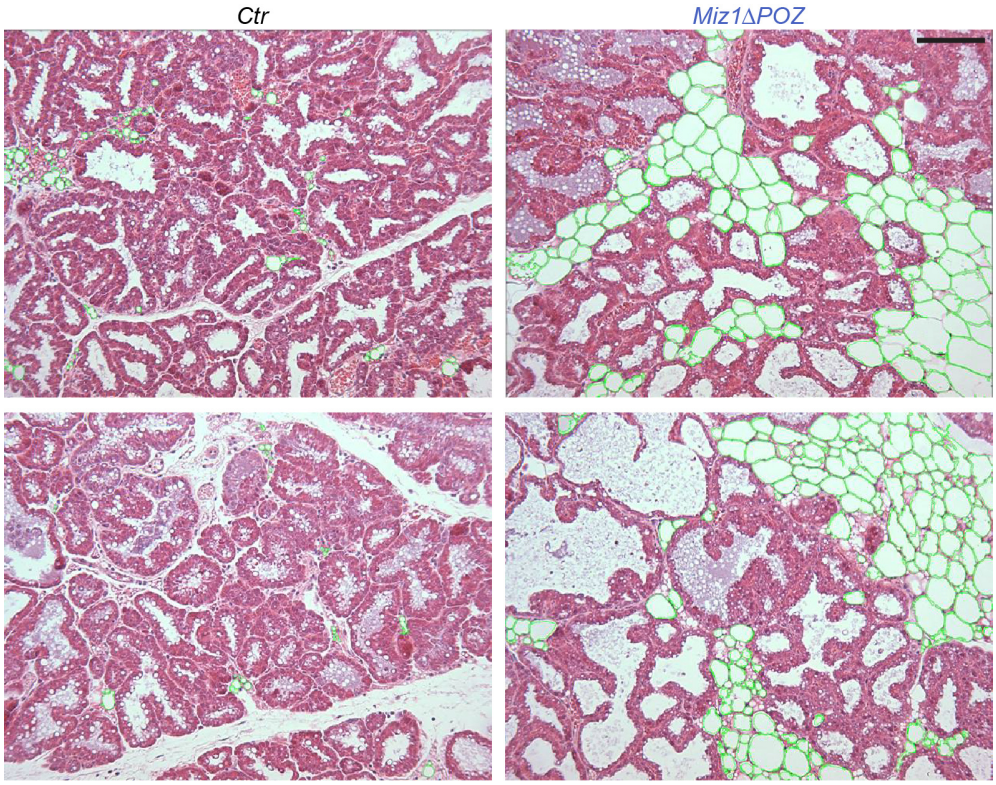

Figure 3.18: Quantification of the proportion of adipose tissue at lactation day 6 using ImageJ software. 10 pictures per animal were used for the analysis of first pregnancy (n=4 per genotype) and second pregnancy (n=3 per genotype) lactation day 6 sections of *Ctr* and *Miz1ΔPOZ* mammary glands. The wand tool of ImageJ 1.43u software was employed to calculate the adipocyte area in relation to the total mammary gland area in each sample. Scale bar: 30 µm.

No marked differences were observed in H&E sections from *Ctr* and *Miz1ΔPOZ* mammary glands at first pregnancy day 18.5 (Fig. 3.19A and B). This observation might be related to the expression of endogenous Miz1 which, as already mentioned in Section 3.1.1, was hardly detectable by Western Blotting at the end of pregnancy.

The reduced alveologenesis phenotype only became apparent at lactation day 1 (Fig. 3.19C and D), obvious at lactation day 6 (Fig. 3.19E and F) and partially rescued by lactation day 10 (Fig. 3.19G and H). Taken together, the data indicate that *Miz1ΔPOZ* glands suffered a delay in alveolar development during early lactation which caused the nursing defect in mutant dams.

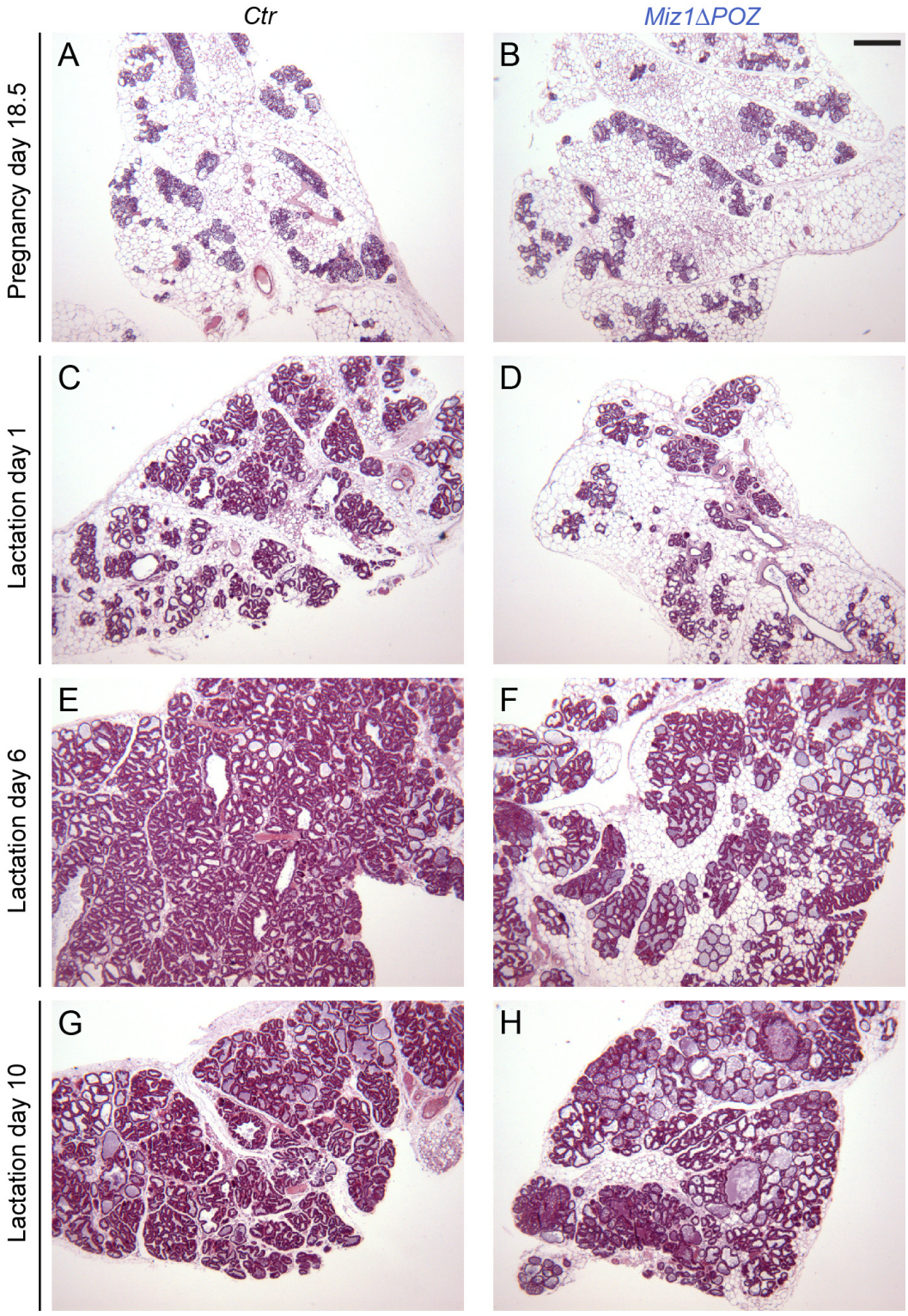

Figure 3.19: Representative H&E sections of *Ctr* and *Miz1ΔPOZ* mammary glands at different stages of pregnancy and lactation. The following time points were analysed: (**A, B**) Pregnancy day 18.5 (n=3). (**C**, **D**) Lactation day 1 (at least n=3). (**E**, **F**) Lactation day 6 (n=8). (**G**, **H**) Lactation day 10 (n=4). Scale bar in B: 300 µm.

3.4.3. Apoptosis during lactation in *Ctr* and *Miz1ΔPOZ* mammary glands.

One possible explanation for the reduced alveologenesis in *Miz1ΔPOZ* animals could be the occurrence of mammary epithelial cell apoptosis in mutant glands. To test this hypothesis, terminal deoxynucleotidyl transferase dUTP nick end labeling (TUNEL) assays (Gavrieli et al., 1992) and cleaved caspase-3 immunohistochemistry were performed on lactation day 1 and 6 samples of *Ctr* and *Miz1ΔPOZ* first pregnancy mammary gland sections. TUNEL positive cells were rare in both *Ctr* and *Miz1ΔPOZ* mammary sections as can be seen in Fig. 3.20A-D.

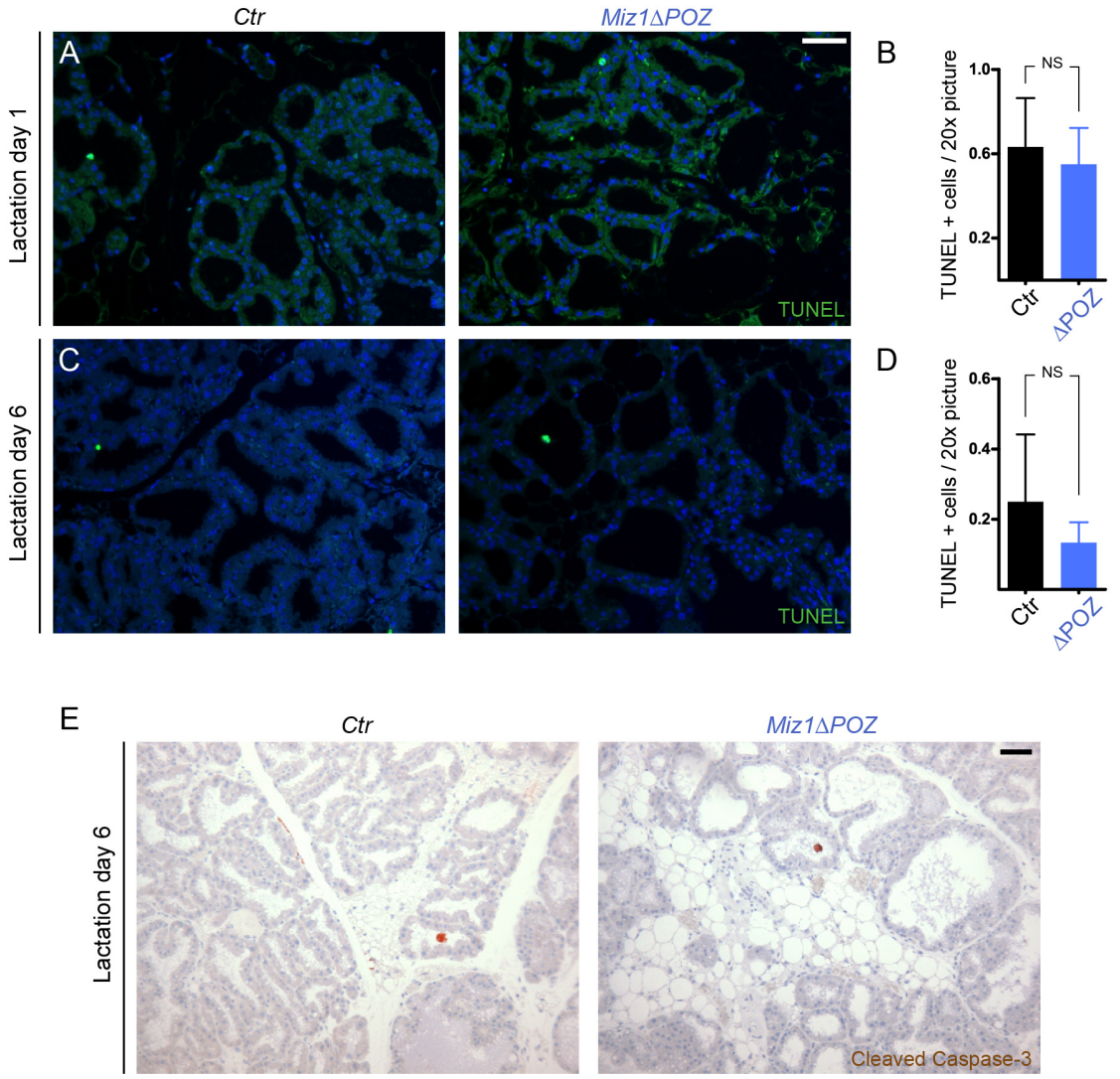

Figure 3.20: Apoptosis during lactation in *Ctr* and *Miz1ΔPOZ* mammary glands. TUNEL assay pictures and quantifications performed on *Ctr* and *Miz1ΔPOZ* sections at lactation days 1 (**A**, **B**) and 6 (**C**, **D**). TUNEL positive cells were quantified in 20x magnification mammary pictures (10 per animal) and at least 3 animals per genotype and time point were analysed. (**E**) Immunohistochemistry against cleaved caspase-3 in lactation day 6. Scale bars: 50 µm.

TUNEL positive cells were quantified in 20x magnification mammary pictures (10 per animal) and at least 3 animals per genotype and time point were analysed. In lactation day 1, 0.63 ± 0.23 TUNEL positive cells per 20x picture were scored in *Ctr* while 0.55 ± 0.17 were found in *Miz1ΔPOZ* sections (Fig. 3.20B; p=0.6059). In lactation day 6, 0.25 ± 0.19 positive cells per 20x picture were observed in *Ctr*, whereas 0.13 ± 0.06 were counted in mutant glands (Fig. 3.20D; p=0.3632). In conclusion, no significant differences in DNA fragmentation, characteristic of a late stage of apoptosis, were found in *Ctr* and *Miz1ΔPOZ* lactation days 1 and 6 sections. These observations were further confirmed by cleaved caspase-3 immunohistochemistry at lactation days 1 (data not shown) and 6 (Fig. 3.20E). As for the TUNEL assay, at least 3 animals per genotype and time point were used. Taken together, apoptosis was not different between *Ctr* and *Miz1ΔPOZ* animals during early lactation and thus this process cannot explain the reduced alveolar density observed in *Miz1ΔPOZ* mice.

3.4.4. Reduced proliferation during lactation in *Miz1ΔPOZ* mammary glands.

Proliferation of mammary cells from *Ctr* and *Miz1ΔPOZ* animals was assessed by Ki67 immunohistochemistry in lactation day 6 histological sections after a first pregnancy. A reduction in the number of positive cells and a decreased staining intensity were observed in *Miz1ΔPOZ* samples as shown in several magnifications in Fig. 3.21. While Ki67 positive cells were detected in the lymph nodes of both *Ctr* and *Miz1ΔPOZ* mammary glands (Fig. 3.21B), alveolar cells from *Miz1ΔPOZ* mice had an obvious reduction in Ki67 staining positivity.

The Ki67 labelling index was then calculated in *Ctr* and *Miz1ΔPOZ* sections at lactation day 6 by counting Ki67 positive cells among all epithelial cells in representative 25x pictures using ImageJ software. More than 1000 cells per animal were scored in 3 animals per genotype (n=3). As represented in Fig. 3.22A, 50.40 ± 3.63% of the cells analysed were positive for Ki67 in *Ctr* animals while only 14.26 ± 0.89% were found to express Ki67 in *Miz1ΔPOZ* sections (p<0.0001). The Ki67 mRNA (*Mki67*) was also reduced in *Miz1ΔPOZ* glands as analysed by qPCR, but this difference was statistically not significant (p=0.0575; Fig. 3.22A). In conclusion, a reduced proliferation was observed in *Miz1ΔPOZ* sections at lactation day 6 compared to *Ctr* mammary glands.

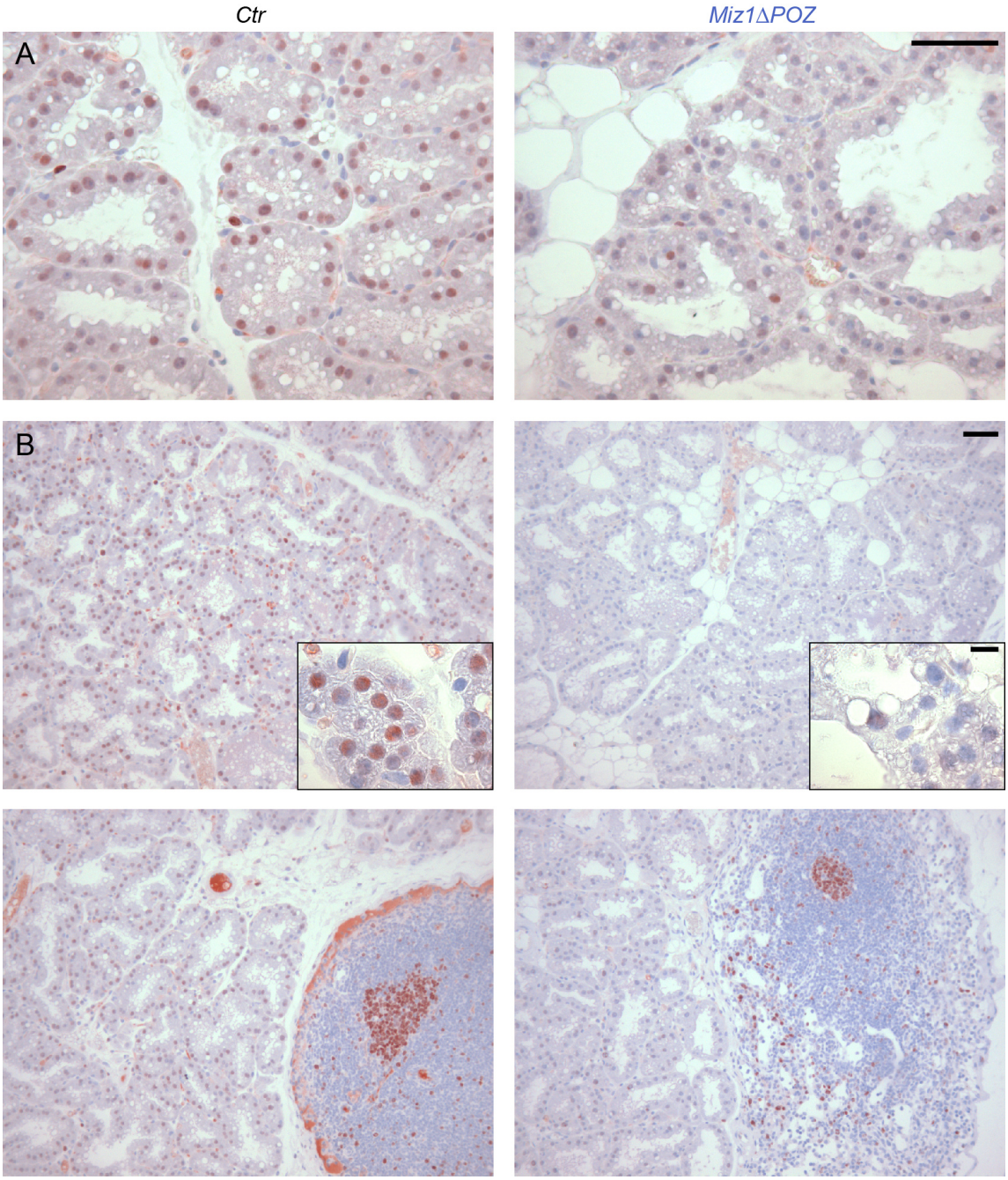

Figure 3.21: Decreased proliferation in *Miz1ΔPOZ* glands at lactation day 6. Ki67 immunostaining is shown in lower and higher magnification for *Ctr* and *Miz1ΔPOZ* glands at lactation day 6 (**A** and **B**). As can be seen in B (lower pictures), lymph nodes exhibit cells strongly stained for Ki67 in both *Ctr* and *Miz1ΔPOZ* animals. In contrast, alveolar mammary gland cells from *Miz1ΔPOZ* mice displayed a much lower number of Ki67 positive nuclei. At least n=3 animals per genotype were used. Scale bars: 50 µm and 10 µm in inset from B.

The Miz1/Myc complex is a critical repressor of the cell cycle arrest gene *Cdkn1a* (Seoane et al., 2002; Wu et al., 2003a; Hönnemann et al., 2012), encoding $p21^{cip1}$, but the expression of *Cdkn1a* (p=0.3823) and *Myc* (p=0.5281) was not significantly altered in *Miz1ΔPOZ* mammary glands at lactation day 6 as analysed by qPCR (Fig. 3.22B). Taken together, the delay in mammary gland alveolar development during early lactation was influenced by a reduced proliferation of *Miz1ΔPOZ* epithelial cells and this was not caused predominantly due to overexpression of $p21^{cip1}$ or an attenuated expression of Myc. Another potential candidate molecule for explaining the reduced proliferation phenotype in *Miz1ΔPOZ* lactating mammary glands will be addressed in the Section 3.4.8.

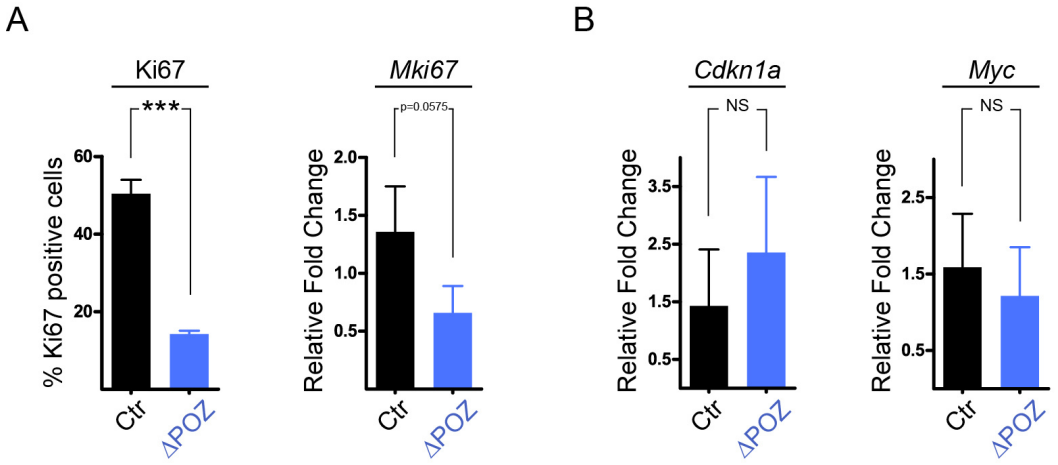

Figure 3.22: Quantification of Ki67 staining and proliferation-related gene expression in *Ctr* and *Miz1ΔPOZ* mammary glands at lactation day 6. (**A**) On the left side, the percentage of Ki67 positive cells in histological sections from lactation day 6 animals was quantified using ImageJ software (p<0.0001). More than 1000 cells per animal were scored in 3 animals per genotype (n=3). On the right side, qPCR data of *Mki67* expression in lactation day 6 samples (p=0.0575). (**B**) qPCR relative expression of *Cdkn1a* and *Myc* in *Ctr* and *Miz1ΔPOZ* glands at lactation day 6 (n=3 for all qPCR data shown).

3.4.5. Morphogenetic 3D culture of HC11 cells and consequences after Miz1 knockdown: unaltered apoptosis, reduced proliferation and delayed acinar lumen formation.

HC11 mammary cells (Ball et al., 1988) were used as an *in vitro* model to study Miz1 function on cellular proliferation and apoptosis trying to test if parallelisms exist with the *in vivo* deletion of the Miz1 POZ domain described above. In addition, the impact of Miz1 in 3D mammary acinar formation was investigated. Stably-transfected HC11 cells with expression vectors encoding for either a scrambled short hairpin RNA used as control (*shscr*) or a Miz1 specific short hairpin

RNA to knockdown Miz1 (*shMiz1*) were generated (Fig. 3.23B). These cells were then cultured in an acinar morphogenetic *in vitro* assay already described (Debnath et al., 2003; Hebner et al., 2008; Xian, 2005) where Cultrex basement membrane extract (Trevigen) was used to coat sterilized coverslips. In these conditions and with medium containing 2% Cultrex, mammary cells proliferate and then form growth-arrested polarized acini. After 6-8 days of culture a lumen starts to be discernible in the center of these structures as a consequence of cellular apoptosis (Debnath et al., 2002) and autophagy (Avivar-Valderas et al., 2011; Debnath, 2008).

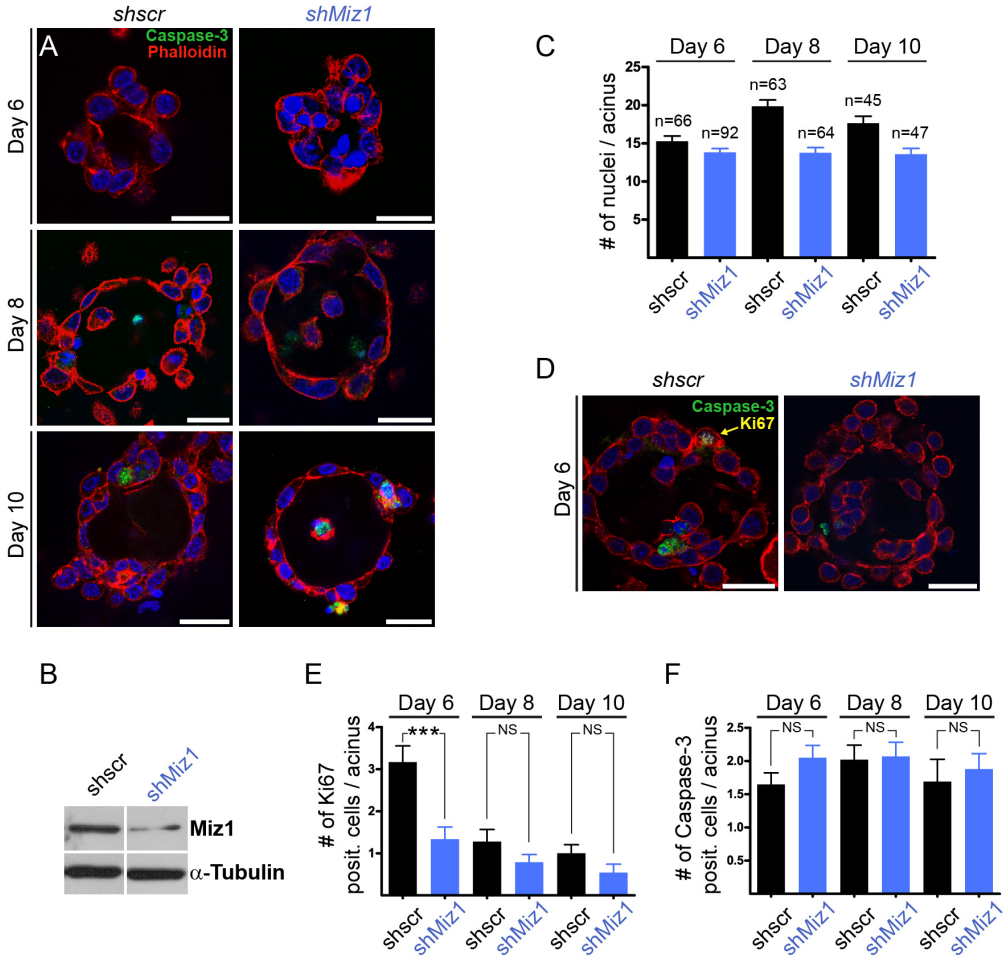

Figure 3.23: Three-dimensional culture of *shscr* and *shMiz1* HC11 cells. (**A**) Representative confocal microscopy pictures of acinar structures formed by *shscr* and *shMiz1* HC11 cells. Nuclei were stained with Hoechst (blue), actin filaments with Phalloidin-TRITC (red) and apoptotic cells with cleaved caspase-3 (green). (**B**) Western blot showing the knock-down of Miz1 in *shMiz1* HC11 cells.
(**C**) Quantification of the number of nuclei per acinus in *shscr* and *shMiz1* HC11 cells merging data from two independent experiments. Acinar cell proliferation and apoptosis were quantified by analysis of Ki67 (**E**) and cleaved Caspase-3 (**F**) positivity (**D**; cleaved Caspase-3: green and Ki67: yellow). Stainings and quantifications were performed by David Fuhrmann. Scale bars: 25 µm.

Representative pictures of acinar structures formed 6, 8 and 10 days after the seeding of *shscr* and *shMiz1* expressing HC11 cells are shown in Fig. 3.23A. In this figure, phalloidin (red) was used to stain actin filaments of the cytoskeleton and cleaved caspase-3 (green) fluorescent immunostaining was employed to assess apoptosis at the indicated time points (Fig. 3.23A). As in *Miz1ΔPOZ* mammary glands *in vivo*, quantification of the number of cleaved caspase-3 positive cells per acinus revealed no significant differences in apoptosis between *shscr* and *shMiz1* expressing HC11 cells (Fig. 3.23F).

The number of nuclei per acinus was quantified at the time points mentioned above. After 6 days of seeding, no significant differences were observed between *shscr* and *shMiz1* HC11 cells. In contrast, after 8 and 10 days of culture, the number of nuclei per acinus was lower in HC11 cells with decreased levels of Miz1 (Fig. 3.23C). Moreover, Ki67 (yellow) fluorescent staining (Fig. 3.23D) and quantification of Ki67 positive cells per acinus (Fig. 3.23E) revealed a significantly diminished proliferation of *shMiz1* HC11 cells at 6 days post-seeding (p=0.0007). Thus, a parallelism can be drawn with the *in vivo* situation where apoptosis is not altered and proliferation is decreased in the absence of a functional Miz1. In addition, the establishment of a lumen was delayed in *shMiz1* HC11 cells (data not shown).

3.4.6. Reduced differentiation during lactation in *Miz1ΔPOZ* mammary glands.

Despite the fact that mammary alveolar cell density was similar between *Ctr* and *Miz1ΔPOZ* animals at lactation day 10 (Fig. 3.19G and H), the difference in pup weights was not rescued and even increased over time (Fig. 3.16A). In order to identify genes potentially regulated by Miz1 which could explain the observed lactation defect phenotype and to assess the relative expression of milk protein genes, a genome-wide cDNA microarray was performed using samples from *Ctr* and *Miz1ΔPOZ* animals obtained at day 6 of lactation (n=4 for each genotype).

The expression of distinct casein genes (*Csn1s1, Csn1s2a, Csn1s2b, Csn2, Csn3*) and the whey acidic protein gene (*Wap*) was up to 2.5fold downregulated in mutant animals (later represented in Fig. 3.32). These observations could be confirmed by qPCR which showed a twofold downregulation in *Miz1ΔPOZ* glands of the genes encoding for α-casein (p=0.0003), ß-casein (p=0.0006) and whey acidic protein (p=0.0058) as represented in Fig. 3.24A. Moreover, less ß casein protein was detected by western blotting in mammary gland tissue from *Miz1ΔPOZ* animals at lactation day 6 (Fig. 3.24B). A decreased amount of milk was observed in the alveoli

from mutant animals compared with control animals (Fig. 3.24C) on sections of lactation day 6 mammary glands, stained with an antibody against mouse milk proteins (Merlo et al., 1994). Collectively, the data show that differentiation of mammary gland epithelial cells is diminished in *Miz1ΔPOZ* glands leading to a reduced synthesis and secretion of several milk proteins.

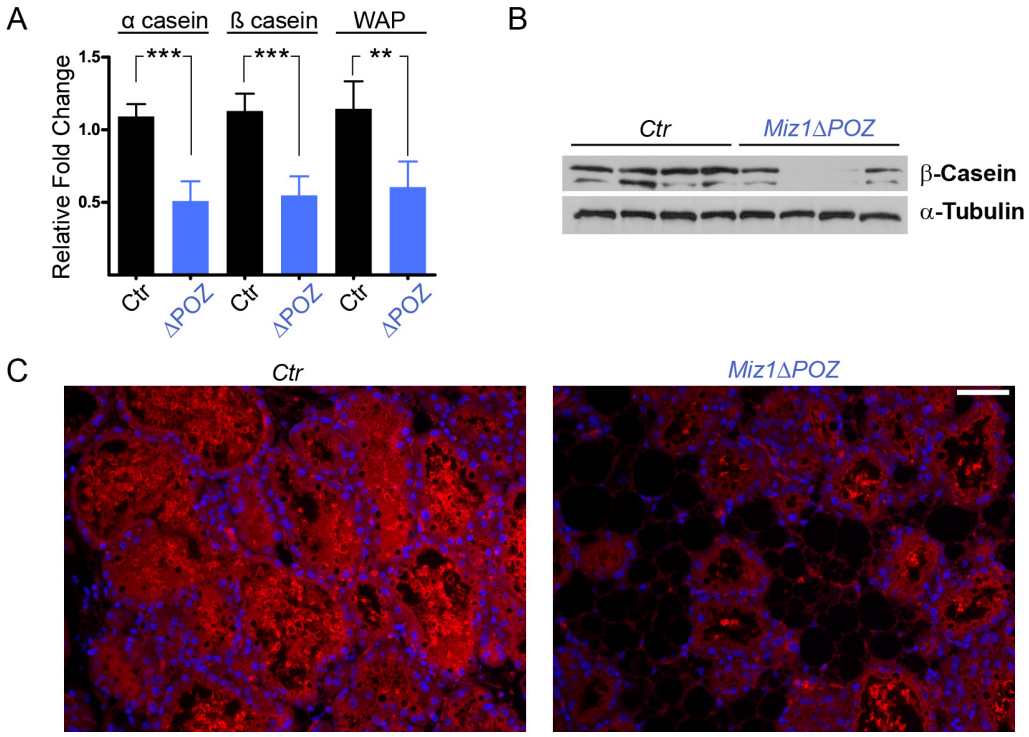

Figure 3.24: Decreased differentiation in *Miz1ΔPOZ* glands at lactation day 6. (**A**) qPCR data of the expression of the genes which code for milk proteins α-casein, β-casein and Wap in samples taken from *Ctr* and *Miz1ΔPOZ* animals at lactation day 6. (**B**) ß-casein western blot at lactation day 6. Each lane represents an individual animal. (**C**) Milk proteins immunofluorescence in mammary tissue from *Ctr* and *Miz1ΔPOZ* mice at lactation day 6. Scale bar in C: 50 µm.

3.4.7. Reduced differentiation in HC11 cells with low levels of Miz1.

In order to investigate whether the reduced differentiation phenotype observed in *Miz1ΔPOZ* animals can also be recapitulated on a cellular basis *in vitro*, we again took advantage of the HC11 cell line. These immortalized mid-pregnant mammary gland cells can undergo a limited differentiation after hormonal treatment and stimulate the synthesis of different milk proteins (Ball et al., 1988). A schematic representation of the protocol followed for HC11 differentiation is shown in Fig. 3.25A and a description of it was already provided in Section 3.1.3. The

expression of the *csn2* gene (Fig. 3.25C) and the amount of translated ß-casein protein (Fig. 3.25D) detected 24, 48 and 72 hours after adding the hormonal cocktail DIP (containing dexamethasone, insulin and prolactin) were lower in HC11 cells with decreased levels of Miz1 (*shMiz1*).

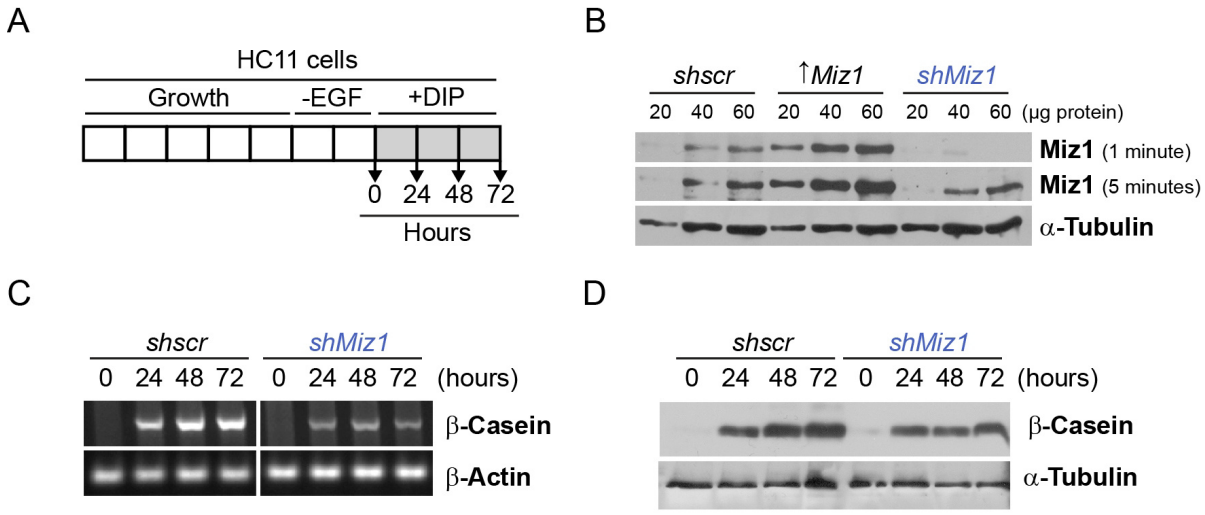

Figure 3.25: Reduced expression of the differentiation marker ß-casein in HC11 cells with low levels of Miz1. (**A**) Protocol for the differentiation of HC11 mammary cells. Each rectangle represents one day. EGF: epidermal growth factor; DIP: differentiation media containing dexamethasone, insulin and prolactin. Time points indicated correlate to the ones in C and D. (**B**) HC11 cells were stably transfected with scrambled short hairpin RNA (*shscr*), a Miz1 shRNA (*shMiz1*) and a vector overexpressing Miz1 as a positive control (↑*Miz1*). Semi-quantitative PCR (**C**) and western blotting (**D**) revealed a decreased expression of ß-casein when Miz1 levels were low (*shMiz1*).

In conclusion, decreasing the levels of Miz1 in HC11 cells *in vitro* led to a reduced expression of the differentiation marker ß-casein. Thus, the diminished expression of milk protein genes observed in *Miz1ΔPOZ* lactating dams *in vivo* could be cell autonomous and not due only to an increased proportion of adipose tissue in mutant glands.

3.4.8. Deficient Stat5 signalling in *Miz1ΔPOZ* mammary glands.

Signal Transducer and Activator of Transcription 5a and 5b (Stat5a/b) are essential for proper adult mammary gland proliferation, differentiation and survival (Furth et al., 2011; Hennighausen and Robinson, 2008). Mammary alveolar formation and lactogenesis are severely impaired in the absence of Stat5 signalling as seen in knockout *in vivo* mouse models (Liu et al., 1997; Teglund et al., 1998; Cui et al., 2004).

In order to investigate whether Stat5a/b levels were altered in *Miz1ΔPOZ* glands, qPCRs and Western blots were performed at lactation day 6 after a first pregnancy. The expression of the genes *Stat5a* (p=0.1671) and *Stat5b* (p=0.0607) was slightly but not significantly decreased in mutant glands. Using an antibody which recognizes both Stat5 isoforms, Western blotting showed an obvious reduction in the levels of Stat5a/b proteins in *Miz1ΔPOZ* glands (Fig. 3.26B). The mammary epithelial cell-specific cytokeratin-18 and α-tubulin, which has a very low expression in adipose tissue (Spiegelman and Farmer, 1982), were employed as loading control. In addition, immunohistochemistry against phosphorylated Stat5 (Tyr694) revealed a diminished number of positive nuclei and a decreased staining intensity in mutant mammary gland tissue at lactation day 6 (Fig. 3.26C).

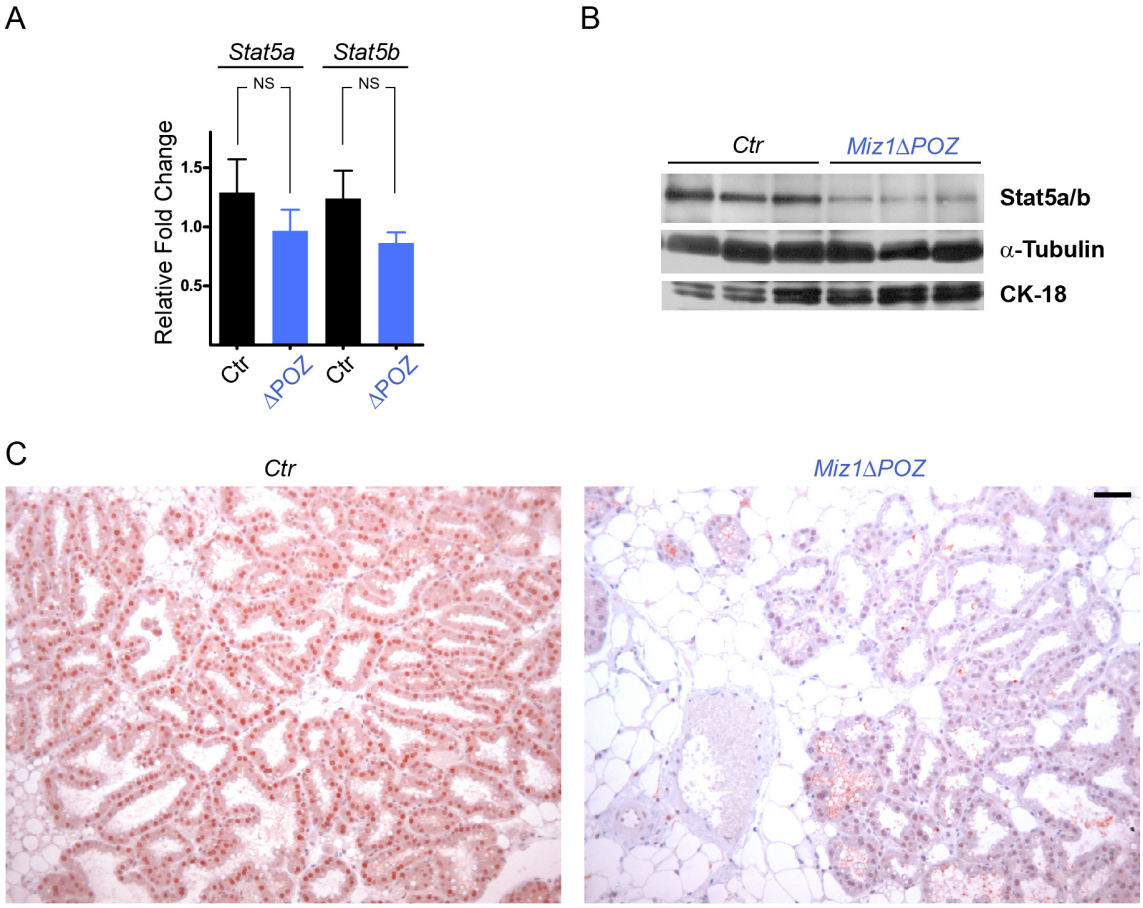

Figure 3.26: Deficient Stat5 signalling in *Miz1ΔPOZ* glands at lactation day 6. (**A**) The expression of the genes *Stat5a* and *Stat5b* was analysed by qPCR in *Ctr* and *Miz1ΔPOZ* mammary glands (n=3) at lactation day 6. (**B**) Western blotting of Stat5a/b protein at lactation day 6. Each lane represents an individual animal. α-Tubulin and cytokeratin-18 were used as loading controls. (**C**) pSTAT5 (Tyr694) protein was detected by immunohistochemistry in lactation day 6 sections of control and mutant glands (first pregnancy samples are shown). Scale bar in C: 50 µm.

A reduced phosphorylation of Stat5 *in vivo* was detected by immunostaining also after a second pregnancy (data not shown). In conclusion, a deficient Stat5 signalling, crucial for proper mammary cell proliferation and differentiation, led to reduced mammary alveolar density and a lactation defect in *Miz1ΔPOZ* mothers.

3.4.9. Deficient Stat5 signalling in *shMiz1* HC11 mammary cells.

HC11 mammary cells were used again to test whether the deficient Stat5 signalling observed in *Miz1ΔPOZ* glands also occurred *in vitro* when Miz1 levels are knocked down. After addition of the lactogenic cocktail (DIP) in the already described HC11 differentiation protocol (Fig. 3.27A), Stat5 was phosphorylated and could be detected after 24 hours of the hormonal induction, as previously reported (Schmitt-Ney et al., 1992). The protein levels of Stat5a/b and pStat5a/b were analysed by western blotting at the moment of adding the hormones (time 0 hours) and 24, 48 and 72 hours after the start of differentiation in control (*shscr*) and low Miz1 expressing (*shMiz1*) HC11 cells. Stat5a/b protein after Miz1 knockdown was not as obviously reduced as *in vivo* but the detected pStat5a/b was greatly decreased in *shMiz1* HC11 cells at the different time points analysed after the induction of differentiation with the lactogenic hormonal cocktail (Fig. 3.27B).

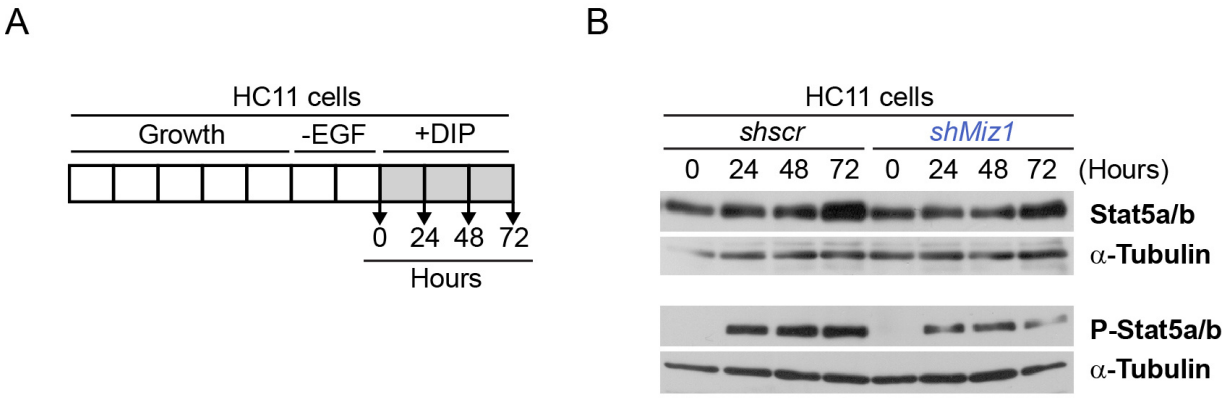

Figure 3.27: Deficient Stat5 signalling in differentiating *shMiz1* HC11 cells. (**A**) HC11 differentiation protocol representing the time points analysed. Protein samples were obtained at the moment of adding the lactogenic hormone cocktail (time 0 hours) and 24, 48 and 72 hours after the induction of differentiation (+DIP). (**B**) The levels of Stat5a/b and pStat5a/b (Tyr 694/699) were detected by Western blotting in control (*shscr*) and low Miz1 (*shMiz*1) HC11 cells at the time points indicated. α-Tubulin was used as a loading control.

To sum up, Stat5 phosphorylation is diminished *in vivo* and *in vitro* when a functional Miz1 is lacking and this observation correlates with the decreased proliferation and differentiation detected in *Miz1ΔPOZ* lactation day 6 mammary glands and *shMiz1* HC11 cells.

3.4.10. Gene expression analysis of Stat5 pathway regulators.

The expression of different Janus kinase 2 (Jak2)/Stat5 pathway components was analysed by qPCR in *Ctr* and *Miz1ΔPOZ* mammary glands at lactation day 6. A number of studies demonstrate that the more upstream components of the Stat5 pathway, namely the prolactin receptor (Ormandy et al., 1997; Grimm et al., 2002) and Jak2 (Shillingford et al., 2002; Wagner et al., 2004), are indispensable for normal alveolar formation and mammary differentiation. Stat5 phosphorylation through activation of the prolactin receptor is mediated by the Jak2 protein (Gallego et al., 2001; Hennighausen and Robinson, 2008). The expression of the prolactin receptor (*Prlr*) was found to be downregulated in *Miz1ΔPOZ* mammary tissue by microarray analysis performed with *Ctr* and *Miz1ΔPOZ* lactation day 6 mammary glands. qPCR analysis further revealed a statistically significant (p=0.0402) decrease in the levels of *Prlr* in mutant glands (Fig. 3.28A).

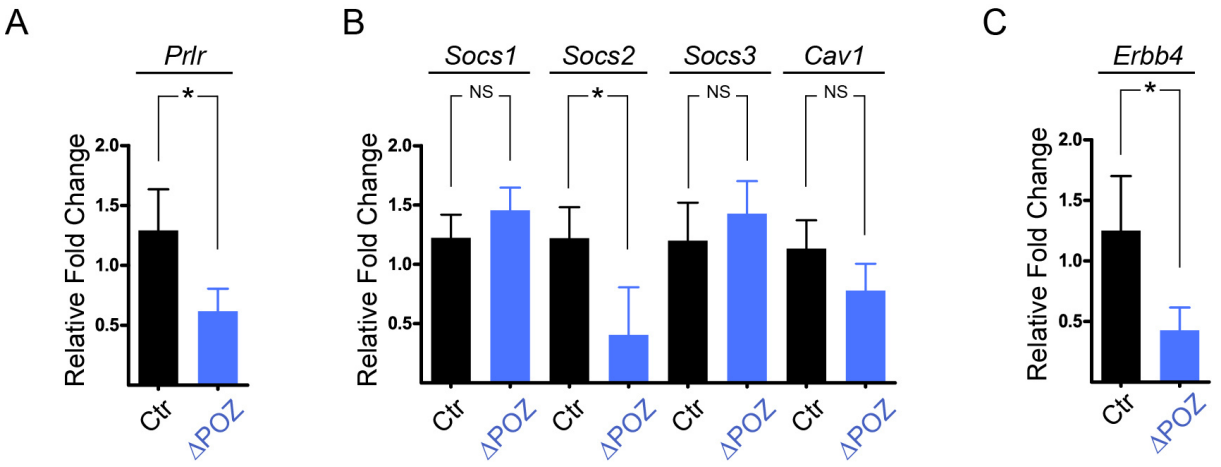

Figure 3.28: Gene expression analysis of Stat5 pathway regulators. qPCR data of the expression of (**A**) *Prlr*, (**B**) *Socs1-3*, *Cav1* and (**C**) *Erbb4* in *Ctr* and *Miz1ΔPOZ* glands (n=3 per genotype) at lactation day 6 of a first pregnancy.

Then, the expression of genes which negatively regulate the Jak2/Stat5 pathway was analysed via qPCR. Suppressor of cytokine signaling (*Socs*) genes are part of a negative feedback loop which

maintains the levels of activated Stat5 under strict control (Sutherland et al., 2007; Tam et al., 2001), although the mechanism of action in the mammary gland of the distinct family members varies (Lindeman et al., 2001; Harris et al., 2006; Nicholson et al., 2000). The expression of *Socs1* (p=0.2132) and *Socs3* (p=0.4060) was not significantly different between *Ctr* and *Miz1ΔPOZ* animals, but the expression of *Socs2*, a direct target of Stat5 (Harris et al., 2006), was downregulated (p=0.0425) in mutant glands (Fig. 3.28B). This observation further pointed to a decreased Stat5 signalling in *Miz1ΔPOZ* animals.

Cav1 (Caveolin-1), component of the caveolae in the plasma membrane, has also been shown to act as a negative regulator of the Jak2/Stat5 pathway by direct interaction with Jak2 (Park et al., 2002). The expression of *Cav1* was found not significantly different (p=0.1368) between *Ctr* and *Miz1ΔPOZ* mice at lactation day 6 by qPCR (Fig. 3.28B).

Stat5 phosphorylation is not only affected by the prolactin receptor/Jak2 pathway but also by ErbB4 (Receptor tyrosine-protein kinase ErbB-4), which directly phosphorylates Stat5 and, after proteolytic cleavage, translocates activated Stat5 into the nucleus (Long et al., 2003; Williams et al., 2004). As shown in Fig. 3.28C, the expression of *Erbb4* was found significantly decreased (p=0.0433) in lactation day 6 samples from *Miz1ΔPOZ* dams.

Taken together, the data point to a downregulation of the prolactin (*Prlr*) and ErbB4 (*Erbb4*) receptors which correlates with decreased Stat5 phosphorylation and nuclear translocation, causing the documented decline in proliferation and differentiation observed in *Miz1ΔPOZ* mammary glands which finally led to a lactation defect.

3.4.11. Lipid aggregation in *Miz1ΔPOZ* lactating mammary glands.

In order to assess the lipid synthesis capabilities of *Ctr* and *Miz1ΔPOZ* mammary glands, a Sudan III lipid staining was performed using lactation day 6 cryosections. As can be seen in Fig. 3.29 at different magnifications, fat droplets coalesced forming very large aggregates in the lumina of *Miz1ΔPOZ* alveoli. These lipid accumulations were much smaller in time-matched *Ctr* glands.

A similar lipid aggregation phenotype was observed in a recent publication (Le Guillou et al., 2012a), where this defect is explained by impaired calcium transport. Calcium positively regulates the size of milk fat globules as previously reported (Valivullah et al., 1988).

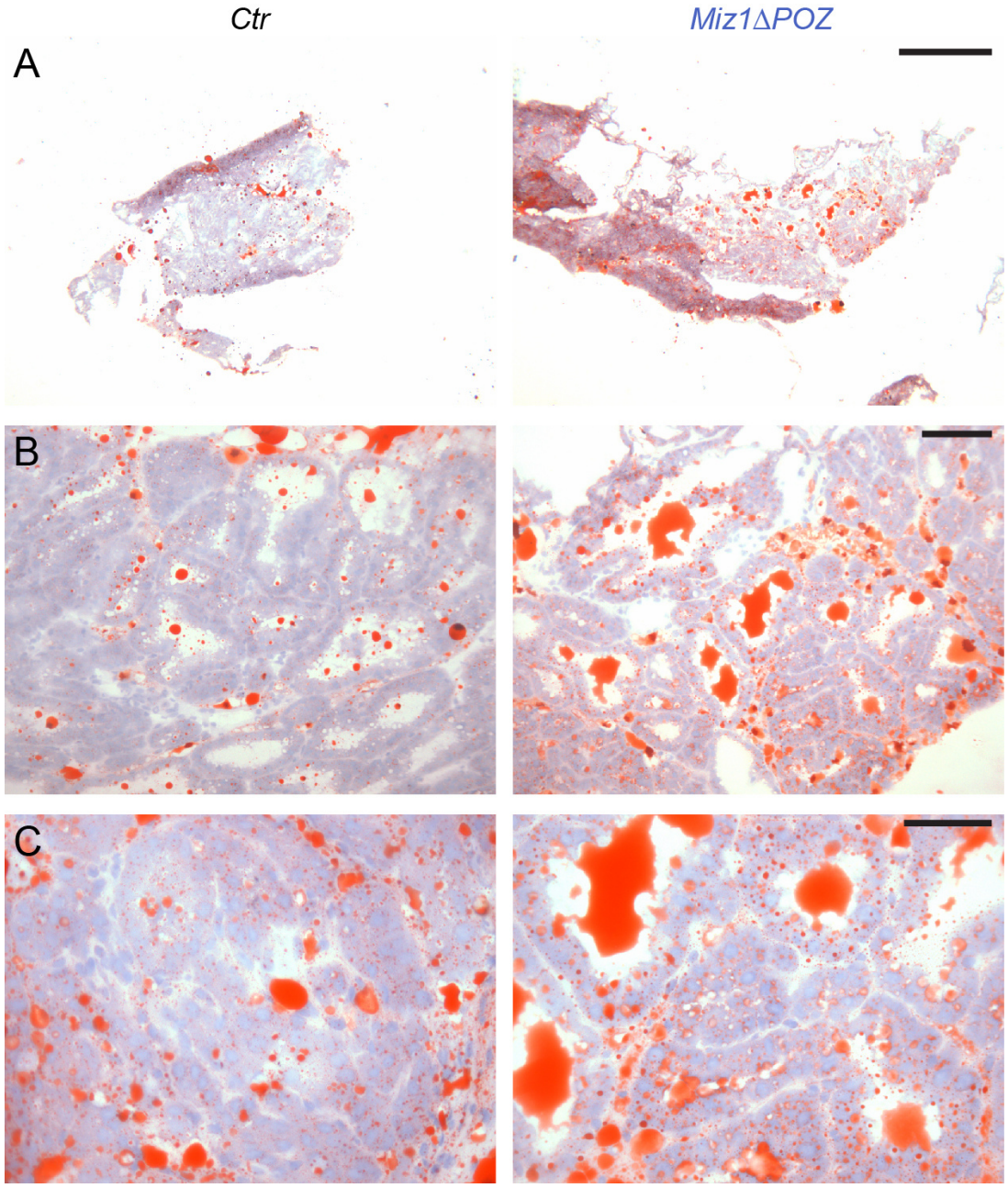

Figure 3.29: Lipid aggregation in lactation day 6 *Miz1ΔPOZ* mammary glands. Sudan III staining was performed on cryosections from *Ctr* and *Miz1ΔPOZ* glands at lactation day 6 (n=4 per genotype). Different magnifications are shown. Scale bars: 500 µm in A, 100 µm in B and 50µm in C.

Le Guillou et al. point to a deregulation of the expression of a number of genes which control calcium transport to explain the fat accumulation in the lumina of alveolar cells observed upon overexpression of miR-30b. Namely, *Clca1* and *Clca2* are upregulated and *Camk2b* and *Ano4* are downregulated in animals which display lipid aggregation.

Interestingly, a similar gene expression pattern was observed in our microarray analysis (see Fig. 3.32) of lactation day 6 samples after comparing *Miz1ΔPOZ* animals in relation to *Ctr* mammary glands (*Clca1*: 4.6-fold up; *Clca2*: 5.4-fold up; *Camk2b*: 3.8-fold down; *Ano4*: 1.6-fold down). This observation was further confirmed by qPCR as shown in Fig. 3.30.

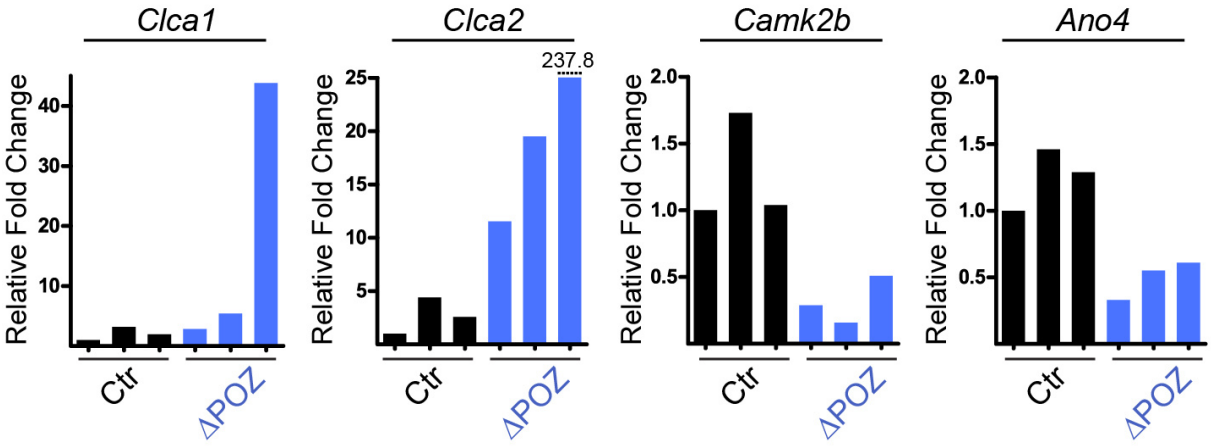

Figure 3.30: Expression data of genes which regulate calcium transport in lactation day 6 samples. qPCRs showing the relative expression of *Clca1*, *Clca2*, *Camk2b* and *Ano4* in *Ctr* and *Miz1ΔPOZ* mammary gland samples at lactation day 6. Each bar represents an individual animal.

Clca1 and Clca2 proteins are chloride channels activated by calcium which share great homology in their sequence but not in tissue pattern expression (Pauli et al., 2000; Leverkoehne et al., 2002; Loewen and Forsyth, 2005). As already described by Leverkoehne et al., *Clca1* expression is very low or negligible during the different stages of mammary gland development while *Clca2* is highly expressed in lactating and involuting mammary glands when compared to other murine tissues. This observation was further supported with our own qPCR data using lactation day 6 samples (*Clca1* expression was found much lower than the one from *Clca2*). The expression of both genes was greatly upregulated in mutant glands (Fig. 3.30).

Calcium/calmodulin-dependent kinase type IIβ (coded by the gene *Camk2b*) is a serine/threonine kinase which is activated upon increase of the intracellular levels of calcium and has an important role in synaptic plasticity in the central (Yamauchi, 2005) and peripheral nervous systems (Waggener et al., 2013), although it is expressed ubiquitously. Anoctamin 4 (coded by *Ano4*) belongs to the family of anoctamins (10 different proteins) which are chloride channels that have been shown to be also transiently activated by an increase of the intracellular levels of calcium (Tian et al., 2012). *Camk2b* and *Ano4* are both downregulated in mutant glands. Taken together,

the deregulation of calcium transport or flux in *Miz1ΔPOZ* mammary glands could account for the accumulation of lipid observed in the lumina of mutant mammary glands as previously described for miR-30b overexpression (Le Guillou et al., 2012a).

3.4.12. Confirmation and extension of the qPCR expression data by microarray analysis.

As already mentioned in Sections 3.4.6 and 3.4.11, a mouse genome Agilent array was performed for the analysis of gene expression on 1st pregnancy lactation day 6 mammary glands (n=4 per genotype). Interestingly, the number of genes downregulated in *Miz1ΔPOZ* glands was much higher than the ones upregulated, when compared with *Ctr* mice. After setting the threshold for fold change (FC) of relative gene expression to ±2, a total of 98 genes were found upregulated and 167 were downregulated in *Miz1ΔPOZ* versus *Ctr* glands. If the threshold was arbitrarily set to 1.5, the list of upregulated genes comprised 478 genes and the one of those with downregulated expression included 1033 genes (see Venn diagrams in Fig. 3.31A). Thus, the data suggest that, at least in the mammary gland, Miz1 is more often an activator of gene transcription than a repressor, taking into account that it is well documented that this protein can carry out both functions (Herkert and Eilers, 2010; Möröy et al., 2011).

A bioinformatic analysis, using David Bioinformatics software, revealed several functional groups formed by the regulated genes obtained after comparison of array data from *Miz1ΔPOZ* versus *Ctr* mammary glands. The four most significant Gene Ontology (GO) terms provided by the software are represented in Fig. 3.31B. The relative abundance of genes between each of these groups is related to the size of the portions of the diagram. Two of the functional groups which systematically appeared in the different analysis of upregulated genes were “Immune response” and “Response to stress”. Miz1 is generally regarded as a cell cycle regulator, so it was not surprising to find this functional group when subjecting the list of upregulated genes in *Miz1ΔPOZ* glands to bioinformatic analysis. The most abundant lists of downregulated genes in mutant animals were the following: “Cellular metabolic process” and “Anatomical structure development”. These very general functional groups probably include some genes which would normally be directly activated by Miz1 and are downregulated in *Miz1ΔPOZ* mice.

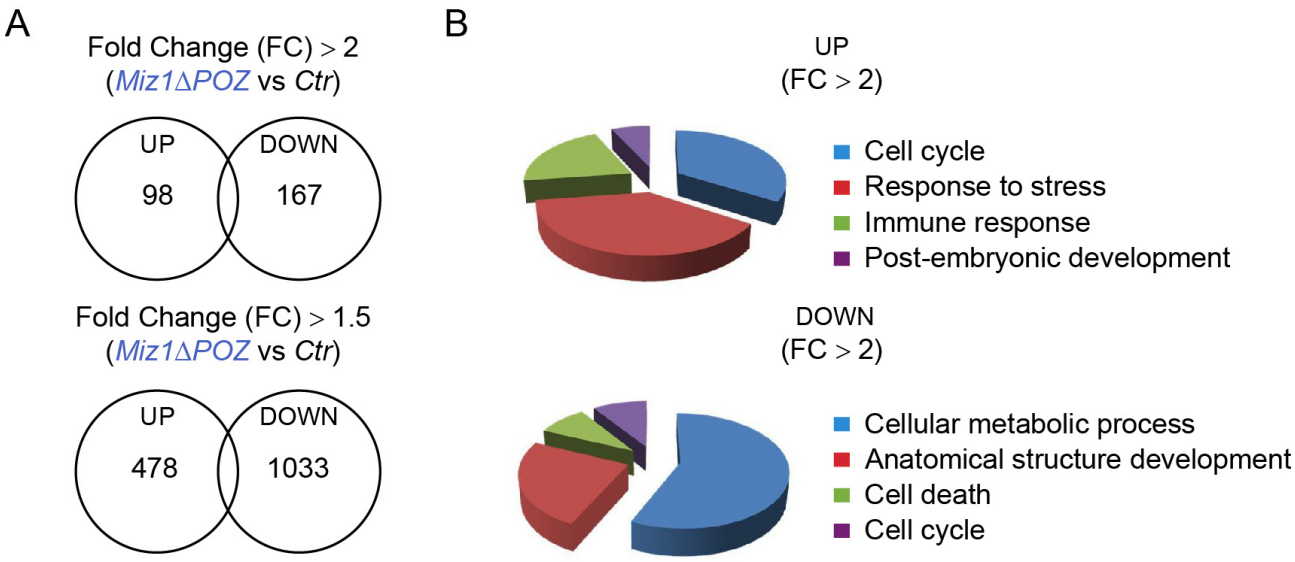

Figure 3.31: Bioinformatic analysis of the lactation day 6 microarray. (**A**) Number of regulated genes in *Miz1ΔPOZ* mammary glands using different Fold Change (FC) thresholds. Note the increased number of genes downregulated in *Miz1ΔPOZ* animals. (**B**) The 4 most significant Gene Ontology (GO) terms were obtained using lists of genes regulated FC>2 and the Functional Annotation tool on David Bioinformatics v6.7. Cell functions are represented by relative gene abundance between groups.

In order to provide a general view or summary of the molecular data obtained in this section dealing with the lactation defect phenotype observed in *Miz1ΔPOZ* dams, the microarray expression values of genes involved in the different cellular functions already discussed are represented in Fig. 3.32. When distinct values of Fold Change (FC) from the microarray analysis were available these were averaged. This is the reason why only some bars have standard deviation. The expression data of most of the genes provided in Figure 3.32 were further validated by qPCR and both approaches led to fairly similar results. Stat5 target genes (Yamaji et al., 2012), of both classes A (*Csn1s2a*, *Csn2*, *Csn1s1* or *Csn3*) and B (*Wap* and *Csn1s2b*), were found downregulated in *Miz1ΔPOZ* glands, providing further evidence of the decreased activation of the Jak2/Stat5 pathway observed in mutant dams. The expression of crucial receptors (*Prlr* and *Erbb4*) that modulate the phosphorylation of Stat5 was also downregulated in *Miz1ΔPOZ* mammary glands. When negative regulators of the Jak2/Stat5 pathway were scrutinized, as already described by qPCR, the expression of *Socs1*, *Socs3* and *Cav1* was found not significantly different in *Miz1ΔPOZ* animals. Only *Socs2*, a Stat5 target gene, was downregulated in mutant mammary glands. Regarding mammary cell proliferation, *Mki67* was

downregulated in *Miz1ΔPOZ* glands, correlating with the immunohistochemistry and qPCR data already provided (see Figures 3.21 and 3.22).

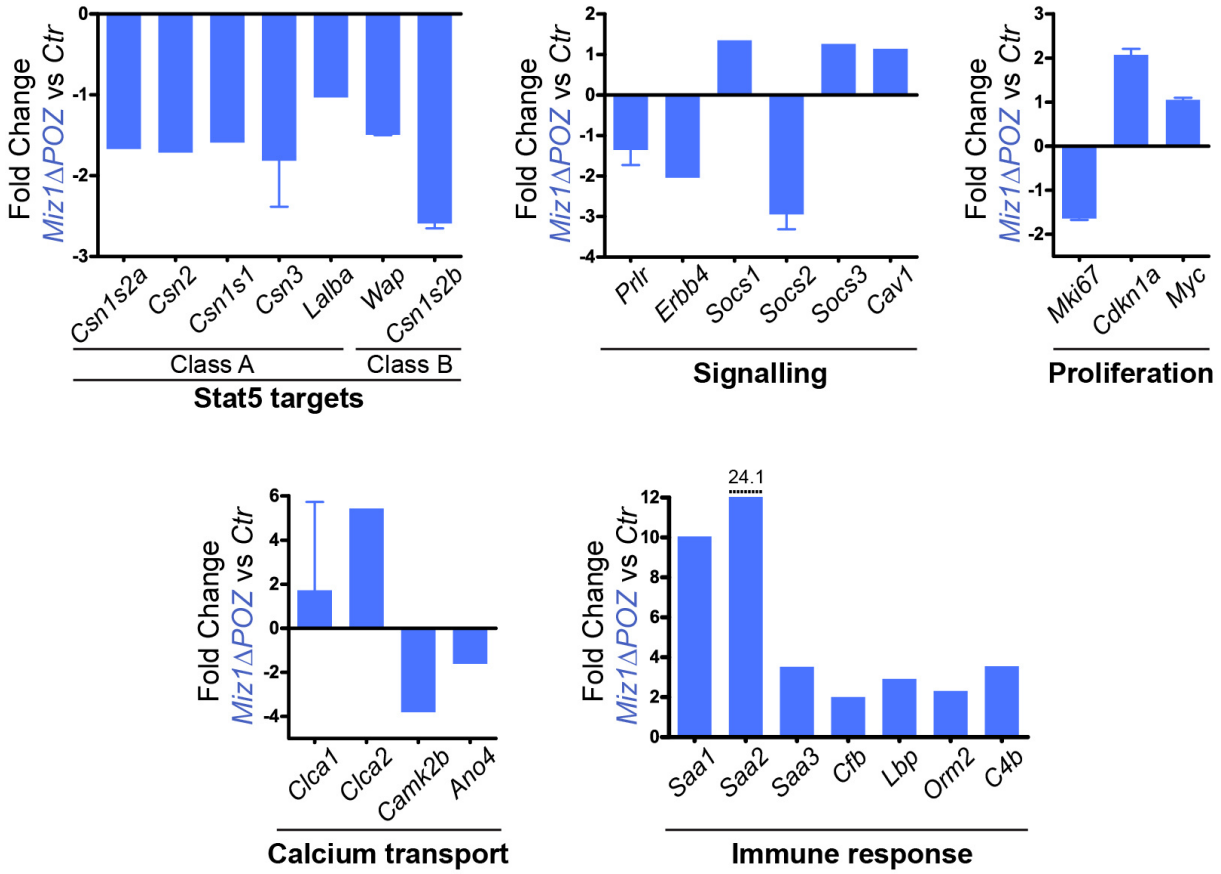

Figure 3.32: Summary of microarray data. Functional gene groups derived from the lactation day 6 microarray after normalization and filtering of the data. The relative gene expression is shown comparing *Miz1ΔPOZ* versus *Ctr* mammary glands. Fold changes were averaged when different values for the same gene were available. See Material and Methods for experimental details related to the Agilent Microarray.

Continuing with the analysis of the array data of lactation day 6 samples, *Myc* expression was not significantly different between genotypes and *Cdkn1a* was upregulated about twofold in *Miz1ΔPOZ* glands. In the case of *Cdkn1a*, the expression of this cell cycle arrest regulator in the mammary glands of *Miz1ΔPOZ* mice was found to be quite heterogeneous when validating the array data by qPCR. Some mutant animals had high mammary levels of *Cdkn1a* mRNA at lactation day 6 while others expressed amounts comparable to those detected in *Ctr* mice. Several qPCRs were performed with n=3, n=4 and n=6 animals per genotype but, as shown in Fig. 3.22B, the expression of *Cdkn1a* was not significantly different in *Miz1ΔPOZ* mammary glands,

independently of the number of biological replicates analysed. In regard to the calcium transport genes, which might regulate lipid aggregation, and also in consonance with the data shown in Fig. 3.30 by qPCR, the expression in the array of *Clca1* and *Clca2* was greatly upregulated, while *Camk2b* and *Ano4* were both downregulated in mutant glands.

As mentioned above, a number of immune response genes were greatly upregulated in lactating mutant glands. The Gene Ontology (GO) terms "Immune response" or "Response to stress" appeared very frequently in the different functional analysis performed with David Bioinformatics comparing mutants to controls (see Fig. 3.31B). Distinct mRNAs which are normally expressed in the acute phase of an inflammatory process were upregulated in mutant glands at lactation day 6: *Saa1*, *Saa2*, *Saa3*, *Lbp* and *Orm2*. In addition, mRNAs related to the activation of the complement system were also highly expressed in mutant glands: *Cfb* and *C4b* (Fig. 3.32). A possible explanation for the "immune response" gene signature observed in mutant dams will be provided in the Discussion section. Despite the expression of these genes, F4/80 immunohistochemistry did not reveal an increased recruitment of macrophages to the mammary alveoli of *Miz1ΔPOZ* mice at lactation day 6 (data not shown).

3.4.13. Miz1 regulates vesicular transport gene expression

In order to gain insight into the mechanism underlying the observed lactation phenotype, data from Miz1 ChIP-Seq experiments using the MDA-MB231 mammary epithelial cell line (Cailleau et al., 1974) were analysed. The data were provided by Dr. Björn von Eyss (Prof. Martin Eilers lab, Biocenter, Würzburg, Germany). In these ChIP-Seq experiments, 830 promoters bound by Miz1 were identified in MDA-MB231 cells. To elucidate how Miz1 regulates these target genes during lactation, Dr. Elmar Wolf (Prof. Martin Eilers lab, Biocenter, Würzburg, Germany) created a gene set with the 100 most strongly Miz1-bound genes (sorting by ChIP-Seq tag number) and correlated this list with the gene expression data from our cDNA microarray experiments performed on day 6 of lactation. This Gene Set Enrichment Analysis (GSEA) showed that a majority of Miz1 direct target genes are down-regulated in *Miz1ΔPOZ* animals (data not shown). All down-regulated genes which had at least 200 binding tags in the ChIP-Seq experiment are represented in Table 3.1. Interestingly, 13 out of the 23 identified genes (represented in grey color in Table 3.1) encode for proteins related to vesicular transport processes.

Gene symbol	Binding [tags]	Regulation ΔPOZ/Ctr [log2FC]	Process/function
Gphn	1355	-0,64397	protein localization, synaptic structure
Exoc2/Sec5	1173	-0.78775	membrane Trafficking, translocation of GLUT4 to the plasma Membrane
Mrps23	1158	-0,41446	structural ribosomal protein
Vamp4	1105	-0.98223	SNARE interactions in vesicular transport
Tbc1d14	1029	-0.40866	regulation of autophagic vacuole assembly
Lrp12	977	-0.74450	endocytosis
Heatr5a	949	-0,55225	unknown
Vps28	899	-0.87396	endocytosis
Wdr13	893	-0,42085	unknown
Dctn6	873	-0.93368	dynein dependent vesicular transport
Tpk1	863	-0.42197	thiamine metabolism
Ambra1	841	-0.48620	regulation of autophagic vacuole assembly
Pdcd5/ TFAR19	795	-1.00497	apoptosis
Vps13d	736	-0.23141	Golgi localisation
Pikfyve	729	-0.48238	phosphatidylinositol metabolic process, endocytosis
Snx18/ Snag1	724	-0.56591	endosomal transport
Tbxas1	702	-0.66024	oxidation-reduction process, iron/heme metabolism
Tcea1	645	-0.83292	regulation of DNA-dependent transcription
Tmbim4	645	-0,49351	apoptosis
Nrip1	445	-0,54765	mammary gland development, energy metabolism
Spast	428	-0.47523	microtubule dependent vesicular transport
Dync2h1	374	-0.56335	dynein dependent vesicular transport
Inpp5A	351	-0.43089	phosphatidylinositol metabolic process, endocytosis

Table 3.1: Miz1 targets in MDA-MB231 mammary cells which are down-regulated in lactating *Miz1ΔPOZ* mammary glands. ChIP-Seq data from MDA-MB231 cells were combined with microarray expression analysis data obtained from control and *Miz1ΔPOZ* mammary gland tissue at lactation day 6. Listed are genes which show a strong Miz1 binding (>200 binding tags) and a down-regulation in *Miz1ΔPOZ* animals. Genes which code for proteins related to vesicular transport processes are highlighted in grey. Table created in collaboration with Prof. Hans-Peter Elsässer (Institute of Cellular Biology, Marburg, Germany), Dr. Elmar Wolf and Dr. Björn von Eyss (both from Prof. Martin Eilers lab, Biocenter, Würzburg, Germany).

Quantitative PCR further validated the lactation microarray analysis data. The expression of several Miz1 targets in MDA-MB231 cells, which code for proteins involved in vesicular transport processes, was downregulated in *Miz1ΔPOZ* mice (Fig. 3.33A). Moreover, ultrastructural analysis of the secretory vacuoles (Fig. 3.33B) revealed a higher percentage of casein micelle containing vacuoles ($p<0.0011$) in *Miz1ΔPOZ* animals (Fig. 3.33C) when lactation day 10 samples were analysed. In addition, a higher, but statistically not significant ($p=0.1127$), mean number of micelles per vacuole was observed in *Miz1ΔPOZ* animals. The data suggests that the formation, transport or sorting of secretory vesicles could be altered in *Miz1ΔPOZ* mammary glands. This observation correlates with the reported direct binding of Miz1 to genes which regulate vesicular transport in MDA-MB231 mammary epithelial cells and the reduced expression of these in *Miz1ΔPOZ* lactating glands.

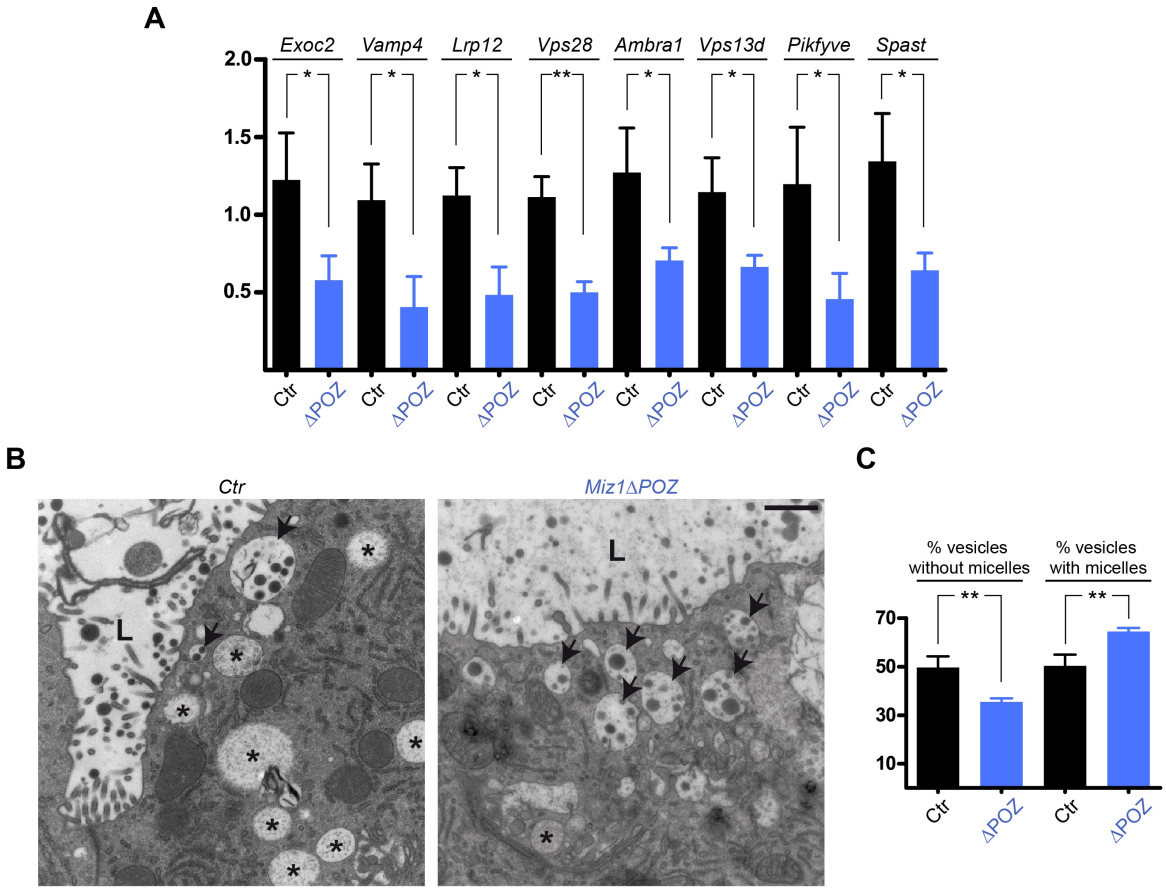

Figure 3.33: Genes related to vesicular transport processes are bound by Miz1 and downregulated in *Miz1ΔPOZ* mammary glands. (**A**) Quantitative PCRs of several genes related to vesicular transport from Table 3.1. (**B**) Electron microscopy showing vesicles with (arrows) and without (asterisks) casein micelles in tissue from control and *Miz1ΔPOZ* animals. (**C**) Vacuole type quantification in mammary glands of control and *Miz1ΔPOZ* animals from lactation day 10 (n=4). Total number of vacuoles counted: Control, 309-379; *Miz1ΔPOZ*, 339-404. Scale bar in B: 1 µm.

More experiments addressing development, maturation and transport of different intracellular vesicles are required to obtain a consistent model about the function of Miz1 in lactating mammary gland cells.

3.4.14. Decreased Prolactin receptor and ErbB4 expression in *Miz1ΔPOZ* lactating glands.

The Prolactin receptor (Ormandy et al., 1997; Grimm et al., 2002) and ErbB4 (Long et al., 2003) are of outstanding importance for proper mammary proliferation and differentiation. They modulate the phosphorylation and activity of Stat5. ErbB4 acts like a chaperone, favoring the nuclear translocation of phosphorylated Stat5 into the cell nucleus (Williams et al., 2004). The ChIP-Seq experiment revealed that Miz1 did neither bind *Prlr* nor *Erbb4* directly. However, by immunofluorescence, prolactin receptor was hardly detectable in the plasma membrane of the epithelial cells from *Miz1ΔPOZ* lactating mammary glands (Fig. 3.34A) and nuclear ErbB4 was also reduced in mutant dams (Fig. 3.34B).

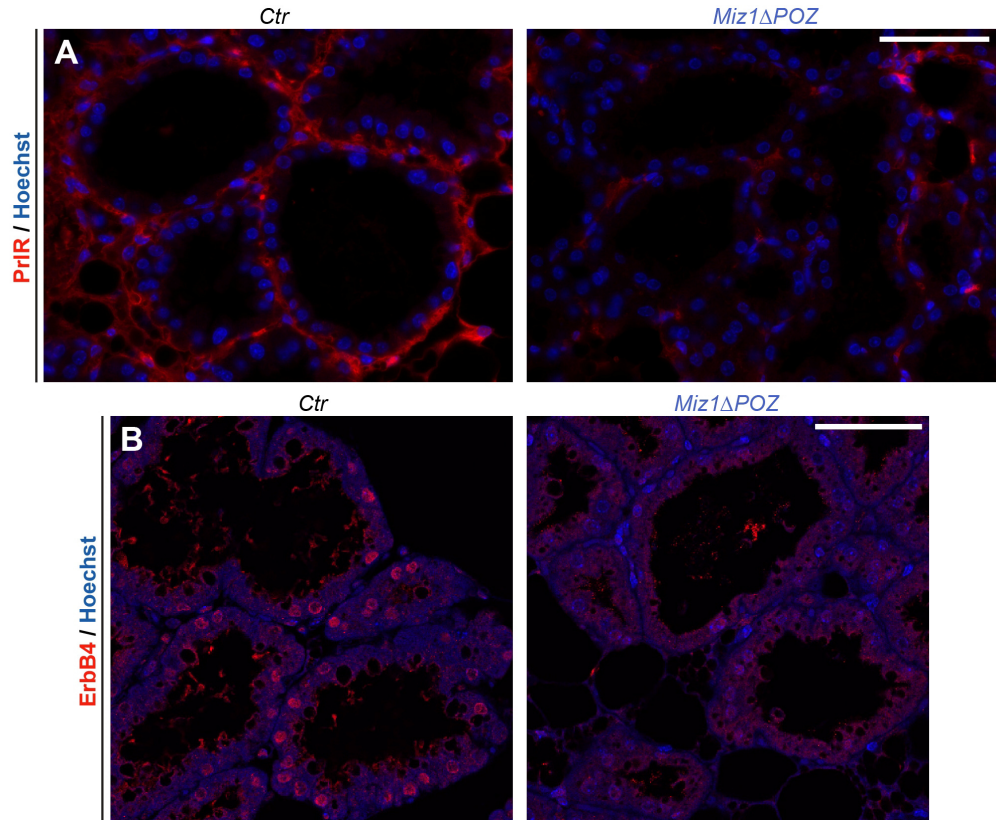

Figure 3.34: Protein expression and localization of the prolactin receptor (PrlR) and ErbB4. PrlR (**A**) and ErbB4 (**B**) immunofluorescence (red) from control and *Miz1ΔPOZ* mammary gland tissue at lactation day 6. Nuclei were stained with Hoechst (blue). Scale bars in A and B: 50 µm.

In conclusion, the deletion of the Miz1 POZ domain in luminal mammary cells had an impact on the expression of a number of genes which regulate distinct intracellular vesicular transport processes. The sorting into the membrane of important receptors for mammary proliferation and differentiation like the Prolactin receptor (PrlR) or ErbB4 could be impaired by deranged vesicular transport. Reduction of PrlR and ErbB4 expression and their diminished availability at the cell surface can explain the decreased amount of phosphorylated Stat5 in the nucleus of *Miz1ΔPOZ* mammary cells during lactation. Thus, the reduced levels of pStat5 cannot adequately activate the transcription of proliferation and differentiation genes in *Miz1ΔPOZ* glands leading to the lactation phenotype observed.

4. DISCUSSION

4.1. Expression of Miz1 and Myc during postnatal mammary development

The study of the expression and function of proteins important for human health in normal development provides valuable information for the design of therapeutical opportunities in the context of disease. Myc is one of the current most promising targets for a number of cancer types including triple-negative breast cancer (Dang, 2012) and Miz1 has been shown to play an important role in Myc-mediated tumorigenesis (Wiese et al., 2013). Precise knowledge about the expression of the Miz1/Myc complex during the different stages of mouse mammary gland development was lacking in the literature and is analysed in this thesis.

A nuclear Miz1 and Myc staining was detected in the ducts of developing virgin mammary glands by immunohistochemistry (Fig. 3.1 and 3.2). As already reported, Myc expression substantially increases during early pregnancy (Master et al., 2002; Blakely, 2005; Stoelzle et al., 2009) and these high levels correlate with the stimulation of cell division during this phase of enhanced proliferation (Fig. 3.2). At the end of pregnancy, the immunohistochemical staining of Myc was detected in lymph nodes (internal positive control), but not in mammary alveolar cells where Miz1 protein was also found at very low levels (Fig. 3.1 and 3.2). In contrast, Miz1 expression in the murine mammary gland was clearly boosted with the onset of lactation. By Western blotting, Miz1 protein could not be detected at the end of pregnancy (day 18.5), but was evident during lactation from day 1 after parturition (Fig. 1B; days 1 and 10 of lactation were also analysed, data not shown). The physiological upregulation of the endogenous levels of Miz1 in this particular developmental stage points to its significance during pup nursing. The lactation defect observed in Wap-Cre *Miz1ΔPOZ* mice supports this notion. The reason for the upregulation of Miz1 during lactation is still not clear. Two hormones play important roles in the mammary gland after parturition: prolactin stimulates milk protein synthesis in the luminal compartment of mammary alveoli, while oxytocin contributes to the contraction of myoepithelial cells for efficient milk ejection (Neville et al., 2002). Addition of prolactin in the DIP lactogenic cocktail (containing also insulin and dexamethasone) to confluent HC11 mammary cells did not result in an upregulation of Miz1 as shown by qPCR and Western blotting (Fig. 3.3). This was tested till 7 days after DIP-mediated induction of HC11 mammary cell differentiation (data not shown). Thus, prolactin does not induce Miz1 expression *in vitro* although a possible *in vivo*

effect should not be excluded. The hormone oxytocin might also constitute the trigger for Miz1 expression during lactation. Thus, oxytocin or prolactin could be directly administered *in vivo* to test whether Miz1 is induced in the mammary gland. Also, obtaining samples earlier than 24 hours after parturition can provide more precise information about the exact time point of Miz1 upregulation. Additional experiments are required to unequivocally identify the molecular events that lead to the increase of Miz1 expression at around parturition and that maintain these high protein levels in the mouse mammary gland throughout lactation. Miz1 was detected in the cell nucleus during most developmental phases analysed, although immunohistochemistry also demonstrated a cytoplasmic staining of Miz1 during lactation. Miz1 has been shown to be associated with microtubules in the cytoplasm (Ziegelbauer et al., 2001; Ziegelbauer et al., 2004) and cellular treatment with the microtubule depolymerization agent T113242 (Lu et al., 2012) results in the translocation of Miz1 from the cytoplasm to the cell nucleus (Ziegelbauer et al., 2001). Also, Myc was reported to sequester Miz1, which lacks an intrinsic nuclear localization signal, into the cell nucleus upon Myc overexpression (Peukert et al., 1997). Although Miz1 function in the cytoplasm remains obscure, some immunosuppressive functions of Miz1 in this cellular compartment were already described (Liu et al., 2009).

Myc levels during lactation remain low although the function of this transcription factor has been shown indispensable for a proper translation of milk proteins and the conditional knockout of Myc in the pregnant mammary gland also leads to a lactation defect (Stoelzle et al., 2009). *In vitro*, Myc expression decreases as HC11 cells become confluent and the protein can hardly be detected during mammary differentiation after DIP addition to the medium (Fig. 3.4; Grolli et al., 1997). As stated earlier, Miz1 can act as a transactivator or as a transrepressor in collaboration with other proteins (Möröy et al., 2011). The decreased levels of Myc during lactation could favor Miz1 function as an activator of transcription as less repressive Miz1/Myc complexes would be available. Microarray analysis of samples from lactating mammary glands corroborate this view as two thirds of significantly regulated genes have a decreased expression in *Miz1ΔPOZ* glands (Fig. 3.31). In addition, acetylated lysine 9 and trimethylated lysine 4 of histone H3 (AcH3K9 and H3K4me3), marks of transcriptionally active chromatin, were found in 553 Miz1 target genes out of the total 734 Miz1-bound genes as shown in human embryonic stem (ES) cells using ChIP-on-chip analysis (Varlakhanova et al., 2011). Miz1 also seems to act predominantly as a transactivator in the lactating mammary gland although its repressive function (e.g. in a Miz1/Myc complex) could have a great significance in other cell types or contexts, like cell cycle

arrest gene control and tumorigenesis (Hönnemann et al., 2012; Wiese et al., 2013). In ES cells, Miz1 and Myc are shown to share binding to 203 genes out of the 734 Miz1-bound genes (Varlakhanova et al., 2011). Thus, Myc-independent functions of Miz1 are obvious and have already been described in the immune system, the cerebellum (Kosan et al., 2010; Saba et al., 2011; Wolf et al., 2013) and now, with this work, in the lactating mammary gland.

ChIP-Seq data generated in Prof. Eilers´ lab point to the regulation by Miz1, through direct binding, of a number of genes important for vesicular transport, endocytosis, autophagy and lysosomal biogenesis (Wolf et al., 2013). The expression of many of these genes bound by Miz1 in cells of a human mammary cell line was downregulated in mutant lactating glands, as observed by microarray analysis and validated by quantitative PCR (Fig. 3.32 and 3.33). An interesting question that derives from these data arises: would Miz1 bind to the same set of genes in a proliferating ductal cell in the virgin gland as in an alveolar cell actively producing milk proteins? Performing ChIP-Seq experiments with chromatin samples from these distinct developmental phases would provide a feasible answer. Miz1 could potentially have different affinity for binding to the variable DNA motifs described (Wolf et al., 2013), as Myc has been shown to have a varying affinity to different canonical and non-canonical E-boxes (Fernandez et al., 2003; Lin et al., 2012). Lower affinity sites would only be occupied when the expression of the protein is high, as in the case of Miz1 in the mammary gland during lactation. A similar analysis was performed studying the occupancy of Miz1 and Myc in *Hox* genes after inducing the differentiation of ES cells into embryoid bodies (EBs) (Varlakhanova et al., 2011). Comparable experiments would be of particular interest in the mammary gland.

After lactation is completed and upon cessation of pup suckling, cell death and tissue remodeling shape the involuting mammary gland in a highly coordinated manner (Watson and Kreuzaler, 2011b). Myc has been described as a mediator of accelerated apoptosis in SOCS3-deficient involuting mammary glands where high levels of pStat3 stimulate Myc expression (Sutherland et al., 2006). A sudden decrease of the expression of Miz1 in the mammary gland was detected 48 hours after removal of the pups from the mother (Fig. 3.1). This suggests that Miz1 is possibly not required when apoptosis is triggered in the early steps of involution. The described function of Miz1 as an activator of the anti-apoptotic gene Bcl2 (Patel and McMahon, 2007) would be in agreement with this view. The analysis of Miz1 expression and apoptosis, comparing wildtype and *Miz1ΔPOZ* glands in more time points after the initiation of involution, would be required to more precisely assess the possible role of Miz1 in this remodeling phase.

4.2. Impact of Miz1 in the virgin gland and mammary stem cells

As stated earlier, a nuclear Miz1 staining was detected in ductal cells of the pubertal mammary gland (Fig. 3.1). To study the function of Miz1 in the virgin gland, MMTV-Cre (Line A) mediated deletion of the POZ domain of this transcription factor in the luminal and basal compartments of the mouse mammary gland was accomplished (Fig. 3.5). Recombination under the MMTV promoter takes place already during embryonic development and occurs also in stem/progenitor cells (Buono et al., 2006; Jiang et al., 2010). Thus, despite some unspecific tissue recombination, MMTV-Cre animals are a good model to study stem cell function and mammary branching in the virgin gland (Wagner et al., 2001), but are not suitable for lactation research due to the fact that the integration of the transgene results in a reduced mammary alveologenesis as recently described (Robinson and Hennighausen, 2011; Yuan et al., 2011).

The development of the ductal epithelial tree through the adipocyte-rich stroma or fat pad was analysed in *Ctr* and *Miz1ΔPOZ* animals by whole-mount preparations after carmine alum staining (Fig. 3.6-3.8). Although the mammary gland finally develops normally in mutant mice (Fig. 3.8), a developmental delay was observed in 30-day old *Miz1ΔPOZ* animals. At this time point, terminal end buds (TEBs) already reach the lymph node in control animals while the rudimentary epithelial tree remains close to the nipple and TEBs are not as obvious in *Miz1ΔPOZ* glands (Fig. 3.6). By 45 dpp, ductal elongation is variable in knockouts allowing the hypothesis of a heterogeneous extent of Cre-mediated recombination of the exons which code for the POZ domain in different animals (see floxed and recombinant bands in the Miz1 genotyping gel of Fig. 3.5B). Two of the three knockout animals analysed had developed normally at 45 dpp, while the other had a clear delay in the migration of the TEBs, not observed in any of the 6 wildtype animals studied at this time point (Fig. 3.7 and data not shown). Finally, no obvious differences were observed in ductal elongation or branching morphogenesis in mammary glands from *Ctr* and *Miz1ΔPOZ* animals at 65 dpp (Fig. 3.8).

TEBs progress through the fat pad by an incompletely understood mechanism which involves collective cell migration (Ewald et al., 2008), regulation of endocrine signals, extracellular matrix (ECM) remodeling, stromal-epithelial interactions and cell adhesion (Hinck and Silberstein, 2005). In regard to this, Miz1 has recently been linked to cellular migration by positively regulating *RhoA* gene expression in a complex with the Myc/Max/p300/Skp2 proteins (Chan et al., 2010). These data are still controversial, considering the existing model of Myc-mediated

repression and the fact that Miz1 binding at the *RhoA* promoter could not be detected in several cell lines recently analysed by ChIP-Seq (Wiese et al., 2013). More experiments would be required to ascertain the possible role of Miz1 in cellular migration. Miz1 levels have been shown to be high in metastatic prostate cancer compared to primary prostate tumors (Chan et al., 2010). Metastatic cells disseminate to secondary organs in a complex mechanism which involves cellular migration (Bravo-Cordero et al., 2012) and it would be interesting to extend the mentioned analysis (Chan et al., 2010) to other tissues and rule out a more general positive correlation between Miz1 expression and metastasis.

Also, E-cadherin was shown to be important for collective cell migration in epithelial sheets maintaining tight cell-cell adhesion contacts (Li et al., 2012). E-cadherin expression was found indistinguishable between control and *Miz1ΔPOZ* virgin ducts by immunofluorescence staining analysis (data not shown; collaboration with Hedyeh Kiaveh). As described earlier, ECM remodeling is important for a proper mammary ductal morphogenesis in the virgin mammary gland. Integrins are crucial trans-membrane receptors necessary for the adhesion between cells and the ECM and for maintaining cell-cell contacts (Raymond et al., 2012; Glukhova and Streuli, 2013). Unexpectedly, MMTV-Cre mediated deletion of ß1 integrin does not impair mammary ductal morphogenesis in the virgin gland (White et al., 2004), but K5-Cre basal ablation does (Taddei et al., 2008). Despite the fact that the Miz1/Myc complex has been shown to regulate ß1 integrin expression in keratinocytes by direct binding (Gebhardt, 2006), we could not detect obvious differences in ß1 integrin expression between control and *Miz1ΔPOZ* virgin ducts by immunohistochemistry (data not shown; collaboration with Hedyeh Kiaveh).

In addition to E-cadherin, ductal cellular architecture was analysed by immunostaining of ß-catenin (luminal marker) and cytokeratin-14 (basal marker) in control and mutant mammary ducts and no differences were observed between both genotypes (data not shown; collaboration with Hedyeh Kiaveh). Interestingly, 45 day-old knockout ducts displayed less cellularity compared to aged-matched controls and the continuity of the luminal cell epithelium was seriously disrupted in various *Miz1ΔPOZ* virgin ducts (Fig. 3.9). In line with these observations, decreased proliferation in mutant glands was observed by Ki67 immunohistochemistry (data not shown; collaboration with Hedyeh Kiaveh). Diminished Ki67 positivity was also observed in WAP-Cre *Miz1ΔPOZ* lactating mammary glands (Fig. 3.21) and in K14-Cre *Miz1ΔPOZ* papillomas in the skin (Hönnemann et al., 2012). Thus, the ability of cells to orderly proliferate in the absence of a functional Miz1 is compromised in different cellular contexts.

Further, qPCR data revealed a reduced expression of the EGF receptor ligand amphiregulin in *Miz1ΔPOZ* virgin glands (data not shown; collaboration with Hedyeh Kiaveh). Amphiregulin is one of the main drivers of estrogen and progesterone mediated pubertal ductal morphogenesis and proliferation, and it is highly expressed in invasive breast carcinomas (McBryan et al., 2008; Aupperlee et al., 2013). The binding of amphiregulin to the EGF receptor can occur after autocrine, paracrine or juxtacrine secretion of the ligand (Willmarth and Ethier, 2008). Although the expression of amphiregulin was clearly downregulated in *Miz1ΔPOZ* virgin glands compared to controls, the lack of a reliable antibody for immunohistochemistry and Western blotting hampered the yield of more conclusive results. In summary, the absence of the POZ domain of Miz1 in the virgin mammary gland led to a modest phenotype characterized by a delay in ductal morphogenesis in mutant glands, while *Miz1ΔPOZ* ducts displayed less cellularity correlating with a decreased Ki67 positivity. The expression of luminal and basal markers in virgin mammary ducts was not affected by Miz1 POZ domain deletion. The mechanism to explain the delay in mammary duct morphogenesis observed in *Miz1ΔPOZ* mammary glands remains to be elucidated.

The mammary gland has emerged as a valuable organ for stem/progenitor cell studies due to the development of *in vivo* (e.g. transplantation of mammary cells or tissue into the cleared fat pad of immunocompromised mice or lineage tracing experiments) and *in vitro* (e.g. mammosphere culture) techniques, which allow the determination of the mammary stem cell frequency in a cellular population and the enrichment of stem/progenitor cells in culture (Deome et al., 1959; Dontu and Wicha, 2005b; Van Keymeulen et al., 2011b). Currently, Myc is recognized as a crucial cellular pluripotency regulator (Kim et al., 2010; Smith et al., 2011; Chappell and Dalton, 2013) and is indispensable for the maintenance of the mammary stem cell compartment (Stoelzle et al., 2009; Moumen et al., 2012; Moumen et al., 2013). On the other hand, the role of Miz1 on stem cell function alone or in association with Myc is still incompletely understood. Of note, the stem cell compartment in the hair follicle bulge region of the skin is not altered by Miz1 POZ domain deletion under the K14-Cre promoter as shown by BrdU labeling and immunofluorescence of the skin stem cell markers cytokeratin 15 and CD34 (Hönnemann et al., 2012). Also, overexpression of Myc in neural progenitor cells (NPCs) leads to an increased neurosphere formation and neural stem/progenitor cell accumulation while forced expression of the $Myc^{VD/VD}$ mutant, unable to bind to Miz1, is unable to stimulate self-renewal as efficiently as wildtype Myc (Kerosuo et al., 2008). Inspired by this neural stem cell culture approach

(Reynolds et al., 1992), mammosphere experiments allow the estimation of the frequency of mammary stem/progenitor cells in a complex cellular population and its propagation through serial passaging by cultivation in serum-free semisolid medium (Dontu et al., 2003; Dey et al., 2009b). As described in this thesis, *Miz1ΔPOZ* mice accumulate mammary stem/progenitor cells after secondary and tertiary mammosphere culture (Fig. 3.10) through a Myc-independent mechanism (Fig. 3.11). Members of the hedgehog pathway (Ptch1, Ptch2, Smo, Gli1, Gli2 and Bmi1) have been shown to be highly upregulated in mammospheres compared to differentiated mammary cells and exogenous addition of Shh to mammary cells increases mammosphere formation in culture (Liu, 2006). However, mammary development is not altered in the absence of Shh *in vivo* (Gallego et al., 2002; Michno et al., 2003), although redundancy in the function of the different Hedgehog ligands (Shh, Dhh and Ihh) could explain the lack of phenotype in Shh mutants (García-Zaragoza et al., 2012). Work from our laboratory revealed a high expression of sonic hedgehog (Shh) by qPCR and Western blotting and a decreased amount of primary cilia in mutant virgin glands after staining acetylated tubulin (Hedyeh Kiaveh; data not shown). Miz1 has recently been shown to positively regulate the hedgehog pathway *in vitro* interacting with Smo and Gli2 by POZ domain-independent and dependent binding, respectively (Lu et al., 2013b). In this publication, Miz1 is shown to be recruited with Smo into the primary cilia, a process that would be possible in *Miz1ΔPOZ* mice, as Miz1 interacts through its C-terminus with Smo. In addition, ablation of the Myc binding domain of Miz1 (amino acids 641-715) has no effect on Gli activation (Lu et al., 2013b) suggesting that the interaction with Myc is not required for Miz1 regulation of the hedgehog pathway. This last point would be in agreement with our own observations on mammosphere formation in Myc and $Myc^{VD/VD}$ mice (Fig. 3.11). Also, binding of Miz1 to Gli2 would facilitate the accumulation of Gli2 at the tips of primary cilia and ciliogenesis seems to be not affected by Miz1 knockdown *in vitro* (Lu et al., 2013b). *In vivo*, Gli2 expression in the virgin mammary gland is only stromal while during pregnancy and lactation it is both epithelial and stromal (Lewis et al., 2001). Miz1 expression in the virgin gland was weak in the stroma and strong in the epithelial compartment (Fig. 3.1), so that the interaction between Miz1 and Gli2 might be rare in the *in vivo* situation and would need to be formally demonstrated. Although Shh is significantly upregulated in *Miz1ΔPOZ* glands, downstream components of the Hedgehog pathway (Ptch1, Bmi1, Gli1 and Gli2; data not shown) are not statistically altered in mutant glands, leading to the hypothesis of an increased Shh ligand secretion in mutant glands to compensate for the reduced amount of primary cilia, essential for hedgehog signalling (Goetz et

al., 2009), in *Miz1ΔPOZ* glands. The high levels of Shh observed in *Miz1ΔPOZ* glands could explain the accumulation of stem/progenitor cells seen in the mammosphere assays already described (Fig. 3.10) but more experiments are necessary to find the possible mechanistical difference between Miz1 regulation of the hedgehog pathway *in vivo* and *in vitro*. A likely function of Miz1 in dynein and kinesin-mediated vesicular transport along microtubules in the cytoplasm (Franker and Hoogenraad, 2013) has not been investigated so far, despite the fact that Miz1 is associated to microtubules (Ziegelbauer et al., 2001). Vesicular transport is required for the transfer of proteins from the cytosol and Golgi apparatus to the primary cilia, which depends on a functional polarized trafficking (Hsiao et al., 2012). Considering that Miz1 has been recently described as an activator of genes related to vesicular transport by direct binding to their promoters (Wolf et al., 2013), it would be interesting to investigate in more depth the requirement of Miz1 for a proper ciliogenesis and its impact on the Hedgehog signalling pathway.

Unequivocal mammary stem cell markers that would allow their prospective isolation are currently not known, although a considerable stem cell enrichment is already possible in virtue of the $Lin^{-}CD24^{+}CD29^{h}CD49f^{h}$ cell surface FACS sorting profile (Shackleton et al., 2006; Stingl et al., 2006; Santos et al., 2013). The two current models of mammary cell hierarchy favor either the existence of a multipotent progenitor that gives rise to luminal (ductal and alveolar cells) and basal (myoepithelial cells) progeny or a model in which two lineage-restricted populations of stem cells repopulate either the luminal or basal mammary compartments but not both (Visvader and Smith, 2011; Joshi and Khokha, 2012). Both hypothetic possibilities were supported recently by two research groups which agree on the fact that the behavior of mammary stem cells differs in transplantation experiments when compared to the physiological situation (Van Keymeulen et al., 2011b; van Amerongen et al., 2012). Although cells with the most repopulating or self-renewal potential in transplantation experiments express basal markers and reside in the basal mammary compartment (Makarem et al., 2013), recent data challenge these ideas pointing to the existence of separated populations of luminal and basal stem cells that contribute exclusively to their own compartment (Van Keymeulen et al., 2011b). Other lineage tracing experiments revealed that expression of Wnt signalling-associated protein Axin2 in the embryo marks the prospective luminal compartment while Axin2 positive cells in the prepubescent mammary gland finally contribute to the basal compartment (van Amerongen et al., 2012). Also, transplanted mouse basal mammary cells are both multipotent and lineage-restricted in primary recipients (Nguyen et al., 2014). In this publication, a novel clonal analysis via barcoding (Schmidt et al.,

2009) revealed that primary luminal clones occasionally transformed into bilineage ones in transplanted secondary mice. Luminal mammary cells seem to have lower repopulating abilities but display multilineage differentiation potential (Shehata et al., 2012). Even more recent data point to the existence of bipotent stem cells and long-lived progenitors based on a new 3D high resolution imaging method combined with inducible lineage tracing (Rios et al., 2014). The plasticity of mammary cells in their commitment in response to environmental cues is astonishing as progenitor cells from other tissues are able to reprogram into the mammary cell fate upon transplantation into the fat pad (Booth et al., 2008; Boulanger et al., 2012; Bruno et al., 2014). Although our understanding of mammary stem cells has increased substantially in the last years, more research will be required to unequivocally delineate the hierarchical cellular organization of the mammary gland.

As described in Section 3.3, the disruption of the interaction between Miz1 and Myc *in vivo*, by culturing $Myc^{+/+}$ and $Myc^{VD/VD}$ knock-in primary cells, neither affected the mammary stem/progenitor cell frequency nor the mammosphere sizes observed (Fig. 3.11). Thus, the accumulation of stem/progenitor cells observed in MMTV-Cre *Miz1ΔPOZ* primary cells cultured as mammospheres could be Myc-independent as described in other systems (Kosan et al., 2010; Saba et al., 2011; Wolf et al., 2013). Unexpectedly, the culture of $Myc^{+/+}$ and $Myc^{VD/VD}$ knock-in primary cells in basement membrane extract (Cultrex) reveals an interesting phenotype concerning lipid droplet formation. As seen in Figs. 3.12 and 3.13, primary mammary cells produce lipid droplets in culture stimulated by the lack of serum in the medium (Deslex et al., 1987; Cabodevilla et al., 2013) and by the proadipogenic properties of Matrigel-like basement membranes (O'Connor et al., 2003; Lewis et al., 2012). While approximately 75% of all $Myc^{+/+}$ primary cells cultured on Cultrex basement membrane differentiated into lipid droplet-forming cells after 10 days of culture, only around 25% of $Myc^{VD/VD}$ knock-in primary cells contained lipid droplets at this time point (Fig. 3.13C). Several possibilities could account for the observed phenotype. As whole mammary glands were disaggregated and digested, a different proportion of preadipocytes might have been already present in the glands of the distinct mice before starting the culture. Another more likely explanation could be that the formation of a functional Miz1/Myc complex is required for proper adipocyte differentiation, which is enhanced by culture in serum-free and basement membrane-containing media. In relation to this, after induction of differentiation using a lactogenic hormone cocktail, HC11 mammary cells overexpressing Myc produced normal levels of ß-casein while forced expression of the $Myc^{VD/VD}$ mutant led to a

disrupted differentiation and hardly discernible ß-casein expression by semiquantitative PCR (data not shown). It would be interesting to assess the function of the Miz1/Myc complex in cellular differentiation also in other tissues examining the relative levels of both proteins before and during the differentiation process (as in Figs. 3.3 and 3.4), while simultaneously testing their DNA binding status in these different developmental stages by ChIP-Seq or ChIP-on-chip. Myc has been shown to be downregulated in many contexts at the onset of differentiation, including the mammary gland (Grolli et al., 1997 and Fig. 3.4), and to inhibit functional differentiation when overexpressed (Eilers and Eisenman, 2008). In spite of this fact, Myc can also promote functional differentiation in epithelial tissues like the skin (Gandarillas and Watt, 1997), sebaceous glands (Cottle et al., 2013) or the mammary gland (Schoenenberger et al., 1988b; Blakely, 2005). Thus, cellular context and Myc levels play an important role in the differentiation process (Watt et al., 2008). The function of Miz1 during mammary gland differentiation is discussed in detail in the section below.

4.3. Miz1 in the lactating mammary gland

Deletion of the Miz1 POZ domain in mammary gland epithelial cells during gestation (Fig. 3.14) rendered a functionally mutated Miz1 protein which causes a lactogenic defect in the first and second pregnancies (Figs. 3.16 and 3.17). Wap-Cre mediated gene deletion is generally regarded as a highly specific and temporally regulated mouse model, which allows the study of mammary differentiation and lactation *in vivo* (Wagner et al., 1997). Cre expression is limited to the luminal alveolar compartment of the mammary gland and starts after the second week of pregnancy (Wagner et al., 1997; Stoelzle et al., 2009 and Fig. 3.15). The lactation defect observed in *Miz1ΔPOZ* dams was characterized by a diminished proliferation and differentiation of the glandular cells which caused a delayed development of the mammary gland during lactation and resulted in malnutrition of the pups. The reduced proliferation and differentiation detected in lactating mutant glands was also recapitulated *in vitro* using mid-pregnant immortalized HC11 mammary cells with normal and low levels of Miz1 cultivated to form three-dimensional acini (Fig. 3.23) or induced to functionally differentiate by addition to the medium of a lactogenic cocktail containing prolactin (Fig. 3.25). As referred to earlier, Miz1 expression in the normal mammary gland is low at late pregnancy (P18.5) but dramatically increases during the transition from pregnancy to lactation (L1), where it remains high until day 2 of involution (Fig. 3.1). In

line with this notion, phenotypical differences of the mammary gland between control and *Miz1ΔPOZ* animals, like a transient reduction of the glandular tissue (Figs. 3.17 and 3.18), a decrease of milk protein expression (Fig. 3.24) and an extracellular coalescence of lipid droplets (Fig. 3.29), become visible not before lactation, although the Cre recombinase under the control of the Wap promoter was expressed already at day 14.5 of pregnancy (Fig. 3.14; Wagner et al., 1997; Stoelzle et al., 2009). The sudden increase and decrease of Miz1 protein levels at the beginning and end of lactation, respectively, supports the data provided showing that Miz1 has an important function in maintaining the lactation state of the mammary gland. Although standardized pup weights from control and *Miz1ΔPOZ* dams (n=6) were not altered at day 3 of lactation, they become statistically significant from day 6 on (Fig. 3.16). *Miz1ΔPOZ* glands finally catched up with controls in alveolar development (Fig. 3.19) but pup weights were not rescued in the 24-day period analysed and differences even increased throughout time (Fig. 3.16). This observation allowed us to think that although alveoli finally fill up mutant fat pads at lactation day 10, Miz1 is required for a proper mammary differentiation in a cell autonomous manner and this supposition was confirmed after inducing differentiaton in HC11 mammary cells with normal and low levels of Miz1 (Figs. 3.24 and 3.25). TUNEL assays and cleaved caspase-3 immunohistochemistry revealed that apoptosis is not playing a role in the phenotype observed in mutant glands (Fig. 3.20) and this observation could be recapitulated *in vitro* (Fig. 3.23F). These results are in line with *Miz1ΔPOZ* ablation in the skin where apoptosis is indistinguishable between control and mutant animals (Hönnemann et al., 2012).

Miz1 was originally found as a Myc binding protein (Peukert et al., 1997) and it was shown that the binding of Myc/Max complexes to Miz1 at the initiation region of a promoter represses gene expression (Seoane et al., 2001; Staller et al., 2001). This has been well documented for *Cdkn1a* and *Cdkn2b*, encoding the cyclin dependent kinase inhibitors $p21^{cip1}$ and $p15^{ink4b}$, respectively. In skin, it was shown that a functional mutation of Miz1 in keratinocytes of the basal epidermal cell layer reveals an increase of $p21^{cip1}$ as a result of the lack of Miz1/Myc repressing complexes. This leads to a reduced proliferation, a maintained or even increased differentiation and an alleviated development and growth of induced skin papillomas, all of which can be rescued on a $p21^{cip1}$ null background (Hönnemann et al., 2012). However, neither *Cdkn1a* nor *Cdkn2b* were present under the 830 genes bound by Miz1 in a ChIP-Seq analysis performed in the mammary gland epithelial cell line MDA-MB231 (Dr. Björn von Eyss; data not shown), indicating that Miz1 does not regulate these genes in this cell type. This is in agreement with the observation

that the expression of *Cdkn1a* was not significantly altered in the mammary gland from *Miz1ΔPOZ* animals compared to controls (Fig. 3.22B), making it unlikely that the reduced proliferation observed is primarily caused by upregulated $p21^{cip1}$. In addition, analysis of $p21^{cip1}$ expression during lactation (L6) by immunohistochemistry did not reveal any obvious differences between both genotypes (data not shown). The Myc protein was found expressed at very low levels during lactation by immunohistochemistry (Fig. 3.2), as previously described for mRNA by microarray analysis (Blakely, 2005). However, when the Myc gene was deleted during mid to late pregnancy in a conditional mouse model using Wap-Cre, a lactation defect phenotype was also observed (Stoelzle et al., 2009). Phenotypically, the authors describe a delayed proliferation and differentiation, impaired translation of milk proteins and a reduction of mammary gland precursor cells. Whether some of these observations are linked to the absence of Myc/Miz1 repressive complexes remains to be elucidated. However, a significant upregulation of $p21^{cip1}$, as observed in *Miz1ΔPOZ* skin (Hönnemann et al., 2012) and Myc-deficient mammary gland (Stoelzle et al., 2009), was not observed in the *Miz1ΔPOZ* mammary gland, suggesting that a relief of *Cdkn1a* repression by Myc/Miz1 is not the main reason for the reduction in proliferation. Moreover, keratinocyte differentiation was enhanced in *Miz1ΔPOZ* skin in a $p21^{cip1}$ dependent manner (Hönnemann et al., 2012) while differentiation of *Miz1ΔPOZ* luminal mammary gland cells was decreased (Fig. 3.24).

The expression of milk protein genes was lower in lactating mammary glands from mutant mice (Fig. 3.24 and 3.32) and in HC11 cells induced to differentiate after stable knockdown of Miz1 (Fig. 3.25). The alveoli of lactating wildtype animals were often filled with milk proteins and this situation was rare in mutant glands (see red fluorescence in Fig. 3.24C). In turn, lumina from *Miz1ΔPOZ* mammary glands were filled with large lipid aggregates as seen after Sudan III lipid staining from lactation day 6 cryosections (Fig. 3.29). These data imply that milk from knockout dams has a low protein and high lipid content. The reduced protein content would affect the proper growth of the pups after suckling and the high lipid composition might complicate milk ejection due to increased milk viscosity (Stinnakre et al., 1994). The reason for the milk fat aggregate accumulation in the lumina of knockout glands is still not clear but could be explained by an altered calcium transport which has been shown to positively regulate lipid aggregation (Valivullah et al., 1988). Information about the regulation of calcium transport and its impact in milk fat aggregation is scarce in the literature but several genes have been shown to influence the process. For instance, overexpression of miR-30b during lactation results in a reduced number of

lipid droplets which, in turn, are characterized by a larger area than those in control animals (Le Guillou et al., 2012b). From the genes which are described to regulate calcium flux in this publication, two are upregulated (*Clca1* and *Clca2*) and two downregulated (*Camk2b* and *Ano4*) after miR-30b overexpression, and these are regulated in a similar fashion in *Miz1ΔPOZ* mammary glands (Figs. 3.30 and 3.32). In line with the lipid droplet aggregation described, a high viscosity of milk in mutant glands could lead to inefficient clearing and subsequent milk stasis in *Miz1ΔPOZ* lumina. Microarray analysis of lactation day 6 samples provided evidence of an increased amount of mRNAs characteristic of an inflammatory response in mutant glands, which comprised acute phase response or complement activation genes (Fig. 3.32). Milk stasis has been shown to induce the expression of acute phase response genes like *Saa3* (Molenaar et al., 2009). However, no immune cells are apparent in *Miz1ΔPOZ* glands after HE staining or immunohistochemical analysis of the macrophage-specific antigen F4/80 (data not shown). An alternative explanation of the stimulation of an immune response genetic program in knockout animals would be related to the already described function of Miz1 as a negative regulator of inflammation by selectively suppressing TNF-α-induced Jnk1 activation (Liu et al., 2009; Do-Umehara et al., 2013). More experimental data would be required to test the cited possibilities.

The signal transducer and activator of transcription (Stat) 5, especially Stat5a, establishes a central signalling node for proliferation and differentiation of the luminal mammary gland epithelium, as well as for alveologenesis during pregnancy and lactation (Hennighausen and Robinson, 2008). When Stat5 was conditionally deleted in late pregnancy using Wap-Cre, a similar reduction in mammary gland tissue was observed as in our animal model (Cui et al., 2004). More sophisticated experiments revealed that the extent of glandular tissue that develops in late pregnancy and lactation depends on the Stat5 concentration in the luminal cells (Yamaji et al., 2012). In parallel to the morphological phenotype, genes encoding milk proteins or proteins involved in the regulation of luminal cell proliferation and differentiation were gradually down-regulated with different Stat5 dosages (Yamaji et al., 2012). In line with these observations is the mammary gland specific knockout of SnoN or Ski novel protein (Jahchan et al., 2012). Deletion of SnoN, which stabilizes the Stat5 protein, reduces Stat5 concentrations in luminal mammary epithelial cells and induces a lactogenic defect resembling the phenotype seen in Stat5 knockouts or in the *Miz1ΔPOZ* mammary gland. *Miz1ΔPOZ* animals also exhibit a reduced amount of Stat5 compared to control tissue when analysed by Western blots. Since the mammary gland epithelial cytokeratin-18 and tubulin, which is expressed at very low levels in adipose tissue (Spiegelman

and Farmer, 1982), were used as loading controls, the difference of Stat5 concentrations cannot be attributed to a different ratio between adipose and glandular tissue (Fig. 3.26). Whether the subtle decrease of Stat5a/b gene expression is sufficient to explain the reduced Stat5 protein in mutant glands, or if the deletion of the Miz1 POZ domain inhibits Stat5 translation or promotes Stat5 degradation, remains to be elucidated. Miz1 could favor stabilization of Stat5 as reported for SnoN (Jahchan et al., 2012) and further experiments would be required to test this hypothesis. As expected, due to the lower concentration of Stat5 in mutant glands, immunohistochemistry also revealed a clear decrease in phosphorylated Stat5 (Fig. 3.26). Taken together, the reduced proliferation and differentiation in the mammary gland of *Miz1ΔPOZ* animals during lactation is the consequence of a lower concentration of activated Stat5.

Stat5 is phosphorylated by a variety of cytokine receptors depending on the cell type (Furth et al., 2011). Cytokine receptors recruit Jak2 resulting in the phosphorylation of Stat5 (Levy and Darnell, 2002). The Jak2/Stat5 pathway is altered in lymphocytes when a functional Miz1 is absent, mainly by the upregulation of the Suppressor of cytokine signalling 1 (SOCS1) in response to interleukin-7 stimulation (Kosan et al., 2010). As already described, SOCS proteins negatively affect Stat5 phosphorylation keeping the Jak2/Stat5 pathway under strict control in a negative feedback loop (Sutherland et al., 2007). In the mammary gland both, *Socs1* and *Socs2*, are target genes of activated Stat5 (Hennighausen and Robinson, 2008), but we observed only a lower *Socs2* expression in *Miz1ΔPOZ* animals, while *Socs1* was not altered and, in particular, not upregulated like in mutant B-cells (Kosan et al., 2010). Interestingly, *Socs1* does not occur in the Miz1 binding list from ChIP-Seq data in MDA-MB231 cells (Dr. Björn von Eyss; data not shown), indicating that this is not a Miz1 target gene in mammary gland cells, in contrast to B-cells, where *Socs1* expression is directly regulated by Miz1 (Kosan et al., 2010). Caveolin-1 prevents the access of Jak2 to the prolactin receptor and, as described, its expression is not increased in mutant glands (Figs. 3.28 and 3.32). In conclusion, neither the three *Socs* genes (*Socs1*, *Socs2* and *Socs3*) nor Caveolin-1 (*Cav1*) are upregulated in *Miz1ΔPOZ* mammary glands (Figs. 3.28 and 3.32) making it unlikely that the decreased activation of Stat5 in knockouts is directly derived from high levels of these negative regulators of the Jak2/Stat5 pathway.

In mammary gland cells, the Jak2/Stat5 pathway is activated by the prolactin receptor (Gallego et al., 2001). The expression of this receptor is significantly downregulated in *Miz1ΔPOZ* animals, providing a possible explanation for the reduced pStat5 (Fig. 3.28). In line with this notion is the observation that heterozygous knockout of the prolactin receptor in the mouse mammary gland

leads to a similar phenotype as seen in the *Miz1ΔPOZ* animals (Harris, 2006). The knockout phenotype was rescued on a *Socs2* null background indicating that half dosage of the prolactin receptor is sufficient when the Jak2 inhibitor SOCS2 is absent. However, although *Socs2* was downregulated in the mammary gland of *Miz1ΔPOZ* mice (Fig. 3.28), Stat5 was less phosphorylated suggesting that either the amount of Stat5 itself was low or the concentration of the prolactin receptor was not in favor of a more efficient Stat5 phosphorylation. In addition, it has been shown that ErbB4 also phosphorylates Stat5 in a Jak2-independent manner in the mammary gland epithelium (Long et al., 2003) and promotes the nuclear translocation of pStat5 (Williams et al., 2004). Of note, the mRNA of this protein is also decreased in *Miz1ΔPOZ* animals providing an additional explanation for the observed decrease of pStat5 (Fig. 3.28). Data obtained using ChIP-Seq technology suggested that *Prlr* and *Erbb4* are not directly regulated by Miz1 (Dr. Björn von Eyss; data not shown). In contrast, about 50% of genes bound by Miz1 in ChIP-Seq analysis (with more than 200 binding tags) and found downregulated in the mammary gland from *Miz1ΔPOZ* animals by microarray analysis are related to vesicular transport processes indicating that Miz1 influences multiple functions related to secretion or intracellular protein targeting including the transport of plasma membrane proteins to their final destination (Table 3.1). The expression of different Miz1-bound genes in ChIP-Seq experiments which were downregulated in mutant glands was validated by qPCR. Genes important for vesicular transport (*Vamp4* and *Spast*) including those related to membrane protein trafficking (*Exoc2* and *Vps13d*), endocytosis (*Lrp12*, *Vps28* and *Pikfyve*) or autophagic vacuole assembly (*Ambra1*) were significantly downregulated in mutant glands (Fig. 3.33). These data are in agreement with a recently published report about Miz1 function in the cerebellum (Wolf et al., 2013). In addition, vesicular transport was found altered in *Miz1ΔPOZ* animals after careful examination of casein micelle formation in lactating mammary gland samples using electron microscopy (Fig. 3.33B and C). It would be interesting to study Miz1 impact on vesicle formation and sorting of membrane receptors using time-lapse microscopy to elucidate whether the prolactin receptor and ErbB4 are correctly sorted to the plasma membrane and which steps of the transport are more influenced by Miz1 transcriptional activity (Rodriguez-Boulan et al., 2005; Chenouard et al., 2014). The altered vesicular transport hypothesis is compatible with the observation that in *Miz1ΔPOZ* animals 1) the composition of the secretory vesicles is altered (Fig. 3.33), 2) ErbB4 concentration in the nucleus is reduced (Fig. 3.34) after proteolytic cleavage of the membrane receptor (Williams et al., 2004) and 3) the prolactin receptor is not properly located in the plasma

membrane (Fig. 3.34). Signalling by the PrlR depends not only on a correct localization at the plasma membrane (Swaminathan et al., 2008), but is also modified by internalization via clathrin dependent or independent endocytosis (Piazza et al., 2009), another branch of vesicular transport. Interestingly, it has been shown that transcriptional expression of *Prlr* is enhanced by prolactin-induced prolactin receptor signalling (Liby et al., 2003; Gutzman et al., 2004), suggesting a link between the observed reduction in the expression of *Prlr* to an impaired vesicular transport.

In vivo studies during the last years revealed that Miz1 has pleiotropic functions in different tissues like skin (Gebhardt et al., 2007; Hönnemann et al., 2012), B- and T-cells (Kosan et al., 2010; Möröy et al., 2011) or cerebellum (Wolf et al., 2013). Interestingly, the absence of functional Miz1 led to attenuated tumorigenesis in mouse skin (Hönnemann et al., 2012) and in a murine lymphoma model (Riggelen et al., 2010b), either by upregulation of *Cdkn1a* expression or by induction of senescence via an autocrine TGFβ signalling loop, respectively. Together with the fact that Miz1 is a central player in mediating the repressive function of the proto-oncogene Myc in cancer (Wiese et al., 2013), relevant roles of Miz1 in different kinds of tumors, also in the mammary gland, are likely. Several mouse models of breast cancer are available and some of them allow the study of metastasis (Hennighausen, 1999; Fantozzi and Christofori, 2006; Taneja et al., 2009). In the course of this thesis, MMTV-Cre (Line A) $Miz1^{lox/lox}$ mice were mated to MMTV-Polyomavirus Middle T Antigen (MMTV-PyMT) animals but no Miz1 knockouts (MMTV-$PyMT^{+}$ and $Miz1^{lox/lox}$) were obtained after several rounds of mating (data not shown). $Miz1^{+/+}$ and $Miz1^{lox/+}$ mice expressing PyMT developed mammary tumors at around 3-4 months of age as previously described for the MMTV-PyMT mouse strain (Lin et al., 2003). The reason for a possible embryonic lethality of mice lacking the POZ domain of Miz1 and simultaneously expressing MMTV-PyMT is currently not known. Other mouse models could be used to study the influence of Miz1 in mammary tumorigenesis as in other tissues (Riggelen et al., 2010b; Hönnemann et al., 2012; Wiese et al., 2013) and to test whether Miz1 has an effect in metastasis *in vivo* as already suggested (Chan et al., 2010).

This is the first report about the physiological function of Miz1 in the mammary gland and documents its importance for an adequate mammary cell proliferation and differentiation during lactation. Miz1 levels increase in the transition from pregnancy to lactation and remain elevated until involution is triggered by cessation of pup suckling. We propose a tentative model (Fig. 4.1) where the lack of functional Miz1 causes a downregulation of a gene set involved in vesicular transport, limiting a proper localization, degradation and recycling of plasma membrane proteins.

This disrupts the Jak2/Stat5 pathway due to impaired signalling via prolactin receptor and ErbB4, reflected by an alleviated expression of Stat5 target genes like *Csn1s1, Csn1s2a, Csn1s2b, Csn2, Csn3, Wap* or *Socs2* as well as *Prlr* and *Erbb4*. This deficiency in Stat5 activation leads to a decrease in mammary proliferation and differentiation which cause the lactation phenotype observed in *Miz1ΔPOZ* animals.

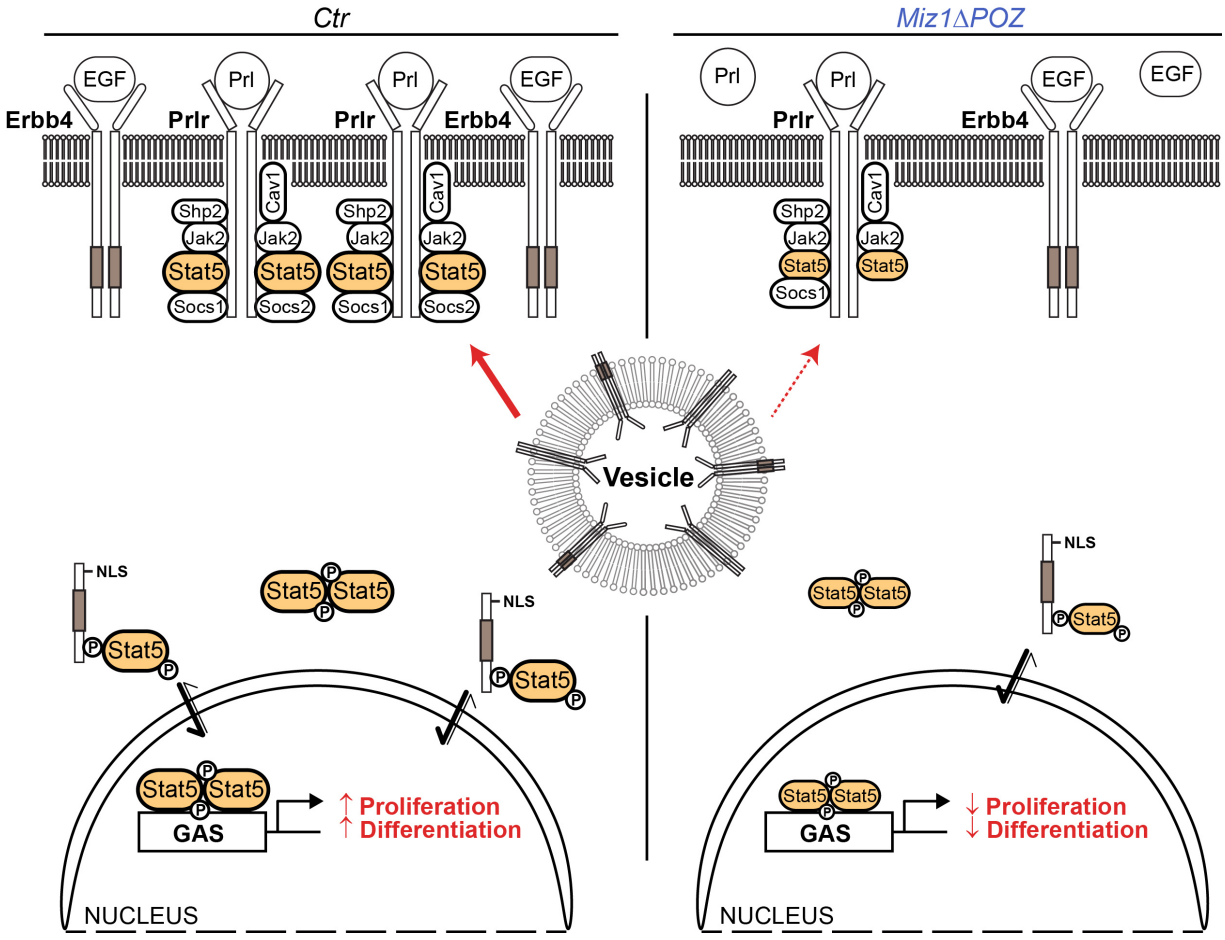

Figure 4.1: Hypothetical model for the function of Miz1 in the lactating mouse mammary gland. Miz1 binds to many genes which are important for vesicular transport and these are downregulated in *Miz1ΔPOZ* glands. Impaired sorting of these vesicles could be the cause of the observed reduction in the exposure of the prolactin receptor and ErbB4 to the plasma membrane leading to a decreased amount of activated Stat5 in mutant glands. In consequence, the reduced levels of phosphorylated Stat5 dimers (represented by smaller symbol size) cannot adequately activate the transcription genes important for proliferation and differentiation in *Miz1ΔPOZ* glands leading to the described lactation defect (Modified according to Williams et al., 2004 and Hennighausen and Robinson, 2008).

REFERENCES

Abbas, T. and Dutta, A. (2009). p21 in cancer: intricate networks and multiple activities. *Nature Reviews Cancer* 9, 400–414.

Adhikary, S., Peukert, K., Karsunky, H., Beuger, V., Lutz, W., Elsasser, H.-P., Moroy, T. and Eilers, M. (2003). Miz1 Is Required for Early Embryonic Development during Gastrulation. *Molecular and Cellular Biology* 23, 7648–7657.

Adhikary, S., Marinoni, F., Hock, A., Hulleman, E., Popov, N., Beier, R., Bernard, S., Quarto, M., Capra, M., Goettig, S., et al. (2005). The Ubiquitin Ligase HectH9 Regulates Transcriptional Activation by Myc and Is Essential for Tumor Cell Proliferation. *Cell* 123, 409–421.

Affolter, M., Bellusci, S., Itoh, N., Shilo, B., Thiery, J.-P. and Werb, Z. (2003). Tube or Not Tube: Remodeling Epithelial Tissues by Branching Morphogenesis. *Developmental Cell* 4, 11–18.

Agarwal, K. L., Büchi, H., Caruthers, M. H., Gupta, N., Khorana, H. G., Kleppe, K., Kumar, A., Ohtsuka, E., Rajbhandary, U. L., Van de Sande, J. H., et al. (1970). Total synthesis of the gene for an alanine transfer ribonucleic acid from yeast. *Nature* 227, 27–34.

Allred, D. C. and Medina, D. (2008). The Relevance of Mouse Models to Understanding the Development and Progression of Human Breast Cancer. *Journal of Mammary Gland Biology and Neoplasia* 13, 279–288.

Amati, B., Brooks, M. W., Levy, N., Littlewood, T. D., Evan, G. I. and Land, H. (1993). Oncogenic activity of the c-Myc protein requires dimerization with Max. *Cell* 72, 233–245.

Andersen, C. L., Jensen, J. L. and Ørntoft, T. F. (2004). Normalization of Real-Time Quantitative Reverse Transcription-PCR Data: A Model-Based Variance Estimation Approach to Identify Genes Suited for Normalization, Applied to Bladder and Colon Cancer Data Sets. *Cancer Res* 64, 5245–5250.

Anderson, S. M., Rudolph, M. C., McManaman, J. L. and Neville, M. C. (2007). Key stages in mammary gland development. Secretory activation in the mammary gland: it's not just about milk protein synthesis! *Breast Cancer Research* 9, 204.

Atwood, C. S., Hovey, R. C., Glover, J. P., Chepko, G., Ginsburg, E., Robison, W. G. and Vonderhaar, B. K. (2000). Progesterone induces side-branching of the ductal epithelium in the mammary glands of peripubertal mice. *J Endocrinol* 167, 39–52.

Aupperlee, M. D., Leipprandt, J. R., Bennett, J. M., Schwartz, R. C. and Haslam, S. Z. (2013). Amphiregulin mediates progesterone-induced mammary ductal development during puberty. *Breast Cancer Res* 15, R44.

Avivar-Valderas, A., Salas, E., Bobrovnikova-Marjon, E., Diehl, J. A., Nagi, C., Debnath, J. and Aguirre-Ghiso, J. A. (2011). PERK Integrates Autophagy and Oxidative Stress Responses To Promote Survival during Extracellular Matrix Detachment. *Molecular and Cellular Biology* 31, 3616–3629.

Bai, L. and Rohrschneider, L. R. (2010). s-SHIP promoter expression marks activated stem cells in developing mouse mammary tissue. *Genes Dev.* 24, 1882–1892.

Ball, R. K., Friis, R. R., Schoenenberger, C. A., Doppler, W. and Groner, B. (1988). Prolactin regulation of beta-casein gene expression and of a cytosolic 120-kd protein in a cloned mouse mammary epithelial cell line. *The EMBO journal* 7, 2089.

Basu, S., Liu, Q., Qiu, Y. and Dong, F. (2009). Gfi-1 represses CDKN2B encoding p15INK4B through interaction with Miz-1. *PNAS* 106, 1433–1438.

Bédard, M., Maltais, L., Beaulieu, M.-E., Bilodeau, J., Bernard, D. and Lavigne, P. (2012). NMR structure note: solution structure of human Miz-1 zinc fingers 8 to 10. *J Biomol NMR* 54, 317–323.

Bernard, D., Bédard, M., Bilodeau, J. and Lavigne, P. (2013). Structural and dynamical characterization of the Miz-1 zinc fingers 5–8 by solution-state NMR. *J Biomol NMR* 57, 103–116.

Blackwell, T. K., Kretzner, L., Blackwood, E. M., Eisenman, R. N. and Weintraub, H. (1990). Sequence-specific DNA binding by the c-Myc protein. *Science* 250, 1149–1151.

Blackwood, E. M. and Eisenman, R. N. (1991). Max: a helix-loop-helix zipper protein that forms a sequence-specific DNA-binding complex with Myc. *Science* 251, 1211–1217.

Blakely, C. M. (2005). Developmental stage determines the effects of MYC in the mammary epithelium. *Development* 132, 1147–1160.

Blanpain, C., Daley, G. Q., Hochedlinger, K., Passegué, E., Rossant, J. and Yamanaka, S. (2012). Stem cells assessed. *Nat Rev Mol Cell Biol* 13, 471–476.

Booth, B. W., Boulanger, C. A. and Smith, G. H. (2007). Alveolar progenitor cells develop in mouse mammary glands independent of pregnancy and lactation. *Journal of Cellular Physiology* 212, 729–736.

Booth, B. W., Mack, D. L., Androutsellis-Theotokis, A., McKay, R. D. G., Boulanger, C. A. and Smith, G. H. (2008). The mammary microenvironment alters the differentiation repertoire of neural stem cells. *Proc Natl Acad Sci U S A* 105, 14891–14896.

Boulanger, C. A., Bruno, R. D., Rosu-Myles, M. and Smith, G. H. (2012). The Mouse Mammary Microenvironment Redirects Mesoderm-Derived Bone Marrow Cells to a Mammary Epithelial Progenitor Cell Fate. *Stem Cells and Development* 21, 948–954.

Bouras, T., Pal, B., Vaillant, F., Harburg, G., Asselin-Labat, M.-L., Oakes, S. R., Lindeman, G. J. and Visvader, J. E. (2008). Notch Signaling Regulates Mammary Stem Cell Function and Luminal Cell-Fate Commitment. *Cell Stem Cell* 3, 429–441.

Bravo-Cordero, J. J., Hodgson, L. and Condeelis, J. (2012). Directed cell invasion and migration during metastasis. *Current Opinion in Cell Biology* 24, 277–283.

Brisken, C. and Rajaram, R. D. (2006). Alveolar and Lactogenic Differentiation. *Journal of Mammary Gland Biology and Neoplasia* 11, 239–248.

Brisken, C., Park, S., Vass, T., Lydon, J. P., O'Malley, B. W. and Weinberg, R. A. (1998). A paracrine role for the epithelial progesterone receptor in mammary gland development. *PNAS* 95, 5076–5081.

Brisken, C., Kaur, S., Chavarria, T. E., Binart, N., Sutherland, R. L., Weinberg, R. A., Kelly, P. A. and Ormandy, C. J. (1999). Prolactin Controls Mammary Gland Development via Direct and Indirect Mechanisms. *Developmental Biology* 210, 96–106.

Bruno, R. D., Boulanger, C. A., Rosenfield, S. M., Anderson, L. H., Lydon, J. P. and Smith, G. H. (2014). Paracrine-rescued lobulogenesis in chimeric outgrowths comprising progesterone-receptor-null mammary epithelium and redirected wild-type testicular cells. *J Cell Sci* 127, 27–32.

Buono, K. D., Robinson, G. W., Martin, C., Shi, S., Stanley, P., Tanigaki, K., Honjo, T. and Hennighausen, L. (2006). The canonical Notch/RBP-J signaling pathway controls the balance of cell lineages in mammary epithelium during pregnancy. *Developmental Biology* 293, 565–580.

Bustin, S. A., Benes, V., Garson, J. A., Hellemans, J., Huggett, J., Kubista, M., Mueller, R., Nolan, T., Pfaffl, M. W., Shipley, G. L., et al. (2009). The MIQE Guidelines: Minimum Information for Publication of Quantitative Real-Time PCR Experiments. *Clinical Chemistry* 55, 611–622.

Cabodevilla, A. G., Sánchez-Caballero, L., Nintou, E., Boiadjieva, V. G., Picatoste, F., Gubern, A. and Claro, E. (2013). Cell Survival during Complete Nutrient Deprivation Depends on Lipid Droplet-fueled β-Oxidation of Fatty Acids. *J. Biol. Chem.* 288, 27777–27788.

Cailleau, R., Mackay, B., Young, R. K. and Reeves, W. J. (1974). Tissue Culture Studies on Pleural Effusions from Breast Carcinoma Patients. *Cancer Res* 34, 801–809.

Campbell, G. S., Argetsinger, L. S., Ihle, J. N., Kelly, P. A., Rillema, J. A. and Carter-Su, C. (1994). Activation of JAK2 tyrosine kinase by prolactin receptors in Nb2 cells and mouse mammary gland explants. *PNAS* 91, 5232–5236.

Carpenter, G. (2003). ErbB-4: mechanism of action and biology. *Experimental Cell Research* 284, 66–77.

Chammas, R., Taverna, D., Cella, N., Santos, C. and Hynes, N. E. (1994). Laminin and tenascin assembly and expression regulate HC11 mouse mammary cell differentiation. *J Cell Sci* 107, 1031–1040.

Chan, C.-H., Lee, S.-W., Li, C.-F., Wang, J., Yang, W.-L., Wu, C.-Y., Wu, J., Nakayama, K. I., Kang, H.-Y., Huang, H.-Y., et al. (2010). Deciphering the transcriptional complex critical for RhoA gene expression and cancer metastasis. *Nat Cell Biol* 12, 457–467.

Chappell, J. and Dalton, S. (2013). Roles for MYC in the Establishment and Maintenance of Pluripotency. *Cold Spring Harb Perspect Med* 3, a014381.

Chenouard, N., Smal, I., de Chaumont, F., Maška, M., Sbalzarini, I. F., Gong, Y., Cardinale, J., Carthel, C., Coraluppi, S., Winter, M., et al. (2014). Objective comparison of particle tracking methods. *Nat Meth* advance online publication,.

Chepko, G. and Smith, G. H. (1997). Three division-competent, structurally-distinct cell populations contribute to murine mammary epithelial renewal. *Tissue and Cell* 29, 239–253.

Chepko, G., Slack, R., Carbott, D., Khan, S., Steadman, L. and Dickson, R. B. (2005). Differential alteration of stem and other cell populations in ducts and lobules of TGFα and c-Myc transgenic mouse mammary epithelium. *Tissue and Cell* 37, 393–412.

Cho, K. B., Cho, M. K., Lee, W. Y. and Kang, K. W. (2010). Overexpression of c-myc induces epithelial mesenchymal transition in mammary epithelial cells. *Cancer Letters* 293, 230–239.

Coons, A. H. and Kaplan, M. H. (1950). Localization of Antigen in Tissue Cells Ii. Improvements in a Method for the Detection of Antigen by Means of Fluorescent Antibody. *J Exp Med* 91, 1–13.

Costoya, J. A. (2007). Functional analysis of the role of POK transcriptional repressors. *Briefings in Functional Genomics and Proteomics* 6, 8–18.

Cottle, D. L., Kretzschmar, K., Schweiger, P. J., Quist, S. R., Gollnick, H. P., Natsuga, K., Aoyagi, S. and Watt, F. M. (2013). c-MYC-Induced Sebaceous Gland Differentiation Is Controlled by an Androgen Receptor/p53 Axis. *Cell Reports* 3, 427–441.

Cui, Y., Riedlinger, G., Miyoshi, K., Tang, W., Li, C., Deng, C.-X., Robinson, G. W. and Hennighausen, L. (2004). Inactivation of Stat5 in Mouse Mammary Epithelium during Pregnancy Reveals Distinct Functions in Cell Proliferation, Survival, and Differentiation. *Molecular and Cellular Biology* 24, 8037–8047.

D'Cruz, C. M., Moody, S. E., Master, S. R., Hartman, J. L., Keiper, E. A., Imielinski, M. B., Cox, J. D., Wang, J. Y., Ha, S. I., Keister, B. A., et al. (2002). Persistent Parity-Induced Changes in Growth Factors, TGF-β3, and Differentiation in the Rodent Mammary Gland. *Molecular Endocrinology* 16, 2034–2051.

Dang, C. V. (2012). MYC on the Path to Cancer. *Cell* 149, 22–35.

Dang, C. V. and Lee, W. M. (1988). Identification of the human c-myc protein nuclear translocation signal. *Mol. Cell. Biol.* 8, 4048–4054.

Dang, C. V., McGuire, M., Buckmire, M. and Lee, W. M. F. (1989). Involvement of the "leucine zipper" region in the oligomerization and transforming activity of human c-myc protein. *Nature* 337, 664–666.

Daniel, C. W. (1975). Regulation of cell division in aging mouse mammary epithelium. *Adv. Exp. Med. Biol.* 61, 1–19.

Danielson, K. G., Oborn, C. J., Durban, E. M., Butel, J. S. and Medina, D. (1984). Epithelial mouse mammary cell line exhibiting normal morphogenesis in vivo and functional differentiation in vitro. *Proc Natl Acad Sci U S A* 81, 3756–3760.

Davis, B. J. (1964). Disc Electrophoresis – Ii Method and Application to Human Serum Proteins*. *Annals of the New York Academy of Sciences* 121, 404–427.

Davis, A. C., Wims, M., Spotts, G. D., Hann, S. R. and Bradley, A. (1993). A null c-myc mutation causes lethality before 10.5 days of gestation in homozygotes and reduced fertility in heterozygous female mice. *Genes Dev.* 7, 671–682.

Debnath, J. (2008). Detachment-induced autophagy during anoikis and lumen formation in epithelial acini. *Autophagy* 4, 351–353.

Debnath, J., Mills, K. R., Collins, N. L., Reginato, M. J., Muthuswamy, S. K. and Brugge, J. S. (2002). The Role of Apoptosis in Creating and Maintaining Luminal Space within Normal and Oncogene-Expressing Mammary Acini. *Cell* 111, 29–40.

Debnath, J., Muthuswamy, S. K. and Brugge, J. S. (2003). Morphogenesis and oncogenesis of MCF-10A mammary epithelial acini grown in three-dimensional basement membrane cultures. *Methods* 30, 256–268.

Deome, K. B., FAULKIN, L. J., Jr, BERN, H. A. and BLAIR, P. B. (1959). Development of mammary tumors from hyperplastic alveolar nodules transplanted into gland-free mammary fat pads of female C3H mice. *Cancer Res.* 19, 515–520.

Deslex, S., Negrel, R. and Ailhaud, G. (1987). Development of a chemically defined serum-free medium for differentiation of rat adipose precursor cells. *Experimental Cell Research* 168, 15–30.

Desprez, P.-Y., Lin, C. Q., Thomasset, N., Sympson, C. J., Bissell, M. J. and Campisi, J. (1998). A Novel Pathway for Mammary Epithelial Cell Invasion Induced by the Helix-Loop-Helix Protein Id-1. *Mol Cell Biol* 18, 4577–4588.

Dey, D., Saxena, M., Paranjape, A. N., Krishnan, V., Giraddi, R., Kumar, M. V., Mukherjee, G. and Rangarajan, A. (2009a). Phenotypic and Functional Characterization of Human Mammary Stem/Progenitor Cells in Long Term Culture. *PLoS ONE* 4, e5329.

Do-Umehara, H. C., Chen, C., Urich, D., Zhou, L., Qiu, J., Jang, S., Zander, A., Baker, M. A., Eilers, M., Sporn, P. H. S., et al. (2013). Suppression of inflammation and acute lung injury by Miz1 via repression of C/EBP-δ. *Nat Immunol* 14, 461–469.

Dontu, G. and Wicha, M. S. (2005a). Survival of Mammary Stem Cells in Suspension Culture: Implications for Stem Cell Biology and Neoplasia. *Journal of Mammary Gland Biology and Neoplasia* 10, 75–86.

Dontu, G., Abdallah, W. M., Foley, J. M., Jackson, K. W., Clarke, M. F., Kawamura, M. J. and Wicha, M. S. (2003). In vitro propagation and transcriptional profiling of human mammary stem/progenitor cells. *Genes Dev.* 17, 1253–1270.

Eilers, M. and Eisenman, R. N. (2008). Myc's broad reach. *Genes Dev.* 22, 2755–2766.

Elias, J. J., Pitelka, D. R. and Armstrong, R. C. (1973). Changes in fat cell morphology during lactation in the mouse. *Anat. Rec.* 177, 533–547.

Ewald, A. J., Brenot, A., Duong, M., Chan, B. S. and Werb, Z. (2008). Collective Epithelial Migration and Cell Rearrangements Drive Mammary Branching Morphogenesis. *Developmental Cell* 14, 570–581.

Fantozzi, A. and Christofori, G. (2006). Mouse models of breast cancer metastasis. *Breast Cancer Res* 8, 212.

Fernandez, P. C., Frank, S. R., Wang, L., Schroeder, M., Liu, S., Greene, J., Cocito, A. and Amati, B. (2003). Genomic targets of the human c-Myc protein. *Genes Dev.* 17, 1115–1129.

Fischer, A. H., Jacobson, K. A., Rose, J. and Zeller, R. (2008). Hematoxylin and Eosin Staining of Tissue and Cell Sections. *Cold Spring Harb Protoc* 2008, pdb.prot4986.

Folmes, C. D. L., Martinez-Fernandez, A., Faustino, R. S., Yamada, S., Perez-Terzic, C., Nelson, T. J. and Terzic, A. (2013). Nuclear Reprogramming with c-Myc Potentiates Glycolytic Capacity of Derived Induced Pluripotent Stem Cells. *J. of Cardiovasc. Trans. Res.* 6, 10–21.

Franker, M. A. M. and Hoogenraad, C. C. (2013). Microtubule-based transport - basic mechanisms, traffic rules and role in neurological pathogenesis. *Journal of Cell Science* 126, 2319–2329.

Fridriksdottir, A. J. R., Petersen, O. W. and Rnnov-Jessen, L. (2011). Mammary gland stem cells: current status and future challenges. *The International Journal of Developmental Biology* 55, 719–729.

Furth, P. A., Nakles, R. E., Millman, S., Diaz-Cruz, E. S. and Cabrera, M. C. (2011). Signal transducer and activator of transcription 5 as a key signaling pathway in normal mammary gland developmental biology and breast cancer. *Breast Cancer Research* 13, 220.

Gallant, P. and Steiger, D. Myc's secret life without Max. *Cell Cycle* 8, 3848–3853.

Gallego, M. I., Binart, N., Robinson, G. W., Okagaki, R., Coschigano, K. T., Perry, J., Kopchick, J. J., Oka, T., Kelly, P. A. and Hennighausen, L. (2001). Prolactin, Growth Hormone, and Epidermal Growth Factor Activate Stat5 in Different Compartments of Mammary Tissue and Exert Different and Overlapping Developmental Effects. *Developmental Biology* 229, 163–175.

Gallego, M. I., Beachy, P. A., Hennighausen, L. and Robinson, G. W. (2002). Differential Requirements for Shh in Mammary Tissue and Hair Follicle Morphogenesis. *Developmental Biology* 249, 131–139.

Gandarillas, A. and Watt, F. M. (1997). c-Myc promotes differentiation of human epidermal stem cells. *Genes Dev.* 11, 2869–2882.

García-Zaragoza, E., Pérez-Tavarez, R., Ballester, A., Lafarga, V., Jiménez-Reinoso, A., Ramírez, Á., Murillas, R. and Gallego, M. I. (2012). Intraepithelial paracrine Hedgehog signaling induces the expansion of ciliated cells that express diverse progenitor cell markers in the basal epithelium of the mouse mammary gland. *Developmental Biology* 372, 28–44.

Gavrieli, Y., Sherman, Y. and Ben-Sasson, S. A. (1992). Identification of programmed cell death in situ via specific labeling of nuclear DNA fragmentation. *J Cell Biol* 119, 493–501.

Gebhardt, A. (2006). Myc regulates keratinocyte adhesion and differentiation via complex formation with Miz1. *The Journal of Cell Biology* 172, 139–149.

Gebhardt, A., Kosan, C., Herkert, B., Moroy, T., Lutz, W., Eilers, M. and Elsasser, H.-P. (2007). Miz1 is required for hair follicle structure and hair morphogenesis. *Journal of Cell Science* 120, 2586–2593.

Gentleman, R. C., Carey, V. J., Bates, D. M., Bolstad, B., Dettling, M., Dudoit, S., Ellis, B., Gautier, L., Ge, Y., Gentry, J., et al. (2004). Bioconductor: open software development for computational biology and bioinformatics. *Genome Biology* 5, R80.

Gill, G. W. (2012). *Cytopreparation: Principles & Practice*. Springer.

Glukhova, M. A. and Streuli, C. H. (2013). How integrins control breast biology. *Curr Opin Cell Biol* 25, 633–641.

Goetz, S. C., Ocbina, P. J. R. and Anderson, K. V. (2009). The Primary Cilium as a Hedgehog Signal Transduction Machine. *Methods Cell Biol* 94, 199–222.

Gouilleux, F., Wakao, H., Mundt, M. and Groner, B. (1994). Prolactin induces phosphorylation of Tyr694 of Stat5 (MGF), a prerequisite for DNA binding and induction of transcription. *EMBO J* 13, 4361–4369.

Gouon-Evans, V., Rothenberg, M. E. and Pollard, J. W. (2000). Postnatal mammary gland development requires macrophages and eosinophils. *Development* 127, 2269–2282.

Grimm, S. L., Seagroves, T. N., Kabotyanski, E. B., Hovey, R. C., Vonderhaar, B. K., Lydon, J. P., Miyoshi, K., Hennighausen, L., Ormandy, C. J., Lee, A. V., et al. (2002). Disruption of Steroid and Prolactin Receptor Patterning in the Mammary Gland Correlates with a Block in Lobuloalveolar Development. *Molecular Endocrinology* 16, 2675–2691.

Grinberg, A. V., Hu, C.-D. and Kerppola, T. K. (2004). Visualization of Myc/Max/Mad Family Dimers and the Competition for Dimerization in Living Cells. *Mol. Cell. Biol.* 24, 4294–4308.

Grolli, S., Accornero, P., Ramoni, R., Donofrio, G. and Whitelaw, C. B. A. (1997). Expression of c-mycIs Down-regulated as Mouse Mammary Epithelial Cells Become Confluent. *Biochemical and Biophysical Research Communications* 239, 566–569.

Gutzman, J. H., Miller, K. K. and Schuler, L. A. (2004). Endogenous human prolactin and not exogenous human prolactin induces estrogen receptor α and prolactin receptor expression and increases estrogen responsiveness in breast cancer cells. *The Journal of Steroid Biochemistry and Molecular Biology* 88, 69–77.

Han, L. Q., Yang, G. Y., Zhu, H. S., Wang, Y. Y., Wang, L. F., Guo, Y. J., Lu, W. F., Li, H. J. and Wang, Y. L. (2010). Selection and use of reference genes in mouse mammary glands. *Genet. Mol. Res.* 9, 449–456.

Hann, S. R. and Eisenman, R. N. (1984). Proteins encoded by the human c-myc oncogene: differential expression in neoplastic cells. *Mol Cell Biol* 4, 2486–2497.

Harris, J., Stanford, P. M., Sutherland, K., Oakes, S. R., Naylor, M. J., Robertson, F. G., Blazek, K. D., Kazlauskas, M., Hilton, H. N., Wittlin, S., et al. (2006). Socs2 and Elf5 Mediate Prolactin-Induced Mammary Gland Development. *Molecular Endocrinology* 20, 1177–1187.

Hazen, S. A., Rowe, W. A. and Lynch, C. J. (1995). Monolayer cell culture of freshly isolated adipocytes using extracellular basement membrane components. *J. Lipid Res.* 36, 868–875.

Hebner, C., Weaver, V. M. and Debnath, J. (2008). Modeling Morphogenesis and Oncogenesis in Three-Dimensional Breast Epithelial Cultures. *Annual Review of Pathology: Mechanisms of Disease* 3, 313–339.

Hennighausen, L. (1999). Mouse models for breast cancer. *Breast Cancer Research* 2, 2.

Hennighausen, L. and Robinson, G. W. (2005). Information networks in the mammary gland. *Nature Reviews Molecular Cell Biology* 6, 715–725.

Hennighausen, L. and Robinson, G. W. (2008). Interpretation of cytokine signaling through the transcription factors STAT5A and STAT5B. *Genes Dev.* 22, 711–721.

Hens, J. R. and Wysolmerski, J. J. (2005). Key stages of mammary gland development: Molecular mechanisms involved in the formation of the embryonic mammary gland. *Breast Cancer Res* 7, 220–224.

Herkert, B. and Eilers, M. (2010). Transcriptional Repression: The Dark Side of Myc. *Genes & Cancer* 1, 580–586.

Herkert, B., Dwertmann, A., Herold, S., Abed, M., Naud, J.-F., Finkernagel, F., Harms, G. S., Orian, A., Wanzel, M. and Eilers, M. (2010). The Arf tumor suppressor protein inhibits Miz1 to suppress cell adhesion and induce apoptosis. *J Cell Biol* 188, 905–918.

Herold, S., Wanzel, M., Beuger, V., Frohme, C., Beul, D., Hillukkala, T., Syvaoja, J., Saluz, H.-P., Haenel, F. and Eilers, M. (2002). Negative Regulation of the Mammalian UV Response by Myc through Association with Miz-1. *Molecular Cell* 10, 509–521.

Herold, S., Hock, A., Herkert, B., Berns, K., Mullenders, J., Beijersbergen, R., Bernards, R. and Eilers, M. (2008). Miz1 and HectH9 regulate the stability of the checkpoint protein, TopBP1. *EMBO J* 27, 2851–2861.

Higuchi, R., Dollinger, G., Walsh, P. S. and Griffith, R. (1992). Simultaneous amplification and detection of specific DNA sequences. *Biotechnology (N.Y.)* 10, 413–417.

Higuchi, R., Fockler, C., Dollinger, G. and Watson, R. (1993). Kinetic PCR analysis: real-time monitoring of DNA amplification reactions. *Biotechnology (N.Y.)* 11, 1026–1030.

Hinck, L. and Silberstein, G. B. (2005). Key stages in mammary gland development: The mammary end bud as a motile organ. *Breast Cancer Research* 7, 245.

Hoffman, B. and Liebermann, D. A. (2008). Apoptotic signaling by c-MYC. *Oncogene* 27, 6462–6472.

Hönnemann, J., Sanz-Moreno, A., Wolf, E., Eilers, M. and Elsässer, H.-P. (2012). Miz1 Is a Critical Repressor of cdkn1a during Skin Tumorigenesis. *PLoS ONE* 7, e34885.

Hovey, R. C. and Aimo, L. (2010). Diverse and Active Roles for Adipocytes During Mammary Gland Growth and Function. *J Mammary Gland Biol Neoplasia* 15, 279–290.

Howlin, J., McBryan, J. and Martin, F. (2006). Pubertal Mammary Gland Development: Insights from Mouse Models. *J Mammary Gland Biol Neoplasia* 11, 283–297.

Hsiao, Y.-C., Tuz, K. and Ferland, R. J. (2012). Trafficking in and to the primary cilium. *Cilia* 1, 4.

Huang, D. W., Sherman, B. T. and Lempicki, R. A. (2008). Systematic and integrative analysis of large gene lists using DAVID bioinformatics resources. *Nat. Protocols* 4, 44–57.

Huang, D. W., Sherman, B. T. and Lempicki, R. A. (2009). Bioinformatics enrichment tools: paths toward the comprehensive functional analysis of large gene lists. *Nucl. Acids Res.* 37, 1–13.

Hunkeler, D. (1991). Mechanism and kinetics of the persulfate-initiated polymerization of acrylamide. *Macromolecules* 24, 2160–2171.

Hynes, N. E. and Stoelzle, T. (2009). Key signalling nodes in mammary gland development and cancer: Myc. *Breast Cancer Research* 11, 210.

Hynes, N. E., Taverna, D., Harwerth, I. M., Ciardiello, F., Salomon, D. S., Yamamoto, T. and Groner, B. (1990). Epidermal growth factor receptor, but not c-erbB-2, activation prevents lactogenic hormone induction of the beta-casein gene in mouse mammary epithelial cells. *Molecular and Cellular Biology* 10, 4027–4034.

Inoue, S., Hao, Z., Elia, A. J., Cescon, D., Zhou, L., Silvester, J., Snow, B., Harris, I. S., Sasaki, M., Li, W. Y., et al. (2013). Mule/Huwe1/Arf-BP1 suppresses Ras-driven tumorigenesis by preventing c-Myc/Miz1-mediated down-regulation of p21 and p15. *Genes & Development* 27, 1101–1114.

Ip, M. M. and Asch, B. B. (2000). *Methods in Mammary Gland Biology and Breast Cancer Research*. Springer.

Jahchan, N. S., Wang, D., Bissell, M. J. and Luo, K. (2012). SnoN regulates mammary gland alveologenesis and onset of lactation by promoting prolactin/Stat5 signaling. *Development* 139, 3147–3156.

Jasmin, J.-F., Mercier, I., Sotgia, F. and Lisanti, M. P. (2006). SOCS proteins and caveolin-1 as negative regulators of endocrine signaling. *Trends in Endocrinology & Metabolism* 17, 150–158.

Jiang, Z., Deng, T., Jones, R., Li, H., Herschkowitz, J. I., Liu, J. C., Weigman, V. J., Tsao, M.-S., Lane, T. F., Perou, C. M., et al. (2010). Rb deletion in mouse mammary progenitors induces luminal-B or basal-like/EMT tumor subtypes depending on p53 status. *J Clin Invest* 120, 3296–3309.

Jones, F. E., Welte, T., Fu, X.-Y. and Stern, D. F. (1999). Erbb4 Signaling in the Mammary Gland Is Required for Lobuloalveolar Development and Stat5 Activation during Lactation. *J Cell Biol* 147, 77–88.

Joshi, P. A. and Khokha, R. (2012). The mammary stem cell conundrum: is it unipotent or multipotent? *Breast Cancer Research* 14, 305.

Joshi, P. A., Jackson, H. W., Beristain, A. G., Di Grappa, M. A., Mote, P. A., Clarke, C. L., Stingl, J., Waterhouse, P. D. and Khokha, R. (2010). Progesterone induces adult mammary stem cell expansion. *Nature* 465, 803–807.

Kelly, K. F. and Daniel, J. M. (2006). POZ for effect – POZ-ZF transcription factors in cancer and development. *Trends in Cell Biology* 16, 578–587.

Kerosuo, L., Piltti, K., Fox, H., Angers-Loustau, A., Hayry, V., Eilers, M., Sariola, H. and Wartiovaara, K. (2008). Myc increases self-renewal in neural progenitor cells through Miz-1. *Journal of Cell Science* 121, 3941–3950.

Kim, J., Woo, A. J., Chu, J., Snow, J. W., Fujiwara, Y., Kim, C. G., Cantor, A. B. and Orkin, S. H. (2010). A Myc Network Accounts for Similarities between Embryonic Stem and Cancer Cell Transcription Programs. *Cell* 143, 313–324.

Kleppe, K., Ohtsuka, E., Kleppe, R., Molineux, I. and Khorana, H. G. (1971). Studies on polynucleotides. XCVI. Repair replications of short synthetic DNA's as catalyzed by DNA polymerases. *J. Mol. Biol.* 56, 341–361.

Klinakis, A., Szabolcs, M., Politi, K., Kiaris, H., Artavanis-Tsakonas, S. and Efstratiadis, A. (2006). Myc is a Notch1 transcriptional target and a requisite for Notch1-induced mammary tumorigenesis in mice. *PNAS* 103, 9262–9267.

Komatsu, M., Waguri, S., Chiba, T., Murata, S., Iwata, J., Tanida, I., Ueno, T., Koike, M., Uchiyama, Y., Kominami, E., et al. (2006). Loss of autophagy in the central nervous system causes neurodegeneration in mice. *Nature* 441, 880–884.

Kosan, C., Saba, I., Godmann, M., Herold, S., Herkert, B., Eilers, M. and Möröy, T. (2010). Transcription Factor Miz-1 Is Required to Regulate Interleukin-7 Receptor Signaling at Early Commitment Stages of B Cell Differentiation. *Immunity* 33, 917–928.

Krimpenfort, P., IJpenberg, A., Song, J.-Y., van der Valk, M., Nawijn, M., Zevenhoven, J. and Berns, A. (2007). p15Ink4b is a critical tumour suppressor in the absence of p16Ink4a. *Nature* 448, 943–946.

Laemmli, U. K. (1970). Cleavage of Structural Proteins during the Assembly of the Head of Bacteriophage T4. *Nature* 227, 680–685.

Laurenti, E., Wilson, A. and Trumpp, A. (2009). Myc's other life: stem cells and beyond. *Current Opinion in Cell Biology* 21, 844–854.

Le Guillou, S., Sdassi, N., Laubier, J., Passet, B., Vilotte, M., Castille, J., Laloë, D., Polyte, J., Bouet, S., Jaffrézic, F., et al. (2012a). Overexpression of miR-30b in the Developing Mouse Mammary Gland Causes a Lactation Defect and Delays Involution. *PLoS ONE* 7, e45727.

Leverkoehne, I., Horstmeier, B. A., von Samson-Himmelstjerna, G., Scholte, B. J. and Gruber, A. D. (2002). Real-time RT-PCR quantitation of mCLCA1 and mCLCA2 reveals differentially regulated expression in pre-and postnatal murine tissues. *Histochemistry and cell biology* 118, 11–17.

Levy, D. E. and Darnell, J. E. (2002). STATs: transcriptional control and biological impact. *Nat Rev Mol Cell Biol* 3, 651–662.

Lewis, M. T., Ross, S., Strickland, P. A., Sugnet, C. W., Jimenez, E., Hui, C. and Daniel, C. W. (2001). The Gli2 Transcription Factor Is Required for Normal Mouse Mammary Gland Development. *Developmental Biology* 238, 133–144.

Lewis, M. T., Landua, J. D., Iii, H. C. A. and Medina, D. (2012). A Mystery Wrapped in an Enigma: Matrigel Enhancement of Mammary Cell Growth and Morphogenesis. *J Mammary Gland Biol Neoplasia* 17, 99–101.

Li, L., Hartley, R., Reiss, B., Sun, Y., Pu, J., Wu, D., Lin, F., Hoang, T., Yamada, S., Jiang, J., et al. (2012). E-cadherin plays an essential role in collective directional migration of large epithelial sheets. *Cell Mol Life Sci* 69, 2779–2789.

Liby, K., Neltner, B., Mohamet, L., Menchen, L. and Ben-Jonathan, N. (2003). Prolactin overexpression by MDA-MB-435 human breast cancer cells accelerates tumor growth. *Breast Cancer Res. Treat.* 79, 241–252.

Lin, E. Y., Jones, J. G., Li, P., Zhu, L., Whitney, K. D., Muller, W. J. and Pollard, J. W. (2003). Progression to Malignancy in the Polyoma Middle T Oncoprotein Mouse Breast Cancer Model Provides a Reliable Model for Human Diseases. *The American Journal of Pathology* 163, 2113–2126.

Lin, C. Y., Lovén, J., Rahl, P. B., Paranal, R. M., Burge, C. B., Bradner, J. E., Lee, T. I. and Young, R. A. (2012). Transcriptional Amplification in Tumor Cells with Elevated c-Myc. *Cell* 151, 56–67.

Lindeman, G. J., Wittlin, S., Lada, H., Naylor, M. J., Santamaria, M., Zhang, J.-G., Starr, R., Hilton, D. J., Alexander, W. S., Ormandy, C. J., et al. (2001). SOCS1 deficiency results in accelerated mammary gland development and rescues lactation in prolactin receptor–deficient mice. *Genes Dev.* 15, 1631–1636.

Liu, S. (2006). Hedgehog Signaling and Bmi-1 Regulate Self-renewal of Normal and Malignant Human Mammary Stem Cells. *Cancer Research* 66, 6063–6071.

Liu, X., Robinson, G. W., Wagner, K. U., Garrett, L., Wynshaw-Boris, A. and Hennighausen, L. (1997). Stat5a is mandatory for adult mammary gland development and lactogenesis. *Genes Dev.* 11, 179–186.

Liu, X., Gallego, M. I., Smith, G. H., Robinson, G. W. and Hennighausen, L. (1998). Functional rescue of Stat5a-null mammary tissue through the activation of compensating signals including Stat5b. *Cell Growth Differ.* 9, 795–803.

Liu, J., Zhao, Y., Eilers, M. and Lin, A. (2009). Miz1 is a signal- and pathway-specific modulator or regulator (SMOR) that suppresses TNF-α-induced JNK1 activation. *PNAS* 106, 18279–18284.

Liu, Q., Basu, S., Qiu, Y., Tang, F. and Dong, F. (2010). A role of Miz-1 in Gfi-1-mediated transcriptional repression of CDKN1A. *Oncogene* 29, 2843–2852.

Liu, J., Yan, J., Jiang, S., Wen, J., Chen, L., Zhao, Y. and Lin, A. (2012). Site-specific ubiquitination is required for relieving the transcription factor Miz1-mediated suppression on TNF-α–induced JNK activation and inflammation. *PNAS* 109, 191–196.

Livak, K. J. and Schmittgen, T. D. (2001). Analysis of Relative Gene Expression Data Using Real-Time Quantitative PCR and the 2−ΔΔCT Method. *Methods* 25, 402–408.

Lkhider, M., Delpal, S., Le Provost, F. and Ollivier-Bousquet, M. (1997). Rat prolactin synthesis by lactating mammary epithelial cells. *FEBS Letters* 401, 117–122.

Loewen, M. E. and Forsyth, G. W. (2005). Structure and Function of CLCA Proteins. *Physiol Rev* 85, 1061–1092.

Long, W., Wagner, K.-U., Lloyd, K. C. K., Binart, N., Shillingford, J. M., Hennighausen, L. and Jones, F. E. (2003). Impaired differentiation and lactational failure of Erbb4-deficient mammary glands identify ERBB4 as an obligate mediator of STAT5. *Development* 130, 5257–5268.

Lu, Y., Chen, J., Xiao, M., Li, W. and Miller, D. D. (2012). An Overview of Tubulin Inhibitors That Interact with the Colchicine Binding Site. *Pharm Res* 29, 2943–2971.

Lu, J., Chen, M., Ren, X.-R., Wang, J., Lyerly, H. K., Barak, L. and Chen, W. (2013a). Regulation of Hedgehog Signaling by Myc-Interacting Zinc Finger Protein 1, Miz1. *PLoS ONE* 8, e63353.

Lüscher, B. and Vervoorts, J. (2012). Regulation of gene transcription by the oncoprotein MYC. *Gene* 494, 145–160.

Lydon, J. P., DeMayo, F. J., Funk, C. R., Mani, S. K., Hughes, A. R., Montgomery, C. A., Shyamala, G., Conneely, O. M. and O'Malley, B. W. (1995). Mice lacking progesterone receptor exhibit pleiotropic reproductive abnormalities. *Genes Dev.* 9, 2266–2278.

Macias, H. and Hinck, L. (2012). Mammary gland development. *Wiley Interdisciplinary Reviews: Developmental Biology* 1, 533–557.

Mailleux, A. A., Overholtzer, M. and Brugge, J. S. (2008). Lumen formation during mammary epithelial morphogenesis: insights from in vitro and in vivo models. *Cell Cycle* 7, 57–62.

Makarem, M., Spike, B. T., Dravis, C., Kannan, N., Wahl, G. M. and Eaves, C. J. (2013). Stem Cells and the Developing Mammary Gland. *J Mammary Gland Biol Neoplasia* 18, 209–219.

Mao, D. Y. L., Watson, J. D., Yan, P. S., Barsyte-Lovejoy, D., Khosravi, F., Wong, W. W.-L., Farnham, P. J., Huang, T. H.-M. and Penn, L. Z. (2003). Analysis of Myc Bound Loci Identified by CpG Island Arrays Shows that Max Is Essential for Myc-Dependent Repression. *Current Biology* 13, 882–886.

Marine, J.-C., McKay, C., Wang, D., Topham, D. J., Parganas, E., Nakajima, H., Pendeville, H., Yasukawa, H., Sasaki, A., Yoshimura, A., et al. (1999). SOCS3 Is Essential in the Regulation of Fetal Liver Erythropoiesis. *Cell* 98, 617–627.

Marte, B. M., Jeschke, M., Graus-Porta, D., Taverna, D., Hofer, P., Groner, B., Yarden, Y. and Hynes, N. E. (1995). Neu differentiation factor/heregulin modulates growth and differentiation of HC11 mammary epithelial cells. *Molecular Endocrinology* 9, 14–23.

Master, S. R., Hartman, J. L., D'Cruz, C. M., Moody, S. E., Keiper, E. A., Ha, S. I., Cox, J. D., Belka, G. K. and Chodosh, L. A. (2002). Functional Microarray Analysis of Mammary Organogenesis Reveals a Developmental Role in Adaptive Thermogenesis. *Molecular Endocrinology* 16, 1185–1203.

Matulka, L. A., Triplett, A. A. and Wagner, K.-U. (2007). Parity-induced mammary epithelial cells are multipotent and express cell surface markers associated with stem cells. *Developmental Biology* 303, 29–44.

McBryan, J., Howlin, J., Napoletano, S. and Martin, F. (2008). Amphiregulin: Role in Mammary Gland Development and Breast Cancer. *Journal of Mammary Gland Biology and Neoplasia* 13, 159–169.

McMahon, S. B., Van Buskirk, H. A., Dugan, K. A., Copeland, T. D. and Cole, M. D. (1998). The Novel ATM-Related Protein TRRAP Is an Essential Cofactor for the c-Myc and E2F Oncoproteins. *Cell* 94, 363–374.

Merlo, G. R., Venesio, T., Taverna, D., Marte, B. M., Callahan, R. and Hynes, N. E. (1994). Growth suppression of normal mammary epithelial cells by wild-type p53. *Oncogene* 9, 443–453.

Meyer, N. and Penn, L. Z. (2008). Reflecting on 25 years with MYC. *Nat Rev Cancer* 8, 976–990.

Miao, L., Song, Z., Jin, L., Zhu, Y. M., Wen, L. P. and Wu, M. (2009). ARF antagonizes the ability of Miz-1 to inhibit p53-mediated transactivation. *Oncogene* 29, 711–722.

Michno, K., Boras-Granic, K., Mill, P., Hui, C. C. and Hamel, P. A. (2003). Shh expression is required for embryonic hair follicle but not mammary gland development. *Developmental Biology* 264, 153–165.

Molenaar, A. J., Harris, D. P., Rajan, G. H., Pearson, M. L., Callaghan, M. R., Sommer, L., Farr, V. C., Oden, K. E., Miles, M. C., Petrova, R. S., et al. (2009). The acute-phase protein serum amyloid A3 is expressed in the bovine mammary gland and plays a role in host defence.

Möröy, T., Saba, I. and Kosan, C. (2011). The role of the transcription factor Miz-1 in lymphocyte development and lymphomagenesis—Binding Myc makes the difference. *Seminars in Immunology* 23, 379–387.

Moumen, M., Chiche, A., Cagnet, S., Petit, V., Raymond, K., Faraldo, M. M., Deugnier, M.-A. and Glukhova, M. A. (2011). The mammary myoepithelial cell. *The International Journal of Developmental Biology* 55, 763–771.

Moumen, M., Chiche, A., Deugnier, M.-A., Petit, V., Gandarillas, A., Glukhova, M. A. and Faraldo, M. M. (2012). The Proto-Oncogene Myc Is Essential for Mammary Stem Cell Function. *STEM CELLS* 30, 1246–1254.

Moumen, M., Chiche, A., Decraene, C., Petit, V., Gandarillas, A., Deugnier, M.-A., Glukhova, M. A. and Faraldo, M. M. (2013). Myc is required for β-catenin-mediated mammary stem cell amplification and tumorigenesis. *Mol. Cancer* 12, 132.

Mulac-Jericevic, B., Lydon, J. P., DeMayo, F. J. and Conneely, O. M. (2003). Defective mammary gland morphogenesis in mice lacking the progesterone receptor B isoform. *PNAS* 100, 9744–9749.

Mullis, K. B. and Faloona, F. A. (1987). [21] Specific synthesis of DNA in vitro via a polymerase-catalyzed chain reaction. In *Methods in Enzymology* (ed. Ray Wu), pp. 335–350. Academic Press.

Muraoka-Cook, R. S., Sandahl, M., Husted, C., Hunter, D., Miraglia, L., Feng, S., Elenius, K. and Earp, H. S. (2006). The Intracellular Domain of ErbB4 Induces Differentiation of Mammary Epithelial Cells. *Mol. Biol. Cell* 17, 4118–4129.

Muraoka-Cook, R. S., Feng, S.-M., Strunk, K. E. and Iii, H. S. E. (2008). ErbB4/HER4: Role in Mammary Gland Development, Differentiation and Growth Inhibition. *J Mammary Gland Biol Neoplasia* 13, 235–246.

Nair, S. K. and Burley, S. K. (2003). X-Ray Structures of Myc-Max and Mad-Max Recognizing DNA: Molecular Bases of Regulation by Proto-Oncogenic Transcription Factors. *Cell* 112, 193–205.

Nakagawa, M., Koyanagi, M., Tanabe, K., Takahashi, K., Ichisaka, T., Aoi, T., Okita, K., Mochiduki, Y., Takizawa, N. and Yamanaka, S. (2008). Generation of induced pluripotent stem cells without Myc from mouse and human fibroblasts. *Nat Biotech* 26, 101–106.

Nakagawa, M., Takizawa, N., Narita, M., Ichisaka, T. and Yamanaka, S. (2010). Promotion of direct reprogramming by transformation-deficient Myc. *Proceedings of the National Academy of Sciences* 107, 14152–14157.

Nau, M. M., Brooks, B. J., Battey, J., Sausville, E., Gazdar, A. F., Kirsch, I. R., McBride, O. W., Bertness, V., Hollis, G. F. and Minna, J. D. (1985). L-myc, a new myc-related gene amplified and expressed in human small cell lung cancer. *Nature* 318, 69–73.

Naylor, M. J., Lockefeer, J. A., Horseman, N. D. and Ormandy, C. J. (2003). Prolactin regulates mammary epithelial cell proliferation via autocrine/paracrine mechanism. *Endocr* 20, 111–114.

Neville, M. C. and Daniel, C. W. (1987). *The Mammary gland: development, regulation, and function*. Plenum Press.

Neville, M. C., McFadden, T. B. and Forsyth, I. (2002). Hormonal regulation of mammary differentiation and milk secretion. *Journal of mammary gland biology and neoplasia* 7, 49–66.

Nguyen, L. V., Vanner, R., Dirks, P. and Eaves, C. J. (2012). Cancer stem cells: an evolving concept. *Nat Rev Cancer* 12, 133–143.

Nguyen, L. V., Makarem, M., Carles, A., Moksa, M., Kannan, N., Pandoh, P., Eirew, P., Osako, T., Kardel, M., Cheung, A. M. S., et al. (2014). Clonal Analysis via Barcoding Reveals Diverse Growth and Differentiation of Transplanted Mouse and Human Mammary Stem Cells. *Cell Stem Cell*.

Nicholson, S. E., Willson, T. A., Farley, A., Starr, R., Zhang, J.-G., Baca, M., Alexander, W. S., Metcalf, D., Hilton, D. J. and Nicola, N. A. (1999). Mutational analyses of the SOCS proteins suggest a dual domain requirement but distinct mechanisms for inhibition of LIF and IL-6 signal transduction. *EMBO J* 18, 375–385.

Nicholson, S. E., De Souza, D., Fabri, L. J., Corbin, J., Willson, T. A., Zhang, J.-G., Silva, A., Asimakis, M., Farley, A., Nash, A. D., et al. (2000). Suppressor of cytokine signaling-3 preferentially binds to the SHP-2-binding site on the shared cytokine receptor subunit gp130. *Proc Natl Acad Sci U S A* 97, 6493–6498.

Nie, Z., Hu, G., Wei, G., Cui, K., Yamane, A., Resch, W., Wang, R., Green, D. R., Tessarollo, L., Casellas, R., et al. (2012). c-Myc Is a Universal Amplifier of Expressed Genes in Lymphocytes and Embryonic Stem Cells. *Cell* 151, 68–79.

O'Connor, K. C., Song, H., Rosenzweig, N. and Jansen, D. A. (2003). Extracellular matrix substrata alter adipocyte yield and lipogenesis in primary cultures of stromal-vascular cells from human adipose. *Biotechnol. Lett.* 25, 1967–1972.

Oakes, S. R., Rogers, R. L., Naylor, M. J. and Ormandy, C. J. (2008). Prolactin Regulation of Mammary Gland Development. *Journal of Mammary Gland Biology and Neoplasia* 13, 13–28.

Oftedal, O. T. (2002). The mammary gland and its origin during synapsid evolution. *J Mammary Gland Biol Neoplasia* 7, 225–252.

Orban, P. C., Chui, D. and Marth, J. D. (1992). Tissue- and site-specific DNA recombination in transgenic mice. *Proc Natl Acad Sci U S A* 89, 6861–6865.

Ormandy, C. J., Camus, A., Barra, J., Damotte, D., Lucas, B., Buteau, H., Edery, M., Brousse, N., Babinet, C., Binart, N., et al. (1997). Null mutation of the prolactin receptor gene produces multiple reproductive defects in the mouse. *Genes Dev.* 11, 167–178.

Ornstein, L. (1964). Disc Electrophoresis-I Background and Theory*. *Annals of the New York Academy of Sciences* 121, 321–349.

Otto, P., Zoltan, B., Zsolt, C. and Ida, G. (2007). Differences in the onset of puberty in selected inbred mouse strains.

Palmer, C. A., Neville, M. C., Anderson, S. M. and McManaman, J. L. (2006). Analysis of Lactation Defects in Transgenic Mice. *Journal of Mammary Gland Biology and Neoplasia* 11, 269–282.

Pankiv, S., Clausen, T. H., Lamark, T., Brech, A., Bruun, J.-A., Outzen, H., Øvervatn, A., Bjørkøy, G. and Johansen, T. (2007). p62/SQSTM1 Binds Directly to Atg8/LC3 to Facilitate Degradation of Ubiquitinated Protein Aggregates by Autophagy. *J. Biol. Chem.* 282, 24131–24145.

Park, D. S., Lee, H., Riedel, C., Hulit, J., Scherer, P. E., Pestell, R. G. and Lisanti, M. P. (2001). Prolactin Negatively Regulates Caveolin-1 Gene Expression in the Mammary Gland during Lactation, via a Ras-dependent Mechanism. *J. Biol. Chem.* 276, 48389–48397.

Park, D. S., Lee, H., Frank, P. G., Razani, B., Nguyen, A. V., Parlow, A. F., Russell, R. G., Hulit, J., Pestell, R. G. and Lisanti, M. P. (2002). Caveolin-1-deficient Mice Show Accelerated Mammary Gland Development During Pregnancy, Premature Lactation, and Hyperactivation of the Jak-2/STAT5a Signaling Cascade. *Mol. Biol. Cell* 13, 3416–3430.

Patani, N., Martin, L.-A., Reis-Filho, J. S. and Dowsett, M. (2012). The role of caveolin-1 in human breast cancer. *Breast Cancer Res Treat* 131, 1–15.

Patel, J. H. and McMahon, S. B. (2006). Targeting of Miz-1 Is Essential for Myc-mediated Apoptosis. *J. Biol. Chem.* 281, 3283–3289.

Patel, J. H. and McMahon, S. B. (2007). BCL2 Is a Downstream Effector of MIZ-1 Essential for Blocking c-MYC-induced Apoptosis. *J. Biol. Chem.* 282, 5–13.

Pauli, B. U., Abdel-Ghany, M., Cheng, H.-C., Gruber, A. D., Archibald, H. A. and Elble, R. C. (2000). Molecular characteristics and functional diversity of CLCA family members. *Clinical and Experimental Pharmacology and Physiology* 27, 901–905.

Peaker, M. (2002). The Mammary Gland in Mammalian Evolution: A Brief Commentary on Some of the Concepts. *J Mammary Gland Biol Neoplasia* 7, 347–353.

Pece, S., Tosoni, D., Confalonieri, S., Mazzarol, G., Vecchi, M., Ronzoni, S., Bernard, L., Viale, G., Pelicci, P. G. and Di Fiore, P. P. (2010). Biological and Molecular Heterogeneity of Breast Cancers Correlates with Their Cancer Stem Cell Content. *Cell* 140, 62–73.

Penn, L. J., Brooks, M. W., Laufer, E. M. and Land, H. (1990). Negative autoregulation of c-myc transcription. *EMBO J* 9, 1113–1121.

Peukert, K., Staller, P., Schneider, A., Carmichael, G., Hanel, F. and Eilers, M. (1997). An alternative pathway for gene regulation by Myc. *EMBO J* 16, 5672–5686.

Phan, R. T., Saito, M., Basso, K., Niu, H. and Dalla-Favera, R. (2005). BCL6 interacts with the transcription factor Miz-1 to suppress the cyclin-dependent kinase inhibitor p21 and cell cycle arrest in germinal center B cells. *Nat Immunol* 6, 1054–1060.

Piazza, T. M., Lu, J.-C., Carver, K. C. and Schuler, L. A. (2009). Src Family Kinases Accelerate Prolactin Receptor Internalization, Modulating Trafficking and Signaling in Breast Cancer Cells. *Molecular Endocrinology* 23, 202–212.

Pittius, C. W., Hennighausen, L., Lee, E., Westphal, H., Nicols, E., Vitale, J. and Gordon, K. (1988). A milk protein gene promoter directs the expression of human tissue plasminogen activator cDNA to the mammary gland in transgenic mice. *PNAS* 85, 5874–5878.

Rahl, P. B., Lin, C. Y., Seila, A. C., Flynn, R. A., McCuine, S., Burge, C. B., Sharp, P. A. and Young, R. A. (2010). c-Myc Regulates Transcriptional Pause Release. *Cell* 141, 432–445.

Raymond, K., Faraldo, M. M., Deugnier, M.-A. and Glukhova, M. A. (2012). Integrins in mammary development. *Seminars in Cell & Developmental Biology* 23, 599–605.

Reversi, A., Cassoni, P. and Chini, B. (2005). Oxytocin Receptor Signaling in Myoepithelial and Cancer Cells. *J Mammary Gland Biol Neoplasia* 10, 221–229.

Reynolds, B. A., Tetzlaff, W. and Weiss, S. (1992). A multipotent EGF-responsive striatal embryonic progenitor cell produces neurons and astrocytes. *J. Neurosci.* 12, 4565–4574.

Riggelen, J. van, Müller, J., Otto, T., Beuger, V., Yetil, A., Choi, P. S., Kosan, C., Möröy, T., Felsher, D. W. and Eilers, M. (2010a). The interaction between Myc and Miz1 is required to antagonize TGFβ-dependent autocrine signaling during lymphoma formation and maintenance. *Genes Dev.* 24, 1281–1294.

Rios, A. C., Fu, N. Y., Lindeman, G. J. and Visvader, J. E. (2014). In situ identification of bipotent stem cells in the mammary gland. *Nature* advance online publication,.

Robinson, G. W. and Hennighausen, L. (2011). MMTV-Cre transgenes can adversely affect lactation: Considerations for conditional gene deletion in mammary tissue. *Analytical Biochemistry* 412, 92–95.

Robinson, G. W., McKnight, R. A., Smith, G. H. and Hennighausen, L. (1995). Mammary epithelial cells undergo secretory differentiation in cycling virgins but require pregnancy for the establishment of terminal differentiation. *Development* 121, 2079–2090.

Robinson, G. W., Karpf, A. B. C. and Kratochwil, K. (1999). Regulation of Mammary Gland Development by Tissue Interaction. *J Mammary Gland Biol Neoplasia* 4, 9–19.

Robinson, G. W., Pacher-Zavisin, M., Zhu, B. M., Yoshimura, A. and Hennighausen, L. (2007). Socs 3 modulates the activity of the transcription factor Stat3 in mammary tissue and controls alveolar homeostasis. *Developmental Dynamics* 236, 654–661.

Rodriguez-Boulan, E., Kreitzer, G. and Müsch, A. (2005). Organization of vesicular trafficking in epithelia. *Nature Reviews Molecular Cell Biology* 6, 233–247.

Rossant, J. and McMahon, A. (1999). “Cre”-ating mouse mutants—a meeting review on conditional mouse genetics. *Genes Dev.* 13, 142–145.

Saba, I., Kosan, C., Vassen, L. and Möröy, T. (2011). IL-7R–dependent survival and differentiation of early T-lineage progenitors is regulated by the BTB/POZ domain transcription factor Miz-1. *Blood* 117, 3370–3381.

Saiki, R. K., Scharf, S., Faloona, F., Mullis, K. B., Horn, G. T., Erlich, H. A. and Arnheim, N. (1985). Enzymatic amplification of beta-globin genomic sequences and restriction site analysis for diagnosis of sickle cell anemia. *Science* 230, 1350–1354.

Saiki, R. K., Gelfand, D. H., Stoffel, S., Scharf, S. J., Higuchi, R., Horn, G. T., Mullis, K. B. and Erlich, H. A. (1988). Primer-directed enzymatic amplification of DNA with a thermostable DNA polymerase. *Science* 239, 487–491.

Saito, M., Novak, U., Piovan, E., Basso, K., Sumazin, P., Schneider, C., Crespo, M., Shen, Q., Bhagat, G., Califano, A., et al. (2009). BCL6 suppression of BCL2 via Miz1 and its disruption in diffuse large B cell lymphoma. *PNAS* 106, 11294–11299.

Sambrook, J., Fritsch, E. F. and Maniatis, T. (1989). *Molecular cloning: a laboratory manual*. Cold Spring Harbor Laboratory.

Santos, C. O. dos, Rebbeck, C., Rozhkova, E., Valentine, A., Samuels, A., Kadiri, L. R., Osten, P., Harris, E. Y., Uren, P. J., Smith, A. D., et al. (2013). Molecular hierarchy of mammary differentiation yields refined markers of mammary stem cells. *PNAS* 110, 7123–7130.

Sarkar, A. (2009). *Human Stem Cells*. Discovery Publishing House.

Schmidt, M., Schwarzwaelder, K., Bartholomae, C. C., Glimm, H. and Kalle, C. von (2009). Detection of Retroviral Integration Sites by Linear Amplification-Mediated PCR and Tracking of Individual Integration Clones in Different Samples. In *Genetic Modification of Hematopoietic Stem Cells* (ed. Baum, C.), pp. 363–372. Humana Press.

Schmitt-Ney, M., Happ, B., Hofer, P., Hynes, N. E. and Groner, B. (1992). Mammary gland-specific nuclear factor activity is positively regulated by lactogenic hormones and negatively by milk stasis. *Molecular Endocrinology* 6, 1988–1997.

Schoenenberger, C. A., Andres, A. C., Groner, B., van der Valk, M., LeMeur, M. and Gerlinger, P. (1988a). Targeted c-myc gene expression in mammary glands of transgenic mice induces mammary tumours with constitutive milk protein gene transcription. *EMBO J* 7, 169–175.

Schroeder, J. A. and Lee, D. C. (1998). Dynamic expression and activation of ERBB receptors in the developing mouse mammary gland. *Cell Growth & Differentiation* 9, 451.

Schulz, T. C., Hopwood, B., Rathjen, P. D. and Wells, J. R. (1995). An unusual arrangement of 13 zinc fingers in the vertebrate gene Z13. *Biochem. J.* 311 (Pt 1), 219–224.

Schwab, M., Alitalo, K., Klempnauer, K. H., Varmus, H. E., Bishop, J. M., Gilbert, F., Brodeur, G., Goldstein, M. and Trent, J. (1983). Amplified DNA with limited homology to myc cellular oncogene is shared by human neuroblastoma cell lines and a neuroblastoma tumour. *Nature* 305, 245–248.

Selbert, S., Bentley, D. J., Melton, D. W., Rannie, D., Lourenço, P., Watson, C. J. and Clarke, A. R. (1998). Efficient BLG-Cre mediated gene deletion in the mammary gland. *Transgenic Res.* 7, 387–396.

Seoane, J., Pouponnot, C., Staller, P., Schader, M., Eilers, M. and Massagué, J. (2001). TGFβ influences Myc, Miz-1 and Smad to control the CDK inhibitor p15INK4b. *Nat Cell Biol* 3, 400–408.

Seoane, J., Le, H.-V. and Massagué, J. (2002). Myc suppression of the p21Cip1 Cdk inhibitor influences the outcome of the p53 response to DNA damage. *Nature* 419, 729–734.

Shackleton, M., Vaillant, F., Simpson, K. J., Stingl, J., Smyth, G. K., Asselin-Labat, M.-L., Wu, L., Lindeman, G. J. and Visvader, J. E. (2006). Generation of a functional mammary gland from a single stem cell. *Nature* 439, 84–88.

Shapiro, A. L., Scharff, M. D., Maizel, J. V. and Uhr, J. W. (1966). Synthesis of Excess Light Chains of Gamma Globulin by Rabbit Lymph Node Cells. *Nature* 211, 243–245.

Shapiro, A. L., Viñuela, E. and V. Maizel Jr., J. (1967). Molecular weight estimation of polypeptide chains by electrophoresis in SDS-polyacrylamide gels. *Biochemical and Biophysical Research Communications* 28, 815–820.

Shehata, M., Teschendorff, A., Sharp, G., Novcic, N., Russell, I. A., Avril, S., Prater, M., Eirew, P., Caldas, C., Watson, C. J., et al. (2012). Phenotypic and functional characterisation of the luminal cell hierarchy of the mammary gland. *Breast Cancer Research* 14, R134.

Sheiness, D., Fanshier, L. and Bishop, J. M. (1978). Identification of nucleotide sequences which may encode the oncogenic capacity of avian retrovirus MC29. *J. Virol.* 28, 600–610.

Shillingford, J. M., Miyoshi, K., Robinson, G. W., Grimm, S. L., Rosen, J. M., Neubauer, H., Pfeffer, K. and Hennighausen, L. (2002). Jak2 Is an Essential Tyrosine Kinase Involved in Pregnancy-Mediated Development of Mammary Secretory Epithelium. *Molecular Endocrinology* 16, 563–570.

Si, J., Yu, X., Zhang, Y. and DeWille, J. W. (2010). Myc interacts with Max and Miz1 to repress C/EBPδ promoter activity and gene expression. *Molecular Cancer* 9, 92.

Smith, P. K., Krohn, R. I., Hermanson, G. T., Mallia, A. K., Gartner, F. H., Provenzano, M. D., Fujimoto, E. K., Goeke, N. M., Olson, B. J. and Klenk, D. C. (1985). Measurement of protein using bicinchoninic acid. *Analytical Biochemistry* 150, 76–85.

Smith, K. N., Lim, J.-M., Wells, L. and Dalton, S. (2011). Myc orchestrates a regulatory network required for the establishment and maintenance of pluripotency. *Cell Cycle* 10, 592–597.

Smyth, G. K. (2004). Linear Models and Empirical Bayes Methods for Assessing Differential Expression in Microarray Experiments. *Statistical Applications in Genetics and Molecular Biology* 3,.

Sobolewska, A., Motyl, T. and Gajewska, M. (2011). Role and regulation of autophagy in the development of acinar structures formed by bovine BME-UV1 mammary epithelial cells. *European Journal of Cell Biology* 90, 854–864.

Spiegelman, B. M. and Farmer, S. R. (1982). Decreases in tubulin and actin gene expression prior to morphological differentiation of 3T3 Adipocytes. *Cell* 29, 53–60.

Staller, P., Peukert, K., Kiermaier, A., Seoane, J., Lukas, J., Karsunky, H., Möröy, T., Bartek, J., Massagué, J., Hänel, F., et al. (2001). Repression of p15INK4b expression by Myc through association with Miz-1. *Nat Cell Biol* 3, 392–399.

Stead, M. A., Trinh, C. H., Garnett, J. A., Carr, S. B., Baron, A. J., Edwards, T. A. and Wright, S. C. (2007). A Beta-Sheet Interaction Interface Directs the Tetramerisation of the Miz-1 POZ Domain. *Journal of Molecular Biology* 373, 820–826.

Stewart, T. A., Pattengale, P. K. and Leder, P. (1984). Spontaneous mammary adenocarcinomas in transgenic mice that carry and express MTV/myc fusion genes. *Cell* 38, 627–637.

Stingl, J., Eirew, P., Ricketson, I., Shackleton, M., Vaillant, F., Choi, D., Li, H. I. and Eaves, C. J. (2006). Purification and unique properties of mammary epithelial stem cells. *Nature* 439, 993–997.

Stinnakre, M. G., Vilotte, J. L., Soulier, S. and Mercier, J. C. (1994). Creation and phenotypic analysis of alpha-lactalbumin-deficient mice. *PNAS* 91, 6544–6548.

Stoelzle, T., Schwarb, P., Trumpp, A. and Hynes, N. E. (2009). c-Myc affects mRNA translation, cell proliferation and progenitor cell function in the mammary gland. *BMC Biology* 7, 63.

Stogios, P. J., Downs, G. S., Jauhal, J. J., Nandra, S. K. and Privé, G. G. (2005). Sequence and structural analysis of BTB domain proteins. *Genome Biology* 6, R82.

Summers, D. F., Maizel, J. V. and Darnell, J. E. (1965). Evidence for virus-specific noncapsid proteins in poliovirus-infected HeLa cells. *Proc Natl Acad Sci U S A* 54, 505–513.

Sutherland, K. D., Vaillant, F., Alexander, W. S., Wintermantel, T. M., Forrest, N. C., Holroyd, S. L., McManus, E. J., Schutz, G., Watson, C. J., Chodosh, L. A., et al. (2006). c-myc as a mediator of accelerated apoptosis and involution in mammary glands lacking Socs3. *EMBO J* 25, 5805–5815.

Sutherland, K. D., Lindeman, G. J. and Visvader, J. E. (2007). Knocking off SOCS genes in the mammary gland. *Cell Cycle* 6, 799–803.

Swaminathan, G., Varghese, B. and Fuchs, S. (2008). Regulation of prolactin receptor levels and activity in breast cancer. *J Mammary Gland Biol Neoplasia* 13, 81–91.

Taddei, I., Deugnier, M.-A., Faraldo, M. M., Petit, V., Bouvard, D., Medina, D., Fässler, R., Thiery, J. P. and Glukhova, M. A. (2008). β1 Integrin deletion from the basal compartment of the mammary epithelium affects stem cells. *Nature Cell Biology* 10, 716–722.

Takahashi, K. and Yamanaka, S. (2006). Induction of Pluripotent Stem Cells from Mouse Embryonic and Adult Fibroblast Cultures by Defined Factors. *Cell* 126, 663–676.

Tam, S. P., Lau, P., Djiane, J., Hilton, D. J. and Waters, M. J. (2001). Tissue-Specific Induction of SOCS Gene Expression by PRL. *Endocrinology* 142, 5015–5026.

Taneja, P., Frazier, D. P., Kendig, R. D., Maglic, D., Sugiyama, T., Kai, F., Taneja, N. K. and Inoue, K. (2009). MMTV mouse models and the diagnostic values of MMTV-like sequences in human breast cancer. *Expert Review of Molecular Diagnostics* 9, 423–440.

Teglund, S., McKay, C., Schuetz, E., van Deursen, J. M., Stravopodis, D., Wang, D., Brown, M., Bodner, S., Grosveld, G. and Ihle, J. N. (1998). Stat5a and Stat5b Proteins Have Essential and Nonessential, or Redundant, Roles in Cytokine Responses. *Cell* 93, 841–850.

Tian, Y., Schreiber, R. and Kunzelmann, K. (2012). Anoctamins are a family of Ca2+-activated Cl− channels. *J Cell Sci* 125, 4991–4998.

Towbin, H., Staehelin, T. and Gordon, J. (1979). Electrophoretic transfer of proteins from polyacrylamide gels to nitrocellulose sheets: procedure and some applications. *Proc Natl Acad Sci U S A* 76, 4350–4354.

Trumpp, A., Refaeli, Y., Oskarsson, T., Gasser, S., Murphy, M., Martin, G. R. and Bishop, J. M. (2001). c-Myc regulates mammalian body size by controlling cell number but not cell size. *Nature* 414, 768–773.

Udy, G. B., Towers, R. P., Snell, R. G., Wilkins, R. J., Park, S.-H., Ram, P. A., Waxman, D. J. and Davey, H. W. (1997). Requirement of STAT5b for sexual dimorphism of body growth rates and liver gene expression. *PNAS* 94, 7239–7244.

Valivullah, H. M., Bevan, D. R., Peat, A. and Keenan, T. W. (1988). Milk lipid globules: control of their size distribution. *Proc Natl Acad Sci U S A* 85, 8775–8779.

Van Amerongen, R., Bowman, A. N. and Nusse, R. (2012). Developmental Stage and Time Dictate the Fate of Wnt/β-Catenin-Responsive Stem Cells in the Mammary Gland. *Cell Stem Cell* 11, 387–400.

Van Keymeulen, A., Rocha, A. S., Ousset, M., Beck, B., Bouvencourt, G., Rock, J., Sharma, N., Dekoninck, S. and Blanpain, C. (2011a). Distinct stem cells contribute to mammary gland development and maintenance. *Nature* 479, 189–193.

Van Riggelen, J., Yetil, A. and Felsher, D. W. (2010). MYC as a regulator of ribosome biogenesis and protein synthesis. *Nat Rev Cancer* 10, 301–309.

Vandesompele, J., De Preter, K., Pattyn, F., Poppe, B., Van Roy, N., De Paepe, A. and Speleman, F. (2002). Accurate normalization of real-time quantitative RT-PCR data by geometric averaging of multiple internal control genes. *Genome Biol* 3, research0034.1–research0034.11.

Varlakhanova, N., Cotterman, R., Bradnam, K., Korf, I. and Knoepfler, P. S. (2011). Myc and Miz-1 have coordinate genomic functions including targeting Hox genes in human embryonic stem cells. *Epigenetics & Chromatin* 4, 20.

Vervoorts, J., Lüscher-Firzlaff, J. and Lüscher, B. (2006). The Ins and Outs of MYC Regulation by Posttranslational Mechanisms. *J. Biol. Chem.* 281, 34725–34729.

Visvader, J. E. (2009). Keeping abreast of the mammary epithelial hierarchy and breast tumorigenesis. *Genes & Development* 23, 2563–2577.

Visvader, J. E. and Smith, G. H. (2011). Murine Mammary Epithelial Stem Cells: Discovery, Function, and Current Status. *Cold Spring Harb Perspect Biol* 3, a004879.

Waggener, C. T., Dupree, J. L., Elgersma, Y. and Fuss, B. (2013). CaMKIIβ Regulates Oligodendrocyte Maturation and CNS Myelination. *J. Neurosci.* 33, 10453–10458.

Wagner, K.-U. and Rui, H. (2008). Jak2/Stat5 Signaling in Mammogenesis, Breast Cancer Initiation and Progression. *Journal of Mammary Gland Biology and Neoplasia* 13, 93–103.

Wagner, K.-U., Wall, R. J., St-Onge, L., Gruss, P., Wynshaw-Boris, A., Garrett, L., Li, M., Furth, P. A. and Hennighausen, L. (1997). Cre-mediated gene deletion in the mammary gland. *Nucleic acids research* 25, 4323–4330.

Wagner, K.-U., Ward, T., Davis, B., Wiseman, R. and Hennighausen, L. (2001). Spatial and temporal expression of the Cre gene under the control of the MMTV-LTR in different lines of transgenic mice. *Transgenic research* 10, 545–553.

Wagner, K.-U., Boulanger, C. A., Henry, M. D., Sgagias, M., Hennighausen, L. and Smith, G. H. (2002). An adjunct mammary epithelial cell population in parous females: its role in functional adaptation and tissue renewal. *Development* 129, 1377–1386.

Wagner, K.-U., Krempler, A., Triplett, A. A., Qi, Y., George, N. M., Zhu, J. and Rui, H. (2004). Impaired Alveologenesis and Maintenance of Secretory Mammary Epithelial Cells in Jak2 Conditional Knockout Mice. *Mol Cell Biol* 24, 5510–5520.

Wakao, H., Gouilleux, F. and Groner, B. (1994). Mammary gland factor (MGF) is a novel member of the cytokine regulated transcription factor gene family and confers the prolactin response. *EMBO J* 13, 2182–2191.

Walisko, O., Izsvák, Z., Szabó, K., Kaufman, C. D., Herold, S. and Ivics, Z. (2006). Sleeping Beauty transposase modulates cell-cycle progression through interaction with Miz-1. *PNAS* 103, 4062–4067.

Wang, X., Cunningham, M., Zhang, X., Tokarz, S., Laraway, B., Troxell, M. and Sears, R. C. (2011). Phosphorylation Regulates c-Myc's Oncogenic Activity in the Mammary Gland. *Cancer Research* 71, 925–936.

Wanzel, M., Kleine-Kohlbrecher, D., Herold, S., Hock, A., Berns, K., Park, J., Hemmings, B. and Eilers, M. (2004). Akt and 14-3-3η regulate Miz1 to control cell-cycle arrest after DNA damage. *Nature Cell Biology* 7, 30–41.

Wanzel, M., Russ, A. C., Kleine-Kohlbrecher, D., Colombo, E., Pelicci, P.-G. and Eilers, M. (2008). A ribosomal protein L23-nucleophosmin circuit coordinates Miz1 function with cell growth. *Nature Cell Biology* 10, 1051–1061.

Watson, C. J. and Khaled, W. T. (2008). Mammary development in the embryo and adult: a journey of morphogenesis and commitment. *Development* 135, 995–1003.

Watson, C. J. and Kreuzaler, P. A. (2011a). Remodeling mechanisms of the mammary gland during involution. *The International Journal of Developmental Biology* 55, 757–762.

Watt, F. M., Frye, M. and Benitah, S. A. (2008). MYC in mammalian epidermis: how can an oncogene stimulate differentiation? *Nat Rev Cancer* 8, 234–242.

Weber, A., Marquardt, J., Elzi, D., Forster, N., Starke, S., Glaum, A., Yamada, D., Defossez, P.-A., Delrow, J., Eisenman, R. N., et al. (2008). Zbtb4 represses transcription of P21CIP1 and controls the cellular response to p53 activation. *EMBO J* 27, 1563–1574.

White, D. E., Kurpios, N. A., Zuo, D., Hassell, J. A., Blaess, S., Mueller, U. and Muller, W. J. (2004). Targeted disruption of β1-integrin in a transgenic mouse model of human breast cancer reveals an essential role in mammary tumor induction. *Cancer Cell* 6, 159–170.

Wiechelman, K. J., Braun, R. D. and Fitzpatrick, J. D. (1988). Investigation of the bicinchoninic acid protein assay: Identification of the groups responsible for color formation. *Analytical Biochemistry* 175, 231–237.

Wiese, K. E., Walz, S., von Eyss, B., Wolf, E., Athineos, D., Sansom, O. and Eilers, M. (2013). The Role of MIZ-1 in MYC-Dependent Tumorigenesis. *Cold Spring Harb Perspect Med* 3,.

Williams, C. C., Allison, J. G., Vidal, G. A., Burow, M. E., Beckman, B. S., Marrero, L. and Jones, F. E. (2004). The ERBB4/HER4 receptor tyrosine kinase regulates gene expression by functioning as a STAT5A nuclear chaperone. *J Cell Biol* 167, 469–478.

Willmarth, N. E. and Ethier, S. P. (2008). Amphiregulin as a Novel Target for Breast Cancer Therapy. *Journal of Mammary Gland Biology and Neoplasia* 13, 171–179.

Wiseman, B. S. and Werb, Z. (2002). Stromal Effects on Mammary Gland Development and Breast Cancer. *Science* 296, 1046–1049.

Wolf, E., Gebhardt, A., Kawauchi, D., Walz, S., von Eyss, B., Wagner, N., Renninger, C., Krohne, G., Asan, E., Roussel, M. F., et al. (2013). Miz1 is required to maintain autophagic flux. *Nat Commun* 4,.

Wolfe, S. A., Nekludova, L. and Pabo, C. O. (2000). DNA RECOGNITION BY Cys2His2 ZINC FINGER PROTEINS. *Annual Review of Biophysics and Biomolecular Structure* 29, 183–212.

Wu, S., Cetinkaya, C., Munoz-Alonso, M. J., von der Lehr, N., Bahram, F., Beuger, V., Eilers, M., Leon, J. and Larsson, L.-G. (2003a). Myc represses differentiation-induced p21CIP1 expression via Miz-1-dependent interaction with the p21 core promoter. *Oncogene* 22, 351–360.

Wu, S., Cetinkaya, C., Munoz-Alonso, M. J., von der Lehr, N., Bahram, F., Beuger, V., Eilers, M., Leon, J. and Larsson, L.-G. (2003b). Myc represses differentiation-induced p21CIP1 expression via Miz-1-dependent interaction with the p21 core promoter. *Oncogene* 22, 351–360.

Xian, W. (2005). Pleiotropic effects of FGFR1 on cell proliferation, survival, and migration in a 3D mammary epithelial cell model. *The Journal of Cell Biology* 171, 663–673.

Yamaji, D., Na, R., Feuermann, Y., Pechhold, S., Chen, W., Robinson, G. W. and Hennighausen, L. (2009). Development of mammary luminal progenitor cells is controlled by the transcription factor STAT5A. *Genes Dev.* 23, 2382–2387.

Yamaji, D., Kang, K., Robinson, G. W. and Hennighausen, L. (2012). Sequential activation of genetic programs in mouse mammary epithelium during pregnancy depends on STAT5A/B concentration. *Nucleic Acids Research* 41, 1622–1636.

Yamauchi, T. (2005). Neuronal Ca 2+/calmodulin-dependent protein kinase II—discovery, progress in a quarter of a century, and perspective: implication for learning and memory. *Biological and Pharmaceutical Bulletin* 28, 1342–1354.

Yang, Y., Do, H., Tian, X., Zhang, C., Liu, X., Dada, L. A., Sznajder, J. I. and Liu, J. (2010). E3 ubiquitin ligase Mule ubiquitinates Miz1 and is required for TNFα-induced JNK activation. *PNAS* 107, 13444–13449.

Yap, P. L., Mirtle, C. L., Harvie, A. and McClelland, D. B. (1980). Milk protein concentrations in neonatal milk (witch's milk). *Clin Exp Immunol* 39, 695–697.

Young, L. J. T., Medina, D., DeOme, K. B. and Daniel, C. W. (1971). The influence of host and tissue age on life span and growth rate of serially transplanted mouse mammary gland. *Experimental Gerontology* 6, 49–56.

Yuan, T., Wang, Y., Pao, L., Anderson, S. M. and Gu, H. (2011). Lactation Defect in a Widely Used MMTV-Cre Transgenic Line of Mice. *PLoS ONE* 6, e19233.

Zarzynska, J. and Motyl, T. (2008). Apoptosis and autophagy in involuting bovine mammary gland. *J. Physiol. Pharmacol.* 59 Suppl 9, 275–288.

Ziegelbauer, J., Shan, B., Yager, D., Larabell, C., Hoffmann, B. and Tjian, R. (2001). Transcription Factor MIZ-1 Is Regulated via Microtubule Association. *Molecular Cell* 8, 339–349.

Ziegelbauer, J., Wei, J. and Tjian, R. (2004). Myc-interacting protein 1 target gene profile: A link to microtubules, extracellular signal-regulated kinase, and cell growth. *PNAS* 101, 458–463.

5. APPENDICES

5.1. Summary

5.1.1. Zusammenfassung

Die Analyse von Proteinen, die für die embryonale Entwicklung sowie für Erkrankungen relevant sind, stellen wertvolle Informationen für die Entwicklung neuer therapeutischer Konzepte zur Verfügung. Das Protooncogen Myc ist zum Beispiel ein vielversprechendes Zielprotein in einer Reihe von unterschiedlichen Tumoren einschließlich des sogenannten „triple negativen" Brustdrüsenkarzinoms. In der vorliegenden Arbeit wurde zum ersten Mal die Funktion des Transkriptionsfaktors Miz1 in der Brustdrüse der Maus untersucht. Hierzu wurde ein konditionelles Miz1 knockout Mausmodell verwendet. Bei diesem Modell wird die POZ Domäne deletiert. Diese ist essentiell für die Ausbildung von Tetrameren, die dann stabil an das Chromatin binden können. Die Deletion wurde mit zwei unterschiedlichen Cre-Stämmen durchgeführt. Ein MMTV-Cre Stamm wurde verwand, um die POZ Domäne in nulliparen Mäusen zu deletieren, wobei die postnatale Morphogenese der Drüse, sowie die Brustdrüsenstammzellen untersucht wurden. Ein Wap-Cre Stamm wurde eingesetzt, um die Alveologenese und die Brustdrüsendifferenzierung während der Schwangerschaft und der anschließenden Laktation zu analysieren.

Die Deletion der POZ Domäne mit MMTV-Cre erfolgt bereits im embryonalen Gewebe und führte zu einer Verzögerung der postnatalen Ausbildung und Verzweigung des Drüsenganges und einem zellärmeren Gangepithel. Weiterhin wurde eine von Myc unabhängige Anreicherung von Stamm- bzw. Vorläuferzellen in *Miz1ΔPOZ* Tieren beobachtet. Unterschiede in der Expression von luminalen und myoepithelialen Markern traten nicht auf. Die Verzögerung der postnatalen Gangentwicklung war in zwei Monate alten Tieren nicht mehr zu beobachten.

Mit Hilfe der Immunhistochemie und mit Western Blots konnte gezeigt werden, dass die Expression von endogenem Miz1 in normalen Tieren während der Laktation stark erhöht ist, während am Ende der Schwangerschaft nur wenig Miz1 nachgewiesen werden konnte. Die Miz1 Expression wird also während bzw. kurz nach der Geburt sprunghaft erhöht. Wird die Involution eingeleitet, fällt die Miz1 Expression innerhalb von 48 Stunden auf Werte zurück, wie sie vor der Laktation beobachtet wurden. Die Deletion der POZ Domäne während der Schwangerschaft mit

Hilfe von Wap-Cre erzeugte einen Laktationsdefekt während der ersten und der zweiten Schwangerschaft. Drüsen mit mutiertem Miz1 zeigte eine reduzierte Alveologenese, sowie eine verminderte Proliferation und Differenzierung. Dies konnte in der HC11 Zelllinie, die aus einer Maus-Brustdrüse isoliert wurde, verifiziert werden. HC11 Zellen mit geringer Miz1 Expression proliferieren langsamer und expremieren weniger β-Casein, wenn sie mit einem „laktogenen Hormoncocktail“, der u.a. Prolactin enthält, behandelt werden. Dabei zeigt sich weder *in vivo* noch *in vitro* eine Änderung der Apoptoserate , wenn die Miz1 POZ Domäne deletiert oder Miz1 ausgeschaltet wird. Brustdrüsen mit mutiertem Miz1 haben geringere Mengen an Stat5, was zu einer Reduktion der Expression entsprechender Zielgene wie α-Casein, β-Casein or whey acidic protein (Wap) führt. Negative Regulatoren des Jak2/Stat5 Signalwegs wie Socs (*Socs1, Socs2, Socs3*) oder Caveolin-1 (*Cav1*) waren in ihrer Expression nicht verändert. Im Gegensatz dazu wurde eine Verringerung des Prolactinrezeptors und von ErbB4 beobachtet. Beide Proteine sind wichtig für die Phosphorylierung von Stat5. Allerdings konnte mit Hilfe von CHIP-Seq Experimenten eine direkte Bindung von Miz1 an die Gene dieser beiden Proteine nicht gezeigt werden. Jedoch bindet Miz1 an verschiedene Gene, die für die Regulation des vesikulären Transportes, der Endozytose und der Autophagie entscheidend sind. Ein Modell, in dem die Störung des vesikulären Transportes der beiden Rezeptorproteine im Mittelpunkt steht, wird vorgeschlagen.

5.1.2. Summary

The study of the expression and function of proteins important for human health in normal development provides valuable information for the design of therapeutical opportunities in the context of disease. Myc is one of the current most promising targets for a number of cancer types including triple-negative breast cancer and Miz1 has been shown to play an important role in Myc-mediated tumorigenesis. In the present work, the function of the Myc-binding protein Miz1 in the mammary gland is investigated for the first time using two different lines of transgenic mice expressing Cre-recombinase to conditionally knockout the POZ domain of Miz1 in the murine mammary gland. Deletion of this evolutionary-conserved region impedes multimerization and stable association of Miz1 with chromatin. MMTV-Cre mediated deletion was used to investigate Miz1 function in the virgin gland, considering branching morphogenesis and mammary stem/progenitor biology. Ablation under the Wap-Cre promoter provided information

about alveologenesis and mammary differentiation. The mammary gland is a very suitable organ for stem cell and developmental studies as rounds of proliferation, differentiation and apoptosis occur after each pregnancy.

POZ domain deletion using MMTV-Cre (Line A), already active in the embryo, led to a delayed ductal tree formation, less cellularity in knockout ducts and a Myc-independent accumulation of stem/progenitor cells in virgin mammary glands of *Miz1ΔPOZ* animals. No differences in the expression of luminal and myoepithelial markers were observed between control and *Miz1ΔPOZ* virgin mice. In addition, the delay in the development of the mammary ductal tree in knockout mice is rescued at around two months of age.

Endogenous Miz1 expression in the mammary gland of control animals was found to be highly boosted during lactation by immunohistochemistry and Western blotting. Very low Miz1 levels were detected at the end of pregnancy, which increased after parturition and diminished upon cessation of pup suckling at around 48 hours of forced involution. Miz1 POZ domain ablation in luminal alveolar mammary cells during pregnancy using the WAP-Cre transgenic line resulted in a lactation defect in mutant dams during the first two pregnancies analysed. Mutant lactating glands display a reduced alveologenesis as a result of a diminished mammary cell proliferation and differentiation. These data were also confirmed *in vitro* using the HC11 murine mammary cell line after retroviral infection for stable knockdown of Miz1. HC11 cells with low levels of Miz1 show a reduced proliferation and a decreased expression of ß-casein after inducing differentiation by addition of a lactogenic hormone cocktail containing prolactin. Apoptosis is unaffected after either Miz1 POZ domain ablation *in vivo* or stable knockdown of Miz1 *in vitro*. Mutant glands display lower levels of activated Stat5 which lead to a reduced expression of its transcriptional targets, mainly genes which code for milk proteins like α-casein, β-casein or whey acidic protein (WAP). Gene expression of negative regulators of the Jak2/Stat5 pathway like Socs (*Socs1*, *Socs2* and *Socs3*) or Caveolin-1 (*Cav1*) is not upregulated in *Miz1ΔPOZ* lactating glands. In contrast, the expression of receptors important for a proper phosphorylation of Stat5, like the prolactin receptor or ErbB4, is decreased in lactating mutant glands. ChIP-Seq experiments revealed that genes encoding the prolactin receptor and ErbB4 are not direct targets of Miz1. Rather, Miz1 binds to genes which regulate vesicular transport and thus alters processes like endocytosis and autophagy in mammary gland cells. A model in which the vesicular transport of these receptors in mutant glands could be disrupted is proposed.

In conclusion, this work shows for the first time that Miz1 is important for mammary stem/progenitor cell regulation in the virgin gland and for a proper proliferation and differentiation in the lactating mammary gland.

5.2. List of abbreviations

AEC	3-amino-9-ethylcarbazole
ANOVA	Analysis of variance
APS	Ammonium Persulfate
BCA	Bicinchoninic acid assay
bFGF	Basic fibroblast growth factor
BME	Basement membrane extract
CD	Cluster of differentiation
cDNA	Complementary DNA
ChIP-Seq	Chromatin immunoprecipitation-sequencing
Cre	Cre recombinase
Ct	Threshold cycle
Ctr	Control
Cy	Cyanine
dd	Double-distilled
DEPC	Diethylpyrocarbonate
DIP	Dexamethasone-insulin-prolactin
DMEM	Dulbecco's modified eagle's medium
dNTPs	Deoxynucleotide triphosphates
EDTA	Ethylenediaminetetraacetic acid
EGF	Epidermal growth factor
EMT	Epithelial to mesenchymal transition
FACS	Fluorescence activated cell sorting
FBS	Fetal bovine serum
FITC	Fluorescein isothiocyanate
GAPDH	Glyceraldehyde 3-phosphate dehydrogenase
GFP	Green fluorescent protein
GSEA	Gene Set Enrichment Analysis
HBS	Hepes buffered saline
HEPES	Hydroxyethyl piperazineethanesulfonic acid

HRP	Horseradish peroxidase
H&E	Hematoxylin and eosin
Ig	Immunoglobulin
iPSC	Induced pluripotent stem cell
K5	Cytokeratin 5
K14	Cytokeratin 14
MEBM	Mammary epithelial basal medium
MMTV	Mouse mammary tumor virus
M-MuLV	Moloney murine leukemia virus
NMR	Nuclear magnetic resonance
NOD/SCID	Nonobese diabetic/severe combined immunodeficiency
OD	Optical density
PCR	Polymerase chain reaction
PFA	Paraformaldehyde
PVDF	Polyvinylidene fluoride
RIPA	Radioimmunoprecipitation assay buffer
RPMI	Roswell Park Memorial Institute
RQI	RNA quality indicator
rTdT	Terminal Deoxynucleotidyl Transferase
SD	Standard deviation
SDS	Sodium dodecyl sulfate
SMA	Smooth muscle actin
TBE	Tris borate EDTA
TDLUs	Terminal ductal lobular units
TEBs	Terminal end buds
TEMED	Tetramethylethylenediamine
TGFβ	Transforming growth factor beta
TNFα	Tumor necrosis factor alpha
TRITC	Tetramethylrhodamine isothiocyanate
UV	Ultraviolet
WAP	Whey acidic protein

5.3. University teachers

Meine akademischen Lehrer in Oviedo und Marburg waren die Damen und Herren:

Acuña-Fernández, Anadón-Álvarez, Braña-Gil, Casares-Sánchez, Cernuda-Cernuda, Egocheaga-Rodríguez, Eilers, Domínguez-Sanjurjo, Elsässer, Fernández-Casado, Fernández-González, Fernández-Sánchez, González-González, Herrero-Espílez, Lastra-López, Manzanal-Sierra, Martínez-Esteban, Miguelez-González, Nava-Fernández, Navarro-Incio, Obeso-Suárez, Pérez-Freije, Piñeiro-Belloso, Rico-Ordás, Rodicio-Rodicio, Rodríguez-Alonso, Rodríguez-Fernández, Sánchez-Cármenes, Toyos-González

5.4. Acknowledgements

I would like to express my deepest gratitude to my thesis supervisor, Prof. Dr. Hans-Peter Elsässer, for his continuous support and constructive guidance throughout the five past years. He has been like a father for me in Germany and I will always be grateful for his patience, sense of humor and passion for research.

Also, thanks to Prof. Dr. Martin Eilers for his helpful scientific advice and Dr. Elmar Wolf and Dr. Björn von Eyss for their ChIP-Seq analysis and collaboration. Microarray data would not have been possible without Dr. Michael Krause, Florian Finkernagel and Lukas Rycak from the Institute of Molecular Biology and Tumor Research (IMT, Marburg) and I acknowledge them for their useful help and availability. Dieter Schäffer and everybody working at the animal house in the Lahnberge deserve great recognition for taking so good care of the mice.

Special thanks to everybody in the Institute of Cytobiology and Cytopathology for the great atmosphere and openness. The technical support of Waltraud Ackermann and Ursula Lehr is greatly acknowledged. I would also like to thank Gisela Lesch, Volkwin Kramer, Ralph Rößer and Dr. Oliver Stehling for their generous help. I cannot miss the opportunity to mention the "famous" Institute music band: The Wildtypes. It has been fun to play together and I wish that this same spirit endures in the Institute and new generations of scientists display their love for music in rehearsals and live concerts.

My PhD program (Transregio 17; "Ras-dependent pathways in human cancer") was of great interest and excellently organized. The people from AG Eilers, Stiewe, Brehm or Gaubatz were always open for scientific discussion and I enjoyed every Retreat or Meeting celebrated where you could learn and have fun at the same time. Thanks to Andrea Schott Heinzmann, Martina Janowski, Katrin Wiese and Anne Catherine Bretz for their outstanding work.

The AG Elsässer has been a formidable place to work and I would like to show my appreciation for so many unforgettable moments. Dr. Jan Hönnemann was fundamental for me in the lab teaching me countless techniques, discussing about our data and being an endless source of entertainment. Thank you, Jan. Dr. Mareike Muller was also of great help taking care of every detail of the day-to-day life in the lab.

I would also like to mention former lab members like Sarah Oppenheimer, Nadime Ünver, Corina Webert, Carina Trojahn or Sophie Berliner, and more recent colleagues David Fuhrmann, Hedyeh Kiaveh, Lara Kern and Elisa Kreibich, for creating a fun and interacting work environment.

Nice greets to my friends in Spain (you know who you are!). Thanks for making me feel at home even when I am 2000 kilometers away from it.

I owe my sincere gratitude to my parents Alfredo and Esther. Thank you for being always there and providing all your love and support. I appreciate your perseverance and faith in me, this is for you. Finally, thanks to my sister Vicky and my brother Alfredo for taking good care of the younger brother.

Last but not least, all my gratitude and love goes to my girlfriend Tanja Paul. I could not have made it without her patience and love. She makes the sun shine in my life and I feel blessed for having her by my side.